

ATTENUATION OF STORMWATER MICROPOLLUTANTS IN
BIOCHAR-AMENDED BIOFILTERS AND ENGINEERED
STREAMBED HYPORHEIC ZONES

by
Andrea C. Portmann

© Copyright by Andrea C. Portmann, 2023

All Rights Reserved

A thesis submitted to the Faculty and the Board of Trustees of the Colorado School of Mines in partial fulfillment of the requirements for the degree of Doctor of Philosophy (Civil & Environmental Engineering).

Golden, Colorado

Date _____

Signed: _____

Andrea C. Portmann

Signed: _____

Dr. Christopher P. Higgins
Thesis Advisor

Signed: _____

Dr. John E. McCray
Thesis Advisor

Golden, Colorado

Date _____

Signed: _____

Dr. Junko Munakata Marr
Professor and Department Head
Department of Civil & Environmental Engineering

ABSTRACT

Urbanization is an important factor in driving water shortages through the increase in impermeable surface areas, which creates greater runoff volumes and less groundwater infiltration. This disruption of the natural water cycle is accompanied by a growing pollution of urban waters – stemming from diffuse anthropogenic sources, i.e., stormwater, and leading to water quality degradation. The use of black carbon adsorbents such as biochar in stormwater control measures (SCMs) has been shown to enhance removal of trace organic contaminants (TOrcs). Though often considered “black box” passive treatment systems, knowledge of the dominant treatment processes impacting long-term system performance can ultimately inform design, maintenance, and lifetime of SCMs. The overall objective of this dissertation was to evaluate the role of biodegradation and biochar in the long-term removal of TOrcs in novel biochar-amended SCMs.

Exhaustive column studies sought to advance our understanding of the impact of a biofilm on TOrc removal and biofilter lifetime (Chapter 2), whereas flume experiments provided insight on the attenuation of TOrcs in engineered hyporheic zones (i.e., streambed biofilters known as Biohydrochemical Enhancements for Streamwater Treatment; BEST) and evaluated the removal of the highly polar diabetes medication metformin in full-scale modules (Chapter 3) and a range of different TOrcs in a pilot-scale flume system (Chapter 4). Findings from Chapter 2 indicated that the presence of an active biofilm prolonged filter lifetime by 2-fold and that biological processes (i.e., biodegradation and biologically enhanced sorption) contributed 20-36% to overall TOrc removal. Chapter 3 revealed that BEST engineered streambeds led to enhanced hyporheic exchange and attenuation of metformin compared to non-engineered sediment. Chapter 4 revealed that 14 consecutive 1-m long modules featuring BEST streambeds amended with 7% biochar (by volume) and sand (8-mesh Unimin) resulted in surface peak concentration reductions of >50% for all TOrcs studied except for one. The research conducted in this dissertation provides critical performance data and design recommendations for biochar-amended SCMs. Resulting water quality improvements in urban areas lead to greater human and ecosystem health. Furthermore, a better understanding of TOrc removal in these novel SCMs may facilitate their regulatory approval and acceptance by stormwater practitioners.

TABLE OF CONTENTS

ABSTRACT	iii
LIST OF FIGURES	viii
LIST OF TABLES	xiv
LIST OF SYMBOLS	xvii
LIST OF ABBREVIATIONS	xix
ACKNOWLEDGMENTS	xxiv
DEDICATION	xxvi
CHAPTER 1 INTRODUCTION	1
1.1 Background and Motivation	2
1.1.1 Biochar as Stormwater Adsorbent	2
1.1.2 Biological Processes in Biochar-Amended Filtration Systems	3
1.1.3 Engineered Hyporheic Zones for Stormwater Treatment	4
1.2 Objectives and Hypotheses	6
1.2.1 Objective 1: The Role of Biofilm in the Removal of Pesticides in Biofilters	6
1.2.2 Objective 2: Attenuation of Metformin in Full-Scale Engineered Streambed Hyporheic Zones	7
1.2.3 Objective 3: TO _r C Removal in Pilot-Scale Engineered Streambed Hyporheic Zones	7
1.3 Dissertation Organization	8
CHAPTER 2 THE REGENERATIVE ROLE OF BIOFILM IN THE REMOVAL OF PESTICIDES FROM STORMWATER IN BIOCHAR-AMENDED BIOFILTERS	10
2.1 Abstract	10
2.2 Introduction	11
2.3 Methods	14
2.3.1 TO _r C Analysis	14
2.3.2 Materials	15
2.3.3 Batch Sorption Experiments	16

2.3.4	Column Experiments	17
2.3.5	Microcosm Experiments	18
2.3.6	Transport Modelling	18
2.4	Results and Discussion	19
2.4.1	Biological Activity of Columns	19
2.4.2	Impact of Fouling/Ageing on Biochar Properties	21
2.4.3	Column Performance: Contaminant Breakthrough Curves	21
2.4.4	Biotic Contributions – Parent Mass Balance (Columns)	23
2.4.5	Biotic Contributions – Known Transformation Products and Pathways	26
2.4.6	Microcosm Mass Balance / Suspect Screening	31
2.4.7	Abiotic Batch Sorption Experiments	33
2.4.8	Transport Modelling	35
2.5	Environmental Implications	37
 CHAPTER 3 BIOCHAR-AMENDED ENGINEERED STREAMBEDS FOR IN-STREAM ATTENUATION OF THE DIABETES MEDICATION METFORMIN AND ITS METABOLITE GUANYLUREA		
3.1	Abstract	39
3.2	Introduction	40
3.3	Methods	43
3.3.1	Field Site and Flume Experiments	43
3.3.2	Engineered Streambeds – Experimental Setup	44
3.3.3	Engineered Streambeds – Materials	45
3.3.4	Analytical Chemical Analysis of Surface and Streambed Water	46
3.3.5	Batch Experiments	47
3.4	Results and Discussion	49
3.4.1	Biochar Batch Sorption	49
3.4.2	HZ Flow and Exchange in Engineered Streambeds	51
3.4.3	Redox Conditions in Engineered Streambeds	51

3.4.4	Attenuation of Metformin/Guanylurea in Engineered Streambeds	53
3.4.5	Biodegradation of Metformin (Suspect Screening)	55
3.5	Conclusions	56
CHAPTER 4 ENGINEERED STREAMBEDS FOR THE REMOVAL OF PESTICIDES AND PHARMACEUTICALS FROM STORMWATER		58
4.1	Abstract	58
4.2	Introduction	59
4.3	Methods	62
4.3.1	Flume Configuration and Operational Conditions	62
4.3.2	Materials	63
4.3.3	Contaminant Experiments	65
4.3.4	TOrC Analysis	68
4.4	Results and Discussion	69
4.4.1	Surface Water TOrC Removal (Reach-Scale)	69
4.4.2	Subsurface Water TOrC Removal (Module-Scale)	73
4.4.3	Extended Reach-Scale Attenuation	76
4.4.4	TOrC Transformation Products	77
4.5	Conclusions	81
CHAPTER 5 CONCLUSIONS		82
5.1	Summary of Findings	82
5.1.1	Objective 1: The Role of Biofilm in the Removal of Pesticides in Biofilters	82
5.1.2	Objective 2: Attenuation of Metformin in Full-Scale Engineered Streambed Hyporheic Zones	83
5.1.3	Objective 3: TOrCs Removal in Pilot-Scale Engineered Streambed Hyporheic Zones	84
5.2	Research Contributions and Significance	85
5.3	Recommendations for Future Research	88
REFERENCES		90
APPENDIX A SUPPORTING INFORMATION FOR CHAPTER 2		107

A.1	TO _r C Analysis	107
A.2	Microbial Transformation Pathways	109
A.3	Materials	115
A.4	Batch Sorption Experiments	117
A.5	Column Experiments	121
A.6	Transformation Products & Suspect Screening	124
A.7	Transport Modelling	131
APPENDIX B SUPPORTING INFORMATION FOR CHAPTER 3		142
B.1	Flume System & Experimental Set-up	142
B.2	TO _r C Analysis	145
B.3	Batch Sorption Experiments	148
B.4	Redox Conditions in Streambeds	151
B.5	Particle Tracing (Transport Model)	152
B.6	Experiment B (10 mg/L Metformin), Suspect Screening	153
APPENDIX C SUPPORTING INFORMATION FOR CHAPTER 4		154
C.1	Pilot-Scale Flume System & Experimental Set-up	154
C.2	TO _r C Analysis	156
C.3	Flume Contaminant Experiments	160
C.4	Transformation Products (Suspect Screening)	162
APPENDIX D COPYRIGHT PERMISSIONS		168

LIST OF FIGURES

Figure 2.1	<p>a) Biological activity of columns: Removal of dissolved oxygen (DO) during days 7-110 and removal of dissolved organic carbon (DOC) during days 11-103; shown are the mean and standard error of the mean (SEM) with sample sizes $n = 54, 18, 18, 18$, respectively. b) Effect of biofilm and ageing on biochar properties: Brunauer-Emmett-Teller specific surface area (BET SSA) and pore volume distribution of fresh MCG-biochar compared to aged biotic and inhibited samples. Ageing consisted of column conditioning with synthetic stormwater containing ~ 10 mg/L DOC (23 days) followed by injection of synthetic stormwater with ~ 10 mg/L DOC and ~ 200 $\mu\text{g/L}$ TOrCs (92 days). 20</p>
Figure 2.2	<p>Column effluent concentrations [$\mu\text{g/L}$] over time [days] for the spiked pesticides: a) Atrazine, b) Imidacloprid, c) Clothianidin. Initial breakthrough (BT) is defined as the time when the effluent concentration $C_{Eff} = 0.05 \cdot C_{In}$, and exhaustive BT is defined as the time when the effluent concentration $C_{Eff} = 0.9 \cdot C_{In}$. BT times for the ‘BC+Sand biotic’ condition (three replicates) are reported as mean \pm standard deviation. Dotted lines represent the mean influent concentrations. 22</p>
Figure 2.3	<p>Mass balance of parent effluent data (area under curve calculation). The share of sorption, inhibited (comprising both sorption to the biochar and biosorption) was estimated from the difference between the inhibited Sand and inhibited BC+Sand breakthrough curves. This portion was then subtracted from the biologically enhanced removal observed in the biotic BC+Sand columns to yield the biotic contribution (consisting of both biologically enhanced sorption and biodegradation). 24</p>
Figure 2.4	<p>Temporal evolution of transformation products (TPs) of atrazine and imidacloprid in column effluents and influent identified by target LC-QToF-MS analysis: a) desethyl-atrazine, b) 2-hydroxy-atrazine, c) desnitro-imidacloprid, d) imidacloprid-olefin. Y-axis shows TP concentrations in effluent normalized by the average parent influent concentration ($C_{W,TP}/C_{W,0,Parent}$). Dotted black lines represent the limit of quantitation (LOQ) for each TP. 28</p>
Figure 2.5	<p>Molar mass balance of microcosm data: Share of transformation products in total parent mass removal at the end of the experiment (369 days). The total parent molar masses removed after 369 days were 71.4 nmol, 119.2 nmol, and 67.8 nmol for atrazine, imidacloprid, and clothianidin, respectively. Initial concentrations for the three compounds were 1923 nM, 1412 nM, and 1458 nM, respectively. “Unknown” indicates that the mass was unaccounted for. Abbreviations: desethyl-atrazine (DEA), desisopropyl-atrazine (DIA), and 2-hydroxy-atrazine (OH-ATZ), desnitro-imidacloprid (desnitro-IMI), imidacloprid-urea (IMI-urea), imidacloprid-olefin (IMI-olefin), 6-chloronicotinic acid (6-CNA), and clothianidin-urea (CLO-urea). Note that calculations for CLO-urea are semi-quantitative. 32</p>
Figure 3.1	<p>Schematic of experimental setup of flume sections amended with engineered structures (BEST plates, submerged dam) and geomeia (biochar). Locations A, B, and C denote HZ sampling locations accessed by vertically introduced MINIPOINT samplers (each at 8 cm depth). Figure is not to scale to better illustrate sampling features and flow paths. 44</p>

Figure 3.2	Biochar batch sorption experiments: a) Kinetic sorption data for metformin and guanylurea (GUA) with pseudo-first order fit of the apparent distribution coefficient ($K_{d,app} = C_S/C_W$) over time. Solid lines represent best fits and dashed lines represent the 95% confidence intervals. b) Sorption isotherms for metformin, GUA, and 1-methylbiguanide (MGB); best-fits of the Freundlich and Langmuir isotherms were obtained via non-linear regression with relative weighting ($1/Y^2$). All analyses were performed in GraphPad Prism (version 9.1.1). Estimated best-fit parameters can be found in the SI (Tables B.4 and B.5). Biochar source: pine wood, gasification process, >1100°C (Gropro, Inc., Etna, CA).	49
Figure 3.3	Subsurface breakthrough curves of bromide (conservative tracer) for different conditions: 1) BEST (top left), 2) BEST + biochar (top right), 3) Surface sand dunes (bottom left), and 4) Plain sediment, non-altered (bottom right). Locations A, B, and C denote subsurface sampling locations (see schematic in Figure 3.1).	50
Figure 3.4	Dissolved oxygen (DO) profiles of subsurface flume sections. Top panel: Left: BEST (May 2018), Right: BEST (June 2018); Bottom panel: Left: BEST+biochar (May 2018), Right: BEST+biochar (June 2018). DO values on color legend are mg/L.	52
Figure 3.5	Subsurface nutrient summarized in a box and whisker plot: a) Iron(II) measurements during the Day 1 to 16 time period; b) Ammonium (NH_4^+) measurements during the Day 1 to 16 time period. A, B, and C denote the subsurface sampling locations in each condition (see Figure 3.1).	53
Figure 3.6	Subsurface breakthrough curves of metformin for different conditions: 1) BEST (top left), 2) BEST + biochar (top right), 3) Surface sand dunes (bottom left), and 4) Plain sediment, non-altered (bottom right). Locations A, B, and C denote HZ sampling locations (see Figure 3.1). Relative standard deviation (%RSD) associated with the analysis was 5% for metformin and 3% for guanylurea, respectively.	54
Figure 3.7	Transformation products (TPs) of metformin measured during Experiment B (10 mg/L spike) for the following conditions: 1) BEST, 2) BEST + biochar, 3) Surface sand dunes, and 4) Plain sediment, non-altered; C1/C2 are samples from the control flume (un-spiked). Locations A, B, and C denote subsurface sampling locations (see Figure 3.1). Sampling time was August 24th 2018, i.e. 10 days after spiking. Response ratios for TPs were determined relative to metformin-d ₆ ($Area_{TP}/Area_{metformin-d6}$). Confidence level of identification according to Schymanski scale: metformin, guanylurea, and 1-methyl-biguanide: 1; others: 3.	55
Figure 4.1	Surface water breakthrough curves (BTCs) for select TOrCs during simulated stormflow experiments (single-pass flume operation). Experimental conditions: Control (F1), BEST (F2), BEST + biochar (F3), and BEST + biochar, slow (F4). Dotted vertical lines indicate the time when dosing stopped: 3h 45min (F1), 3h 25min (F2), 4h (F3, F4). Samples with concentrations below the LOQ, which frequently occurred for the Su samples after dosing stopped, were not plotted.	70
Figure 4.2	Mass balance for each TOrC and flume (F1-F4) for simulated stormflow experiments (single-pass flume operation). Mass differences per flume were calculated as follows: $\Delta M [\%] = (M_{in} - M_{out})/M_{in} * 100$ whereas M_{in} was the nominal mass added to each flume; $M_{out} = \Sigma(C_{out} * t) * Q$ with $Q = 681.37 \text{ L/h} = \text{constant}$. Experimental conditions: Control (F1), BEST (F2), BEST + biochar (F3), and BEST + biochar, slow (F4).	72

Figure 4.3	Porewater breakthrough curves (BTCs) for select TOrcs and modules (#3, #7, #11) during simulated stormflow experiments (single-pass flume operation). Conditions: BEST (F2), BEST+biochar (F3), and BEST+biochar, slow (F4). Dotted vertical lines indicate dosing end: 3h 25min (F2), 4h (F3, F4).	74
Figure 4.4	Removal of TOrcs during recirculation experiments at 24 hours after dosing onset (T1) and at 15 days (T15); calculated based on concentration reductions between Su and Sd. Net negative removal at T15 for carbamazepine in F1 and F2 is not shown (-28.3% and -43.1%, respectively). Experimental conditions: Control (F1), BEST (F2), BEST + biochar (F3), and BEST + biochar, slow (F4).	76
Figure 4.5	Transformation products (TPs) detected in samples from recirculation experiments via suspect screening for the following parent compounds: a) Atenolol (C_0 F1: 4.9 nM; C_0 F2: 8.5 nM); b) Ibuprofen (13.0 nM; 8.2 nM); c) Isoproturon (25.0 nM; 32.5 nM); d) Diazinon (16.7 nM; 16.0 nM). Please note that concentrations for all suspects are semi-quantitative; calibrants were the corresponding parent compounds. Abbreviations: 1/2-hydroxy-ibuprofen (1/2-OH-IBU); carboxy-ibuprofen (carboxy-IBU); 1,2-dihydroxy-ibuprofen (1,2-diOH-IBU); monodesmethyl-isoproturon (MDIPU); 2-hydroxy-isoproturon (2-OH-IPU); 2-isopropyl-6-methyl-4-pyrimidinol (IMHP); hydroxy-diazinon (OH-diazinon).	78
Figure A.1	Literature-established major microbial transformation pathways for atrazine. Sources: Fang <i>et al.</i> ; Kolekar <i>et al.</i> ; Mudhoo & Garg; Sagarkar <i>et al.</i> ; Singh & Cameotra; Singh <i>et al.</i>	113
Figure A.2	Literature-established major microbial transformation pathways for imidacloprid. Sources: Hussain <i>et al.</i> ; Pandey <i>et al.</i> ; Sharma <i>et al.</i> ; Sharma <i>et al.</i>	114
Figure A.3	Literature-established major microbial transformation pathways for clothianidin. Sources: Mori <i>et al.</i> ; Van der Velde-Koerts <i>et al.</i> ; Zhang <i>et al.</i>	115
Figure A.4	Solid lines represent best fits of the Freundlich and Langmuir equations to batch sorption isotherm data using non-linear regression and relative weighting ($1/Y^2$). Dotted lines represent the 95% confidence intervals of the fitted curves. The systematic error in the observed datapoints across all three pesticides was likely caused by uncertainties in dry biochar mass (due to its extremely light weight and hydrostatic behavior).	117
Figure A.5	Kinetic batch sorption data plotted as apparent distribution coefficient, $K_d = C_S/C_W$ (C_S = biochar-sorbed concentration, C_W = aqueous concentration). The solid lines represent pseudo-first order fits and the dashed lines represent the 95% confidence intervals; the fit was simply done for better visualization.	119
Figure A.6	Salt tracer breakthrough curves in column effluents using a potassium bromide (KBr) tracer. Data is adjusted for hold-up time outside of porous media; ideal plug-flow conditions were assumed in tubing and in glass beads/glass wool mixture at the inlet and outlet of columns.	121
Figure A.7	Seeding cultures used for column inoculation and microcosms during the last stage (4 days) of the second inoculation cycle. Optical density (O.D.) at 600 nm of the culture was measured in a subsample each day and was as follows (chronological order): a) 0.183, b) 0.585, c) 0.643, d) 0.474. The seeding culture depicted in d) was used for column and microcosms inoculation the following day.	122

Figure A.8	Optical density (O.D.) measurements of column enrichment cultures or seeding cultures (SC). In the beginning, several replicate batches were incubated and only the ones with most observed growth (highest O.D. values) were kept for continued multi-cycle inoculation. Cultures 3.5B and 3.5C were combined for stage II incubation, which resulted in the final culture 3.5B+C, which was used for column and microcosm biofilm seeding. Error bars during stage I represent standard deviation occurring from repeated measurement of the same sample (analytical variability).	123
Figure A.9	Representative MS and MS ² scans for 5-Hydroxyimidacloprid. a) Precursor ion extracted chromatogram, b) Isotope spectrum of precursor ion, c) MS ² scan, d) Zoomed in MS ² scan at 225.05 Da (fragment), e) Zoomed in MS ² scan at 191.09 Da (fragment).	125
Figure A.10	Representative MS and MS ² scans for Nitrosoguanidine-Imidacloprid. a) Precursor ion extracted chromatogram, b) Isotope spectrum of precursor ion, c) MS ² scan including fragments at 209.05 Da and 175.09 Da.	125
Figure A.11	Representative MS and MS ² scans for Clothianidin-Urea. a) Precursor ion extracted chromatogram, b) Isotope spectrum of precursor ion, c) MS ² scan including fragments at 131.96 Da and 119.96 Da.	126
Figure A.12	Target and suspect transformation products in microcosms over time. Error bars represent the standard deviation between experimental replicates (n=2). Abbreviations: desethylatrazine (DEA), desisopropylatrazine (DIA), and 2-hydroxy-atrazine (OH-ATZ), desnitro-imidacloprid (desnitro-IMI), imidacloprid-urea (IMI-urea), imidacloprid-olefin (IMI-olefin), 6-chloronicotinic acid (6-CNA), nitrosoguanidine-imidacloprid (NG-IMI), and clothianidin-urea (CLO-urea). Note that concentrations for NG-IMI and CLO-urea are semi-quantitative.	126
Figure A.13	Additional target and suspect transformation products (TPs) of atrazine, imidacloprid, and clothianidin in column effluents (and influent) identified by LC-QToF-MS analysis: a) deisopropyl-atrazine, b) imidacloprid-urea, c) clothianidin-urea (suspect; semi-quantitative), d) nitrosoguanidine-imidacloprid (suspect; semi-quantitative). Y-axis shows TP concentrations normalized by the average parent influent concentration ($C_{W,TP}/C_{W,0,Parent}$). Dotted black lines represent the limit of quantitation (LOQ) for each TP (not available for suspects). . . .	127
Figure A.14	The suspect deisopropylhydroxy-atrazine as a product of in-source fragmentation of 2-hydroxy-atrazine (OH-ATZ) at identical retention times of 4.73 min, found both in microcosm samples (a) and analytical standards (b). Both precursor peaks were confirmed by library hits (score >99).	129
Figure A.15	The suspect desethyldeisopropyl-atrazine (or didealkyl-atrazine) as a product of in-source fragmentation of desethyl-atrazine (DEA) at identical retention times of 5.17 min, found both in microcosm samples (a) and analytical standards (b). Both precursor peaks were confirmed by library hits (score >93). The peak to the left in panel b) is the product of in-source fragmentation of deisopropyl-atrazine (DIA) in the analytical standard, but was not found in the sample.	130
Figure A.16	Prediction of <u>inhibited</u> BC+Sand column breakthrough curves using the batch-derived Freundlich sorption isotherm (K_F, n) and kinetic (tortuosity) parameters in the MATLAB transport model. a) Atrazine, b) imidacloprid, c) clothianidin.	137

Figure A.17	Prediction of <u>biotic</u> BC+Sand column breakthrough curves using the batch-derived Freundlich sorption isotherm (K_F , n) and kinetic (tortuosity) parameters in the MATLAB transport model. a) Atrazine, b) imidacloprid, c) clothianidin.	137
Figure A.18	Best-fit simulations of <u>inhibited</u> BC+Sand column breakthrough curves using the transport model in MATLAB and assuming Freundlich non-linear sorption behavior. a) Atrazine, b) imidacloprid, c) clothianidin.	138
Figure A.19	Best-fit simulations of <u>biotic</u> BC+Sand column breakthrough curves using the transport model in MATLAB and assuming Freundlich non-linear sorption behavior. a) Atrazine, b) imidacloprid, c) clothianidin.	138
Figure A.20	Estimation of first-order biodegradation rate (k_{deg}) for <u>biotic</u> BC+Sand column breakthrough curves using the transport model in MATLAB and assuming Freundlich non-linear sorption behavior. Input values for the sorption and kinetic parameters were taken from the best-fit shown in Figure A.18 (best-fit to inhibited BC+Sand data). a) Atrazine, b) imidacloprid, c) clothianidin.	140
Figure B.1	Full-scale outdoors flume system at the German Environment Agency (Umweltbundesamt; UBA) in Berlin, Germany. Photo was taken in 2018.	142
Figure B.2	Preliminary evaluation of experimental set-up and impact of different BEST streambed structures (submerged dam, subsurface steel plates) on HZ flow and residence times of flowpaths in a 1-D flow model in COMSOL Multiphysics®. Finally, the configuration of condition 6 was chosen for the full-scale flume study (with and without biochar).	143
Figure B.3	Flume surface water concentrations of metformin over time during Experiment A (10 µg/L spike). Data is volume-corrected (using lithium-bromide tracer data).	143
Figure B.4	Kinetic sorption of metformin and guanylurea to MCG biochar; shown as relative aqueous concentrations over time (67 days total). Initial TOC concentration was 10 µg/L each. Control batches were set up without biochar (water only).	148
Figure B.5	Removal of metformin during bottle incubation experiment (75 days). Error bars represent standard deviation from triplicate experiments. All experiments were carried out outside to mimic temperature and sunlight exposure conditions of flumes. Biotic experiments were aerated continuously.	150
Figure B.6	Subsurface dissolved oxygen (DO) profiles of plain sand (un-altered) streambed sections. Measurements were taken in May and June 2018.	151
Figure B.7	Particle tracing in a 1-D flow model using COMSOL Multiphysics®. The coupled surface-subsurface model was built based on geometry measurements, material properties and flow information (not calibrated).	152
Figure B.8	Metformin and guanylurea concentrations in the subsurface of different conditions during Experiment B (~10 mg/L spike) measured at t = 10 days after spiking. Conditions: 1) BEST, 2) BEST + biochar, 3) Surface sand dunes, 4) Plain sediment (un-altered).	153
Figure C.1	Process diagram of the pilot-scale outdoor stream flumes at the Mines Park Water Reclamation Facility at the Colorado School of Mines in Golden, CO. Four individual flumes with different configurations can be operated in parallel in recirculation mode or one at a time in single-pass mode.	154

Figure C.2	Location of porewater sampling points in BEST modules. The “X” denotes the location of the tip of the sampling rod, from where pore water was drawn. Black triangles represent BEST walls.	154
Figure C.3	Subsurface bromide breakthrough curves (BTCs) during simulated stormflow experiments: a) Control (F1), b) BEST (F2), c) BEST + biochar (F3), and d) BEST + biochar, slow (F4). Please note the difference in scaling of the y-axis for F1 and the x-axis for F4.	160

LIST OF TABLES

Table 2.1	Biofilter lifetime simulations based on different case study scenarios. Bold numbers indicate biofilter lifetime estimates when treating 16 inches of annual rainfall (Denver, CO), and numbers in parentheses represent biofilter lifetimes assuming continuous flow/operation. Freundlich parameters represent best-fit values to biotic BC+Sand column data, assuming kinetic diffusion limitations. Abbreviations: M_{BC} = biochar application rate, C_{In} = influent concentration.	37
Table 3.1	Physical and chemical properties of streambed materials: flume sediment, sediment / biochar mixture, and biochar. K_{Sat} , porosity, and organic matter content data are provided as average \pm standard deviation.	46
Table 4.1	Flume configurations with saturated hydraulic conductivity (K_{Sat}) and porosity measurements of the corresponding materials (or mixtures). Values are given for loose (L) packing conditions, with values in parentheses representing measurements from tight (T) packing conditions. Red / orange / yellow crosses denote the location of porewater sampling points; for dimensions and exact locations see Figure C.2. Surface water sampling points: Su = surface water upstream; Sm = surface water midstream; Sd = surface water downstream.	64
Table A.1	Native and surrogate standard sources for investigated trace organic chemicals (TOrcs).	107
Table A.2	LC-QToF-MS parameters for target analytes including parent compounds, transformation products, and surrogates. Analysis was performed in ESI+ ionization mode.	108
Table A.3	Extracted ion chromatogram (XIC) list of microbial transformation products of atrazine, imidacloprid, and clothianidin.	110
Table A.4	Best-fit values for Freundlich and Langmuir parameters obtained in GraphPad Prism (version 9.1.1). AICc designates the Akaike's Information Criterion corrected for low sample size. Please note that the K_F values are not significantly different from each other ($p=0.1261$), the same is true for the parameter n ($p=0.7542$; One-way ANOVA, $\alpha = 0.05$). Abbreviations: Confidence interval (CI), Root Mean Square Error (RMSE).	118
Table A.5	Equilibrium K_d (\pm standard deviation) calculated from kinetic batch sorption data at timepoint $t=67$ days ($K_{d,eq} = C_{S,eq}/C_{W,eq}$). It was concluded that sorption equilibrium had been established for all compounds since linear regression analysis between $t=29$ days and 67 days revealed that slopes did not significantly deviate from zero ($p \geq 0.7498$). Tukey's multiple comparisons test (following ANOVA) was computed in GraphPad Prism (version 9.1.1). "ns" denotes "not significant". Abbreviations: Confidence interval (CI), Difference (Diff.); others: see Table A.1.	120
Table A.6	MRM transitions of suspect analytes (all in ESI+ mode): The exact precursor mass was used for compound identification and at least one of the exact fragment masses was used for compound verification. The level of suspect confidence refers to the scale proposed by E. Schymanski, Schymanski <i>et al.</i>	124

Table A.7	Range of (average) TP concentrations observed in the biotic BC+Sand columns and in the microcosms. Please note that concentrations for NG-IMI and CLO-urea are semi-quantitative.	128
Table A.8	Independent and dependent column model variables and input parameters and their dimensions.	132
Table A.9	General input parameters for column pollutant transport model for parameter estimation (fitting).	136
Table A.10	Freundlich sorption parameters, kinetic fitting parameter (tortuosity), goodness of fit, and linearized distribution coefficients for batch (abiotic) and column systems (inhibited and biotic) (Figures A.16-A.19). Linearization of isotherms is presented for comparison only.	139
Table A.11	Calculations to adjust simulated continuous filter lifetimes based on a representative field-scale biofilter (infiltration basin) for a residential area of 3 acres and 16 inches per year of average annual rainfall in Denver, CO.	141
Table B.1	Representative surface water quality data for the treatment flume. Nitrite, phosphate, and ammonia were 0 mg/L at all measured timepoints; nitrate was consistently <0.5 mg/L.	144
Table B.2	List of target analytes analyzed by LC-QToF-MS including information on the source of analytical standards and surrogates.	145
Table B.3	LC-QToF-MS parameters for target analytes including native compounds and surrogates, plus suspect compounds (transformation products (TPs) of metformin). All analytes were analyzed in positive electrospray ionization (ESI+) mode. Abbreviations: 2-amino-4-methylamino-1,3,5-triazine (2,4-AMT), 4-amino-2-imino-1-methyl-1,2-dihydro-1,3,5-triazine (4,2,1-AIMT), and 2,4-diamino-1,3,5-triazine (2,4-DAT).	146
Table B.4	Kinetic data: Pseudo-first order fit of the apparent distribution coefficient ($K_{d,app} = C_S/C_W$) over time using GraphPad Prism (version 9.1.1).	149
Table B.5	Best-fit values for Freundlich and Langmuir parameters obtained from equilibrium biochar sorption data using non-linear regression with relative weighting ($1/Y^2$) in GraphPad Prism (version 9.1.1). AICc designates the Akaike's Information Criterion corrected for low sample size.	149
Table C.1	Representative water quality data for the Membrane Batch Reactor (MBR) system treating wastewater from nearby university student housing. The effluent of the MBR served as the source water for all flume experiments conducted in this study (August-October 2020). Abbreviations: sCOD = soluble chemical oxygen demand; pCOD = particulate chemical oxygen demand; T-N = total nitrogen; T-P = total phosphorus.	155
Table C.2	List of spiked target compounds analyzed by LC-QToF-MS including information on hydrophobicity ($\log K_{OW}$) and biodegradability (BIOWIN3). $\log K_{OW}$ = octanol-water partition coefficient; source: KOWWIN v1.68 estimates (EPI Suite TM).	156

Table C.3	LC-QToF-MS parameters for target analytes including native compounds and surrogates. § Variabilities in limit of quantitation (LOQ) were due to instrument variability (ESI-) or lab blank contamination (ESI+). * Spike Recovery was assessed by adding 10 μ L of Standard solution (in MeOH) to 500 mL deionized water. Unfiltered samples were compared with PVDF (0.2 μ m, 13 mm) filtered samples to determine the average recovery (n = 2) during sample processing.	158
Table C.4	TOrC concentration peak reductions observed during single-pass experiments (4h-rainfall simulation). Surface attenuation was determined as peak reduction in Sd (effluent) compared to influent concentrations (Su); subsurface attenuation was determined exemplarily in Module #3 (across all flumes), as measured removal between HZ sampling locations D and U2.	161
Table C.5	TOrC mass balance conducted for each TOrC and flume for simulated stormflow data (single-pass), using the method of moments for the downstream concentration (Sd) and the nominal TOrC mass added to each flume (M_{in}). M_{in} = 36 mg of each TOrC in F1/F3/F4, and 30 mg in F2.	163
Table C.6	Suspect transformation products (TPs) detected in surface and subsurface samples of recirculation experiments via LC-HRMS Positive Ionization Mode (ESI+). Experimental conditions: Control (F1), BEST (F2), BEST + biochar (F3), and BEST + biochar, slow (F4).	164
Table C.7	Suspect transformation products (TPs) detected in surface and subsurface samples of recirculation experiments via LC-HRMS Negative Ionization Mode (ESI-). Note: Metolachlor oxanilic acid and metolachlor ethane sulfonic acid had to be analyzed in ESI- mode despite the parent (metolachlor) being an ESI+ compound, see Li <i>et al.</i> . For Fipronil sulfone, impurities may be present in calibration standards, possibly due to in-vial oxidation. References: Miller <i>et al.</i> refers to the following online dataset: https://www.sciencebase.gov/catalog/item/5e6cdf5e4b01d509265a1fc	167

LIST OF SYMBOLS

Adsorption kinetic rate constant	k_{ad}
Apparent biochar-water distribution coefficient	$K_{d,app}$
Aquatic life threshold concentration	C_{Th}
Biochar application rate	M_{BC}
Biochar-water partition coefficient	K_d
Effluent concentration	C_{Eff}
Equilibrium biochar-water partition coefficient	$K_{d,eq}$
Flume 1: Sand-only streambeds	$F1$
Flume 2: BEST streambeds	$F2$
Flume 3: BEST streambeds amended with biochar	$F3$
Flume 4: BEST streambeds with fine-grain sand and biochar	$F4$
Freundlich isotherm coefficient	K_F
Freundlich isotherm exponent	n
Influent concentration	C_{In}
Initial TO _o C aqueous concentration	C_0 or $C_{W,0}$
Langmuir isotherm coefficient	K_L
Langmuir isotherm sorption capacity	Q_{max}
Mass balance difference	ΔM
Maximum concentration in the influent (upstream)	$C_{Su,max}$
Octanol-water partition coefficient	K_{OW}
Organic carbon content	f_{OC}
Organic carbon-water partition coefficient	K_{OC}
Organic matter content	f_{OM}
Porewater concentration	C_{PW}
Saturated hydraulic conductivity	K_{Sat}

Surface water concentration	C_{SW}
TOrC aqueous concentration	C_W
TOrC aqueous concentration at equilibrium	$C_{W,eq}$
TOrC biochar-sorbed concentration at equilibrium	$C_{S,eq}$
Tortuosity	τ

Transport Model

Sand particle-water partitioning coefficient for the pollutant	K_S
First-order kinetic sorption rate for pollutants sorbed by the sand particles	k_S
First-order biodegradation rate	k_{deg}
Freundlich isotherm coefficient for the pollutant	$K_{Fr,BC}$
Freundlich isotherm exponent for the pollutant	$1/n_{Fr,BC}$

LIST OF ABBREVIATIONS

1,2-dihydroxy-ibuprofen	1,2-diOH-IBU
1-(3,4-Dichlorophenyl)-3-methylurea	DCPMU
1-methylbiguanide	MBG
1/2-hydroxy-ibuprofen	1/2-OH-IBU
2,4-diamino-1,3,5-triazine	2,4-DAT
2,4-dichlorophenoxyacetic acid	2,4-D
2-4-[(dimethyl-carbamoyl)amino]phenylpropanoic acid	TP237
2-amino-4-methylamino-1,3,5-triazine	2,4-AMT
2-hydroxy-atrazine	OH-ATZ
2-hydroxy-isoproturon	2-OH-IPU
2-isopropyl-6-methyl-4-pyrimidinol	IMHP
2-methyl-4-chlorophenoxyacetic acid	MCPA
4-amino-2-imino-1-methyl-1,2-dihydro-1,3,5-triazine	4,2,1-AIMT
4-isopropylaniline	4-IA
5-hydroxy-imidacloprid	5-OH-IMI
6-chloronicotinic acid	6-CNA
Acrylonitrile butadiene styrene	ABS
Activated carbon	AC
Akaike's Information Criterion	AIC
American Society for Testing and Materials	ASTM
Analysis of variance	ANOVA
Atrazine	ATZ
Background	BG
Barrett, Joyner, and Halenda	BJH
Biochar	BC

Biohydrochemical Enhancements for Streamwater Treatment	BEST
Biological activated carbon filter	BAF
Breakthrough	BT
Breakthrough curve	BTC
Brunauer-Emmett-Teller specific surface area	BET SSA
Carboxy-ibuprofen	carboxy-IBU
Cation exchange capacity	CEC
Chemical oxygen demand	COD
Clothianidin	CLO
Clothianidin-urea	CLO-urea
Confidence interval	CI
Deionized	DI
Desethylatrazine	DEA
Desisopropylatrazine	DIA
Desnitro-imidacloprid	desnitro-IMI
Dissolved organic carbon	DOC
Dissolved oxygen	DO
Electrical conductivity	EC
Electron-donor acceptor	EDA
Environmental Quality Standard	EQS
Ethylene propylene diene monomer	EPDM
Extracted ion chromatogram	XIC
Granular activated carbon	GAC
Guanylurea	GUA
High resolution mass spectrometry	HRMS
High-performance liquid chromatography	HPLC
Humic acid	HA

Hydraulic conductivity	K
Hydraulic residence time	HRT
Hydroxy-diazinon	OH-diazinon
Hyporheic zone	HZ
Imidacloprid	IMI
Imidacloprid-olefin	IMI-olefin
Imidacloprid-urea	IMI-urea
Internal standard	IS
Ion chromatography	IC
Limit of detection	LOD
Limit of quantitation	LOQ
Liquid chromatography quadrupole time-of-flight mass spectrometry	LC-QToF-MS
Mass spectrometry	MS
Membrane Batch Reactor	MBR
Methanol	MeOH
Monodesmethyl-isoproturon	MDIPU
Mountain Crest Gardens	MCG
Multiple reaction monitoring	MRM
N-(2-chlorothiazol-5-yl-methyl)-N'-methylurea	TZMU
N-(2-chlorothiazol-5-yl-methyl)-N'-nitroguanidine	TZNG
N-methyl-N'-nitroguanidine	MNG
National Pollutant Discharge Elimination System	NPDES
Nicotinic acetylcholine receptor	nAChR
Nitrosoguanidine-imidacloprid	NG-IMI
Optical density	O.D.
Organisation for Economic Co-operation and Development	OECD
Pentachlorophenol	PCP

Per-and polyfluoroalkyl substances	PFASs
Perfluorohexanoic acid	PFHxA
Pharmaceuticals and personal care products	PPCPs
Polychlorinated biphenyls	PCBs
Polycyclic aromatic hydrocarbons	PAHs
Polyetheretherketone	PEEK
Polyvinyl chloride	PVC
Polyvinylidene difluoride	PVDF
Pore volume	PV
Positive / Negative electrospray ionization	ESI+/ESI-
Predicted no-effect concentration	PNEC
Pseudo-first order	PFO
Relative standard deviation	%RSD
Response factor	RF
Retention time	RT
Root Mean Square Error	RMSE
Sequential window acquisition of all theoretical fragment ion spectra	SWATH
Standard error of the mean	SEM
Stormwater Control Measures	SCMs
Sum of squared residuals	SSR
Supporting Information	SI
Total Maximum Daily Load	TMDL
Total nitrogen	TN
Total organic carbon	TOC
Trace organic contaminants	TOrCs
Transformation product	TP
Tris(2-carboxyethyl)phosphine	TCEP

Ultra high-performance liquid chromatography tandem mass spectrometry	UHPLC-MS/MS
Umweltbundesamt / German Environment Agency	UBA
United States Environmental Protection Agency	U.S. EPA
Wastewater treatment plant	WWTP

ACKNOWLEDGMENTS

After my research stay at Stanford, I knew that I wanted to become an environmental researcher, because I felt that I could make an important contribution to the protection of our Earth and its resources and the life on it. The journey to become a doctor is never just an academic challenge, but also a personal one. I am deeply grateful for all the support of my friends, family, and colleagues, who accompanied me on my PhD path and continue to do so today.

Most importantly, I could not have made this journey without the support of my advisor, Dr. Chris Higgins, who had the courage to hire a Swiss PhD student in his group. I admire his incredible knowledge about all things PFASs and non-PFASs and his willingness to always find a way. He never lost sight of the big picture and the things that matter, and graciously offered me guidance, feedback and encouragement, whenever I got stuck. I am honored to be one of his PhD researchers.

I am thankful to have received guidance and mentorship from various other researchers. First and foremost, I would like to thank Dr. Greg LeFevre for showing me the ropes of experimental research and for believing in my ability to achieve great things – I would not have become a researcher if it was not for him. He is a true inspiration! I also would like to thank the other members of my PhD committee for their expertise and valuable feedback, Dr. John McCray, who also served as my co-advisor, Dr. Alexis Sitchler, Dr. Junko Munakata-Marr, and Dr. Josh Sharp. I am also grateful to Prof. Dick Luthy, who generously welcomed me into his research group at Stanford University back in 2014 and gave me the opportunity to experience the fun, thrill, and hard work of conducting your own research experiments.

A big thank you goes to all my group mates in the Higgins group and the McCray group – thank you for the help in the lab, impromptu hallway conversations, and words of encouragement when the days in the lab seemed endless (especially when working with high-resolution mass spectrometers). Particularly, I would like to thank Brittnee Halpin, my research collaborator and friend. I am grateful to her for being such a reliable person and researcher, for never giving up, and for working side-by-side amidst most challenging conditions involving a global pandemic, natural wildfires, and the Colorado summer heat. In Europe, I would like to thank the various HypoTRAIN researchers and our collaborators at the German Environment Agency in Berlin. It was exciting to learn how to conduct flume experiments while I visited, and I appreciate your collaborative spirit and hospitality.

My time at Mines would not have been as fun without spending time with my fellow students and researchers in the environmental engineering department. Thank you, Rudy Maltos, Johan Vanneste and Hooman Vatankhah, and many more, for our conversations about life beyond research and for never

forgetting how to have fun! I am also grateful for the long-time friendships with Samantha Medina, Juliane Brown, Tanja Alther and Sabin Amstutz – thank you for supporting me through the ups and downs of life and for all the good memories we created! This list would not be complete without mentioning the Swiss-American Friendship Society in Colorado; thank you for making me feel at home and for sharing the joy of Swiss food together. I am especially grateful to Christie Moran and Markus Groner for pulling me out of the lab to undertake beautiful nature trips and hikes.

Lastly, I would like to thank my entire family, most importantly my Mom, who has always been there for me – in the good times and in the difficult times. I admire your strength and willingness to fight, even when others would have already given up. You are my rock. Also, I should mention that my sister has visited me wherever my research adventures have brought me – Stanford, Golden, Berlin. You are an incredibly creative and warmhearted soul, and manage to make me smile even when things get tough – I cannot thank you enough for this and I am very proud of you.

For those who dare to tell uncomfortable truths.

CHAPTER 1

INTRODUCTION

Climate change and the world’s increasing demand for water supply are aggravating water scarcity, which is one of the major challenges today’s society is facing (Liu *et al.*, 2017b). Urbanization is an important factor in driving water shortages, because of the increase in impermeable surfaces, which create greater runoff volumes and less evaporation and groundwater infiltration compared to undeveloped areas (Grebel *et al.*, 2013). This disruption of the natural water cycle is accompanied by an increasing emission of pollutants in urban spaces – stemming from vehicle traffic, building roofs and facades (e.g. heavy metals), urban green space management (e.g., pesticide application), health management practices (e.g., pharmaceuticals) and household animal waste (e.g., bacteria). Stormwater runoff accumulates many of these anthropogenic contaminants and is thus a major non-point source of pollution – often highly variable in occurrence, runoff volume, and composition/quality (Burant *et al.*, 2018). More and more, stormwater is being viewed as a resource (Luthy *et al.*, 2019) and harnessing it through capture and treatment is a promising strategy to help address both water scarcity and contamination (Clark & Pitt, 2012; Luthy *et al.*, 2019). However, to make stormwater runoff a viable and safe water resource, efficient and cost-effective technologies for water quality improvements are essential. In recent past, the implementation of green infrastructure systems and stormwater control measures (SCMs) has gained traction among practitioners, especially the use of infiltration applications (Grebel *et al.*, 2013). Traditionally, SCMs have focused on flow reduction and water capture, but they have not been designed for stormwater pollutant removal (Grebel *et al.*, 2013; LeFevre *et al.*, 2015).

Among the key drivers of concerns for stormwater use as a water resource is the presence of trace organic contaminants (TOrCs), some of which may be present at unacceptable levels. Common TOrCs found in stormwater and urban streams are polycyclic aromatic hydrocarbons (PAHs), pesticides, vehicle-associated compounds, flame retardants, and pharmaceuticals (LeFevre *et al.*, 2015; Masoner *et al.*, 2019; Spahr *et al.*, 2020). Exposure of TOrCs may lead to substantial aquatic health impacts including acute/chronic toxicity (Tian *et al.*, 2021; Vignet *et al.*, 2019; Young *et al.*, 2018) and endocrine disruption (Mnif *et al.*, 2011; Niemuth & Klaper, 2015), surface water quality degradation (LeFevre *et al.*, 2015), and groundwater pollution (Kiefer *et al.*, 2019; Loos *et al.*, 2010). Specifically, polar TOrCs pose one of the greatest risks for groundwater contamination (Pitt *et al.*, 1999) and ecosystem threats due to their high mobility and low sorptive affinity towards soil and conventional infiltration media such as sand (Spahr *et al.*, 2020). In light of the challenge dissolved and hydrophilic (i.e., polar) TOrCs are imposing on the

aquatic cycle and ecosystem health, amending stormwater treatment systems with geomedia such as biochar has become a strategy of interest to improve contaminant removal (Grebel *et al.*, 2013; Miles *et al.*, 2016; Mohanty *et al.*, 2018). Biochar is a carbonaceous adsorbent similar to activated carbon and is a cost effective means of improving the removal of polar TOrCs as has been shown in laboratory batch and column studies (Ray *et al.*, 2019; Ulrich *et al.*, 2015), as well as pilot-scale biofilters (Ulrich *et al.*, 2017a) and woodchips reactors (Ashoori *et al.*, 2019).

1.1 Background and Motivation

This section provides relevant background literature on 1) the use of biochar as a stormwater adsorbent (i.e., abiotic TOrC sorption mechanisms, biochar properties, diffusion-limited sorption kinetics), 2) biological TOrC removal processes in filtration systems in the presence of biochar and microbial biofilms (i.e., biochar as an electron donor/acceptor, TOrC biodegradation in the dissolved vs. sorbed phase, bioregeneration), and 3) engineered hyporheic zones (e.g., streambed biofilters) for stormwater quality improvements (i.e., natural hyporheic zone, BEST engineered streambeds as a novel SCM technology for TOrC removal).

1.1.1 Biochar as Stormwater Adsorbent

One of the primary challenges in designing biochar-amended biofilters is the selection of the biochar media itself. The material properties of biochar, in contrast to engineered geomedia such as activated carbon (AC), vary widely (Ulrich *et al.*, 2015). Properties are dependent on the source material (feedstock) and the production process (i.e., temperature), resulting in variation in removal performances between different biochars. As the dominant abiotic removal process for TOrCs is adsorption, biochar properties such as surface area, aromaticity, and internal pore size distribution (i.e., microporosity) seem to be governing the adsorption of organic contaminants (Mohanty *et al.*, 2018). Specifically, a high degree of mesoporosity was indicative of improved removal of pesticides in batch studies comparing different types of biochar (Ulrich *et al.*, 2015). Typically, these properties are more pronounced in high temperature biochars (Ahmad *et al.*, 2014), although biochar performance always also depends on the pollutant being evaluated. Depending on the physical-chemical properties and functional group(s) of the target pollutant, different mechanisms can be responsible for the interaction between organic contaminant and biochar surface. Typically, adsorption between organic contaminants and carbonaceous adsorbents (i.e. AC, biochar) is assumed to be governed by π - π electron-donor-acceptor interactions involving the carbon's aromatic structures (Tong *et al.*, 2019). In addition to hydrophobic interactions, this is presumably the predominant sorption mechanism for neutral and non-polar compounds, while polar compounds engage in hydrogen

bonds with the biochar's polar surface groups (Ahmad *et al.*, 2014). Charged organic compounds may be retained via electrostatic attraction (Ahmad *et al.*, 2014) and a combination of cation- π and π - π interactions, a process which is pH-dependent (Kah *et al.*, 2017). Cationic compounds may thus exhibit greater removal than anions since most biochar surfaces are negatively charged (Ahmad *et al.*, 2014). Ultimately, knowledge of the dominant adsorption processes for a given contaminant group of interest is important for biofilter design and the optimal choice of biochar (i.e., feedstock, production temperature).

Furthermore, when studying flow-through systems, the assumption of sorption equilibrium between TOrCs and biochar may no longer be adequate due to elevated water velocities. Werner *et al.* (2012) studied sorption kinetics in high permeability aquifers mixed with low amounts of carbonaceous particles and determined that sorption can be diffusion limited. Similarly, taking intraparticle diffusion kinetics into account in reactive transport modelling of TOrC transport through biochar-amended sand columns substantially improved predictions of column breakthrough curves (Ulrich *et al.*, 2015).

1.1.2 Biological Processes in Biochar-Amended Filtration Systems

In addition to abiotic removal dominated by adsorption, biochar has been shown to increase microbial activity and is known to exhibit electron transfer properties due to its redox-active moieties and aromaticity (Klöpffel *et al.*, 2014; Saquing *et al.*, 2016). Mechanisms of electron transfer involve both electron conductivity (Chen *et al.*, 2014) and electron storage (i.e. by quinone structures) (Saquing *et al.*, 2016). Specifically, one study reported that biochar can function as both electron donor and acceptor, and thus should be seen as rechargeable reservoir of bioavailable electrons (Saquing *et al.*, 2016) – a feature which could potentially promote the biodegradation of contaminants in bioretention systems. The stimulating effect of biochar on microbial processes involving inorganics has been demonstrated for Fe(III) minerals reduction (Kappler *et al.*, 2014) and nitrate reduction (i.e., denitrification) (Saquing *et al.*, 2016).

Contrary to the common assumption that only freely dissolved organic contaminants are available for transformation reactions, a recent study suggested that in the presence of biochar, different coexisting degradation pathways contributed to the biological reduction of pentachlorophenol (PCP): 59% of the degradation involved PCP in the aqueous phase and 41% was attributed to electrical conductor mediated reduction of biochar-bound PCP (Yu *et al.*, 2015). The suitability of biochar to serve as habitat and inoculum carrier for microorganisms has been described before (Hale *et al.*, 2015; Luo *et al.*, 2013). Indeed, biofilm-coated biochar was found to be beneficial for TOrC removal, possibly due to microbial biodegradation (Liu *et al.*, 2017a; Ulrich *et al.*, 2017b) – even though overall removal and bioavailability may be heavily influenced by biochar application rate (Jones *et al.*, 2011; Liu *et al.*, 2017a) and biochar particle size. Frankel *et al.* (2016) reported that biochar-attached biofilms resulted in higher removal of

naphthenic acids (42-72%) compared to sterile biochar experiments (22-25%). The authors suggested that a synergistic relationship between microbial degradation and adsorption to the biochar was responsible for the metabolism of biochar-bound organics. This process, coined bioregeneration, has been described for biological granular activated carbon (GAC) filters in water treatment, and suggests that the sorptive capacity of adsorbents can be restored by microorganisms by freeing up sorption sites (Aktaş & Çeçen, 2007). For example, the role of biofilm in filter regeneration was crucial for the removal of the pharmaceutical carbamazepine in onsite wastewater treatment filters (Dalahmeh *et al.*, 2018).

Generally, there are only a few studies providing insights on long-term performance of biochar-amended stormwater treatment systems (Boehm *et al.*, 2020), and in practice, SCMs are often considered “black box” passive systems when it comes to water quality improvement (Grebel *et al.*, 2013). Studies focusing on biodegradation in already installed SCMs, e.g. bioretention cells (LeFevre *et al.*, 2012), are rare – even in the case of conventional systems without biochar amendments. There is only one study that investigated the formation of transformation products (TPs) of polar TORCs by biofilm-coated biochar in laboratory-scale microcosm and column experiments (Ulrich *et al.*, 2017b). Major TPs that were detected in the microcosms included desethylatrazine, fipronil sulfone, and DCPMU (TP of diuron). Therefore, a better understanding of the effect of an active microbial biofilm (i.e., biodegradation) on overall TORC removal, metabolite production, and biofilter lifetime under flow-conditions is warranted to inform design, maintenance, and risk assessment of biochar-amended SCMs.

1.1.3 Engineered Hyporheic Zones for Stormwater Treatment

The natural hyporheic zone (HZ) plays a major role in the attenuation of nutrients and organic micropollutants in streams and rivers (Lewandowski *et al.*, 2011; Posselt *et al.*, 2018), as it hosts a multitude of physical, biological, and chemical processes occurring simultaneously (Boulton *et al.*, 1998). Due to its unique properties, the HZ has been called a natural bioreactor and the “River’s Liver” (Fischer *et al.*, 2005), and some of its characteristics are similar to a horizontal biofilter. Nevertheless, HZs in urban streams are often biologically degraded and poorly connected with surface water – mostly due to decreased channel morphology or impermeable channel linings (Walsh *et al.*, 2005). A fully developed HZ could provide important habitat, foster biodiversity, and supply water quality treatment (Lawrence *et al.*, 2013). Crucial drivers for hyporheic exchange, i.e. the exchange of surface water with porewater, include channel morphology (e.g. bedforms), hydraulic head differences, streambed properties, and surface flow rates (Cardenas, 2015). Specifically, modifications of streambed permeability are known to augment hyporheic exchange (Herzog *et al.*, 2016; Vaux, 1968; Ward *et al.*, 2011). Engineered HZs have been increasingly gaining attention in stream restoration for improving stream water quality and aquatic habitat in addition

to water quantity benefits (Lawrence *et al.*, 2013; Peter *et al.*, 2019). Additionally, engineered streambeds have great potential as application to in-stream stormwater treatment systems (Herzog *et al.*, 2019). With the ultimate goal of water quality improvements, Herzog *et al.* (2016) introduced a novel technique of HZ engineering employing modifications to subsurface hydraulic conductivity and reactivity called Biohydrochemical Enhancements for Streamwater Treatment (BEST). BEST alterations include subsurface modules that employ impermeable walls that drive hyporheic exchange and control HZ residence times, and use permeable reactive geomeedia amendments to enhance biogeochemical reaction rates within the HZ. The efficiency of the BEST modules has been tested experimentally for the reactive tracer resazurin, which is an indicator for metabolically active transient storage, and hence can serve as surrogate for a reactive pollutant degraded aerobically (Herzog *et al.*, 2018). In constructed flume experiments, a BEST flume of 15 m with impermeable walls and woodchip-amended sand streambed increased both resazurin transformation and the size of the effective hyporheic transient storage by >50% compared to an all-sand control of the same length and essentially identical bed volume (Herzog *et al.*, 2018).

Depending on the location or potential space limitations and site-specific priority contaminants, a horizontal stream-like flow-through system like BEST may be preferable to vertical bioinfiltration systems. BEST engineered streambeds may have great potential to attenuate urban surface water pollution due to the technology's flexible application as stream-like SCMs: this could be extremely effective as it provides treatment to stormwater runoff from the entire upstream catchment. Alternatively, Herzog *et al.* (2019) recommended to install BEST streambeds in conjunction with stormwater detention ponds, treating the flow-metered effluent: taking this "treatment train" approach by pairing BEST with an existing SCM technology could also facilitate regulatory approval. Stormwater detention ponds offer fast runoff volume capture and promote (particulate) pollutant sedimentation, while BEST flumes could be designed to treat dissolved and polar contaminants (Herzog *et al.*, 2019). Analogous to biochar-amended (vertical) bioinfiltration systems – which were needed to meet aquatic benchmarks and load reduction requirements for pesticides in an urban watershed (Wolfand *et al.*, 2019) – geomeedia amendments to the HZ of engineered streambeds may be necessary to provide efficient removal of challenging TOrCs (i.e., polar). Such performance data for a wide range of stormwater-relevant TOrCs showing efficient removal in BEST flumes – and the impact of a strong geosorbent such as biochar on TOrC attenuation – are still missing. Furthermore, it is essential to assess the biotransformation potential of BEST streambeds and determine if they could be a major source of TPs into the environment. TPs of pesticides and pharmaceuticals are increasingly found in various aquatic bodies such as urban streams (Mahler *et al.*, 2021) and groundwater (Kiefer *et al.*, 2019) – sometimes even at higher concentrations than the parent compounds (Ferrando-Climent *et al.*, 2012; Kiefer *et al.*, 2019; Posselt *et al.*, 2018). Finally, design recommendations

for BEST systems that are scalable and adaptable to site-specific pollutants of concern (e.g., via select geomedia amendments) are needed. Collecting contaminant performance data will be crucial to facilitate regulatory approval and increase acceptance of the technology by stormwater practitioners.

1.2 Objectives and Hypotheses

This section introduces the objectives for the three research chapters (projects) of this dissertation and the corresponding hypotheses that were tested to achieve the research objectives. The first objective focuses on gaining an improved understanding of the effect of a biofilm layer and potentially biodegradation on TORC removal and filter lifetime in biochar-amended biofilters, while the second and third objectives aim to study the attenuation of TORCs in engineered hyporheic zone streambeds (BEST) at the field- and pilot-scale and whether biochar amendments are beneficial for hyporheic exchange and TORC removal.

1.2.1 Objective 1: The Role of Biofilm in the Removal of Pesticides in Biofilters

The aim of the first research objective was to gain a better understanding of the effect of a biofilm and potentially biodegradation processes on TORC removal and filter lifetime in biochar-amended biofilters. There is a knowledge gap concerning the long-term performance of biochar-amended filters (i.e., filter exhaustion). A better understanding of the effect of an active microbial biofilm (i.e., biodegradation) on overall TORC removal and biofilter lifetime could help inform the design, maintenance, and risk assessment (e.g., toxicity of metabolites) of real-world biochar-amended SCM systems. Neonicotinoid insecticides (imidacloprid, clothianidin) were included in this study based on their emerging nature, toxicity, and lack of environmental research data, specifically their fate and removal in SCMs and in the context of biochar amendments. To address these research gaps, the following hypothesis was tested:

Hypothesis 1: Biodegradation in biofilm-biochar filters is a relevant removal process of TORCs in the long-term and the presence of a biofilm layer prolongs filter lifetime by >50%. This hypothesis was tested in laboratory-scale exhaustive column tests: after columns were seeded with a microbial seeding solution sourced from river sediments, they were dosed with a representative synthetic stormwater solution containing three select pesticides (atrazine, imidacloprid, clothianidin). Contaminant breakthrough curves were monitored over the course of three months to quantify the impact of an active biofilm layer on overall pesticide removal and biofilter lifetime (exhaustive breakthrough). Pesticide TPs were studied in column effluents to determine major degradation pathways and to assess if biochar-amended biofilters could be a potential source of TPs into the environment. Finally, column breakthrough curves were used to estimate parameters of a contaminant transport model in porous media to simulate representative biofilter lifetimes in different case study scenarios.

1.2.2 Objective 2: Attenuation of Metformin in Full-Scale Engineered Streambed Hyporheic Zones

The second research objective was focused on determining the effect of BEST engineered streambeds on HZ flow and exchange, redox conditions, and the subsurface attenuation and potential biotransformation of metformin. Metformin – a highly polar medication for diabetes – is one of the most frequently detected organic contaminants in natural and urban streams (Bradley *et al.*, 2016). Both metformin and its microbial degradation product guanylyurea are highly mobile in the aquatic environment and their retention in soils/sediments is limited due to their strong hydrophilic nature ($\log K_{OW} \leq -2$). Their ecotoxicity and endocrine disruption potential poses a great threat to aquatic organisms (Niemuth & Klaper, 2015; Ussery *et al.*, 2019). Overall, these findings highlight the need for a HZ and SCM technology that increases the biogeochemical reactivity of the streambed to enhance the attenuation of challenging pollutants such as metformin and guanylyurea. To address this research objective, the following hypothesis was tested:

Hypothesis 2: a) BEST engineered streambeds will lead to enhanced attenuation of metformin and guanylyurea due to increased HZ exchange and streambed redox conditions favorable for their degradation; and b) Biochar addition to BEST engineered streambeds will further accelerate removal along hyporheic flowpaths due to biochar's high sorption capacity. This hypothesis was tested in full-scale BEST modules installed in a recirculating flume at an outdoor flume facility (German Environment Agency in Berlin, Germany) under near-natural conditions. To increase the reactivity of the engineered HZ and thus promote the removal of metformin (and potentially guanylyurea), the stream sediments in select BEST modules were amended with pine-wood biochar. Separate batch studies confirmed the removal of metformin and guanylyurea via biochar. The attenuation of metformin in the surface and subsurface flume water was monitored over several months to determine HZ breakthrough curves. Predominant subsurface redox conditions were determined via dissolved oxygen (DO) profiles and measurement of redox-active species (i.e., Fe(II), NH_4^+). Spiking metformin to the flume at a higher dose allowed to study the formation of TPs of metformin beyond guanylyurea.

1.2.3 Objective 3: TOrC Removal in Pilot-Scale Engineered Streambed Hyporheic Zones

Although previous studies have confirmed the suitability of BEST engineered streambeds to provide metabolically active transient storage (Herzog *et al.*, 2018), performance data for a wide range of stormwater-relevant TOrCs (e.g., pesticides, pharmaceuticals, etc.) showing efficient removal in BEST flumes are still missing. Furthermore, it is important to assess the biotransformation potential of BEST streambeds and the possibility of a chronic exposure risk via TPs towards aquatic organisms. Lastly, formulating design recommendations for BEST systems are needed to inform practical applications of this

novel technology and facilitate acceptance by stormwater managers. Therefore, the aim of the third research objective was to investigate the removal efficiency of different BEST engineered streambed configurations (with/without biochar) for a wide range of TOrcs with different biogeochemical properties. To achieve this objective, the following hypothesis was tested:

Hypothesis 3: The addition of biochar to engineered hyporheic zone streambeds will enhance the removal of TOrcs and will result in measurable reach-scale attenuation along 15 meters of BEST streambeds. This hypothesis was tested in several contaminant experiments using a pilot-scale outdoor constructed flumes system (Mines Park Water Reclamation Facility at the Colorado School of Mines in Golden, CO) fed by recycled municipal wastewater. The following streambed configurations were evaluated: sand-only control streambed (F1), BEST streambeds (F2), BEST streambeds amended with biochar (F3), and BEST streambeds containing fine-grain sand mixed with biochar (F4). 4-hour simulated stormflow events (single-pass mode) allowed to study TOrc surface and porewater breakthrough curves and to determine the reach-scale attenuation. The goal of flume experiments run in recirculation mode (15 days) was the assessment of longer-term performance and the potential for TOrc biotransformation of the different streambed configurations. Specifically, the effect of biochar in BEST streambeds on HZ flow and reach-scale TOrc removal was investigated.

1.3 Dissertation Organization

This dissertation is composed of five chapters. This chapter (Chapter 1) has provided a literature review of relevant prior research and outlines the research objectives and hypotheses for the material in the main body of this dissertation. The closing chapter (Chapter 5) summarizes the conclusions drawn from the research presented in the main body and their broader significance, and recommends directions for future research. The main body of this dissertation (Chapters 2 to 4) describes the motivation, experimental approach, and the main results and conclusions from each of the three research projects that were conducted to address the corresponding research objectives. Relevant supporting information for each of the three chapters is provided in Appendices A, B, and C. Appendix D contains the copyright permission information (reference to Supplemental File). The research chapters have either been published (Chapter 2) or are in the preparation phase for submission to a scientific journal (Chapters 3 and 4). An overview of each of the chapters in the main body of the dissertation is presented in the following:

Chapter 2, “The Regenerative Role of Biofilm in the Removal of Pesticides from Stormwater in Biochar-Amended Biofilters” by Andrea C. Portmann (primary researcher and author), Gregory H. LeFevre (Associate Professor at the University of Iowa that provided experimental guidance and manuscript review), Rennosuke Hankawa (former Bachelor’s student at the Colorado School of Mines that

provided significant laboratory assistance and biotransformation literature review), David Werner (Lecturer at Newcastle University in the United Kingdom that provided modelling assistance), and Christopher P. Higgins (Professor at the Colorado School of Mines, principal investigator and corresponding author), has been published in *Environmental Science: Water Research & Technology* (Portmann *et al.*, 2022). This paper addresses Objective 1 and Hypothesis 1, and relevant supporting information can be found in Appendix A. *Environmental Science: Water Research & Technology* granted permission to reproduce the published manuscript in this dissertation and approval for republication of the manuscript was confirmed from all co-authors (see Appendix D).

Chapter 3, “Biochar-Amended Engineered Streambeds for In-Stream Attenuation of the Diabetes Medication Metformin and its Transformation Product Guanylurea” by Andrea C. Portmann (primary researcher and author), Malte Posselt (Postdoctoral researcher at Stockholm University in Sweden that provided significant contributions in experimental design, sampling, and sample analysis), Anna Jaeger (PhD candidate at Humboldt University in Germany that provided assistance in sampling and sample analysis), Skuylar P. Herzog (Assistant Professor at Oregon State University-Cascades that provided assistance in experimental design and sampling), Reza Abdi (former Postdoctoral researcher at Colorado School of Mines that provided assistance with data post-processing), Chuhui Zhang (Postdoctoral researcher at Colorado School of Mines that provided assistance with sample analysis), René Sahn (Researcher at the German Environment Agency in Germany that provided guidance in experimental design and sampling), Björn Kusebauch (Researcher at the German Environment Agency in Germany that provided guidance in experimental design and sample analysis), John E. McCray (Professor at the Colorado School of Mines that provided experimental guidance and manuscript review), and Christopher P. Higgins (Professor at the Colorado School of Mines, principal investigator and corresponding author), is a manuscript being prepared for submission to a scientific journal. This paper addresses Objective 2 and Hypothesis 2. Relevant supporting information for this chapter are provided in Appendix B.

Chapter 4, “Engineered Streambeds for the Removal of Pesticides and Pharmaceuticals from Stormwater” by Andrea C. Portmann (primary researcher and author), Brittnee N. Halpin (PhD candidate at the Colorado School of Mines that provided significant contributions in experimental design, flume construction, and experiment execution), Donovan Keohane (Bachelor’s student at the Colorado School of Mines that provided assistance with data post-processing in R), John E. McCray (Professor at the Colorado School of Mines that provided experimental guidance), and Christopher P. Higgins (Professor at the Colorado School of Mines, principal investigator and corresponding author), is a manuscript being prepared for submission to a scientific journal. This paper addresses Objective 3 and Hypothesis 3. Relevant supporting information for this chapter are presented in Appendix C.

CHAPTER 2

THE REGENERATIVE ROLE OF BIOFILM IN THE REMOVAL OF PESTICIDES FROM STORMWATER IN BIOCHAR-AMENDED BIOFILTERS

Modified from an article published in *Environmental Science: Water Research & Technology*¹
Andrea C. Portmann^{2,3}, Gregory H. LeFevre⁴, Rennosuke Hankawa², David Werner⁵, Christopher P.
Higgins^{2,6}

2.1 Abstract

Low-impact, green infrastructure systems such as biofilters, particularly when amended with biochar, can help address chemical pollution conveyed via stormwater that is increasingly posing a threat to aquatic ecosystems and groundwater quality. Although removal of organic contaminants including pesticides by biochar-amended systems has been studied, the role of a biofouling layer on contaminant removal, biotransformation, and filter lifetime remains poorly understood. This study evaluated the removal of the pesticides atrazine, imidacloprid, and clothianidin in biologically active biochar-amended columns through complete exhaustion of contaminant removal capacity. The resultant data indicate that biological processes accounted for 20-36% of overall removal in the biochar-amended sand columns. In addition, a combined target and suspect screening approach using liquid chromatography quadrupole time-of-flight mass spectrometry (LC-QToF-MS) was employed to evaluate the potential transformation of these three pesticides and release of the transformation products (TPs). All TPs detected in the effluent remained below 2.5% of their respective parent influent concentrations for the duration of the experiment. Furthermore, at a biochar application rate of 0.5 wt%, the presence of an active biofilm prolonged the filter lifetime by 1.8-2.3 times compared to a fouled but inactive filter, where removal was presumably dominated by adsorption only. Scenario modelling estimates showed that biochar-amended biofilters could last at least 17 years before exceeding aquatic life threshold values at biochar-application rates as low as 1 wt% (5 vol%) in a representative case study. Results of this study provide novel insight on pesticide TP formation in biochar-amended biofilters and estimation of filter lifetimes.

¹Reprinted with permission from *Environ. Sci.: Water Res. Technol.*, 2022, 8, 1092-1110. Copyright 2022 Royal Society of Chemistry. Online access: <https://doi.org/10.1039/D1EW00870F>

²Department of Civil & Environmental Engineering, Colorado School of Mines

³Primary researcher and author

⁴Department of Civil & Environmental Engineering and IIHR-Hydroscience & Engineering, University of Iowa

⁵School of Engineering, Newcastle University, UK

⁶Corresponding author

2.2 Introduction

Harnessing alternative water resources such as stormwater through capture and treatment is a promising strategy to help address both water scarcity and contamination (Clark & Pitt, 2012; Luthy *et al.*, 2019; Mohanty *et al.*, 2018). Nevertheless, to make stormwater runoff a viable and safe water resource, effective methods for water quality improvements are essential. In recent years, the implementation of green infrastructure systems and stormwater control measures (SCMs) has gained attention among practitioners, especially the use of infiltration techniques (Grebel *et al.*, 2013). Traditionally, however, SCMs have focused on flow reduction and water capture but have not been designed for water quality improvement (Grebel *et al.*, 2013; LeFevre *et al.*, 2015). Contamination of urban streams with trace organic contaminants (TOrcs) stemming from stormwater runoff such as polycyclic aromatic hydrocarbons (PAHs) (Burant *et al.*, 2018; Gasperi *et al.*, 2014; LeFevre *et al.*, 2015), pesticides (Gasperi *et al.*, 2014; LeFevre *et al.*, 2015; Rippey *et al.*, 2017; Spahr *et al.*, 2020; Stone *et al.*, 2014; Wolfand *et al.*, 2019), vehicle-associated compounds (Peter *et al.*, 2018), flame retardants (Burant *et al.*, 2018; Spahr *et al.*, 2020), and pharmaceuticals (Burant *et al.*, 2018; Masoner *et al.*, 2019; Spahr *et al.*, 2020) may lead to substantial aquatic health impacts such as acute/chronic toxicity (Anderson *et al.*, 2016; Tian *et al.*, 2021; Vignet *et al.*, 2019; Young *et al.*, 2018) and endocrine disruption (Mnif *et al.*, 2011; Zhang *et al.*, 2020), surface water quality degradation (LeFevre *et al.*, 2015), and drinking water impairments of groundwater aquifers (Kiefer *et al.*, 2019; Loos *et al.*, 2010). During the past 20 years, decentralized biofilters or bioretention systems have been increasingly gaining traction as a viable alternative to centralized stormwater treatment systems (Boehm *et al.*, 2020). Biofilters amended with conventional media (i.e., soil, sand) are typically effective at removing suspended solids and thus particulate-bound organics (e.g. petroleum hydrocarbons, PAHs) with removal values commonly as high as 80-90% (Flanagan *et al.*, 2018; Zhang *et al.*, 2014). However, limited removal in conventional biofilters was observed for less hydrophobic organic contaminants (Zhang *et al.*, 2014) and our understanding of the attenuation of dissolved organic contaminants remains limited (LeFevre *et al.*, 2015). Specifically, TOrcs such as hydrophilic pesticides pose one of the greatest risks for groundwater contamination (Pitt *et al.*, 1999) due to their high mobility and low sorptive affinity towards soil and conventional infiltration media such as sand (LeFevre *et al.*, 2015; Spahr *et al.*, 2020). These findings highlight the need to modify conventional green infrastructure systems for the removal of this class of contaminants (Anderson *et al.*, 2016; Spahr *et al.*, 2020).

In light of the challenge that dissolved and hydrophilic TOrcs pose to maintaining or improving water quality, amending stormwater treatment systems with black carbon adsorbents like biochar has become a strategy of interest to improve contaminant removal (Grebel *et al.*, 2013; Miles *et al.*, 2016; Mohanty *et al.*,

2018). Biochar is a cost-effective means of improving the removal of hydrophilic TOrCs, as has been demonstrated in laboratory batch and column studies (Ray *et al.*, 2019; Ulrich *et al.*, 2015), as well as in pilot-scale biofilters (Ulrich *et al.*, 2017a). As the dominant abiotic removal process for TOrCs is adsorption, biochar properties such as surface area, aromaticity, and internal pore size distribution – especially microporosity and mesoporosity (Ulrich *et al.*, 2015; Xiao & Pignatello, 2015a) – appear to control the removal of organic contaminants (Mohanty *et al.*, 2018). Depending on the functional group(s) of the target pollutant, different mechanisms can be responsible for the interaction between the organic contaminant and biochar surface: non-polar compounds attach to hydrophobic sites on the biochar surface, whereas polar compounds engage in hydrogen bonds with polar surface groups (Ahmad *et al.*, 2014). Charged organic compounds may also be retained via electrostatic attraction, especially cationic compounds, since most biochar surfaces are negatively charged (Ahmad *et al.*, 2014).

In addition to abiotic sorptive removal, the microbial activity of stormwater filters is thought to play an important role for TOrC attenuation (Frankel *et al.*, 2016; Ulrich *et al.*, 2017b). Immobilized microbial biofilms have long been used in water and wastewater treatment (Shieh & Keenan, 1986) and also in the bioremediation of xenobiotics (Oh & Tuovinen, 1994; Puhakka *et al.*, 1995). The suitability of biochar to serve as habitat and inoculum carrier for microorganisms has been described previously (Hale *et al.*, 2015; Luo *et al.*, 2013), although not all literature agrees (Quilliam *et al.*, 2013). The suitability of a biochar to serve as biofilm attachment site may be highly dependent on specific properties, including surface area, hydrophobicity, water holding capacity (Hale *et al.*, 2015) and biochar carbon availability (Luo *et al.*, 2013). Further, Saquing *et al.* (2016) reported that biochar can function as both electron donor and acceptor, and thus should be seen as rechargeable reservoir of bioavailable electrons, a feature which could potentially promote the biodegradation of contaminants in bioretention systems. The stimulating effect of biochar on microbial processes involving inorganics has been demonstrated for Fe(III) reduction (Kappler *et al.*, 2014) and nitrate reduction (i.e., denitrification) (Saquing *et al.*, 2016). Moreover, biological degradation may act directly on biochar-bound organic contaminants (Yu *et al.*, 2015) which has important mechanistic implications. Furthermore, biofilm-coated biochar is reported to benefit TOrCs removal, possibly due to microbial biodegradation (Liu *et al.*, 2017a; Ulrich *et al.*, 2017b). Thus, biochar-attached biofilms could facilitate sustained contaminant removal, potentially via a synergistic relationship between microbial degradation and biochar adsorption (Frankel *et al.*, 2016). This process, coined bioregeneration, has been described for biologically active granular activated carbon (GAC) filters in water treatment, and implies that the sorptive capacity of adsorbents can be restored by microbial degradation freeing up sorption sites (Aktaş & Çeçen, 2007).

Overall, disambiguating the contributions of individual processes on total removal is challenging, and very limited research is available on the disentangling of sorptive and biological processes in biochar-amended systems (Tang *et al.*, 2016; Yan *et al.*, 2017). In practice, SCMs are often considered “black box” passive water treatment systems (Grebel *et al.*, 2013). The design of biochar-amended biofilters is further complicated by processes that are difficult to simulate in the laboratory but inherently arise in field-scale systems, such as the impact of variable saturation conditions, clogging, or biofouling on biochar sorption. For instance, the addition of an external carbon source (e.g. woodchips, compost, humic acid) is known to facilitate biological processes and can benefit contaminant removal (Ashoori *et al.*, 2019; Ulrich *et al.*, 2017b; Zhang *et al.*, 2019) but may also lead to accelerated exhaustion of adsorption sites or pore clogging and concomitant biochar aging (Kwon & Pignatello, 2005; Pignatello *et al.*, 2006). Generally, there are only a few studies providing insight into long-term performance of biochar-amended stormwater treatment systems (Boehm *et al.*, 2020). Thus, a better understanding of the effect of an active microbial biofilm (i.e., biodegradation) on overall TO_{OC} removal over one full lifetime of a biofilter is warranted to inform design, maintenance, lifetime, and risk assessment (e.g., toxicity of metabolites) of biochar-amended SCM systems. Moreover, inclusion of transformation products (TPs) in the analysis of biochar-amended biofilter effluents is lacking in the literature, even though TPs of pesticides are a concern and increasingly found in drinking water sources (Guillon *et al.*, 2018) and in groundwater - sometimes at higher concentrations than their parent compounds (Kiefer *et al.*, 2019). Thus, it is essential to determine if biochar-amended biofilters could be a potential source of TPs into the environment. As biodegradation in biofilm-biochar filters may potentially prolong biofilter lifetime in the long term, the primary objectives of this study were to: i) assess the role of biofilm in overall pesticide removal in biochar-amended biofilters and determine the relative importance of biodegradation compared to sorption; ii) evaluate the effect of the combined biofilm-biochar presence and thus biodegradation on filter lifetime; and iii) elucidate the main transformation pathways of select pesticides occurring in biotic biochar-sand systems compared to controls. To address these objectives, we studied the removal and transformation of atrazine, imidacloprid, and clothianidin in laboratory-scale biochar-amended sand columns over four months and compared the findings to results from inhibited (i.e., inactivated biofilm) biochar-sand columns and sand-only columns (both biotic and inhibited). Hydrophilic pesticides, including atrazine and neonicotinoids, are increasingly being discovered in urban stormwater (Masoner *et al.*, 2019). Our decision to study neonicotinoids in biochar-amended biofilters was based on their emerging nature and lack of environmental research data (personal communication by the California Department of Pesticide Regulation). The resultant column breakthrough curves of the three pesticides were used to estimate parameters of a contaminant transport model to simulate representative biofilter lifetimes in different case study scenarios.

2.3 Methods

This section describes the experimental methods, materials, and procedures used for this study.

2.3.1 TOrC Analysis

The TOrCs suite selected for target analysis in this study included the parent compounds atrazine, imidacloprid, and clothianidin. TPs also targeted for analysis included desethylatrazine (DEA), desisopropylatrazine (DIA), 2-hydroxy-atrazine (OH-ATZ), desnitro-imidacloprid (desnitro-IMI), imidacloprid-urea (IMI-urea), imidacloprid-olefin (IMI-olefin), and 6-chloronicotinic acid (6-CNA). Analytical standards for TPs of clothianidin were not commercially available and therefore not included in the target analysis. Isotope dilution was conducted using the surrogate standards atrazine-d5, imidacloprid-d4, and clothianidin-d3. Information and details on source and purity of analytical standards (natives and surrogates) can be found in the Supporting Information (SI) in Appendix A, Table A.1. Literature-derived microbial transformation pathways for atrazine, imidacloprid, and clothianidin can be found in Figures A.1-A.3. Concentrations of TOrCs in aqueous samples were quantified by liquid chromatography quadrupole time-of-flight mass spectrometry (LC-QToF-MS) using a SCIEX ExionLC™ high-performance liquid chromatography (HPLC) system equipped with a Biphenyl analytical column (3 μm , 100x3 mm; Phenomenex, Torrance, CA), coupled to a SCIEX X500R QToF-MS system (Framingham, MA) using electrospray ionization in positive mode (ESI+) with SWATH® Data-Independent Acquisition for both ToFMS and MS/MS mode. Details on the MS parameters and LC conditions can be found in Appendix A.

Target Analysis. Target analytes were identified based on precursor accurate mass (mass error < 10 ppm), isotopic pattern (isotopic ratio error < 40%), and retention time (ΔRT < 0.05 min) compared to analytical (native) standards, and quantified using calibration standards in the range of 0.005 $\mu\text{g/L}$ to 25 $\mu\text{g/L}$. Surrogate concentrations in calibration standards (and samples) were 0.4 $\mu\text{g/L}$ for atrazine-d5 and 0.8 $\mu\text{g/L}$ for both imidacloprid-d4 and clothianidin-d3. Accuracy of calibration standards was required to be within +/- 30% and the calibration curve had to be linear ($R \geq 0.99$). The limit of quantitation (LOQ) for most analytes was between 0.005 $\mu\text{g/L}$ and 0.01 $\mu\text{g/L}$, except for 6-CNA, for which the LOQ was 0.05 $\mu\text{g/L}$. Considerably lower sensitivity of 6-CNA in LC-MS analysis compared to other neonicotinoid compounds has been reported previously (Hao *et al.*, 2016; Muerdter & LeFevre, 2019). Table A.2 contains the LC-QToF-MS parameters for each target analyte; specifically, retention time, precursor accurate mass (quantitation), MS/MS fragment masses (qualitative confirmation), LOQ, and spike recovery data.

Suspect Screening. To identify additional TPs of atrazine, imidacloprid, and clothianidin, a suspect screening approach was also employed. LC-QToF-MS data acquired in SWATH® mode was screened

using a custom extracted ion chromatogram (XIC) list (Table A.3) containing molecular formulas and accurate masses for TPs identified using the EAWAG Biocatalysis/Biodegradation Database and Pathway Prediction System (EAWAG-BBD/PPS; <http://eawag-bbd.ethz.ch/index.html>) and a review of extant literature (Figures A.1-A.3). Identification of unknown pesticide TPs was based on accurate mass measurement for the molecular ion, isotopic pattern matching scores, and verification of MS/MS spectra. Samples were screened by searching for the protonated molecular ion $[M+H]^+$ using an XIC window of 0.02 Da, a signal to noise threshold of 10:1, and a noise percentage of 90%. For additional analyte confirmation, acquired MS/MS spectra were compared to fragment masses previously reported in literature (Table A.2). Suspects were confirmed by identification of at least one unique product ion accurate mass that matched known fragments (mass error < 10 ppm). In a first screening of the data, only matches with precursor ion mass error < 5 ppm and isotopic pattern error < 40% were considered for subsequent MS/MS fragment analysis. The precursor mass error criterion was chosen to be more restrictive than the target analysis because of the absence of analytical standards. A confidence level was assigned to each suspect compound on the basis of the Schymanski scale (Schymanski *et al.*, 2014).

2.3.2 Materials

Biochar. The biochar used in this study was Mountain Crest Gardens biochar (MCG-biochar) produced by high temperature (> 1100°C) gasification of pinewood (Gropro, Inc., Etna, CA) and was selected for this study due to its superior TOrC removal performance in laboratory-scale (Ray *et al.*, 2019; Ulrich *et al.*, 2015) and pilot-scale biofilters treating stormwater (Ashoori *et al.*, 2019). The biochar was sieved to a particle size range of 53-250 μm , rinsed by deionized (DI) water, and subsequently allowed to air dry. The standard laboratory sand was of uniform particle size (210-297 μm ; Sigma-Aldrich) and was used as received. Additional details related to surface area analysis and pore-size characterization of the biochar is provided in the SI (section A.3).

Dissolved Organic Carbon (DOC) Extract Solutions. All experiments (batch sorption, column, and microcosm experiments) were conducted with representative synthetic stormwater based on a recipe from Grebel *et al.* (2016). Dissolved organic carbon (DOC) was added from DOC extract solutions obtained by infusing local creek water with grass, leaves, and compost over several weeks based on a recipe described elsewhere (Ulrich *et al.*, 2017b). DOC obtained from natural carbon sources provides a more complex DOC source for microbial growth than from single sources (e.g., humic acid) and is thought to be more representative of actual field conditions. Details on the preparation of the DOC extract solutions can be found in the SI (section A.3).

Microbial Enrichment Solutions. Microbial enrichment solutions for column inoculation were prepared following a modified procedure described elsewhere (Ulrich *et al.*, 2017b). In brief, a sediment-creek water slurry was obtained from a local creek (Clear Creek, Golden, CO) and served as the inoculum to the enrichment solutions. The same DOC extract that was used for batch and column experiments was used as growth media for the enrichment solutions. Microbial cultures for the enrichment solutions were grown over two stages of three successive inoculation-incubation cycles. Further details on the microbial enrichment procedure can be found in the SI (section A.3).

2.3.3 Batch Sorption Experiments

Isotherm and kinetic batch experiments were carried out in 250 mL amber glass bottles (Quorpak; Clinton, PA) with representative synthetic stormwater. Batch experiments were conducted following the method described in Ulrich *et al.* (2015). Briefly, after amber glass bottles were autoclaved at 135°C for 25 min, 200 mL of representative synthetic stormwater (including 100 mg/L sodium azide) and 3.8 ± 0.3 mg of fresh MCG biochar were added to each bottle. The batches were placed on a shaker table overnight to allow for pre-equilibration of the biochar with DOC. The following day, batches were spiked with a mixture of the native parent TOrC solution using a methanol carrier (less than 0.05% of total volume), which marked time zero of the batch experiments. Isotherm batch tests were carried out in triplicates at five different initial concentrations ($C_{W,0} = 3, 10, 20, 50,$ and 100 $\mu\text{g/L}$ for each TOrC individually) and including controls (no biochar) to account for abiotic losses of TOrCs. Samples were taken in the beginning ($t = 1.5$ h) from controls only and at the end ($t = 92$ d) from biochar batches and controls. Samples (2 mL) were taken after 0.5 hours of settling using sterile pipet tips and were transferred into glass centrifuge vials (Kimble Chase; Rockwood, TN / DWK Life Sciences, LLC). After addition of a surrogate solution in methanol (10% of final volume), vials were centrifuged at 2600 rcf for 18 min to spin down potential biochar particles. The supernatant was transferred to amber storage vials and stored at 4°C until analysis. Kinetic batch tests were carried out with the serial method following OECD guidelines 106 (OECD, 2000) using an initial TOrC concentration of 10 $\mu\text{g/L}$ (for each TOrC individually). TOrCs sampling was performed at 1.5 h, 1 d, 3 d, 7 d, 15 d, 29 d, and 67 d and the sample preparation and storage followed the same procedure as for isotherm batches.

Best-fit parameters of the Freundlich and Langmuir isotherms were obtained from the equilibrium sorption data using non-linear regression with relative weighting ($1/Y^2$) in GraphPad Prism (version 9.1.1); the corresponding figures can be found in the SI (Figure A.4). Akaike's Information Criterion (AIC) was used to compare the goodness of fit of both sorption equations and demonstrated better fits for the Freundlich isotherm for all three parent compounds. Both the AIC and best-fit values of the non-linear

Freundlich isotherm coefficient K_F and the Freundlich isotherm exponent n are reported in Table A.4.

2.3.4 Column Experiments

Column experiments were conducted using Kimble Chase flex-columns (2.5 x 5 cm) (DWK Life Sciences, LLC) and an effective length of 5.6 cm was dry-packed with a mixture of sand and biochar (0.5 wt%). The media mixture was fixed with glass beads and glass wool at both the inlet and outlet to prevent loss of media under flow conditions. Attachment of a biofilm on the sand-biochar media and start-up of biotic columns followed a procedure described elsewhere (Ulrich *et al.*, 2017b). Columns were purged with CO₂ gas right before startup to ensure fully saturated conditions and were subsequently injected with one pore volume (PV) of microbial enrichment solution at a flow rate of 0.9 mL/min, allowed to sit overnight, and then slowly recirculated at 0.08 mL/min for 48 h to promote microbial attachment. After seeding of a biofilm, columns were conditioned with representative (un-spiked) synthetic stormwater containing 10 mg/L DOC at a flowrate of 0.21 mL/min for 23 days. During conditioning, a salt tracer test was performed using a conservative tracer KBr solution (300 mg/L) to assess mean hydraulic residence times (HRT) of the columns. Effluent samples (1 mL) were taken every 20 min, diluted with Milli-Q water and analyzed by ion chromatography (IC). Based on the salt tracer data, mean HRTs of the columns were between 90-125 min (consistent with a recent bioretention study, Gu *et al.* 2021), with the variance likely due to experimental variation rather than the presence of biochar or a biofilm (see Figure A.6). After the dissolved oxygen (DO) levels in the effluent stabilized, columns were injected with representative synthetic stormwater containing 10 mg/L DOC and 200 µg/L of each TOrC (atrazine, imidacloprid, clothianidin) for 92 days at a flowrate of 0.21 mL/min. This flow rate corresponds to an infiltration rate of 2.58 cm/h and thus meets the infiltration requirement for bioretention systems (>2 cm/h) (LeFevre *et al.*, 2015). Influent reservoirs (aerated) were refreshed daily to minimize microbial growth and TOrC degradation, and the methanol of the TOrC carrier solution was evaporated under N₂ in a conical glass tube. The dried TOrC residue was redissolved and added to the influent reservoirs by repeatedly (6X) adding synthetic stormwater to the glass tube and vigorous shaking, then letting it sit for 10-15 min each time. Influent of inhibited control columns (one for sand and sand+BC each) contained 200 mg/L of sodium azide (NaN₃) for continued biofilm inactivation. Influent and effluent samples were taken regularly (on average, every 2-3 days over the course of 92 days) and preserved by filtration with Millex syringe filters (0.22 µm, 13 mm, Durapore, PVDF membrane; Millipore Sigma) and stored at 4°C until analysis. However, not all of these samples were submitted for TOrC analysis.

General column performance was monitored by analyzing influent and effluent samples for standard water quality parameters. DO concentrations and pH were measured twice a week during the first three

weeks (column conditioning) and once a week afterwards using a portable Hach multimeter (HQ40D) and DO / pH probes. DOC and total nitrogen (TN) concentrations were measured weekly (twice a week during the first seven weeks) by a TOC-L Laboratory Total Organic Carbon Analyzer (Shimadzu), and major anions were analyzed using a Dionex ICS-900 Ion Chromatography System (Thermo Fisher Scientific). Samples were diluted with in-house Milli-Q water as necessary to meet instrument specifications and calibration ranges.

2.3.5 Microcosm Experiments

Biotic microcosms (two replicates: M1, M2) were started in autoclaved 1000 mL Erlenmeyer flasks by combining 100 mL of DOC extract solution (~250 mg/L) with 10 mL of the same microbial seeding solution used for column inoculation. Flasks were aerobically incubated at 30°C in the dark for two weeks (17 days). After incubation, replicates M1 and M2 were spiked with TOrCs (atrazine, imidacloprid, and clothianidin; final concentration: 400 µg/L each) by adding 140 mL of autoclaved synthetic stormwater solution (no DOC). As with the column influent solutions, the methanol of the TOrC carrier solution was evaporated under N₂ before addition to the flasks. An un-spiked control (M3) was prepared to monitor microbial growth under non-exposure conditions. In addition, an inhibited control (M4) was initiated by combining 100 mL of DOC extract solution, 10 mL of NaN₃ in Milli-Q water (final concentration: 200 mg/L) instead of the microbial enrichment solution, and 140 mL of autoclaved synthetic stormwater solution (no DOC). Unfortunately, it was not possible to maintain the inhibited control as uncontaminated over the duration of the experiment and thus it was excluded from further analysis. All flasks were shaken continuously for 369 days at room temperature and sampled regularly (weekly during the first 14 weeks, then bimonthly during the next 15 weeks, and again after six months at the end of the experiment). Sample volumes were kept as low as 0.5-1.0 mL and were prepared for storage following the same method as described for column samples. To account for evaporative water losses, microcosms were weighed before each sampling event and the appropriate volume of autoclaved Milli-Q water was added to each microcosm prior to sampling.

2.3.6 Transport Modelling

Contaminant breakthrough data were assessed using a model in MATLAB (R2019b, MathWorks, Massachusetts, United States) describing one-dimensional solute transport in porous media assuming sorption-retarded intraparticle diffusion kinetics and a Freundlich sorption isotherm (column model variables and input parameters are listed in Tables A.8 and A.9). Tortuosity (τ) was used as a fitting parameter to account for intraparticle diffusion. This model was originally designed to determine the fate

and transport of organic contaminants in black carbon-amended sediments or aquifers (Werner *et al.*, 2006, 2012). Ulrich *et al.* (2015) used an adapted version to demonstrate that including diffusion-limited sorption kinetics allows the prediction of TOrC breakthrough curves (BTCs) in abiotic biochar-amended sand filters based on sorption parameters derived from abiotic batch tests. The same model has been successfully employed to model the breakthrough of per- and polyfluoroalkyl substances (PFASs) in a pilot-scale GAC filtration system, even though it was found that assuming local sorption equilibrium generated a better fit to the observed data (Liu *et al.*, 2019). In the present study, the original model was adapted for constant influent concentration (as opposed to a pulse).

Estimation of sorption and kinetic parameters (i.e., tortuosity) based on batch equilibrium and kinetic sorption data for use in column breakthrough prediction was successfully demonstrated previously (Ulrich *et al.*, 2015); however, in the current study, results were not deemed satisfactory (Figures A.16 and A.17). We assume that the presence of a biofilm layer in the porous media limited the transferability of parameters from abiotic batch studies (microbial growth inhibited by NaN_3) to biologically active flow-through systems. Best-fit Freundlich sorption (K_F , n) and kinetic parameters (τ) for each compound were therefore directly estimated based on the effluent data observed in the biotic BC+Sand columns (Figure A.19). The best-fit parameters were then used to predict TOrC breakthrough and biofilter lifetime in several case study simulations (scenarios). Assuming that the biofilter effluent were discharged into receiving surface waters, the “biofilter lifetime” or “breakthrough” was defined as the time when the effluent concentrations would exceed chronic aquatic life benchmarks specified by the European Union or the United States Environmental Protection Agency (U.S. EPA). Representative stormwater influent concentration ranges were estimated based on reported surface water data in the literature (storm- and stream water), with the corresponding maximum concentrations being used to simulate worst-case scenarios. The simulated continuous filter lifetimes were then adjusted based on a representative field-scale biofilter (infiltration basin) for a residential area in Denver, CO, receiving a representative amount of rainfall. Detailed calculations are provided in Table A.11.

2.4 Results and Discussion

2.4.1 Biological Activity of Columns

The average column influent DO concentration of 7.12 (± 0.11) mg/L consistently decreased in the column effluent for all four tested conditions (Figure 2.1a; $p = 9.10\text{e-}4$, Ranksum Test, $\alpha = 0.05$), indicating continued aerobic microbial activity throughout the study. Nevertheless, DO removal was significantly greater in biotic columns (both with and without biochar) compared to inhibited conditions ($p = 1.96\text{e-}4$; Wilcoxon Sign Rank Test, $\alpha = 0.05$). Similar results occurred for removal of DOC in the

columns (Figure 2.1a): the overall DOC removal in the biotic systems (both Sand and BC+Sand) was significantly greater (45%) compared to the inhibited controls (12%; $p = 3.85e-6$, Paired-sample t-test, $\alpha = 0.05$). However, there was some comparably minor microbial activity in the inhibited columns, indicating that the addition of sodium azide was not sufficient to suppress all microbial activity. This is supported by the fact that the observed average DOC removal was significantly non-zero ($p = 0.0269$ and $p = 0.0086$ for Sand, inhibited and BC+Sand, inhibited, respectively; One-sample t-test, $\alpha = 0.05$). We believe that the term “inhibited” sufficiently reflects this circumstance (compared to, e.g., “abiotic”).

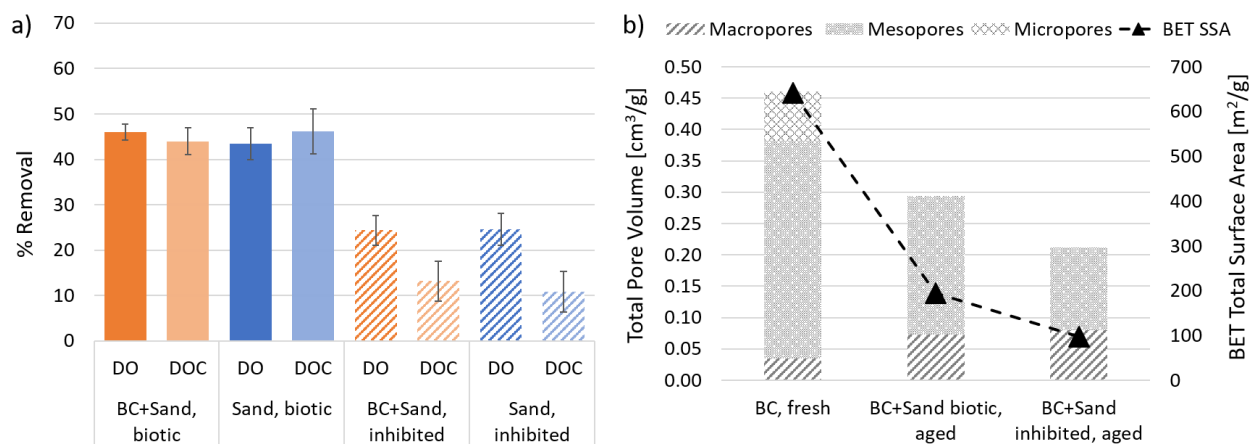


Figure 2.1 a) Biological activity of columns: Removal of dissolved oxygen (DO) during days 7-110 and removal of dissolved organic carbon (DOC) during days 11-103; shown are the mean and standard error of the mean (SEM) with sample sizes $n = 54, 18, 18, 18$, respectively. b) Effect of biofilm and ageing on biochar properties: Brunauer-Emmett-Teller specific surface area (BET SSA) and pore volume distribution of fresh MCG-biochar compared to aged biotic and inhibited samples. Ageing consisted of column conditioning with synthetic stormwater containing ~ 10 mg/L DOC (23 days) followed by injection of synthetic stormwater with ~ 10 mg/L DOC and ~ 200 μ g/L TOxCs (92 days).

The significantly greater removal of DO and DOC in biotic columns indicated the presence of an active biofilm, which we presumed to be responsible for the observed microbial activity. Based on the observations, we further concluded that aerobic conditions dominated in the columns (except for anoxic niches, which may be present in biochar/porous media). Because there was no significant difference in DOC removal between “Sand, biotic” and “BC+Sand, biotic” conditions ($p=0.27$; Paired-sample t-test, $\alpha = 0.05$), we concluded that DOC removal after initial conditioning (\sim Day 11 after column inoculation) was governed by microbial activity rather than adsorption to the biochar. These findings correspond well to another study comparing chemical oxygen demand (COD) between sand and activated carbon (AC) biofilters, concluding that the type of filter material did not affect the activity of the heterotrophic biomass and hence that biotransformation was the main mechanism responsible for COD removal (Yu *et al.*, 2007).

2.4.2 Impact of Fouling/Ageing on Biochar Properties

To comparatively assess the impact of biological fouling and ageing (over 115 days total) on biochar physical properties and thus sorption, fresh and aged (both biotic and inhibited) biochar samples collected from columns were analyzed for total pore volume (PV) and BET specific surface area (BET SSA) (Figure 2.1b). The largest portion (75.4%) of the total PV of fresh MCG biochar was attributed to the mesopore fraction (pore sizes 20-500 Å or 2-50 nm), followed by micropore volume (17.0%; < 20 Å or < 2 nm), whereas the smallest fraction was comprised of macropores (7.6%; > 500 Å or > 50 nm). A high degree of mesoporosity is reportedly crucial for the sorption of triazine herbicides to biochar: Mesopores were beneficial in minimizing steric hindrance effects and may provide pathways for contaminants to diffuse into deeper pores (Xiao & Pignatello, 2015a). The BET SSA of fresh MCG biochar was 641 m²/g, and is approximately double the value reported elsewhere (Ulrich *et al.*, 2015) for the same type of biochar (317 m²/g). As both biochars were acquired from the same production facility but originated from different production batches, this may explain the variability in physical properties. Interestingly, the relative reduction in BET SSA and PV over time was more pronounced under inhibited fouling conditions compared to biologically active conditions (reduction by 85% and 45%, respectively, for inhibited vs. 70% and 23%, respectively, for biotic), which could be indicative of a regenerative effect of microbial activity, potentially through elevated DOC consumption over time that frees up sorption sites at the biochar surface.

2.4.3 Column Performance: Contaminant Breakthrough Curves

The removal of the parent compounds atrazine, imidacloprid, and clothianidin followed a similar pattern in the different treatment conditions (Figure 2.2): Sand columns (both biotic and inhibited) broke through ($C_{Eff} = 0.05 * C_{In}$) nearly immediately (< 0.71 d) for all three compounds. Breakthrough curves (BTCs) for the TORCs indicated relatively rapid initial breakthrough in the inhibited BC+Sand column as well (3.03 d, 3.14 d, and 4.45 d to initial breakthrough for clothianidin, atrazine, and imidacloprid, respectively), but in a more gradual manner compared to the biotic treatment (linear vs. s-shaped BTCs). Initial breakthrough times of biotic BC+Sand columns occurred in the following order: clothianidin \leq atrazine < imidacloprid. When the batch isotherm-derived Freundlich parameters (Table A.4, discussed further below) are used to calculate K_d values at $C_W = 10$ µg/L ($K_d = 151000$, 117000, and 114000 L/kg for imidacloprid, atrazine, and clothianidin, respectively), these coefficients appear to be good predictors of initial column breakthrough order in the biotic BC+Sand columns, despite isotherm nonlinearity. However, the order of compounds did shift slightly when it came to average exhaustive breakthrough time (defined as the time when $C_{Eff} = 0.9 * C_{In}$) and was as follows: clothianidin < imidacloprid \leq atrazine.

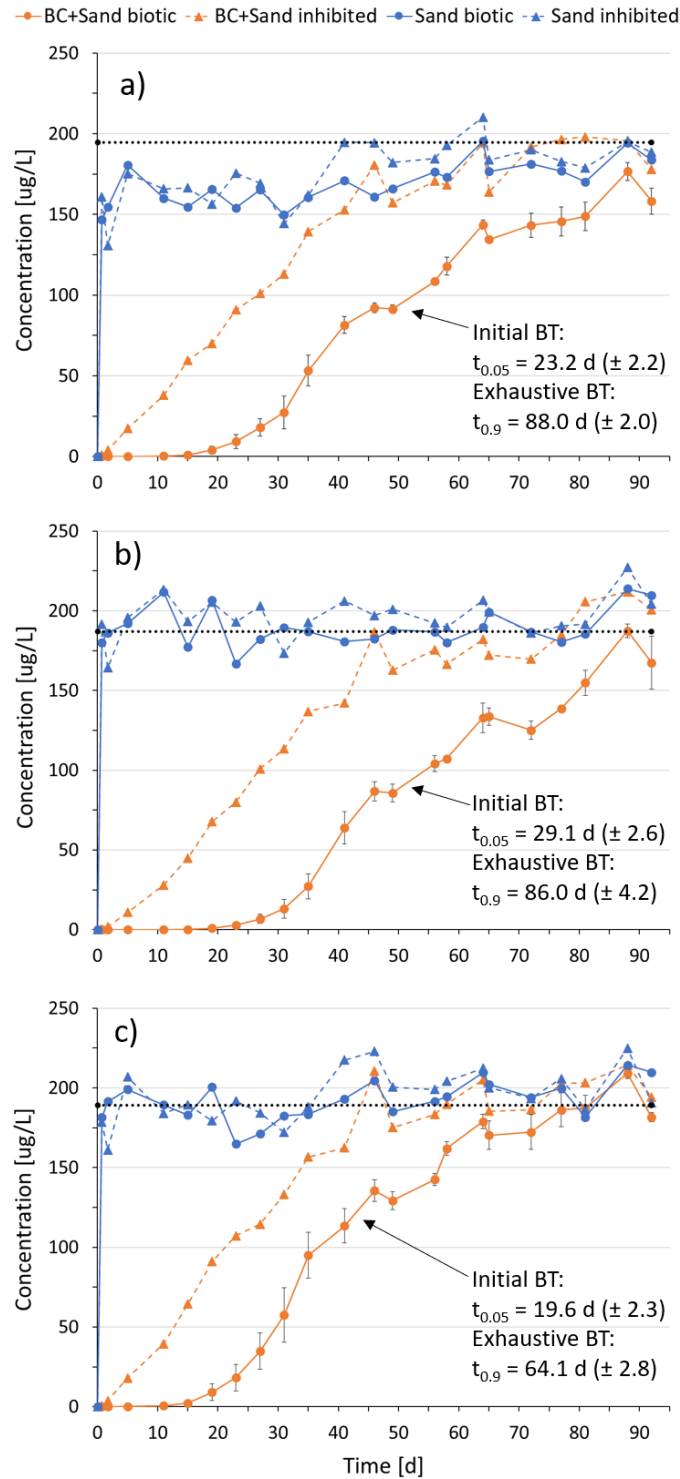


Figure 2.2 Column effluent concentrations [$\mu\text{g/L}$] over time [days] for the spiked pesticides: a) Atrazine, b) Imidacloprid, c) Clothianidin. Initial breakthrough (BT) is defined as the time when the effluent concentration $C_{Eff} = 0.05 \cdot C_{In}$, and exhaustive BT is defined as the time when the effluent concentration $C_{Eff} = 0.9 \cdot C_{In}$. BT times for the 'BC+Sand biotic' condition (three replicates) are reported as mean \pm standard deviation. Dotted lines represent the mean influent concentrations.

The enhanced performance with respect to pesticide removal in the biotic BC+Sand columns is likely due to the combined presence of biochar and (active) microbial biofilm. Because sand was the dominant material in our study (from a mass perspective) and biochar was only present at 0.5 wt%, the biofilm may have been primarily located on the sand particles. Despite this, the data suggest that the biochar played a crucial role for pesticide fate and removal involving the biofilm: even though DO and DOC removal in the biotic sand columns (without biochar) were similar to those with biochar (Figure 2.1), there was a major difference in pesticide removal between these two conditions (Figure 2.2). There was almost no removal of pesticides in the biotic sand column (no biochar) despite comparable DOC and DO removal. In short, there is a clear difference between the fate of DOC and pesticides in these systems: this is evident from the differences in removal between the biotic and inhibited systems and it does point to a clear role of biochar in promoting pesticide removal.

2.4.4 Biotic Contributions – Parent Mass Balance (Columns)

To study the relative importance of biodegradation in overall TOrC removal, the cumulative mass removal for each of the conditions was calculated over the course of the experiment. Because both biotic and inhibited BC+Sand systems were inoculated with a microbial biofilm, we attribute the difference in long-term TOrC removal to microbial activity (and not simply biosorption), potentially involving biodegradation. The mass balance in Figure 2.3 was developed based on area under the curve calculations of BTCs of TOrC effluent concentrations shown in Figure 2.2. The difference in cumulative mass removal at specific timepoints (Figure 2.3) between biotic BC+Sand and inhibited BC+Sand (assumption: sorption only) was assumed to yield the “biotic contribution” or biodegradation portion of the overall removal.

The contributions of both sorption and biodegradation to overall removal varied through time (Figure 2.3). As can be expected based on exhaustion of sorption sites and pore filling, the share of sorption in overall mass removal decreased over time. Concurrently, the share of biodegradation increased between 30 and 60 days. We estimated biotic contributions to account for 20-36% of overall biologically enhanced removal in biotic BC-amended sand columns. These results correspond well with findings from a previous study (Sbardella *et al.*, 2018), which reported that the presence of a biofilm improved the removal of nine pharmaceuticals in a biological activated carbon filter (BAF) and that the contribution of biofilm in overall removal of these compounds was in the range of 22-35%. Indeed, Frankel *et al.* (2016) reported that biochar-attached biofilms resulted in higher removal of naphthenic acids (42-72%) compared to sterile biochar experiments (22-25%). Nevertheless, the dominant removal mechanism may change over time, which was the case in a system simulating natural groundwater recharge when prevalence shifted from sorption to biodegradation (Yan *et al.*, 2017).

In the present study, our mass balance indicates that a biochar application rate of 0.5 wt% and the presence of an active biofilm prolonged the observed biofilter lifetime by 1.8-2.3 times compared to a fouled but inactive filter dominated by adsorptive removal only (inhibited BC+Sand) (Figure 2.3). This finding contradicts the common concept (e.g., in the case of recalcitrant compounds) that biofilm growth (or biofouling) may decrease the lifetime of adsorptive biochar filtration systems (Ray *et al.*, 2019). A mass balance of the parent compounds, however, does not allow for any firm mechanistic conclusions: the biotic contributions may be due to a combination of biotransformation and biologically enhanced sorptive removal. The latter process may be separately studied only in the case of non-biodegradable compounds such as PFASs: a recent study investigated removal of PFASs from wastewater in laboratory column experiments and showed that the activity of the microbial biofilm appeared positively related to the enhanced sorptive removal of PFASs (Dalahmeh *et al.*, 2019). The authors argued that – compared to the inactive biofilm-biochar – the activity of the biofilm may have led to an increased number of available sorption sites on the biochar by continuously degrading organic matter (i.e., DOC in the influent). Our findings of decreased fouling (lessened decline of SSA and PV; see section 2.4.2) under biologically active conditions are consistent with this hypothesis and potentially point towards biologically enhanced sorption and thus a regenerative effect of microbial activity restoring some of the sorption capacity over time.

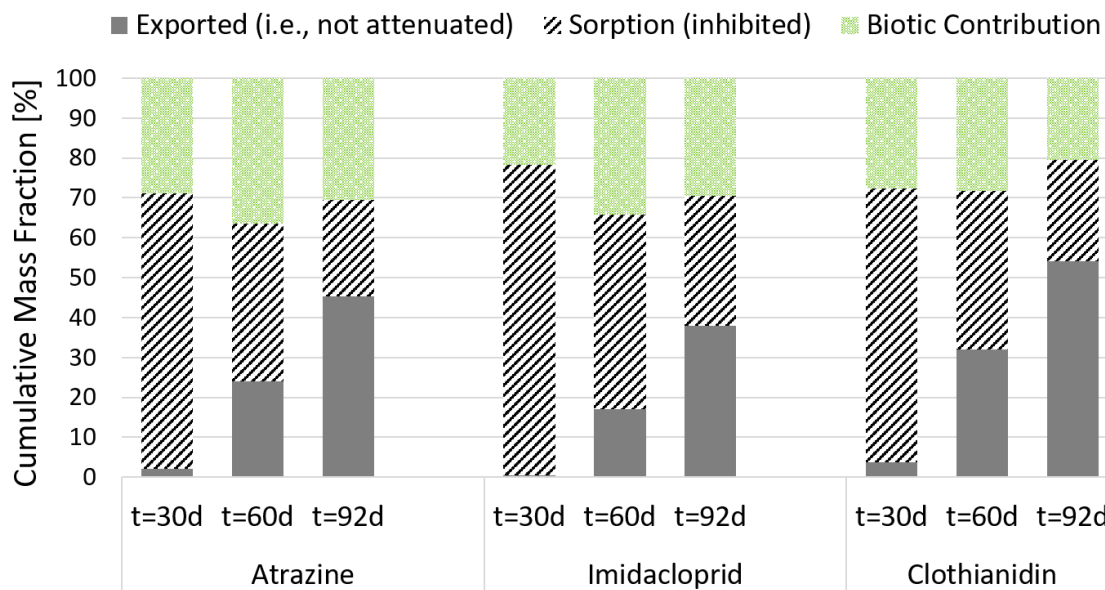


Figure 2.3 Mass balance of parent effluent data (area under curve calculation). The share of sorption, inhibited (comprising both sorption to the biochar and biosorption) was estimated from the difference between the inhibited Sand and inhibited BC+Sand breakthrough curves. This portion was then subtracted from the biologically enhanced removal observed in the biotic BC+Sand columns to yield the biotic contribution (consisting of both biologically enhanced sorption and biodegradation).

Biotransformation of organic chemicals in the combined presence of a microbial biofilm and biochar may involve several mechanisms, which may occur simultaneously and are thus not mutually exclusive. In addition to degradation in the aqueous phase, literature indicates that biodegradation of biochar-bound organic compounds may be possible due to bioregeneration (Klimenko *et al.*, 2003) or enhanced desorption (Zhang *et al.*, 2019) and due to the biochar's ability to serve as redox catalyst between microorganisms and organic compounds (Yu *et al.*, 2015). Bioregeneration occurs during water treatment employing combined biological and adsorptive processes, in which microorganisms renew the adsorption capacity of the black carbon (Aktaş & Çeçen, 2007). Traditionally, it is thought that a concentration gradient between the carbon surface and the bulk liquid is a prerequisite for bioregeneration (Aktaş & Çeçen, 2007). This gradient leads to the desorption of activated carbon-bound organics and renders them available for microorganisms in the aqueous phase (Aktaş & Çeçen, 2007). Abromaitis *et al.* (2016) argue that the reversibility of adsorption is highly dependent on the activation energy of desorption. Because of this, mesoporous adsorbents might be more favorable for desorption and hence bioregeneration than microporous, e.g., commercially available GAC (Abromaitis *et al.*, 2016; Klimenko *et al.*, 2003). The biochar used in our study was predominantly mesoporous (75.4% of total PV) and might thus be well suited for bioregenerative processes. Yu *et al.* (2006) studied the desorption behavior of the pesticide diuron in soil and the role of biochar microporosity and found a high correlation between adsorption-desorption hysteresis and micropore volume. Assuming that bioregeneration is dependent on a concentration gradient, activated carbon regeneration may only be induced after major changes in the loading or operation of the treatment system, e.g., wash-out in a BAC system, which lowers the bulk concentration (Abromaitis *et al.*, 2016). We posit that from this perspective, variable influent systems such as stormwater treatment structures may create conditions favorable for bioregeneration. For example, some catchments may exhibit a first flush phenomenon for certain contaminants, meaning that highly concentrated water is followed by cleaner stormwater runoff (Bach *et al.*, 2010; Bertrand-Krajewski *et al.*, 1998). In other cases, however, stormwater pollutographs may be more complex than the simple first flush concept (Peter *et al.*, 2020), or pollutant concentrations may be subject to seasonal variability (Lee *et al.*, 2004).

Microbial degradation processes of biochar-sorbed organic chemicals are different compared to organics present in the dissolved phase and DOC may substantially impact their desorption and mineralization rates. Zhang *et al.* (2019) demonstrated that the presence of humic acid (HA) increased the mineralization rate of biochar-bound phenanthrene by accelerating its desorption rate into the aqueous phase. Desorption was negatively correlated with the microporosity of biochars: the authors argued that organics bound to the intraparticle surfaces and micropores may be inaccessible (Zhang *et al.*, 2019). In our study, it is possible that a continuous source of DOC in the presence of a predominantly mesoporous biochar led to

increased desorption rates and facilitated transport of atrazine, imidacloprid, and clothianidin in our biologically active columns.

Further, biochar may be crucial in facilitating reduction/oxidation reactions with organic chemicals (Saquing *et al.*, 2016). In the presence of biochar, several coexisting degradation pathways were proposed to contribute to the biological reduction of pentachlorophenol (PCP): 41% of the PCP loss was attributed to electrical conductor mediated reduction of adsorbed PCP (Yu *et al.*, 2015). Unlike the mechanisms described for bioregeneration or DOC-enhanced desorption, this process is thought to act directly on the biochar-bound organics. Similarly, an alternative explanation for observed bioregeneration invokes the release of microbial exoenzymes, which react with the carbon-bound substrates/compounds (Aktaş & Çeçen, 2007), thus increasing the bioaccessibility of the compounds (Ogbonnaya & Semple, 2013). This process may be comparable to plant root exudates stimulating the degradation of organic compounds by rhizosphere-associated microbes (Muerdter & LeFevre, 2019; Ogata *et al.*, 2013). Though it remains uncertain whether and to what extent these alternative mechanisms are responsible for the enhanced removal of clothianidin, atrazine, and imidacloprid in the biochar-amended columns studied here, it is clear that the biologically active systems had a greater capacity for removal of these contaminants than the inhibited systems. The observed enhanced removal may possibly involve a combination of several coexisting processes (i.e., degradation in the aqueous phase, bioregeneration, DOC-enhanced desorption and transport, biochar-bound microbial degradation).

2.4.5 Biotic Contributions – Known Transformation Products and Pathways

TP analysis offers another line of evidence to probe answers about biological processes occurring in the biofiltration columns. We detected multiple TPs of atrazine and imidacloprid in column effluents at timepoints during column operation (Figure 2.4 on page 28): desethyl-atrazine (DEA), 2-hydroxy-atrazine (OH-ATZ), desnitro-imidacloprid (desnitro-IMI), and imidacloprid-olefin (IMI-olefin). Concentrations were generally highest in biotic BC+Sand systems and of greater consistency compared to control conditions (Figure 2.4), although fractions of TPs normalized to parent influent concentrations remained below 2.5% for all conditions throughout the entire experiment. This indicates that biodegradation was occurring, but quantitative estimations are complicated by a lack of authentic standards, yet unknown TPs, as well as the uncertainty as to the degree of mineralization vs. transformation. Interestingly, in the early stage of the experiment (at $t = 23$ d), TPs were primarily detected in biotic Sand columns, but not yet in biotic BC+Sand systems (with the exception of OH-ATZ). Suspect TP peaks were also found for deisopropylhydroxy-atrazine and didealkylatrazine, with both offering some MS2 data to provide more confidence in their detection (i.e., some had library scores >90); however, the peaks were deemed to be

false positives caused by in-source fragmentation of OH-ATZ and DEA, respectively, based on their respective retention times and their presence in analytical standards containing OH-ATZ and DEA (Figures A.14 and A.15).

Among all the TPs examined, the highest production was found for OH-ATZ. Levels of OH-ATZ in the effluent of the biotic BC+Sand columns exhibited a clear increasing trend over time ($R^2 = 0.98$, linear regression). Differences in concentrations between the four tested conditions in the time range 46-92 days were only statistically significant between biotic BC+Sand and each of the biotic and inhibited sand controls ($p=0.0423$ and $p=0.0036$, respectively; Dunn's multiple comparisons test). Detections of OH-ATZ in both biotic and inhibited sand controls were in the range of levels observed in the influent, which were most likely attributable to aqueous hydrolysis governed by solution pH (Zhang *et al.*, 2013). OH-ATZ in inhibited BC+Sand columns was likely produced via surface-catalyzed hydrolysis induced by the biochar, a process that has been described for atrazine (Zhang *et al.*, 2013). Possible mechanisms behind the biochar-enhanced hydrolysis of atrazine include surface-bound metal atoms facilitating the nucleophilic attack of water molecules and surface hydroxyl groups acting as nucleophiles. Biochar-catalyzed reductive transformation was also reported for the dinitro herbicides pendimethalin and trifluralin via similar mechanisms (Oh *et al.*, 2013). Production of DEA in the columns is likely related to the presence of the microbial biofilm, as DEA was almost exclusively observed in the biotic BC+Sand columns, although also (inconsistently) in biotic Sand columns. Over the entire course of the experiment, concentrations of DEA were lower compared to OH-ATZ (in biotic BC+Sand columns: $p=0.0048$; Paired-sample t-test, $\alpha=0.05$), consistent with observations in soil and aquatic systems, where the hydroxylation pathway is generally more common for atrazine (Mudhoo & Garg, 2011). From an environmental risk perspective, hydroxylation renders OH-ATZ non-herbicidal (unlike DEA and DIA) and thus is considered a more straightforward detoxification pathway (Meyer *et al.*, 2009; Wackett *et al.*, 2002). The prevailing redox conditions may have a strong impact on atrazine degradation, and generally, degradation rates are faster under aerobic compared to anaerobic conditions. For example, Douglass *et al.* (2014) studied the mineralization of atrazine in wetland sediments and the aerobic half-life of atrazine was roughly a week, whereas half-lives under anaerobic conditions were up to 50 days. In the present study, the DO levels in effluents of biotic columns were 3.84 ± 0.91 mg/L (BC+Sand) and 4.03 ± 1.05 mg/L (Sand), indicating predominantly aerobic conditions, except for potential anoxic/anaerobic microniches present in the porous media.

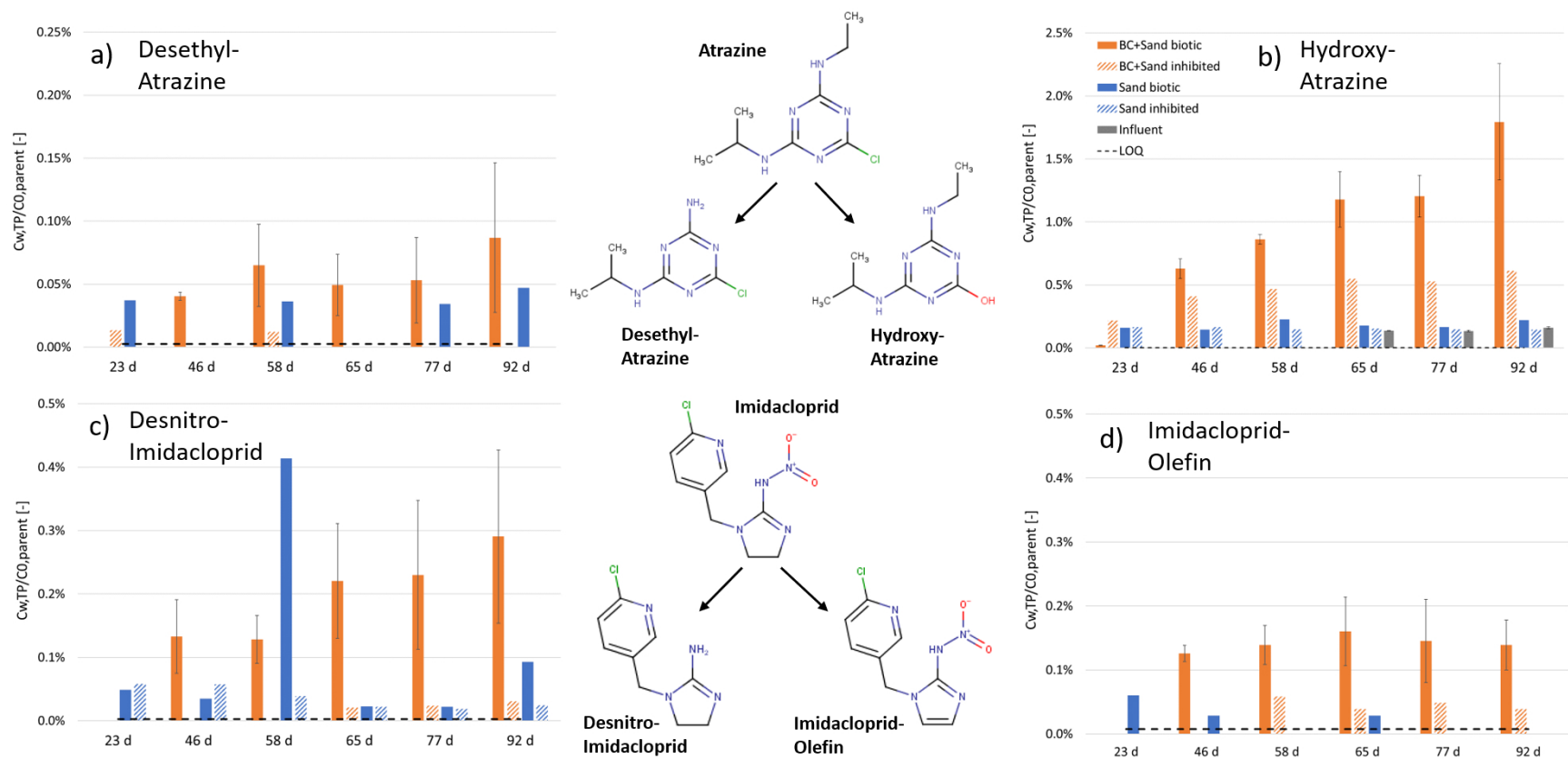


Figure 2.4 Temporal evolution of transformation products (TPs) of atrazine and imidacloprid in column effluents and influent identified by target LC-QToF-MS analysis: a) desethyl-atrazine, b) 2-hydroxy-atrazine, c) desnitro-imidacloprid, d) imidacloprid-olefin. Y-axis shows TP concentrations in effluent normalized by the average parent influent concentration ($C_{W,TP}/C_{W,0,Parent}$). Dotted black lines represent the limit of quantitation (LOQ) for each TP.

Among imidacloprid TPs, concentrations of desnitro-IMI were highest in biotic BC+Sand columns (except for t=58 d) and followed a clear temporal trend ($R^2 = 0.88$, linear regression; Figure 2.4). Desnitro-IMI was detected in effluents of all control columns, but at variable levels. The presence of desnitro-IMI in inhibited Sand columns suggests that either abiotic degradation occurred (although, hydrolysis of imidacloprid under environmentally relevant conditions is very unlikely; Thompson *et al.* 2020) or that sufficient biological activity in the inhibited columns transformed imidacloprid to desnitro-IMI. Similarly, concentrations of IMI-olefin were highest in biotic BC+Sand columns, but IMI-olefin was also present (to a lower extent) in biotic Sand and inhibited BC+Sand systems. 5-hydroxy-imidacloprid (5-OH-IMI) and nitrosoguanidine-imidacloprid (NG-IMI) were detected via suspect screening of column effluent samples. Precursor peaks for both NG-IMI and 5-OH-IMI were consistently detected in biotic BC+Sand samples over time, but only NG-IMI could consistently be confirmed by one accurate mass fragment (209.0591 Da; for details see Table A.6). We presume that 5-OH-IMI precursor peaks were too small for consistent fragment accurate mass confirmation. This led to the assignment of different suspect confidence levels according to the Schymanski scale (Schymanski *et al.*, 2014): Level 3 for NG-IMI and Level 4 for 5-OH-IMI (Table A.6).

Typically, biotransformation is associated with detoxification mechanisms that render metabolites less toxic than their parent compound. However, for some ‘target-specific’ pesticides such as imidacloprid and other neonicotinoids (i.e., pesticides that are designed to impart enhanced toxicity to certain pests via enhanced receptor binding specificity), decreased toxicity does not necessarily occur with degradation. Specifically, insect selectivity (i.e., differential binding propensity toward insect receptors) and thus the toxicity of neonicotinoids is due to favorably binding to the insect nicotinic acetylcholine receptor (nAChR) and is effectively repelled by vertebrate nAChRs (including mammalian) (Tomizawa & Casida, 2003). Replacing the =NNO₂ group in imidacloprid by =NH to yield desnitro-IMI inverts the selectivity for insect versus mammalian receptors, rendering desnitro-IMI >300 times more toxic (based on binding affinity data) toward mammals while at the same time greatly decreasing its insect toxicity (Tomizawa & Casida, 2003). In contrast, the acute toxicity of IMI-olefin towards insects is even higher than imidacloprid, as highlighted in exposure studies on cotton whiteflies (Nauen *et al.*, 1999) and honey bees (Suchail *et al.*, 2001). IMI-olefin and desnitro-IMI are part of two distinct transformation pathways of imidacloprid: IMI-olefin is considered a “dead-end product”, whereas the latter is an intermediate product in the pathway that may lead to complete mineralization via IMI-urea (Figure A.2). Therefore, despite the increased mammalian toxicity, degradation into desnitro-IMI might still be preferred from an environmental risk perspective, because it may further transform into TPs that are, during acute exposure, reportedly less insecticidal (lower bee mortality) compared to imidacloprid (Suchail *et al.*, 2001).

6-chloronicotinic-acid (6-CNA) is a TP of imidacloprid and other neonicotinoids, e.g., acetamiprid (Bonmatin *et al.*, 2015), and is to be found at the “lower end” of the microbial degradation pathway of imidacloprid (Figure A.2). In some bacterial biodegradation studies, 6-CNA was reported as a dead-end metabolite, whereas most evidence indicates full mineralization is possible (Hussain *et al.*, 2016). In the present study, 6-CNA was detected at low concentrations in effluents of biotic BC+Sand columns towards the end of the column experiment. At 92 days after the onset of spiking, 6-CNA was measured at 0.091 µg/L in one column replicate and detected below the LOQ of 0.05 µg/L in another replicate. The relatively low concentrations of 6-CNA observed argues against it being a dead-end metabolite. As for the other experimental conditions, 6-CNA was neither detected in any of the inhibited column controls (Sand or BC+Sand, respectively) nor in the influent water. Although 6-CNA causes considerably less bee mortality than the parent imidacloprid (Suchail *et al.*, 2001), it may still induce some oxidative stress towards aquatic non-target organisms such as freshwater algae and crustacean amphipods (Malev *et al.*, 2012). Moreover, the chronic toxicity towards bees was found to be equally high for imidacloprid and its major TPs, including 6-CNA (Suchail *et al.*, 2001).

At the time of the analysis, there were no analytical standards or entries in spectral libraries available for the identification of clothianidin TPs. Employing a suspect screening approach (Table A.3), we confirmed the presence of one potential TP in effluents of biotic BC+Sand columns, namely clothianidin-urea (CLO-urea) with a protonated precursor accurate mass of 206.01494 Da (Table A.6). All reported peaks fulfilled the suspect precursor quality criteria (<5 ppm mass error, <40% difference in isotope ratio) and the peak identity was further confirmed via at least one known unique fragment ion accurate mass (<10 ppm fragment mass error). The peak area counts in select column effluent samples were converted into concentration values using a semi-quantitation approach with clothianidin as the calibrant (calculations see section A.5). The resulting concentrations of CLO-urea were in the range of 1 µg/L and were highest at the end of the experiment (t=92 days) (Figure A.13c). Thus, CLO-urea levels were likely in the same order of magnitude as other target TPs and were only surpassed by OH-ATZ concentrations.

N-(2-chlorothiazol-5-yl-methyl)-N'-nitroguanidine (TZNG) and N-methyl-N'-nitroguanidine (MNG) are among the most common biodegradation TPs of clothianidin, based on results of soil degradation studies under dark aerobic conditions at 20°C (Van der Velde-Koerts *et al.*, 2011). Mori *et al.* (2017) conducted a degradation study of clothianidin under nitrogen-limited conditions using a specific microorganism, the white-rot fungus *P. sordida*, which is known to produce enzymes that catalyze the degradation of recalcitrant organic chemicals. The fungus degraded 37% of clothianidin in 20 days and CLO-urea (or N-(2-chlorothiazol-5-yl-methyl)-N'-methylurea; TZMU) was the main observed metabolite (Mori *et al.*, 2017). A study investigating the biodegradation of clothianidin in agricultural soils from China identified

CLO-urea and a second compound ($m/z = 170.9$; potentially dechlorinated form of CLO-urea) as degradation products (Zhang *et al.*, 2018a). In contrast to atrazine and imidacloprid, clothianidin undergoes faster biodegradation under anaerobic compared to aerobic conditions, with degradation rates also dependent on factors such as temperature, nutrient levels, and initial concentration (Mulligan *et al.*, 2016). CLO-urea has also been reported as a hydrolysis product of clothianidin (at $\geq 50^\circ\text{C}$ and pH 9) (Van der Velde-Koerts *et al.*, 2011); however, at ambient temperatures, clothianidin is considered hydrolytically stable in the pH range of 4-9 (Klarich *et al.*, 2017; Van der Velde-Koerts *et al.*, 2011). In short, while there are limited clothianidin biodegradation data available, CLO-urea was one of the metabolites that was commonly reported in other degradation studies. The prevailing environmental conditions in our study (aerobic except for micro niches, $T = 20^\circ\text{C}$) may not have been optimal for clothianidin degradation. From a toxicity standpoint, it appears that CLO-urea may be less toxic than its parent compound, as clothianidin significantly decreased the viability of neuroblastoma cells, while CLO-urea did not show significant effects (up to $300\ \mu\text{M}$) (Mori *et al.*, 2017): transformation of clothianidin to CLO-urea would likely be a desired goal of a biofilter. Our combined suspect screening and semi-quantitation approach revealed that CLO-urea was indeed an important TP of clothianidin and should be considered in future studies.

Overall, our findings suggest that biodegradation is predominantly occurring in both the “traditional” (Sand biotic) and the biochar-amended biofilters (BC+Sand biotic), however, only the latter offers the crucial benefit of contaminant retention that ultimately leads to treatment of the stormwater.

2.4.6 Microcosm Mass Balance / Suspect Screening

We conducted microcosm experiments to study the transformation of atrazine, imidacloprid and clothianidin under non-sorptive conditions (no biochar) and using the same microbial enrichment solution that was used for column inoculation. The goal was to determine if differences in TPs between microcosms and column effluents could be attributed to the presence of biochar. Initial concentrations in the microcosms ($415\ \mu\text{g/L}$, $361\ \mu\text{g/L}$, and $364\ \mu\text{g/L}$ for atrazine, imidacloprid, and clothianidin, respectively) were higher than in column influents to increase the opportunity for detecting TPs produced at very low levels. After 369 days, overall parent mass removal in the two biotic microcosm replicates were 15.0% (± 4.73), 34.1% (± 0.01), and 18.8% (± 0.08) for atrazine, imidacloprid, and clothianidin, respectively. In a biotransformation experiment using biofilms collected from natural streams, Desiante *et al.* (2021) considered imidacloprid recalcitrant since concentration decreases of $<20\%$ were observed over the course of 72 hours. Imidacloprid was also classified persistent according to REACH and EMA guidelines in lake/river sediment suspension experiments (Seller *et al.*, 2020). For atrazine, however, average removal of

45% was observed in biotic microcosms over the duration of 76 days (Ulrich *et al.*, 2017b).

All seven target TPs that were detected in column effluents were present in the microcosm solutions as well (Figure 2.5; Table A.7). The most abundant TP of atrazine was OH-ATZ, while for imidacloprid, the highest concentrations were detected for IMI-urea, followed by 6-CNA. Similarly, Muerdter & LeFevre (2019) recently found IMI-urea and 6-CNA - which are both less potent insecticides compared to their parent (Malev *et al.*, 2012; Suchail *et al.*, 2001) - as the main degradation products of imidacloprid in a synergistic duckweed-microbial system. Again, when it comes to chronic insect toxicity, however, there may be no difference between imidacloprid and its major TPs (Suchail *et al.*, 2001).

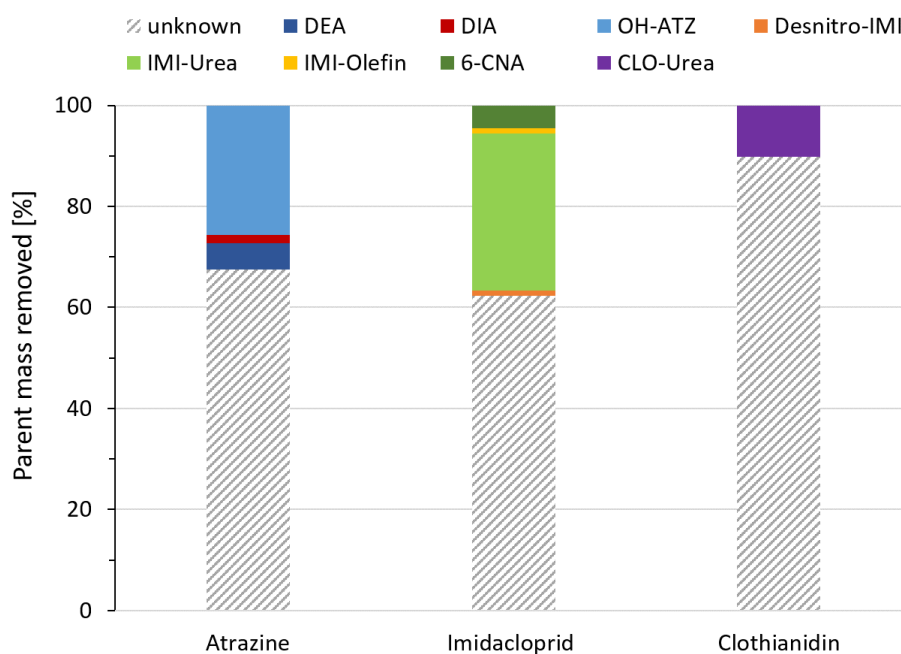


Figure 2.5 Molar mass balance of microcosm data: Share of transformation products in total parent mass removal at the end of the experiment (369 days). The total parent molar masses removed after 369 days were 71.4 nmol, 119.2 nmol, and 67.8 nmol for atrazine, imidacloprid, and clothianidin, respectively. Initial concentrations for the three compounds were 1923 nM, 1412 nM, and 1458 nM, respectively. “Unknown” indicates that the mass was unaccounted for. Abbreviations: desethyl-atrazine (DEA), desisopropyl-atrazine (DIA), and 2-hydroxy-atrazine (OH-ATZ), desnitro-imidacloprid (desnitro-IMI), imidacloprid-urea (IMI-urea), imidacloprid-olefin (IMI-olefin), 6-chloronicotinic acid (6-CNA), and clothianidin-urea (CLO-urea). Note that calculations for CLO-urea are semi-quantitative.

Suspect screening of microcosm samples revealed the presence of the same TPs that were also found in biotic column samples: 5-OH-IMI, NG-IMI, and CLO-urea. Precursor peaks for all three suspects were consistently detected in microcosm samples over time, but only CLO-urea could be confirmed by one accurate mass fragment at the end of the experiment (369 days). 5-OH-IMI precursor peaks were too small for consistent fragment accurate mass confirmation, and NG-IMI peaked during earlier stages of the

experiment and peaks were too low to be confirmed at the end (Figure A.12). Suspect concentrations were estimated employing a semi-quantitation approach using calibrants that share similar ionizable functional groups (for details see section A.5). Suspect precursor and fragment masses, as well as representative MS and MS/MS scans for each suspect can be found in the SI (Table A.6 and Figures A.9-A.11).

Our results indicate that the target and suspect products only account for <40% of total parent mass removed (after 369 days; Figure 2.5). Without authentic standards for the suspect compounds or tracking of radio-labelled parent compounds, it is unclear to what extent errors in estimated concentrations would account for the missing mass. Hence, even without the presence of biochar, potentially unknown TPs for all three pesticides makes closing the mass balance difficult. As all TPs reported here are likely semi-stable intermediates, we recognize that TP production and further degradation (i.e., mineralization) may be dynamic and not well captured in a simple mass balance approach like the one employed here. Nevertheless, biodegradation was active in the microcosms, and the observed TPs were the same as in biotic column systems (both Sand and BC+Sand).

2.4.7 Abiotic Batch Sorption Experiments

Both Freundlich and Langmuir sorption equations were fit to the batch isotherm data up to equilibrium solution concentrations of 45 $\mu\text{g/L}$ (Figure A.4). Akaike’s Information Criterion (AIC) was used to compare the goodness-of-fit for both sorption equations, and demonstrated better fits for the Freundlich isotherm for all three parent compounds. The corresponding AIC and best-fit values of the non-linear Freundlich isotherm coefficient K_F (sorption affinity) and the Freundlich isotherm exponent n are reported in the SI (Table A.4). The Freundlich isotherm has been used in previous studies to describe sorption of hydrophilic TOrCs to MCG-biochar (Ashoori *et al.*, 2019) and of neonicotinoids to pig manure and maize straw-derived biochars (Zhang *et al.*, 2018b).

Atrazine is a weak base ($\text{pK}_a = 1.6$) and exists in its neutral form at environmentally relevant pH values (Kah *et al.*, 2017). Besides hydrophobic effects, $\pi - \pi$ electron-donor acceptor (EDA) interactions are relevant for atrazine sorption to biochar, due to the electron donor nature of atrazine’s ring substituents (Xiao & Pignatello, 2015a). Imidacloprid and clothianidin are not charged at circumneutral pH (Tomizawa *et al.*, 2003) but have a charge distribution at their nitro group ($-\text{NO}_2$) and thus exhibit a distinct pharmacophore (see Figures A.2 and A.3). Zhang *et al.* (2018b) investigated the biochar sorption mechanisms of imidacloprid and clothianidin and concluded that at higher production temperatures ($>500^\circ\text{C}$), hydrophobic partitioning became less important, and instead specific interactions such as $\pi - \pi$ EDA complexes were more prominent. Similarly, Webb *et al.* (2020) suggested that imidacloprid (and imidacloprid-urea) sorption may be primarily driven by $\pi - \pi$ or $\pi^+ - \pi$ interactions (in contrast to

desnitro-imidacloprid). $\log K_{OC}/\log K_{OW}$ ratios can be used as a semi-quantitative approach to assess the importance of hydrophobic effects in overall sorption and higher ratios generally indicate greater importance of specific interactions (Xiao & Pignatello, 2015b). At $C_W = 50 \mu\text{g/L}$ and using the K_d values from section 2.4.3 for K_{OC} , we observed larger $\log K_{OC}/\log K_{OW}$ ratios for imidacloprid (9.26) compared to clothianidin (7.85), which were in line with results for de-ashed maize straw biochars produced at 700°C (Zhang *et al.*, 2018b). Greater ratios may indicate that polar specific interactions were more important for imidacloprid sorption compared to clothianidin (Zhang *et al.*, 2018b). For atrazine, we calculated a $\log K_{OC}/\log K_{OW}$ ratio of 1.83, which indicates a higher importance of hydrophobic interactions compared to the two neonicotinoids.

Kinetic sorption data were used to compare the biochar sorption affinity at equilibrium ($K_{d,Eq} = C_{S,Eq}/C_{W,Eq}$; see Table A.5; Figure A.5) between parent compounds and TPs at an environmentally relevant initial concentration of $10 \mu\text{g/L}$. The equilibrium K_d values of all TPs were lower compared to their respective parent compounds, which is in line with the observation that TPs are generally more polar than their parents and thus potentially more mobile in the environment (Kiefer *et al.*, 2019; Menger *et al.*, 2021). In the case of atrazine TPs, the difference in $K_{d,Eq}$ values compared to atrazine was statistically significant in the cases of DEA and DIA ($p < 0.001$ for both) but not OH-ATZ ($p = 5.47\text{e-}2$). Among imidacloprid TPs, only IMI-urea exhibited a significantly different equilibrium K_d compared to the parent compound ($p < 0.001$). Moreover, the differences in sorption affinity between the three parent compounds were not statistically significant (see Table A.5), even though the octanol-water partition coefficient of atrazine is different by two orders of magnitude from the two neonicotinoids ($\log K_{OW} = 2.82, 0.56,$ and 0.64^7 for atrazine, imidacloprid, and clothianidin, respectively). Interestingly, the loss of the electronegative pharmacophore (nitro group) during the transformation of imidacloprid to desnitro-IMI changes the metabolite's pharmacophore charge distribution to positive (amine group), which was demonstrated to have significant effects on sorption to black carbon primarily due to electrostatic interactions (Webb *et al.*, 2020, 2022). However, alteration of the pharmacophore did not explain our findings regarding imidacloprid and desnitro-IMI: for MCG-biochar, the equilibrium sorption capacities ($K_{d,Eq}$) were similar for the parent compound and the TP. Though an assessment of the surface functionalization of the biochar employed here was beyond the scope of the study, prior research indicates that sorption of desnitro-IMI is greatly impacted by surface functionalization (Webb *et al.*, 2020).

⁷KOWWIN v1.68 estimates

2.4.8 Transport Modelling

Parameter Estimation (Fitting). Preliminary results of the modelling of atrazine, imidacloprid, and clothianidin BTCs in MATLAB revealed that sorption parameters derived from abiotic batch data were poor estimators of column performance for both the inhibited and biotic BC+Sand conditions (see Figures A.16 and A.17). As the batch data set was a strong predictor of the sorption *capacity* in the inhibited BC+Sand case (great agreement of linear distribution coefficients K_d at $C_W = 50 \mu\text{g/L}$; Table A.10), we attribute the difficulties in BTC prediction mainly to kinetics. Furthermore, it should be noted that tortuosity (τ) in this transport model should be regarded as a kinetic fitting parameter rather than a physically meaningful parameter (observed tortuosity values are typically below 3). The inaccuracies of the tortuosity values are likely caused by inaccuracies of other model parameters, i.e. diffusion coefficients. For example, as was shown for PFASs, the fitted tortuosity values might be in error due to inaccurate estimations of diffusion coefficients (Schaefer *et al.*, 2019). Hence, forward prediction of effluent BTCs based on batch data was not possible for conditions with a biofilm present (active or inactivated), unlike what was demonstrated for abiotic biochar-sand columns previously (Ulrich *et al.*, 2015). Similarly, Liu *et al.* (2019) showed that GAC batch study distribution coefficients (K_d) for PFASs were not representative of model K_d values obtained from the GAC pilot-scale study.

In the present study, all model parameters were directly derived from the observed column data. We estimated the sorption to the non-BC materials using the inhibited sand column data set and these parameters (K_S , k_S ; reported in section A.6) were subsequently used to derive the sorption to the BC in the other columns. Freundlich model sorption parameters used in the subsequent scenario modelling (Table 2.1) were estimated based on best-fit simulations of biotic BC+Sand breakthrough curves for atrazine, imidacloprid, and clothianidin (Figure A.19). Though the intended use of this model fitting of the observed column data was primarily for estimating filter lifetimes (i.e., scenario modeling), fitting of the breakthrough data revealed that the model assuming sorption-retarded intraparticle diffusion provided a better description of the data than the model assuming instantaneous sorption equilibrium. Best-fit values for the Freundlich isotherm coefficient, $K_{Fr,BC}$, were 1519, 1499, and 892 $(\mu\text{g/g})^*(\text{L}/\mu\text{g})^n$ for atrazine, imidacloprid, and clothianidin, respectively.

In the column model used in this study, biodegradation can be accounted for through the parameter k_{deg} , which is the first-order biodegradation rate for the pollutant in the mobile water (see section A.6 for more information). The model assumes that a biodegradation rate of $k_{deg} > 0$ will lead to a reduction of the maximum possible breakthrough concentration ($C_W/C_{W,0} < 1$) at steady state. However, in our case, these assumptions may not hold: 1) pesticide breakthrough in the biotic BC+Sand columns was dynamic

and not at steady state, and; 2) the mass removal rate of biodegradation was likely sufficiently smaller than the mass loading rate at full breakthrough. In light of the evidence discussed above, various biological and synergistic processes may have contributed to the removal of the pesticides in the biologically active columns. Biodegradation was likely more complex in the present study and may not be appropriately represented by a first-order degradation rate acting only on dissolved phase contaminants (as biodegradation could also happen in the sorbed phase). Therefore, we did not explicitly quantify the rate of biodegradation in this model and decided to assume that for our modelling purposes, the observed mass removal difference between biotic and inhibited BC+Sand columns was due to biologically enhanced sorption only (in order to be conservative and not overestimate the contribution of biodegradation in the subsequent scenario modelling). Thus, the removal due to regenerated sorption capacity over time (biologically enhanced sorption) was lumped into the sorption parameters of the Freundlich isotherm equation during the fitting process. This was reflected in 2.5-3.6 times greater values for the linear distribution coefficients K_d (derived at $C_W = 10 \mu\text{g/L}$ using the fitted Freundlich sorption parameters; see Table A.10) in the biotic BC+Sand condition (Figure A.19) compared to the inhibited biochar control (Figure A.18).

Biofilter Lifetime Simulations (Scenarios). Table 2.1 lists simulation results from Scenarios 1-3, which describe how long a biologically active biochar-amended biofilter could run in a representative field-scale scenario (Table A.11) for a residential area in Denver, CO, until it reached a defined aquatic life threshold value, C_{Th} . As expected, filter lifetimes increased with increasing biochar application rate (M_{BC}) for all three pesticides, and lifetimes were highly dependent on the respective aquatic life threshold values and influent concentrations. The shortest breakthrough times were observed for atrazine with 17.5 years (Scenario 1, stream water), followed by clothianidin with 32.3 years (Scenario 1, stormwater) and imidacloprid with 68.5 years (Scenario 1, stormwater). Our simulations indicate that even in a worst-case scenario with 5% biochar (by volume) only, the biofilter could effectively remove these pesticides from an impacted water for at least 17 years without endangering aquatic life in receiving waters.

Table 2.1 Biofilter lifetime simulations based on different case study scenarios. Bold numbers indicate biofilter lifetime estimates when treating 16 inches of annual rainfall (Denver, CO), and numbers in parentheses represent biofilter lifetimes assuming continuous flow/operation. Freundlich parameters represent best-fit values to biotic BC+Sand column data, assuming kinetic diffusion limitations. Abbreviations: M_{BC} = biochar application rate, C_{In} = influent concentration.

	Atrazine	Imidacloprid	Clothianidin
Freundlich Model Parameters:			
$K_{Fr,BC}$ [($\mu\text{g/g}$)($\text{L}/\mu\text{g}$) ⁽ⁿ⁾]	1519	1499	892
$n = 1/n_{Fr,BC}$ [-]	0.402	0.417	0.457
Tortuosity [-]	25.1	17.8	19.9
Aquatic Life Threshold Value:			
C_{Th} [$\mu\text{g/L}$]	0.60 ^a	0.01 ^b	0.05 ^b
Scenario 1:			
M_{BC} [wt%]	1.0 (~5 vol%)		
A: Stormwater - C_{In} [$\mu\text{g/L}$]	0.624 ^c	0.428 ^c	0.666 ^d
Time to reach C_{Th} [years]	112 (11.8)	68.5 (7.2)	32.3 (3.4)
B: Stream - C_{In} [$\mu\text{g/L}$]	5.17 ^e	0.1428 ^e	0.0663 ^e
Time to reach C_{Th} [years]	17.5 (1.8)	141 (14.9)	390 (41.1)
Scenario 2:			
M_{BC} [wt%]	4.0 (~20 vol%)		
A: Stormwater - C_{In} [$\mu\text{g/L}$]	0.624	0.428	0.666
Time to reach C_{Th} [years]	377 (39.7)	343 (36.2)	158 (16.7)
B: Stream - C_{In} [$\mu\text{g/L}$]	5.17	0.1428	0.0663
Time to reach C_{Th} [years]	83.2 (8.8)	672 (70.9)	779 (82.2)
Scenario 3:			
M_{BC} [wt%]	6.5 (~32 vol%)		
A: Stormwater - C_{In} [$\mu\text{g/L}$]	0.624	0.428	0.666
Time to reach C_{Th} [years]	593 (62.6)	579 (61.1)	266 (28)
B: Stream - C_{In} [$\mu\text{g/L}$]	5.17	0.1428	0.0663
Time to reach C_{Th} [years]	139 (14.7)	1120 (119)	1300 (137)

^a Environmental Quality Standard (EQS) value, annual average for surface waters (European Union). ^b Chronic Aquatic Life Benchmark for invertebrates, for freshwater (U.S. EPA). ^c Spahr *et al.* (2020) ^d Sutton *et al.* (2019) ^e Bradley *et al.* (2017)

2.5 Environmental Implications

Biochar amendments of biofiltration systems offer a promising solution to mitigate the environmental and ecotoxicological impacts of hydrophilic TORCs such as herbicides and insecticides. The distributed implementation of these green infrastructure systems in an urban watershed can decrease stormwater runoff peak flows, while at the same time decreasing concentration peaks via enhanced contaminant removal. The latter has been shown in a watershed-scale model for the insecticide fipronil (Wolfand *et al.*, 2019) and may help to protect the aquatic and human health of local surface and groundwater bodies. In

this study, we demonstrated the benefit of the combined presence of biochar and biofilm in a biofilter, which promoted conditions favorable for biodegradation, enhanced-sorptive removal, and possibly a regenerative effect to restore some of the biochar's sorption capacity over time. Our findings provide insight into the design of biofilter systems in practice: the addition of biochar in conjunction with a relatively porous media such as sand may help to establish an active microbial community in the biofilter with an estimated filter lifetime of over 15 years. A self-restoring system would certainly lead to less maintenance efforts and costs over the filter's lifetime. In practice, the presence of biofilms would most likely not be a design choice but instead an inevitable feature of biofilters due to the presence of DOC and microorganisms in stormwater and various surfaces supporting microbial attachment. Furthermore, the results of our study indicate that biochar-amended biofilters are not a significant source of TPs into the environment. More importantly, most of the TPs that were detected are less toxic than their respective parent compounds, which has important environmental risk implications. Biofilters are relatively non-invasive and, especially when vegetated, add important green space to urban areas, which may offer co-benefits beyond flood control and water quality enhancement (Venkataramanan *et al.*, 2019).

CHAPTER 3

BIOCHAR-AMENDED ENGINEERED STREAMBEDS FOR IN-STREAM ATTENUATION OF THE DIABETES MEDICATION METFORMIN AND ITS METABOLITE GUANYLUREA

Manuscript in preparation for publication.

Andrea C. Portmann^{8,9}, Malte Posselt¹⁰, Anna Jaeger¹¹, Skuyler P. Herzog¹², Reza Abdi⁸, Chuhui Zhang⁸, René Sahn¹³, Björn Kusebauch¹³, John E. McCray⁸, Christopher P. Higgins^{8,14}

3.1 Abstract

Despite the worldwide rise of point and nonpoint source contamination of surface waters and groundwaters, stormwater practitioners typically prioritize water quantity management over pollutant removal. A novel technique of hyporheic zone (HZ) engineering targeting water quality improvement was recently introduced under the acronym BEST: Biohydrochemical Enhancements for Streamwater Treatment. Although previous studies have shown increased transformation of a reactive tracer (i.e. resazurin) in a BEST flume compared to a sand control, removal of challenging compounds such as hydrophilic organic contaminants have not been investigated. This study evaluated the fate of the ubiquitous, ecotoxic contaminant metformin ($\log K_{OW} = -2.64$) in BEST engineered streambeds in a long-term experiment (73 days) at “full-scale”, using an outdoor flume facility (100x1.0x0.45m) at the Umweltbundesamt in Berlin, Germany. Performance data for metformin attenuation were collected for both a BEST streambed modification and a BEST with biochar (at 30% volume) streambed modification. Metformin removal in the HZ of BEST was greater with longer flowpaths, suggesting greater HZ residence time leads to enhanced attenuation. Metformin’s degradation product guanylurea was not detected above a C/C_0 of 8% in the subsurface, suggesting further degradation (possibly mineralization). Amendment of BEST with biochar resulted in a pronounced decrease in breakthrough curve amplitude in the downwelling zone, plus complete removal of metformin along the flowpaths. Dissolved oxygen penetration depths in the down-welling area of the HZ were greater in BEST streambeds compared to controls (i.e. surface dunes, un-altered streambed sediment), likely due to increased hyporheic exchange, and redox conditions became more reducing along flowpaths. In addition to guanylurea, four transformation products were identified in

⁸Department of Civil & Environmental Engineering, Colorado School of Mines

⁹Primary researcher and author

¹⁰Department of Environmental Science, Stockholm University, Sweden

¹¹Department Ecohydrology, Leibniz Institute of Freshwater Ecology & Inland Fisheries, Berlin, Germany

¹²Natural Resources Program, Oregon State University-Cascades

¹³German Environment Agency in Berlin, Germany

¹⁴Corresponding author

the surface water and HZ porewater when metformin was added at a higher dose ($C_0 = 10$ mg/L): 1-methyl-biguanide, 2-4-AMT / 4-2-1-AIMT, 2-4-DAT, and biguanide. In addition to full-scale treatment performance data for a ubiquitous hydrophilic contaminant, results of this study provide novel insight on HZ exchange, redox conditions, biochar sorption, and biotransformation in engineered streambeds.

3.2 Introduction

The natural hyporheic zone (HZ) - the saturated sediment region below and alongside the streambed - plays a major role in the attenuation of nutrients and organic micropollutants in rivers and surface streams (Jaeger *et al.*, 2019; Lewandowski *et al.*, 2011; Schaper *et al.*, 2019). HZs in urban streams are often degraded and poorly connected with surface water (Lawrence *et al.*, 2013; Walsh *et al.*, 2005). Contamination of urban streams with trace organic contaminants (TOrcs) stemming from anthropogenic sources in stormwater, wastewater, and urban dry-weather flows, may lead to substantial aquatic health impacts in surface waters (LeFevre *et al.*, 2015; Masoner *et al.*, 2019; McKnight *et al.*, 2015; Spahr *et al.*, 2020; Vignet *et al.*, 2019) and drinking water impairments of groundwater aquifers (Kiefer *et al.*, 2019; Loos *et al.*, 2010). For example, elevated TOrcs contamination has been reported in a stream during stormflow as compared to baseflow conditions (Peter *et al.*, 2019). Some of these compounds have been associated with sources such as road runoff (e.g. tire wear) and are similar to compounds associated with stormwater-derived coho salmon acute toxicity (Peter *et al.*, 2019). However, despite substantial water quality challenges, current stormwater management strategies typically prioritize water quantity issues rather than pollutant removal (Grebel *et al.*, 2013). Removal of non-point source contaminants in a stream could be highly effective because it integrates runoff pollution from the entire upstream catchment, compared to most stormwater treatment green infrastructure that treat relatively small areas (e.g., parking lots or developments). Besides its potential for application to in-stream stormwater treatment systems (Herzog *et al.*, 2019), engineered HZs have been increasingly gaining attention in stream restoration for improving stream water quality and aquatic habitat in addition to water quantity benefits (Lawrence *et al.*, 2013; Peter *et al.*, 2019).

A novel technique of HZ engineering targeting water quality degradation was introduced by Herzog *et al.* (2016) under the acronym BEST (Biohydrochemical Enhancements for Streamwater Treatment). BEST alterations include subsurface engineered hyporheic-zone modules that employ 1) vertical impermeable walls across the stream width that drive hyporheic exchange and control HZ residence times, and 2) permeable reactive geomedia amendments in the HZ to enhance biogeochemical reaction rates. In addition to the initial proof of concept (Herzog *et al.*, 2016), the efficiency of the BEST modules has been tested experimentally for the reactive tracer resazurin, which indicates metabolically active transient

storage, and hence served as surrogate for a reactive pollutant degraded aerobically (Herzog *et al.*, 2018). In constructed flume experiments, a BEST flume of 15 m with impermeable walls and woodchip-amended sand streambed increased both resazurin transformation and the size of the effective hyporheic transient storage by >50% compared to an all-sand control of the same length (Herzog *et al.*, 2018). Stream exchange models calibrated to the experimental data suggested that a stream enhanced with BEST modules in series over less than 150 m would remove about 95% of resazurin (Herzog *et al.*, 2018). These results show great promise that BEST modules paired with an appropriate geomedia amendment (depending on the contaminant of interest) can substantially attenuate chemical pollution in stream water. In a larger scale application of methods to enhance hyporheic exchange in an actual urban stream, a reduction of 15-50% of targeted organic contaminants was observed, and the resulting increased hydraulic residence times (HRTs) in the HZ were especially important for increased removal of polar compounds (Peter *et al.*, 2019). However, no significant differences in removal of highly hydrophilic compounds (with $\log K_{OW} < 1$) between the surface water and porewater of shorter HRT flowpaths were found (Peter *et al.*, 2019). Furthermore, hydrophilic TOrCs are a great challenge for stormwater treatment in terms of their toxicological effects and their limited removal in conventional stormwater control measures (SCMs) (Spahr *et al.*, 2020). Overall, these findings highlight the need for a HZ and SCM technology that controls HRTs, while also increasing the biogeochemical reactivity of the streambed to augment the attenuation of challenging pollutants such as hydrophilic TOrCs.

The diabetes medication metformin is an example of a hydrophilic contaminant and one of the most frequently detected organic contaminants in natural and urban streams at concentrations in the $\mu\text{g/L}$ range (Bradley *et al.*, 2016, 2017; Jaeger *et al.*, 2019; Scheurer *et al.*, 2012). Several studies highlighted metformin's endocrine disruption potential associated with intersex and reduced fecundity in fish (Crago *et al.*, 2016; Niemuth & Klaper, 2015, 2018). Typically, the occurrence of metformin has been largely attributed to wastewater treatment plants (WWTPs) (Scheurer *et al.*, 2012), however, it has more recently been widely detected at comparable concentrations in stormwater (Masoner *et al.*, 2019). Furthermore, Bradley *et al.* (2017) found metformin in 89% of samples at 97% of sites in streams of the southeastern U.S. and argued that the near ubiquity of metformin could not be explained by point source discharges (i.e., NPDES discharges). The ubiquitous occurrence of metformin in the water cycle may be due to the fact that it is one of the most prescribed pharmaceuticals worldwide (Scheurer *et al.*, 2012). Unlike other pharmaceuticals, metformin is not metabolized in the human body; therefore, it is excreted unchanged in urine (~70%) or feces, which can lead to very high concentrations in wastewater influents (up to 100 $\mu\text{g/L}$) (Scheurer *et al.*, 2012).

Under aerobic conditions, metformin is degraded to guanyurea (GUA), which has been considered a dead-end transformation product (Trautwein & Kümmerer, 2011), and removal of metformin in WWTPs has been reported in the 53-99% range (Blair *et al.*, 2013; Kosma *et al.*, 2015; Scheurer *et al.*, 2012). Therefore, both metformin and guanyurea are regularly released into receiving surface waters, and the concentration of guanyurea in WWTP effluents may even exceed the concentration of its parent (Kosma *et al.*, 2015). Indeed, in a small wastewater effluent-impacted urban stream in Germany, guanyurea (av. 153 µg/L, max. 222 µg/L) was present at a far greater concentration than metformin (av. 1.0 µg/L, max. 1.66 µg/L) (Posselt *et al.*, 2018). The measured surface water concentrations occasionally exceed the predicted no-effect concentration (PNEC) of 160 µg/L determined for guanyurea (Caldwell *et al.*, 2019). However, others have observed adverse impacts from guanyurea at much lower concentrations towards aquatic organisms: Ussery *et al.* (2019) found that guanyurea negatively impacted the growth of early life stage in fish (Japanese medaka) at concentrations in the ng/L range (compared to µg/L for metformin). When considered alongside the occurrence data, this evidence suggests that guanyurea may pose even more of an imminent threat to aquatic life than metformin, though additional ecotoxicity studies for guanyurea are clearly warranted.

Due to their strong hydrophilic nature (metformin: $\log K_{OW} = -2.64$; GUA: $\log K_{OW} = -1.89$ or -3.57 ; Cui & Schröder (2016)), both metformin and guanyurea are expected to be highly mobile in the aquatic environment (Scheurer *et al.*, 2012). Sorption of metformin to soils and sediments is highly variable, even when accounting for soil type and properties (e.g. organic carbon content, pH, CEC): reported K_d values for metformin range from 3 to 2079 L/kg, with an average of 501 L/kg, whereas literature K_{OC} values spanned five orders of magnitude (Straub *et al.*, 2019). The results of one of the few studies including guanyurea in sorption tests indicate that guanyurea may undergo stronger sorption than metformin (K_{OC} values of 680-1300 L/kg and 270-430 L/kg for guanyurea and metformin, respectively) (Scheurer *et al.*, 2012). Plant uptake and in-planta metabolism of metformin to 1-methylbiguanide (MBG) can be an important loss process from aqueous solution (Cui & Schröder, 2016). In a study on the fate of metformin during riverbank filtration and groundwater recharge, metformin and guanyurea were completely removed to below the limits of quantitation (LOQ), presumably via aerobic degradation (Scheurer *et al.*, 2012). Attempts to enhance removal of metformin via black carbon have met with limited success: removal of metformin from water in laboratory columns packed with activated charcoal (Hormazabal & Ostensvik, 2011), and in activated carbon small scale filter tests (Scheurer *et al.*, 2012), was very limited. However, others have observed metformin removal by granular activated carbon (GAC) filters in different drinking water treatment plants, although biodegradation may have contributed significantly to the observed removal (Scheurer *et al.*, 2012), as a recent assessment concluded that metformin was transformed by the

biofilm on GAC (Piai *et al.*, 2020). Biochar is another black carbon that has shown promise for contaminant removal in pilot-scale biochar-enhanced biofilters (Ashoori *et al.*, 2019; Ulrich *et al.*, 2017a). When targeting a specific contaminant for attenuation by engineered HZs such as BEST, the choice of geomedia (its ability to remove or transform pollutants), manipulation of redox conditions, and the control of subsurface residence times (i.e., HRTs) via hydraulic conductivity modifications are essential design considerations (Herzog *et al.*, 2019).

Streambeds engineered with BEST may have great potential to attenuate ubiquitous TOrCs such as metformin due to the technology's potentially wide application as restoration structures in natural or urban streams, as stream-like SCMs, in the flow-metered effluent of stormwater detention ponds, in persistent dry-weather flows, or as wastewater effluent polishing step before release into receiving surface waters. For this study, we installed full-scale BEST modules in a recirculating flume at an outdoor flume facility (Umweltbundesamt in Berlin, Germany) to test if BEST can efficiently remove a highly polar compound from water. Specifically, we studied the attenuation of metformin in the surface and subsurface over several months under near-natural conditions. To increase the reactivity of the engineered HZ and thus promote the removal of metformin (and potentially guanylurea), the stream sediments in select BEST modules were amended with a pine-wood biochar. Herein, the objectives of this study were to determine the effect of BEST on HZ flow and exchange, redox conditions, and the subsurface attenuation and potential biotransformation of metformin and guanylurea. We specifically designed the BEST modules to 1) increase HZ exchange between surface and subsurface water, and thus 2) create favorable redox conditions for the aerobic degradation of metformin in the downwelling zones of the engineered HZ.

3.3 Methods

This section describes the experimental methods, materials, and procedures used for this study.

3.3.1 Field Site and Flume Experiments

The flume experiments were conducted using an outdoor flume facility (100x1.0x0.45m) at the Umweltbundesamt (UBA; German Environment Agency) in Berlin, Germany (Figure B.1). One treatment flume (spiked) and one control flume (un-spiked) were both operated in recirculation mode (in parallel) in two consecutive experiments: Experiment A (May-August 2018), with a duration of 97 days, and Experiment B (August-November 2018) lasting 98 days. Porewater samples were taken at eight time points during the first 73 days of Experiment A, while only one sample was taken for Experiment B at $t = 10$ days after spiking. Experiment A consisted of spiking the surface water with metformin at ~ 10 $\mu\text{g/L}$ and with the conservative tracer lithium bromide (LiBr; final concentration: ~ 6 mg/L bromide) to account for

total water volume changes of the treatment flume, whereas in Experiment B an elevated concentration of ~ 10 mg/L metformin (and ~ 6 mg/L of bromide) was added. The main focus of Experiment B was to study the formation of transformation products and plant uptake/metabolization of metformin (as part of a companion study). Both flumes (treatment and control) were amended with fine natural sediment and rainwater at a sediment to water ratio of 1:2.5 and incorporated stilling pool sections (slower flow sections) containing different aquatic macrophytes.

3.3.2 Engineered Streambeds – Experimental Setup

Before installation, we investigated several potential experimental set-ups in a simplified 2-D model in COMSOL Multiphysics® to determine the conditions inducing most HZ exchange. This pre-analysis revealed that the combination of a submerged dam and two subsurface BEST plates (upstream: 10 cm distance from dam, downstream: 20 cm distance from dam) would induce a strong downwelling zone as well as flowpaths of varying residence times (see Figure B.2 for COMSOL model results). Figure 3.1 illustrates the subsequent field experimental design. Sections of field-scale constructed streambeds (0.38x1.0x0.45m) were amended with a submerged dam (made of square rocks) and two subsurface BEST walls (stainless steel plates) upstream and downstream of the dam, with or without biochar geomeia. All constructed streambed sections were tested under field-conditions in two consecutive spiking experiments (Experiments A and B).

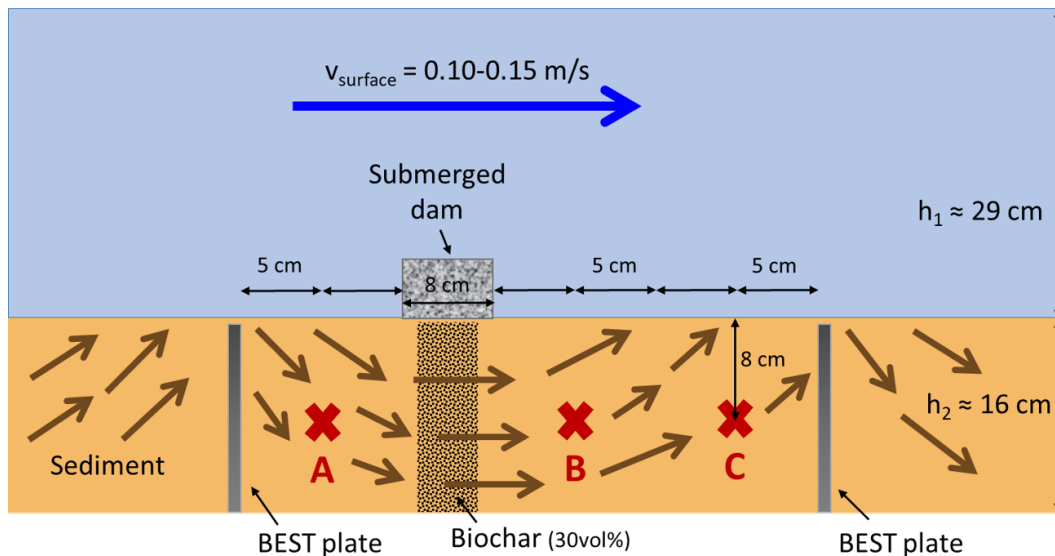


Figure 3.1 Schematic of experimental setup of flume sections amended with engineered structures (BEST plates, submerged dam) and geomeia (biochar). Locations A, B, and C denote HZ sampling locations accessed by vertically introduced MINIPPOINT samplers (each at 8 cm depth). Figure is not to scale to better illustrate sampling features and flow paths.

The tested treatment conditions were as follows: 1) Submerged dam + BEST plates (at 10/20 cm distance from dam): denoted “BEST”; and 2) Submerged dam + BEST plates (at 10/20 cm distance from dam) plus biochar: denoted “BEST+bc”.

The control experimental apparatus included the following: 3) Surface sand dunes (conventional in-stream surface structures) without engineered streambed features: denoted “Dunes”; and 4) Plain sediment (non-altered): denoted “Plain sediment” or “Control”.

Custom-built MINIPPOINT samplers (design based on Posselt *et al.* 2018) were vertically introduced into the flume sediment at a depth of 8 cm from the surface-subsurface interface at three different sampling locations (A – downwelling zone, B and C – upwelling zone). The total length of one BEST module (distance between two BEST plates) was 38 cm (see Figure 3.1). Porewater samples were obtained using syringe pumps at a low flow rate to minimize perturbations of HZ flow due to sample collection.

3.3.3 Engineered Streambeds – Materials

The biochar used in this study was Mountain Crest Gardens biochar (MCG-biochar) produced by high temperature ($> 1100^{\circ}\text{C}$) gasification of pinewood (Gropro, Inc., Etna, CA) and was selected for this study due to its superior performance regarding TOrC removal from water (Ashoori *et al.*, 2019; Ray *et al.*, 2019; Ulrich *et al.*, 2015). Biochar was crushed and sieved to achieve a final particle size range of 0.25-1.00 mm. This range was chosen to blend in optimally with the flume sediment (70% between 0.63–2.00 mm and 26% between 0.18–0.63 mm) to avoid significant reductions in hydraulic conductivity of the final mixture, while keeping the biochar particles as small as possible for faster sorption kinetics. Biochar was analyzed for Brunauer-Emmett-Teller specific surface area (BET SSA) and total pore volume by an external laboratory (Intertek; Allentown, PA, USA). The N_2 isotherms used for BET SSA and total pore volume analyses were measured on a Micromeritics TriStar II Plus unit to full saturation (i.e., a relative pressure of approximately 1.0 at 77 K) and sample activation was performed by degassing at 150°C under dynamic vacuum (Smart VacPrep degas unit). Flume sediment properties and results of the biochar analysis are shown in Table 3.1.

Grain size distribution of the sediment was determined using consecutive sieving (mesh sizes for sediment sieving: 6.3 mm; 2 mm; 0.63 mm; 0.18 mm; 0.063 mm; 0.02 mm). Hydraulic conductivity was measured in three replicate sediment and sediment/biochar cores, respectively, using a KSAT conductivity meter (Meter Group, Pullman, USA). Porosity of the sediment and sediment/biochar mixture was determined by oven-drying three sediment cores of distinct volume. Sediment organic matter content (unamended) was measured by loss on ignition at 450°C of three sediment samples and amounted to 0.152% (± 0.012).

Table 3.1 Physical and chemical properties of streambed materials: flume sediment, sediment / biochar mixture, and biochar. K_{Sat} , porosity, and organic matter content data are provided as average \pm standard deviation.

Properties	Sediment	Sediment/Biochar	Biochar
Particle size range [mm]	0.63 – 2.00 (70%), 0.18 – 0.63 (26%)	0.18 – 2.00	0.25 – 1.00
Saturated hydraulic conductivity (25°C) [m/s], K_{Sat}	1.82E-04 (\pm 3.16E-05)	1.72E-04 (\pm 5.76E-05)	^b
Porosity [-], n	0.33 (\pm 0.01)	0.44 (\pm 0.01)	^b
Organic matter content [%], f_{OM} ^a	0.152 (\pm 0.012)	^b	^b
Specific surface area [m ² /g], SSA	^b	^b	627
Total pore volume [cm ³ /g], PV	^b	^b	0.337 (61% micro PV)

^a $f_{OC} = 0.076 \pm 0.006$, with $f_{OC} = f_{OM}/2$.

^b Parameter not measured.

Temperature, dissolved oxygen (DO), turbidity, electric conductivity (600 ± 50 μ S/cm) and pH (8.2 ± 0.4) in the stream surface water were measured hourly via online systems. The surface water flow was set to 8 cm/s and was confirmed using a handheld electromagnetic water flow meter (OTT MF Pro, OTT HydroMet, Kempton, Germany). DO profiles in streambed pore water were determined in situ using needle sensors (Unisense A/S, Århus, Danmark) attached to an aluminum pole (0.5 cm diameter), which was height-adjusted using a micromanipulator (MM 33, Märzhäuser Wetzlar GmbH & Co., Wetzlar, Germany).

3.3.4 Analytical Chemical Analysis of Surface and Streambed Water

Nutrients and Tracers. Nutrients (i.e. ammonium, NH_4^+ , and iron, mainly present in the form of Fe(II)) were determined in sediment pore water using a microtiter plate reader (Sunrise, Tecan) combined with a small-volume photometry method published previously (Laskov et al., 2007). For Fe(II) and NH_4^+ , six timepoints were analyzed during Experiment A: background (BG) concentration and five samples (T1-T5) after spiking between May 08 – May 24, 2018 (first 16 days). The samples were analyzed in duplicate (BG, T1, T2) or triplicate (T3-T5). Lithium (Li^+), bromide (Br^-) and sulfate (SO_4^{2-}) were determined photometrically at UBA via ion chromatography (IC) using a 930 Compact IC Flex system (Metrohm, Switzerland).

Target Analysis of Metformin and Guanylylurea. Surface and pore water samples were analyzed at Stockholm University for metformin and guanylylurea (GUA) using a small volume direct injection-ultra

high-performance liquid chromatography method coupled to tandem mass spectrometry (UHPLC-MS/MS) following a standard protocol described in detail by Posselt *et al.* (2018). The quality control relative standard deviation (%RSD) associated with the analysis was 5% for metformin and 3% for GUA, respectively. Method limits of detection (LOD) for metformin and GUA were 0.2 and 0.4 $\mu\text{g/L}$, while limits of quantitation (LOQ) values were at 0.4 and 0.8 $\mu\text{g/L}$, respectively. Measured metformin surface water concentrations were adjusted with the tracer bromide to correct for water volume changes in the flume as a consequence of evaporation and precipitation (rainfall).

Samples from batch sorption experiments and select flume samples for suspect screening (described below) were quantified at the Colorado School of Mines by liquid chromatography quadrupole time-of-flight mass spectrometry (LC-QToF-MS) using a SCIEX ExionLCTM high-performance liquid chromatography (HPLC) system equipped with a Luna Omega Polar C-18 analytical column (3 μm , 150x4.6 mm; Phenomenex, Torrance, CA), coupled to a SCIEX X500R QToF-MS system (Framingham, MA) using electrospray ionization in positive mode (ESI+) with SWATH[®] Data-Independent Acquisition for both ToFMS and MS/MS mode. Further details on the MS parameters and chromatography conditions can be found in Appendix B. LOQs were 0.25 $\mu\text{g/L}$ for both metformin and MBG, and 1 $\mu\text{g/L}$ for GUA. Quality control samples were run every ten samples to ensure data consistency and quality over the entire run time.

LC-HRMS Suspect Screening. For a subset of samples collected from the flume experiments (subsurface samples from Experiment B at $t = 10$ days after spiking), we employed a suspect screening approach to identify additional transformation products (TPs) of metformin, which was spiked at ~ 10 mg/L. LC-QToF-MS data acquired in SWATH[®] mode was screened using a custom extracted ion chromatogram (XIC) list (Table B.3) containing molecular formulas and exact masses for potential TPs. Identification of suspect TPs was based on accurate mass measurement for the molecular precursor ion (mass error < 5 ppm) and retention time consistency across samples (ΔRT within 0.1 min). Isotope patterns were not used as a quality control measure due to high isotopic pattern errors ($> 40\%$) at low aqueous concentrations for all suspects studied. Samples were screened by searching for the protonated molecular ion $[\text{M}+\text{H}]^+$ using an XIC window of 0.02 Da, a signal to noise threshold of 10:1, and a noise percentage of 90%. A confidence level was assigned to each suspect compound on the basis of the Schymanski scale (Schymanski *et al.*, 2014).

3.3.5 Batch Experiments

Batch Sorption Experiments with Biochar. Laboratory-scale batch sorption experiments were conducted to study the sorption kinetics of metformin, GUA, and MBG to the selected pine-wood biochar. Experimental methods and batch sample preparation steps were as described previously (Portmann *et al.*, 2022). In brief, the kinetic batch tests were carried out in triplicates with the serial method following

OECD guidelines 106 (OECD, 2000) using 6.5 ± 0.1 mg of biochar and an initial TOxC concentration of 10 $\mu\text{g/L}$ (each for metformin and GUA). Isotherm batch tests were carried out in triplicate autoclaved glass bottles at five different initial concentrations (metformin and MBG: $C_0 = 3, 10, 20, 50,$ and $100 \mu\text{g/L}$ each; GUA: $C_0 = 12, 40, 80, 200,$ and $400 \mu\text{g/L}$) and an average biochar mass per batch of 25.0 ± 0.6 mg. Control batches without biochar were set up to account for abiotic losses of TOxCs such as sorption to glass or aqueous hydrolysis. Samples were taken in the beginning ($t = 1$ d) from controls only and at the end ($t = 67$ d) from treatments and controls.

Best-fit parameters of the Freundlich and Langmuir isotherms were obtained from the equilibrium sorption data (biochar) using non-linear regression with relative weighting ($1/Y^2$) in the statistics software GraphPad Prism (version 9.1.1). Akaike's Information Criterion (AIC) was used to compare the goodness of fit of both sorption equations for each compound. Both the AIC and best-fit parameters of the non-linear Freundlich isotherm (Freundlich coefficient K_F , exponent n) and the best-fit values of the non-linear Langmuir isotherm (adsorption capacity Q_{max} , constant K_L) are reported in the SI (Table B.5). In terms of kinetics, a pseudo-first order adsorption model (assumption: desorption is negligible) was fitted to the apparent distribution coefficient ($K_{d,app} = C_S/C_W$) data over time to estimate the adsorption kinetic rate constant k_{ad} and the distribution coefficient at equilibrium $K_{d,eq}$ (Table B.4). All statistical follow-up tests were performed in GraphPad Prism.

In-Field Bottle Experiments with Sediment/Biochar. In the field, removal of metformin was studied under semi-controlled batch conditions using glass bottles partially submerged in flume water over a duration of 75 days during flume Experiment A. This experimental set-up was chosen to mimic environmental temperature, sunlight exposure, and microbial community present in the flumes, while removing the dynamic flow aspect. The five studied conditions (each in triplicate) were as follows: sediment + biochar biotic, sediment biotic, sediment + biochar abiotic, sediment abiotic, and abiotic control (water only). The setup of the bottles was carried out according to the following procedure: 100 mL of media (either 100% sediment or sediment containing 33 vol% biochar) were added to 500 mL Pyrex glass bottles and combined with 300 mL of un-spiked flume water to reach a final media:water ratio of 1:3, similar to the ratio employed in the flumes (1:2.5). Abiotic bottles were autoclaved at 121°C for 20 min prior to the start of the experiment. The target concentration of metformin in the bottles was $100 \mu\text{g/L}$ and was spiked by adding 0.5 mL of spiking solution (60 mg/L metformin-HCl in deionized water) to each bottle, which marked $t = 0$ of the experiment. Biotic bottles were aerated continuously throughout the experiment using fish tank aeration devices, whereas the lids of autoclaved bottles were kept closed to avoid microbial contamination (except during sampling).

3.4 Results and Discussion

3.4.1 Biochar Batch Sorption

Results from kinetic batch sorption experiments showed that after 67 days of exposure to MCG biochar, removal of metformin and GUA amounted to 18% and 69%, respectively (Figure 3.2a). The treatment data (exposed to MCG-biochar) is statistically significantly different from the control data for both metformin and GUA ($p = 0.0341$ and $p = 0.0145$, respectively; Paired t-test; $\alpha = 0.05$). The concentration over time data indicates that equilibrium conditions in the case of metformin were reached after three days, because the concentration stayed relatively constant for the remainder of the experiment. These results indicate that sorption may have been limited by the number or availability of suitable sorption sites, and that simply adding a greater mass of biochar may lead to a greater removal of metformin (which was demonstrated in on-site bottles experiments; see Figure B.5).

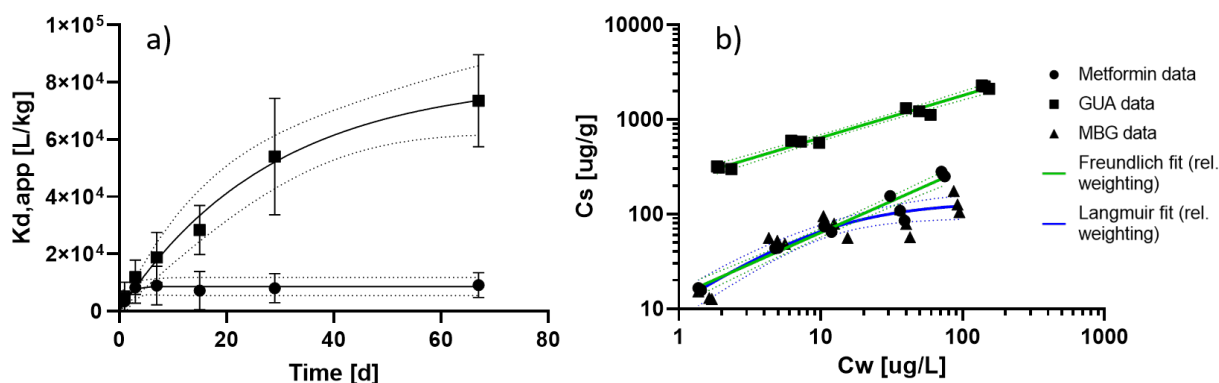


Figure 3.2 Biochar batch sorption experiments: a) Kinetic sorption data for metformin and guanylurea (GUA) with pseudo-first order fit of the apparent distribution coefficient ($K_{d,app} = C_S/C_W$) over time. Solid lines represent best fits and dashed lines represent the 95% confidence intervals. b) Sorption isotherms for metformin, GUA, and 1-methylbiguanide (MGB); best-fits of the Freundlich and Langmuir isotherms were obtained via non-linear regression with relative weighting ($1/Y^2$). All analyses were performed in GraphPad Prism (version 9.1.1). Estimated best-fit parameters can be found in the SI (Tables B.4 and B.5). Biochar source: pine wood, gasification process, $>1100^\circ\text{C}$ (Gropro, Inc., Etna, CA).

Within a wide pH range (pH 7 ± 4), metformin is present as monoprotonated cation (Hernández *et al.*, 2015). Thus, mechanistically, sorption of metformin likely occurred via electrostatic interactions with the biochar surface (negatively charged), although $\pi - \pi$ electron donor acceptor (EDA) interactions, chemisorption, and pore filling via diffusion have been suggested as well (Shearer *et al.*, 2022). Contrary to metformin, its degradation product GUA showed promising removal by biochar even at low biochar mass percentages (~ 6.5 mg biochar in 200 mL synthetic stormwater) with 10 $\mu\text{g/L}$ initial concentration. The equilibrium sorption coefficient, $K_{d,eq}$, was significantly greater for GUA (73,560 L/kg) compared to

metformin (9112 L/kg; t-test: $p = 0.0026$; $\alpha = 0.05$) and corresponded well with the estimated $K_{d,eq}$ (best-fit; Table B.4). Comparable results with greater sorption for GUA compared to metformin were reported from laboratory batch experiments using autoclaved biological GAC: the removal of metformin at 20°C after 53 days was 15%, whereas GUA was removed by 79% under the same conditions (Piai *et al.*, 2020).

Fitting of sorption isotherms to equilibrium data revealed that sorption of metformin and GUA are best described by a Freundlich isotherm, whereas MBG follows a Langmuir sorption behavior (Figure 3.2b). Figure 3.2b illustrates the significantly greater sorption capacity for GUA to biochar compared to metformin for a wider spectrum of aqueous concentrations (Freundlich coefficient $K_F = 13$ and 230 (ug/g)/(ug/L)ⁿ for metformin and GUA, respectively; Table B.5). Similarly, sorption of metformin to macroalgae biochar was well described by the Freundlich model with up to 76% metformin removal, mainly attributed to surface functional group interactions (De Bhowmick *et al.*, 2022).

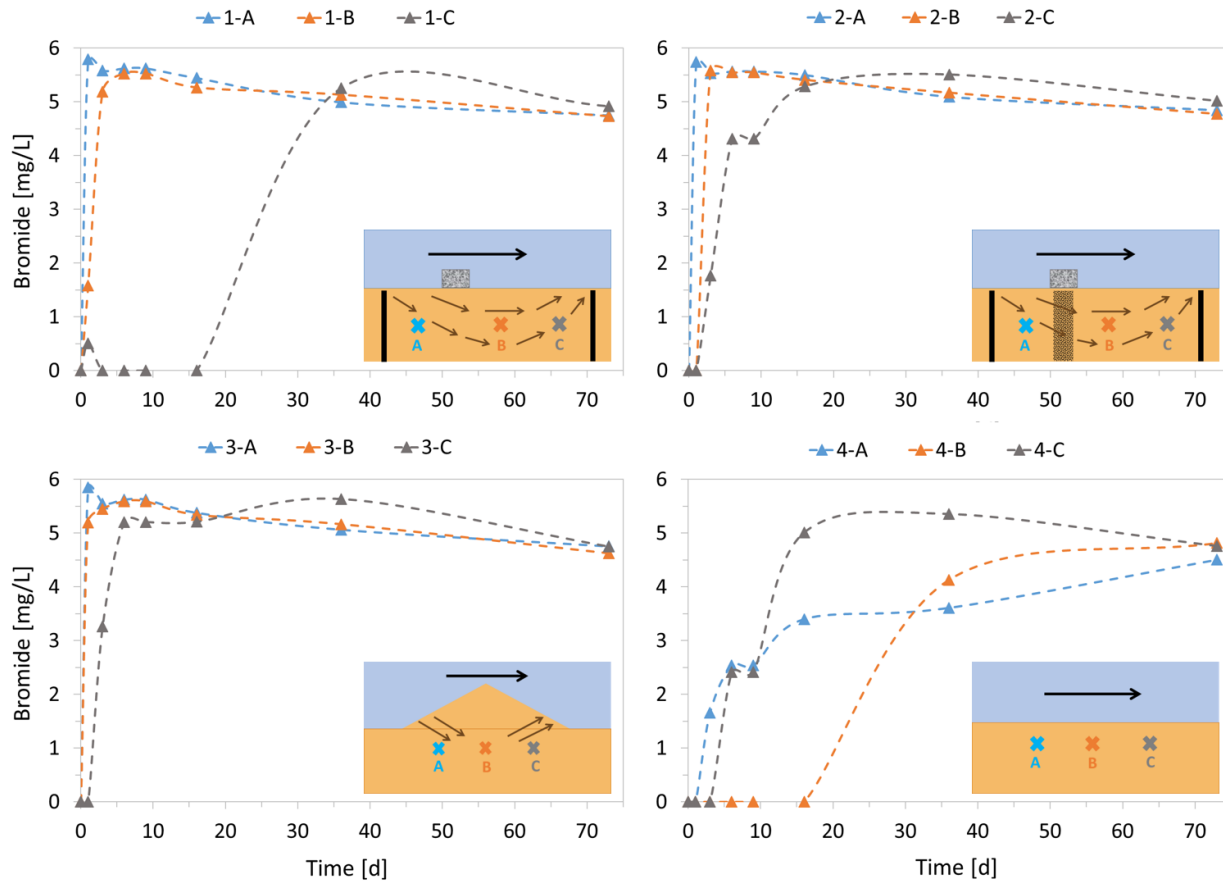


Figure 3.3 Subsurface breakthrough curves of bromide (conservative tracer) for different conditions: 1) BEST (top left), 2) BEST + biochar (top right), 3) Surface sand dunes (bottom left), and 4) Plain sediment, non-altered (bottom right). Locations A, B, and C denote subsurface sampling locations (see schematic in Figure 3.1).

3.4.2 HZ Flow and Exchange in Engineered Streambeds

In the flume, breakthrough (BT) of the conservative tracer bromide was observed to be faster in engineered sections (BEST, BEST+bc, sand dunes) compared to the non-altered plain sand section (see Figure 3.3 on page 50), and initial BT time (defined as the time when $C_{PW} = 0.05 * C_{SW}$) was consistent with distance along flow paths ($BT_A < BT_B < BT_C$). Mean values of saturated hydraulic conductivity measured in triplicates from fresh sample cores of flume sediment and sediment+biochar mixtures (1.82E-04 m/s and 1.72E-04 m/s, respectively; see Table 3.1) were not significantly different from each other ($p = 0.7991$; unpaired t-test, $\alpha = 0.05$): the presence of MCG-biochar at 30 vol% and at the particle size range applied (0.25-1.00 mm) did not compromise hydraulic conductivity of the mixture, at least for initial (unaged biochar) conditions. This is important, because hydraulic conductivity of the streambed is one of the most crucial factors governing the extent and magnitude of hyporheic exchange in streams (Cardenas, 2015; Ward *et al.*, 2011).

3.4.3 Redox Conditions in Engineered Streambeds

DO penetration depth (i.e., increased DO in the streambed porewater with depth from penetrating higher-DO surface water) in the downwelling area of the HZ was greatest in the case of biochar-amended BEST for both May and June measurements, and the maximum depth where $DO > 0$ mg/L was generally larger for the engineered sections (BEST, BEST+bc) (Figure 3.4) vs. a non-altered control section (Figure B.6). Results from a field study in an actual stream indicated that higher HZ exchange fluxes led to deeper oxygen penetration depths (Harvey *et al.*, 2013), which could explain the greater size and distribution (down-welling vs. upwelling) of oxygenated zones in the engineered flume sections (BEST and BEST+bc) compared to the plain sand control.

The distinct succession of redox conditions created along the HZ flowpaths of BEST (and BEST+bc) seems to be well suited to attenuate both metformin and GUA: recent batch experiments with activated sludge studying the biodegradation of metformin and GUA revealed that while metformin degradation was faster under aerobic conditions, degradation kinetics for GUA were more rapid under low oxygen concentrations (suboxic/anoxic) (Tisler & Zwiener, 2019). Whereas the highly oxygenated downwelling zone of BEST favors the microbial transformation of metformin to GUA, the further degradation of GUA would be enhanced as the water moves along the increasingly anoxic hyporheic flowpaths. Observed DO oversaturation (up to 35 mg/L; Figure 3.4) was attributed to photosynthetic activity of algae biofilms growing near the sediment and surface water interface.

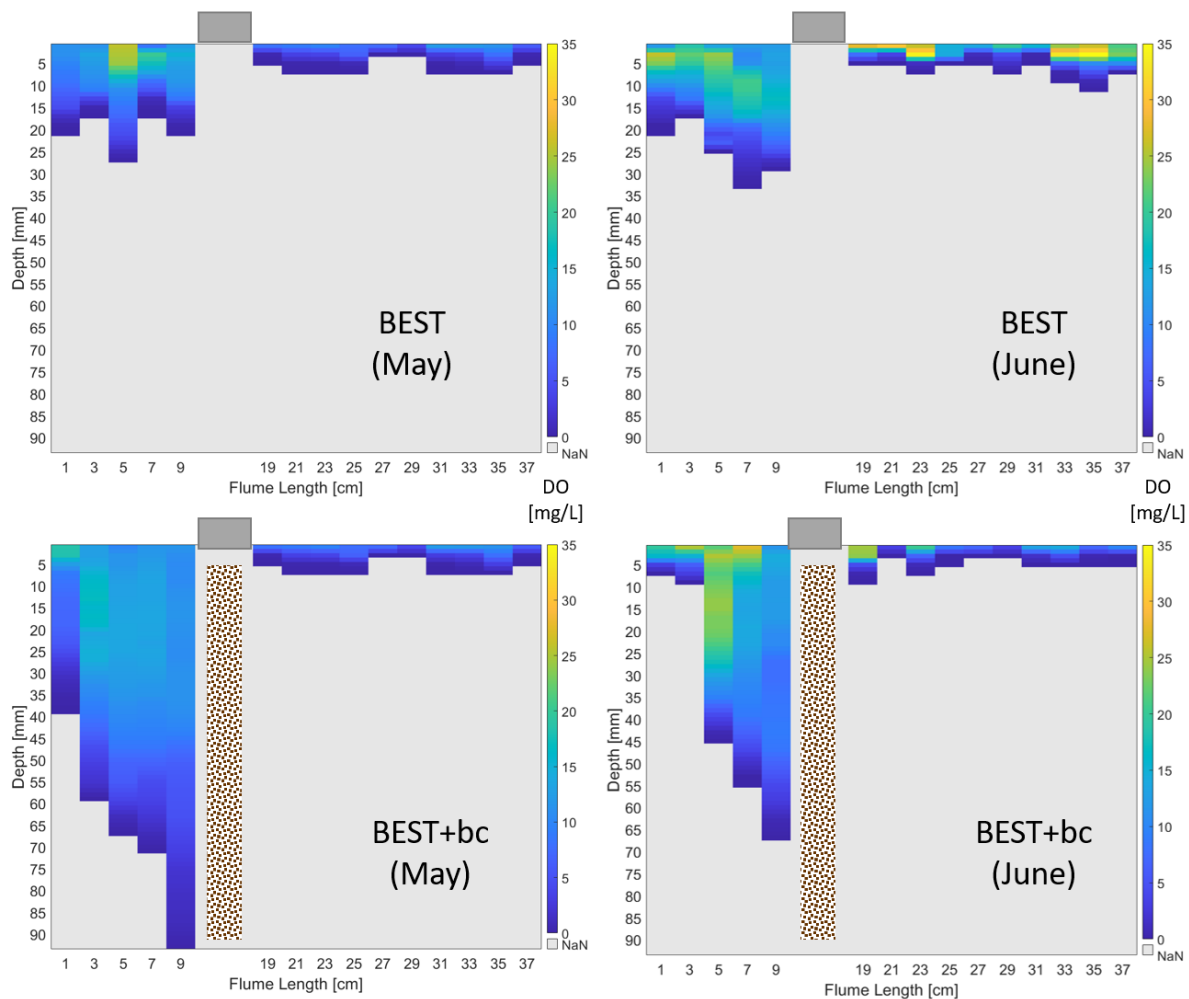


Figure 3.4 Dissolved oxygen (DO) profiles of subsurface flume sections. Top panel: Left: BEST (May 2018), Right: BEST (June 2018); Bottom panel: Left: BEST+biochar (May 2018), Right: BEST+biochar (June 2018). DO values on color legend are mg/L.

As can be seen in Figure 3.5, both BEST and BEST+bc engineered streambeds lead to increasingly reducing conditions (as evidenced by Fe(II)) along hyporheic flowpaths, specifically in the upwelling zone of the flowpath with longer HRT (sampling point C), but also along the deeper downwelling flowpaths. This was not the case in the dunes or in the plain sand control section; which showed the opposite trend with increasingly oxygenating conditions along sampling locations A to C. The measured concentrations of dissolved Fe(II) at upwelling location C were greater in BEST (without biochar) compared to all other conditions. Ammonia (NH_4^+) concentrations were generally lowest in the downwelling zone (location A) of the engineered sections (BEST, BEST+bc, dunes) – probably because nitrification (conversion of NH_4^+ to NO_3^- and/or NO_2^-) was elevated in the downwelling zone due to higher oxygen concentrations (see DO profiles in Figure 3.4). The distinct succession of highly oxygenated porewater observed in the downwelling

zone of BEST due to greater HZ exchange and the subsequently greater reducing conditions in the upwelling zone of the longer HRT flowpath C is remarkable and may explain the observed greater and faster attenuation of metformin (oxygenated downwelling zone) and also potentially GUA (reducing upwelling zone) in the HZ of BEST compared to surface sand dunes or unamended control areas.

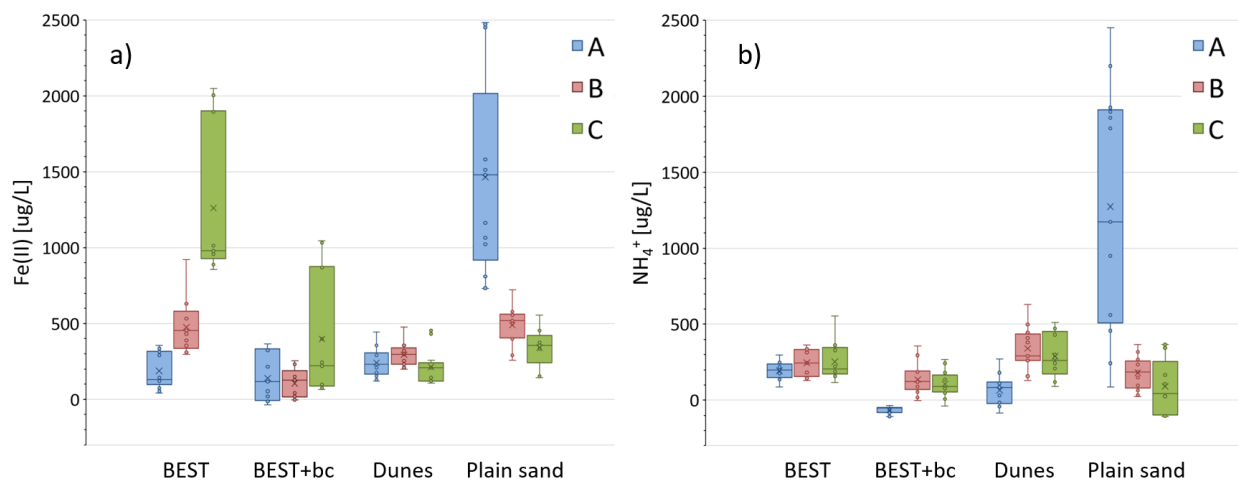


Figure 3.5 Subsurface nutrient summarized in a box and whisker plot: a) Iron(II) measurements during the Day 1 to 16 time period; b) Ammonium (NH_4^+) measurements during the Day 1 to 16 time period. A, B, and C denote the subsurface sampling locations in each condition (see Figure 3.1).

3.4.4 Attenuation of Metformin/Guanylurea in Engineered Streambeds

Metformin BTCs in the HZ of different conditions in the pilot-scale streambed measured during Experiment A are shown in Figure 3.6. Removal of metformin in the HZ of BEST (condition 1; top left panel, Figure 3.6) was greater with longer flowpaths, suggesting greater HZ residence times lead to enhanced attenuation. GUA was not detected above the LOQ of 0.8 µg/L in the subsurface, suggesting further degradation (possibly mineralization). As no metformin nor GUA were detected in the porewater of upwelling zones (B, C) in BEST+bc (condition 2; top right panel, Figure 3.6), the amendment of BEST with biochar likely resulted in the complete removal of metformin along the flowpaths.

Comparing the metformin BTCs of BEST with a conventional surface restoration structure, i.e. sand dunes (condition 3; bottom left panel, Figure 3.6), revealed that BEST structures led to a larger decrease in concentration in both the downwelling and upwelling zones: the maximum measured concentrations in location A were 6.31 µg/L and 7.85 µg/L for BEST and the sand dunes, respectively. The decrease in BTC amplitude in the downwelling zone was even more pronounced when biochar was added to the BEST structure (peak metformin concentration: 3.02 µg/L). Furthermore, we observed pronounced concentration differences at the last sampling time point ($t = 73$ days) between BEST and the sand dunes structures: the

metformin surface water concentration had diminished from 10 to ~ 3.5 $\mu\text{g/L}$ at this timepoint (see Figure B.3), which was well reflected in all HZ sampling points of the sand dunes. In the BEST condition, however, only the downwelling zone was showing a metformin concentration (3.07 $\mu\text{g/L}$) close to the surface water concentration, whereas concentrations at both sampling points B and C were clearly diminished (1.42 $\mu\text{g/L}$ and $<\text{LOQ}$, respectively). This means that the attenuation of metformin between both flowpaths A-B and B-C was significant as compared to the surface water.

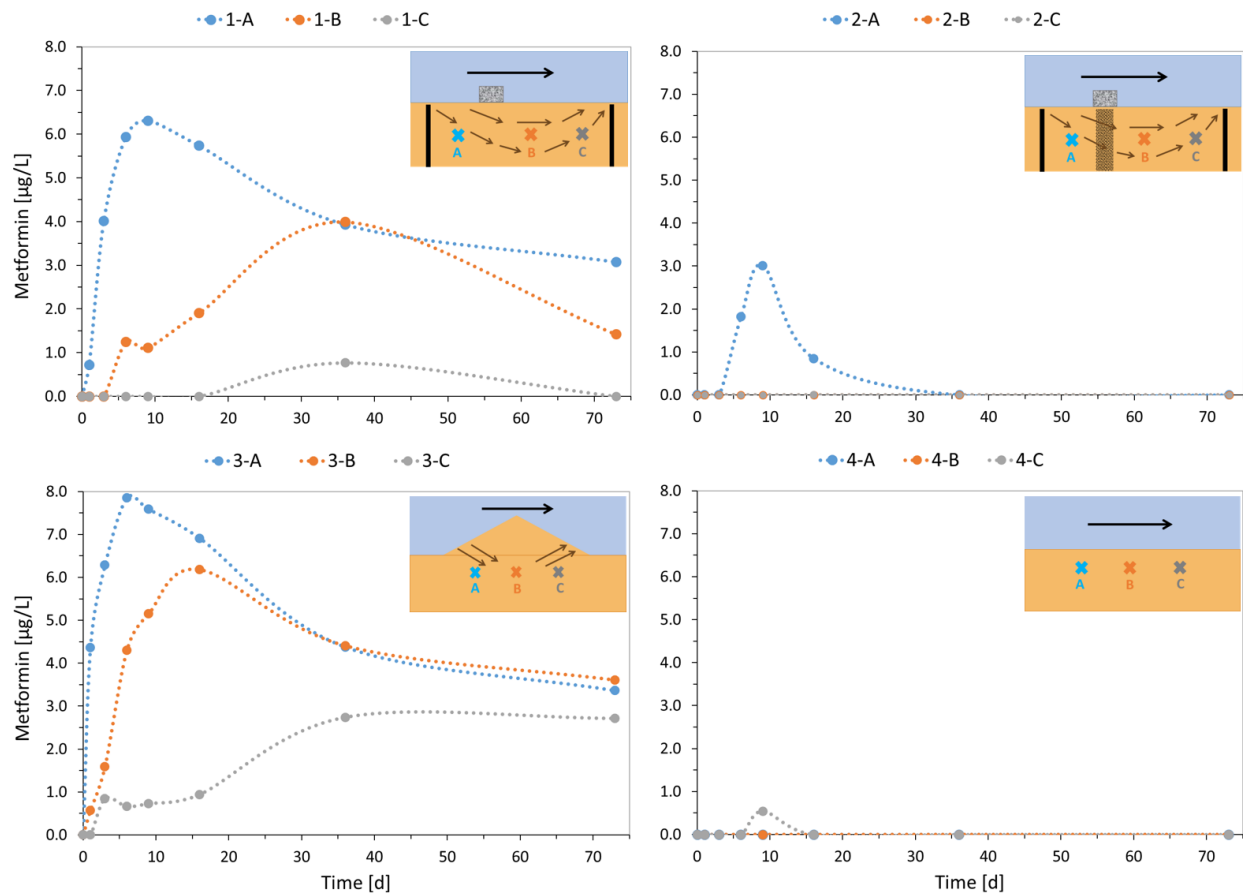


Figure 3.6 Subsurface breakthrough curves of metformin for different conditions: 1) BEST (top left), 2) BEST + biochar (top right), 3) Surface sand dunes (bottom left), and 4) Plain sediment, non-altered (bottom right). Locations A, B, and C denote HZ sampling locations (see Figure 3.1). Relative standard deviation (%RSD) associated with the analysis was 5% for metformin and 3% for guanylyurea, respectively.

Removal rate constants of TORCs in the HZ may vary greatly depending on prevailing redox conditions (Greskowiak *et al.*, 2017; Schaper *et al.*, 2018). The spatial distribution of subsurface redox zones is a combined function of hydrologic conditions (e.g. vertical exchange fluxes), biogeochemical parameters (e.g. availability of electron donors/acceptors, microbial activity, and sediment organic matter content) (Schaper *et al.*, 2018), as well as temperature (Burke *et al.*, 2014). Schaper *et al.* (2018) reported significantly higher

removal rates for several pharmaceuticals under predominantly suboxic (i.e. denitrifying) compared to anoxic (i.e. Fe and Mn reducing) conditions, whereas shorter first-order half-lives of the pesticide fipronil were determined in anaerobic (reducing) sediments (4.6-18.5 days) compared to facultative (aerobic) conditions (25-91 days) (Lin *et al.*, 2008). In this manner, BEST streambeds may offer a great variety of redox conditions (from highly oxygenated to reducing to potentially fully anaerobic) along hyporheic flowpaths and may thus be suited to create favorable microbial degradation environments for a wide range of TOxCs – not only metformin and/or GUA.

3.4.5 Biodegradation of Metformin (Suspect Screening)

During Experiment B (10 mg/L spike of metformin), four TPs in addition to GUA were identified in surface and subsurface water samples (Figure 3.7; surface water data not shown): MBG, 2-4-AMT / 4-2-1-AIMT, 2-4-DAT, and biguanide. Note that the structural isomers 2-4-AMT and 4-2-1-AIMT (see Table B.3) were not distinguished here based on the LC-HRMS data collected.

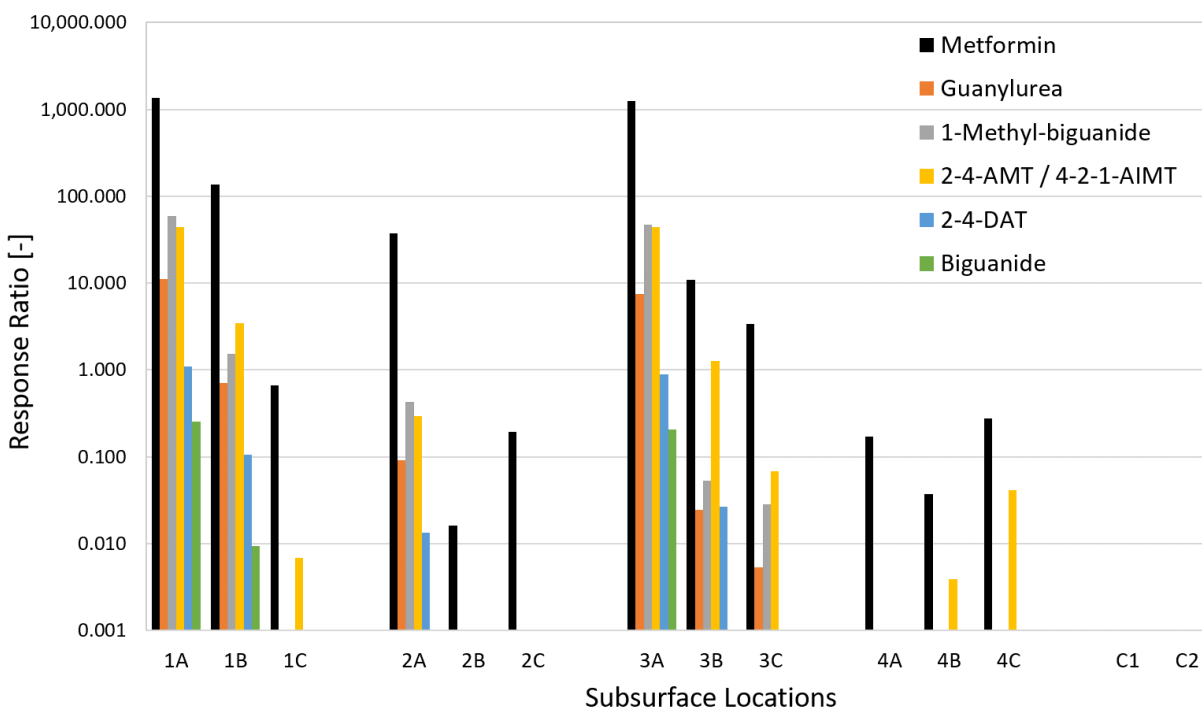


Figure 3.7 Transformation products (TPs) of metformin measured during Experiment B (10 mg/L spike) for the following conditions: 1) BEST, 2) BEST + biochar, 3) Surface sand dunes, and 4) Plain sediment, non-altered; C1/C2 are samples from the control flume (un-spiked). Locations A, B, and C denote subsurface sampling locations (see Figure 3.1). Sampling time was August 24th 2018, i.e. 10 days after spiking. Response ratios for TPs were determined relative to metformin- d_6 ($Area_{TP}/Area_{metformin-d_6}$). Confidence level of identification according to Schymanski scale: metformin, guanylurea, and 1-methyl-biguanide: 1; others: 3.

For the engineered conditions (BEST, BEST+bc, sand dunes), the highest production of TPs occurred in the zone of sampling point A (downwelling), with decreasing amounts detected along the HZ flowpaths (locations B, C). The patterns found in locations 1-A (BEST) and 3-A (dunes) are very similar, indicating that the downwelling zones of BEST and conventional surface structures lead to comparable biotransformation environments.

Locations B and C (upwelling) of the BEST+bc structure show remaining metformin concentrations but no suspect compounds, likely due to the strong sorption properties of the pine-wood biochar. Biochar is also known for creating favorable conditions for microbial attachment and biofilm formation (Hale *et al.*, 2015; Luo *et al.*, 2013), which has been shown to enhance overall TOrC removal and biodegradation (Frankel *et al.*, 2016; Liu *et al.*, 2017a; Portmann *et al.*, 2022). In the joint presence of biochar and biofilm, biodegradation of organic compounds may happen in the sorbed phase (Yu *et al.*, 2015); in this case, the detection of degradation products in the aqueous/dissolved phase is expected to be limited. The plain sand section (condition 4; Figure 3.7) showed no clear pattern of TP formation along the flowpaths and the only TP detected was 2-4-AMT / 4-2-1-AIMT. All four TPs were detected in surface water samples of the treatment flume, at levels comparable to the ones observed in HZ sampling locations A. However, none of the suspect TPs were detected in surface water or porewater samples from the un-spiked control flume (porewater samples denoted as "C1", "C2"; Figure 3.7).

3.5 Conclusions

Both metformin and GUA were effectively removed when exposed to biochar in an aqueous batch solution, although GUA exhibited a significantly greater sorption capacity at equilibrium: after 67 days, we observed 18% and 69% removal for metformin and GUA, respectively ($\log K_{d,eq} = 3.96$ L/kg and 4.87 L/kg for metformin and GUA, respectively). Biochar sorption isotherms for both compounds were best described by the Freundlich equation. Hydraulic conductivity testing confirmed that the presence of the pine-wood biochar at 30 vol% and at the particle size range applied (0.25-1.00 mm) did not compromise the saturated hydraulic conductivity of the sediment-biochar mixture, since the parameter was similar for sediment cores with and without biochar. In both BEST and BEST+bc streambeds, initial BT time of the tracer bromide in the porewater was consistent with distance along HZ flow paths ($BT_A < BT_B < BT_C$). When metformin was added at $C_0 = 10$ $\mu\text{g/L}$ to the stream surface water, removal in the HZ of BEST was greater with longer flowpaths, suggesting that engineered streambeds with greater HZ residence times lead to enhanced adsorption and potentially biodegradation of metformin. Guanylurea (TP of metformin) was not detected above 0.8 $\mu\text{g/L}$ in the subsurface, suggesting further degradation was occurring (possibly full mineralization). Amendment of a BEST streambed with biochar resulted in a pronounced decrease in

metformin breakthrough curve amplitude in the downwelling zone of the HZ. No metformin was detected in the porewater of the upwelling zone, thus the presence of biochar in the engineered streambed resulted in complete removal of metformin along the flowpaths. Next, we studied the prevailing redox conditions in BEST streambeds: Dissolved oxygen penetration depths in the downwelling area of the HZ were greater in BEST streambeds compared to controls (i.e. surface dunes, un-altered sediment), likely due to increased hyporheic exchange with the oxygen-rich surface water. Redox conditions became more reduced along flowpaths, as evidenced by greater Fe(II) concentrations in the upwelling zones of the streambeds. The unique succession of redox conditions along hyporheic flowpaths in BEST streambeds presented ideal biotransformation conditions for the studied TOrCs: Whereas the highly oxygenated downwelling zone favors the microbial transformation of metformin to GUA, further degradation of GUA would be enhanced along the increasingly anoxic hyporheic flowpaths. When metformin was spiked to the flume at a higher dose ($C_0 = 10$ mg/L) to further study biodegradation, four additional transformation products were identified in surface water and porewater samples: 1-methyl-biguanide, 2-4-AMT / 4-2-1-AIMT, 2-4-DAT, and biguanide. We conclude that BEST streambeds attenuated metformin through a combination of adsorption and microbial transformation. Altogether, these results show that BEST engineered streambeds – especially when amended with a strong geosorbent (e.g. biochar) – may be an effective novel HZ technology for improving streamwater quality by attenuating highly polar and ecotoxic contaminants such as metformin and GUA, which pose a substantial threat to aquatic life, surface water quality, and drinking water resources.

CHAPTER 4
ENGINEERED STREAMBEDS FOR THE REMOVAL OF PESTICIDES AND PHARMACEUTICALS
FROM STORMWATER

Manuscript in preparation for publication.

Andrea C. Portmann^{15,16}, Brittnee N. Halpin¹⁵, Donovan Keohane¹⁵, John E. McCray¹⁵, Christopher P. Higgins^{15,17}

4.1 Abstract

This study evaluated the efficiency of hyporheic zone (HZ) engineered streambeds for the attenuation of a broad suite of stormwater-relevant trace organic chemicals (TOrcs), including pesticides, pharmaceuticals and personal care products (PPCPs), and a perfluoroalkyl acid. The performance of several different Biohydrochemical Enhancements for Streamwater Treatment (BEST) streambed modifications to artificial flumes was experimentally evaluated: 1) BEST streambeds, 2) BEST streambeds amended with biochar, 3) BEST streambeds containing fine-grain sand mixed with biochar, and 4) a sand-only control streambed. We conducted two types of experiments for each of the four flumes: simulated stormflow experiments to study TOrc surface and porewater breakthrough behavior, as well as recirculation experiments (over 15 days) to collect long-term performance data and to examine TOrc transformation product (TP) formation over time. We found that under stormflow conditions and at limited flume length (15 m, 14 BEST modules), biochar-amendment of BEST streambeds was necessary to provide both efficient reductions in TOrc concentration peaks and mass loadings. Extended contact time (15 days) was needed to increase removal in the sand-only systems, however, removal was only >78% for compounds that were either fairly hydrophobic (diazinon, fipronil, ibuprofen), or more easily biodegradable (atenolol, caffeine, ibuprofen, MCPA). On the module-scale, removal was greater in streambeds containing fine-grain sand (creating longer hydraulic residence times) or in the presence of biochar. A total of 30 different TPs were detected in the surface and subsurface water of the flumes – predominantly in sand-only systems. Insights gained from these pilot-scale flume experiments allow for the establishment of design recommendations for BEST engineered streambed applications.

¹⁵Department of Civil & Environmental Engineering, Colorado School of Mines

¹⁶Primary researcher and author

¹⁷Corresponding author

4.2 Introduction

A common feature of urban spaces is the increased share of impermeable surfaces, which create greater runoff volumes and less infiltration compared to undeveloped areas (Grebel *et al.*, 2013). At the same time, anthropogenic spaces are characterized by emissions of multiple man-made chemicals and pollutants – stemming from vehicle traffic, building roofs, urban green space management (e.g., pesticide application), and health management practices (e.g., pharmaceuticals). These diffuse sources of trace organic chemicals (TOrcs) contribute to stormwater runoff pollution and water quality degradation of urban streams or nearby water bodies (LeFevre *et al.*, 2015; Masoner *et al.*, 2019). Polar TOrcs, which are typically predominantly in the dissolved phase, are specifically challenging for urban stormwater management due to their limited removal in conventional stormwater control measures (SCMs) (Spahr *et al.*, 2020). Furthermore, many TOrcs are (eco)toxic and may pose human or ecological health risks, specifically towards aquatic biota (LeFevre *et al.*, 2015). Toxicological effects may be multifaceted and impact different aspects of aquatic life: reported effects include coho salmon acute toxicity (Peter *et al.*, 2019) and endocrine disruption potential associated with intersex and reduced fecundity in fish (Niemuth & Klaper, 2015). Some neonicotinoid insecticides (and their metabolites) showed adverse effects on early life stages in fish (Vignet *et al.*, 2019), increased bee mortality (Suchail *et al.*, 2001), and oxidative stress towards aquatic non-target organisms such as freshwater algae (Malev *et al.*, 2012). Pesticides are *the* most prevalent organic substance class in urban stormwater in the United States (Masoner *et al.*, 2019). Minimizing such impacts on receiving water bodies from TOrcs is increasingly recognized as an urgent need for urban stormwater management (Wolfand *et al.*, 2019).

To date, stormwater management has primarily focused on capturing large runoff volumes quickly (e.g., detention ponds) and depending on physical processes (e.g., settling, filtration) to remove particles from the water (LeFevre *et al.*, 2015). An analysis of organic chemicals in stormwater pond sediments revealed that the dominant substance classes were legacy contaminants such as polychlorinated biphenyls (PCBs), polycyclic aromatic hydrocarbons (PAHs), organotins, hydrocarbons, and phthalates, while only 13 out of the 114 investigated pesticides were detected in sediments (Flanagan *et al.*, 2021). Thus, it appears that sedimentation is an unfeasible treatment process for polar TOrcs, which are more often present in the dissolved phase (and thus not particle-bound), including for most pesticides (Spahr *et al.*, 2020).

Specific classes of organic contaminants have historically been associated with stormwater (diffuse sources), e.g. herbicides, while others are typically denoted as wastewater-derived (point sources), e.g. pharmaceuticals and personal care products (PPCPs) (Launay *et al.*, 2016). However, a recent study analyzing contaminant pollutographs during storm- and baseflow reported that pesticides (e.g., diuron)

were present during baseflow conditions, while unexpectedly high concentrations of PPCPs (i.e., ibuprofen, caffeine) appeared during stormflow (Peter *et al.*, 2020). Similar observations were made by Masoner *et al.* (2019); the authors found that both stormwater and wastewater effluents can be sources for over-the-counter pharmaceuticals and household chemicals. Therefore, since many supposedly wastewater-derived contaminants are also commonly detected in stormwater, this sort of characterization is insufficient and non-point source pollution may be more complex (Peter *et al.*, 2020).

Small urban creeks have limited dilution capacities for large volumes of untreated stormwater (Peter *et al.*, 2020), even more so because the hyporheic zone (HZ) in urban streams is often poorly developed or nonexistent (e.g., due to impermeable channel linings) (Lawrence *et al.*, 2013). A functional and rich HZ could provide important habitat, foster biodiversity, and aid in water quality improvement (Lawrence *et al.*, 2013). Fully developed, natural HZs play an important role in the attenuation of nutrients and organic contaminants in streams (Lewandowski *et al.*, 2011; Posselt *et al.*, 2018). Major drivers for hyporheic exchange, i.e. exchange of surface water with porewater, include channel morphology (e.g. bedforms), head differences, streambed hydraulic conductivity, and surface flow rates (Cardenas, 2015; Ward *et al.*, 2011). Efforts to engineer the HZ in urban streams for stormwater treatment purposes led to the introduction of a novel HZ engineered streambeds technology termed BEST: Biohydrochemical Enhancements for Streamwater Treatment (Herzog *et al.*, 2016). BEST modifications of the HZ include engineered subsurface modules that contain 1) vertical impermeable walls that drive hyporheic exchange and control HZ residence times, and 2) permeable reactive geomedia additions to increase biogeochemical reaction rates. Previous constructed flume experiments have shown >50% greater size of the effective hyporheic transient storage and enhanced transformation of the reactive tracer resazurin (i.e., metabolically active transient storage) in a 15 m-long BEST flume containing woodchip-amended sand streambeds compared to a sand-only control without subsurface walls (Herzog *et al.*, 2018). The application of similar HZ restoration techniques in an urban stream resulted in a reduction of 15-50% of targeted organic contaminants, and the observed greater hydraulic residence times (HRTs) in the HZ induced greater pollutant removal (Peter *et al.*, 2019).

The strategy of adding geomedia to existing (vertical) infiltration-based stormwater treatment systems (e.g., biofilters) has been previously suggested to meet aquatic benchmarks and load reduction requirements in urban watersheds (Wolfand *et al.*, 2019). Applications at the pilot-scale level have successfully demonstrated the suitability of biochar-amended biofilters for the efficient removal of hydrophilic (polar) TOxCs and other common stormwater contaminants (Ashoori *et al.*, 2019; Ulrich *et al.*, 2017a). However, depending on the location or potential space limitations and site-specific priority contaminants, a horizontal stream-like flow-through system like BEST may be preferable to a vertical infiltration-based system. BEST engineered streambeds may have great potential to attenuate surface

water pollution due to the technology's flexible application in stream restoration and as stream-like SCMs in urban settings. The latter application could be extremely effective as it provides treatment to stormwater runoff from the entire upstream catchment. Alternatively, Herzog *et al.* (2019) recommended to install BEST streambeds in conjunction with stormwater detention ponds, treating its flow-metered effluent: taking this “treatment train” approach by pairing BEST with an existing SCM technology could also facilitate regulatory approval. Stormwater detention ponds offer fast runoff volume capture and promote (particulate) pollutant sedimentation, while BEST flumes are designed to treat dissolved and polar contaminants (Herzog *et al.*, 2019).

Although previous studies have confirmed the initial proof of concept (Herzog *et al.*, 2016) and have shown the suitability of BEST engineered streambeds to provide metabolically active transient storage (Herzog *et al.*, 2018), performance data for a wide range of stormwater-relevant TOrCs showing efficient removal in BEST flumes are still missing. Similar to stormwater bioinfiltration, the addition of reactive/sorptive geomedia to BEST streambeds may be needed to guarantee efficiency in the removal of dissolved and hydrophilic TOrCs, which are a substantial challenge for the entire aquatic cycle due to their ubiquitous occurrence and high bioavailability (Spahr *et al.*, 2020). Furthermore, it is important to assess the biotransformation potential of BEST streambeds and determine if they could be a major source of transformation products (TPs) into the environment. TPs of pesticides and pharmaceuticals are increasingly found in various aquatic bodies such as urban streams (Mahler *et al.*, 2021; Posselt *et al.*, 2018), river water and wastewater effluents (Ferrando-Climent *et al.*, 2012), drinking water sources (Guillon *et al.*, 2018), and groundwater (Kiefer *et al.*, 2019) – sometimes even at higher concentrations than their respective parent compounds (Ferrando-Climent *et al.*, 2012; Kiefer *et al.*, 2019; Posselt *et al.*, 2018). Finally, design recommendations for BEST systems that are scalable – both in terms of the number and spacing of subsurface modules (i.e., portion of streambed between two impermeable walls), but also total reach length – and adaptable to site-specific pollutants of concern (e.g., via geomedia amendments) are needed. Collecting contaminant performance data will be crucial to facilitate regulatory approval and broad acceptance of the technology by stormwater practitioners.

The overarching goal of this study was to evaluate the removal efficiency of different BEST engineered streambed configurations for a wide range of TOrCs with different biogeochemical properties. We constructed a pilot-scale outdoor flume system treating recycled municipal wastewater amended with a suite of representative stormwater contaminants (metals and TOrCs). Alterations of the hydraulic conductivity (K) in the HZ of the streambeds, either through impermeable BEST walls (i.e., $K = 0$) or a fine-grain sand (i.e., lower K compared to coarse-type sand), were major modifiers of the hyporheic exchange between surface water and porewater. In addition, we employed biochar amendments to the HZ

sediment to enhance sorptive removal. Two types of experiments were conducted for each of the four flumes: 4-hour simulated storm events (single pass mode) for which the surface and subsurface water was monitored for 24 hours; and recirculation mode (over 15 days) experiments for assessment of longer-term performance and the potential for TOrC biotransformation. The primary objectives of this study were to: i) determine the reach-scale attenuation of TOrCs in the surface water of BEST engineered streambed flumes (with and without biochar); ii) determine the effect of HZ residence time and the presence of biochar in the sediment on TOrC retention along hyporheic flowpaths; and iii) evaluate the biotransformation potential of different BEST streambed configurations.

4.3 Methods

This section describes the experimental methods, materials, and procedures used for this study.

4.3.1 Flume Configuration and Operational Conditions

Experiments were conducted in pilot-scale outdoor stream flumes at the Mines Park Water Reclamation Facility at the Colorado School of Mines in Golden, CO. Four identical flumes (dimensions: 15.2-m long, 0.2-m wide, 0.4-m tall) were constructed above-ground from plywood contained in an aluminum frame at a $\sim 1\%$ slope. Each flume was separately contained within impermeable ethylene propylene diene monomer (EPDM) liners. The boundary conditions were the same for each flume: Upstream, the flumes were constrained by a 0.5-m long and 0.3-m deep compartment filled with natural river rocks for flow dissipation, bounded by a permeable mesh (Matala U.S.A.; Laguna Hills, CA, USA) above an impermeable wall holding back the rocks. Downstream, impermeable walls were placed into the streambed at $x = 14.5$ m to maintain saturation; surface water spilled over the wall into another flow-dissipation compartment covered with river rocks (approximately 0.05 m deep). All plumbing consisted of PVC materials.

One flume (F1, “Control”) was filled with 8-mesh Unimin sand (details below) to 0.32 m depth and served as a control condition. The remaining three flumes utilized custom triangular plastic blocks (“BEST walls”; 0.3 m tall, 0.2 m wide, with 0.2 m triangular base) made of ABS (acrylonitrile butadiene styrene) material, sealed to the EPDM using silicone caulk, to form impermeable BEST modules. For each of these three flumes, 15 blocks total were placed at 1-m intervals starting from $x = 0.5$ m to create 14 BEST modules in series. Each of the three BEST flumes was filled with a different type of sand or materials mix: The modules of one flume (F2, “BEST”) were filled with 8-mesh Unimin sand to 0.32 m depth, whereas the second BEST flume (F3, “BEST + biochar”) was amended with a mix of 8-mesh Unimin sand and biochar (7% biochar by vol). The streambed of the last flume (F4, “BEST + biochar, slow”) was filled with a mixture of 16-mesh Unimin sand and biochar (7% biochar by vol); the smaller particle size of this

sand led to decreased hydraulic conductivity (K_{Sat}) and thus longer subsurface residence times compared to the coarse sand (8-mesh). Table 4.1 provides an overview of the four different flume configurations and the materials' properties (K_{Sat} , porosity; see section 4.3.2).

The water source to the flumes was recycled wastewater effluent from a Membrane Bioreactor (MBR) system treating municipal wastewater from nearby university housing. Representative water quality parameters (i.e., pH, alkalinity), major anions, and dissolved organic carbon (DOC) data for the recycled wastewater are summarized in the Supporting Information (SI) (Table C.1). The influent water was pumped to the flume system by four self-priming centrifugal pumps (Dayton® Transfer Pumps, model 6GPG4, aluminum frame; Lake Forest, IL, USA), one for each flume. The operating flow rate in each flume was set to 3 gpm (0.19 L/s) and was continuously monitored over the course of the experiments. The average measured flow velocity in the flumes ranged from 21 to 27 cm/s. A conical-shaped plastic dosing tank (Ace Roto-Mold, Den Hartog Industries Inc.; Hospers, IA, USA) contained the concentrated dosing solution with experiment-specific salts, nutrients, and contaminants (see section 4.3.3). The dosing solution was continuously stirred with a baffle on a drill for all experiments and was added to the source water via injection check valves (WALCHEM / Iwaki America Inc.; Holliston, MA, USA) immediately prior to the water entering the flumes using an electronic metering pump (WALCHEM / Iwaki America Inc.; Holliston, MA, USA). After reaching the downstream flow-dissipation compartment (river rocks), the water of each flume overflowed into a 22-gal rectangular end tank made of polypropylene (RONCO PLASTICS INC; Tustin, CA, US). When not run in recirculation mode, the water was overflowing directly into the sanitary sewer system. A simplified process diagram of the pilot-scale flume system is depicted in Figure C.1.

4.3.2 Materials

The materials used for the engineered streambeds were an 8-mesh Unimin sand (Granusil 2095; 71 vol% between 1.19-2.38 mm and 23 vol% between 0.84-1.19 mm), a smaller size 16-mesh Unimin sand (Granusil 4075; 31 vol% between 0.60-0.84 mm and 50 vol% between 0.42-0.60 mm), and Mountain Crest Gardens biochar (MCG-biochar) produced by high temperature (>1100°C) gasification of pinewood (Gropro, Inc., Etna, CA, USA). The biochar was selected due to its superior TO_{OC} removal performance as previously demonstrated in stormwater biofilters (Ashoori *et al.*, 2019; Ray *et al.*, 2019; Ulrich *et al.*, 2015). The biochar was crushed and sieved to achieve a particle size range of 0.5-1.41 mm. It was subsequently rinsed with deionized water to remove any fine particles <0.5 mm and the remaining fraction was allowed to air dry over the course of several days. The sand and biochar were mixed moist at a ratio of 93:7 by volume (i.e., 7% biochar by vol), subsequently installed in the streambed modules (where applicable) and covered with 1-2 cm of coarse sand (8-mesh Unimin) to prevent transport of material down the flume.

Table 4.1 Flume configurations with saturated hydraulic conductivity (K_{Sat}) and porosity measurements of the corresponding materials (or mixtures). Values are given for loose (L) packing conditions, with values in parentheses representing measurements from tight (T) packing conditions. Red / orange / yellow crosses denote the location of porewater sampling points; for dimensions and exact locations see Figure C.2. Surface water sampling points: Su = surface water upstream; Sm = surface water midstream; Sd = surface water downstream.

Flume #	Configuration	Sand Type	Subsurface Modification	Geomedia Amendment	K_{Sat} [cm/s]		Porosity [%]	
					Loose (L)	Tight (T)	Loose (L)	Tight (T)
F1	Control	8-mesh Unimin (Granusil 2095)	none	none	1.48 ± 0.25 (L) 0.73 ± 0.06 (T)		43.1 ± 0.2 (L) 34.8 ± 1.0 (T)	
F2	BEST	8-mesh Unimin (Granusil 2095)	BEST walls	none	1.48 ± 0.25 (L) 0.73 ± 0.06 (T)		43.1 ± 0.2 (L) 34.8 ± 1.0 (T)	
F3	BEST + biochar	8-mesh Unimin (Granusil 2095)	BEST walls	Biochar (7vol%)	2.32 ± 0.19 (L) 0.67 ± 0.17 (T)		47.4 ± 1.5 (L) <i>n.a.</i> (T)	
F4	BEST + biochar, slow (low K_{Sat})	16-mesh Unimin (Granusil 4075)	BEST walls	Biochar (7vol%)	0.37 ± 0.04 (L) 0.20 ± 0.01 (T)		53.6 ± 4.2 (L) <i>n.a.</i> (T)	

The following salts were used as conservative tracers or nutrient amendment (ammonia) in the different contaminant experiments: potassium bromide (KBr; Sigma-Aldrich, ACS reagent, $\geq 99\%$, anhydrous); sodium bromide (NaBr; Sigma-Aldrich, ACS reagent, $\geq 99\%$, anhydrous); sodium chloride (NaCl; Diamond Crystal); and ammonium chloride (NH_4Cl ; Fisher Chemical, certified ACS, crystalline).

Hydraulic Conductivity and Porosity. The saturated hydraulic conductivity (K_{Sat}) of the different streambed materials and mixtures was measured using a constant head permeameter built and operated according to the specifications in ASTM D-2434-68 (2006), except when operated with sand/biochar mixtures, which required a wet packing method – rather than the standard dry packing method – to achieve a homogeneous mixture. The sand/biochar mixtures were packed at 5% moisture in 2 cm lifts, which were added by gravity (rather than the funnels specified for dry packing), tamped according to ASTM specifications, and scarified between lifts to promote homogeneity within the permeameter. For each material or material mix, separate hydraulic conductivity tests (triplicates) were conducted for both loosely packed (i.e., 0% relative density) and tightly packed conditions (i.e., 100% relative density). K_{Sat} is a crucial design parameter as it influences HZ exchange flow and residence times in the streambeds and potentially the resulting redox conditions. The porosity of each streambed material (for both loosely and tightly packed conditions) was determined via bulk density and particle density measurements.

Biochar Analysis. Biochar analyses for Brunauer-Emmett-Teller specific surface area (BET SSA) and total pore volume were conducted by an external laboratory (Intertek; Allentown, PA, USA). The N_2 isotherms used for BET SSA and total pore volume analyses were measured on a Micromeritics TriStar II Plus unit to full saturation (i.e., a relative pressure of approximately 1.0 at 77 K). The samples were activated on a Smart VacPrep degas unit by degassing at 150°C under dynamic vacuum. Measurement accuracy was estimated to be within approximately 5%. The BET SSA of the biochar was measured as 569 m^2/g and the total pore volume was 0.316 cm^3/g , with a micropore volume of 0.168 cm^3/g (53%).

4.3.3 Contaminant Experiments

The broad suite of TORCs – containing relevant compounds that are typically associated with stormwater and urban water/recycled water – was added to the influent water aiming for an in-stream concentration of approximately 10 $\mu\text{g}/\text{L}$ each, which corresponds to roughly 1000x the limit of quantitation (LOQ) of most TORCs when analyzed via direct injection liquid chromatography tandem mass spectrometry (LC-MS/MS; LOQs typically at 0.005-0.01 $\mu\text{g}/\text{L}$). The TORCs selected for dosing were categorized in terms of their hydrophobicity ($\log K_{OW}$) and potential for biodegradability; this information was used to evaluate how well these parameters were predictive of TORC removal. EPI (Estimation Programs Interface) SuiteTM (version 4.1) was used to estimate the relative biodegradability of all TORCs

listed in Table C.2. The BIOWINTM models, which predict aerobic and anaerobic biodegradability solely based on chemical structure, were specifically employed. As recommended by Aronson *et al.* (2006), the BIOWINTM models were only used for relative binning purposes (to ensure the selected TOxCs represented a broad range of biodegradability potential) and not for quantitatively predicting biodegradation. The TOxC suite selected for target analysis in this study included stormwater and urban water-associated compounds from a variety of classes: herbicides, fungicides, insecticides (neonicotinoids and other), corrosion inhibitors, flame retardants, pharmaceuticals, personal care products, and a perfluoroalkyl acid (PFAA). A full compound list including material source and chemical purity is provided in Table C.2.

Simulated Single-Pass Stormflow Experiments. To determine the reach-scale attenuation of TOxCs in the surface water, we conducted a single-pass experiment in each flume simulating a stormflow event that was monitored over the course of 24 hours. After collecting background samples from surface and pore water, we dosed for approximately 4 hours to add potassium bromide (KBr), sodium chloride (NaCl), ammonium chloride (NH₄Cl), plus a suite of metals and TOxCs to the recycled wastewater. All salts and solids were measured out the day before the experiment and were added to the dosing tank water and premixed via a baffle on a drill right before the start of the experiment

Over the course of each experiment, TOxC concentrations were monitored in the surface water by taking grab samples at the inlet (denoted “surface upstream”, Su; Module #1, at $x \approx 1$ m) and at the outlet (denoted “surface downstream”, Sd; Module #14, at $x \approx 14$ m). In flume F1 (“Control”) only, an additional surface water location was sampled about half-way between the middle and the outlet of the stream (denoted “surface midstream”, Sm; Module #12, at $x \approx 12$ m). Additionally, these experiments allowed to determine the HZ breakthrough of the contaminants and their retention in the subsurface modules. Custom-made porewater samplers (PushPoint samplers; MHE Products, Michigan, US) were used to obtain discrete subsurface samples concurrently with surface water samples. PushPoint samplers consisted of 0.8 m-long stainless-steel tubes (1/8 in / 3.175 mm OD) with four 0.635 mm wide horizontal slits at the tip. The stainless-steel tubes were internally equipped with PEEK tubing (3.05 m long and 0.03 in / 0.762 mm ID) starting from the tip (bottom end). The slit ends were covered by 33 mm long “screen socks” to prevent clogging of the slit openings by small sediment particles. During sampling, the PEEK tubing of each PushPoint sampler was connected to a syringe.

In flumes equipped with BEST modules (F2-F4), three PushPoint samplers were installed in each of the modules #3, 7, and 11 (in total nine samplers/flume). In each module, the samplers were installed along the centerline at a distance of 22 cm (D), 62 cm (U1), and 78 cm (U2) downstream of the centerline of the upstream BEST triangle. Location D was presumably in the down-welling zone of the BEST module, while the other two samplers (U1, U2) were located in the presumably up-welling zone. In flume F1 (Control, no

BEST modules), two PushPoint samplers each were installed at locations equivalent to the D and U2 locations of modules #3, 7, and 11 in the homogeneous streambed (six total samplers for F1). For dimensions and the exact placement of the PushPoint samplers in a module see Figure C.2. Porewater samples were slowly (10 mL/min) withdrawn from the HZ using 50-mL syringes (plastic, NORM-JECT®; VWR/avantor) operated by automated syringe pumps (NE-1600; New Era Pump Systems Inc., New York, US) to minimize disturbance of HZ flow.

In each single-pass stormflow experiment, KBr (26.7 g) and NH₄Cl (53.2 g) were dosed to the influent water, resulting in a final bromide concentration of approximately 7 mg/L. Bromide tracer experiments were conducted to ensure appropriate mixing in the upstream dosing tanks and to characterize the HZ hydrology of each flume's streambed. More specifically, the addition of an ideal tracer allowed to estimate the HZ residence times of the subsurface modules. Module residence times were estimated by extracting pore water samples from the upwelling zones (U2) of the BEST modules (modules #3, 7, and 11) along the length of each flume. In addition to bromide, the injection water contained a small amount of NaCl (343.7 g) to further increase the electrical conductivity (EC) of the source water, allowing for the development of real-time breakthrough curves in the surface water. EC sensors (Decagon ES-2, METER Group, Inc.; Pullman, WA, USA) connected to portable data loggers (Em50®, METER Group, Inc.; Pullman, WA, USA) were installed close to the inlet (three sensors above Module #1, at $x \approx 1$ m) and outlet (three sensors above Module #14, at $x \approx 14$ m) of the flumes to continuously measure the EC in the surface water during the experiments.

The TOrC mass balance was conducted using the method of moments for the downstream concentration (Sd), compared to the nominal TOrC mass added to each flume. Efforts to calculate the mass input into the system based on upstream concentrations (i.e., Su) indicated a significant fraction of the mass was likely missed as a result of low temporal sampling resolution. A summary of the mass balance results for each flume and compound can be found in Table C.5.

Recirculation Experiments. To study the effect of HZ residence times on long-term TOrC sorption and biotic / abiotic transformation along hyporheic flowpaths, the same suite of TOrCs was spiked to the influent and monitored over 15 days with the flumes in continuous recirculation mode (no discharge to sewer). After collecting background samples from surface and pore water, the influent of each flume was dosed for approximately 60 min with NaBr (2.87 g), NH₄Cl (6.61 g), and the same suite of metals and TOrCs as during the single-pass stormflow experiments. The resulting bromide concentration in the flume water was approximately 4 mg/L. The four flumes were identically dosed on a staggered schedule on Day 0. Over the course of 15 days, discrete surface water samples (Su and Sd for F2-F4; Su, Sm, and Sd for F1) and subsurface water samples (via PushPoint samplers) were collected at geometrically progressing time

intervals (e.g., at 4 h, 16 h, 1 d, 2 d, 4 d, 6 d, 9 d, 12 d, and 15 d). In F2, F3, and F4, three samplers were installed in each of the modules #3 and 11 (six samplers per flume), while in F1, three samplers were installed at the locations corresponding to the down-welling zone (D) of modules #3, 7, and 11. Flume water volumes were monitored daily and adjusted with recycled wastewater to account for losses due to evaporation.

Sample Processing and Analysis. The sample processing and analysis was the same for all contaminant experiments: as soon as the water samples were retrieved from the surface or subsurface, they were filtered using 0.45 μm syringe filters (polypropylene membrane, 13 or 25 mm; VWR/avantor or Tisch Scientific) and aliquots were placed into different sample containers and stored at 4°C or analyzed immediately (i.e., DO, pH, temperature). Samples for TOrC analysis were processed differently (see below). Dissolved oxygen (DO) concentrations and pH were measured directly in the field using a portable Hach multimeter (HQ40D) and DO / pH probes. Dissolved organic carbon (DOC) and total nitrogen (TN) concentrations were analyzed in the laboratory by a TOC-L Laboratory Total Organic Carbon Analyzer (Shimadzu), and major anions were analyzed using a Dionex ICS-900 Ion Chromatography System (Thermo Fisher Scientific). Samples were diluted with in-house Milli-Q water as necessary to meet instrument specifications and calibration ranges. Select samples were analyzed for nitrate and ammonia using Hach TNTplus® tests (TNT 830, 831, 835) and a spectrophotometer (Hach). Samples for TOrC analysis were filtered in the field using 0.22 μm pore size syringe filters (Millex-GV Durapore® (PVDF) membrane, 13 or 33 mm; MilliporeSigma) for sample sterilization and were stored in amber glass vials (Qorpak®; VWR/avantor) at 4°C until analysis. Field Blanks were prepared in the field using in-house Milli-Q water.

4.3.4 TOrC Analysis

Concentrations of TOrCs in aqueous samples were quantified by liquid chromatography quadrupole time-of-flight mass spectrometry (LC-QToF-MS) using a SCIEX ExionLC™ high-performance liquid chromatography (HPLC) system, coupled to a SCIEX X500R QToF-MS system (Framingham, MA). Samples were analyzed via isotope dilution and employing electrospray ionization in both positive mode (ESI+) and negative mode (ESI-) with SWATH® Data-Independent Acquisition for both ToFMS and MS/MS mode (details provided in Table C.3). Compounds analyzed in ESI+ mode were eluted on a Kinetex Biphenyl analytical column (2.6 μm , 100x3 mm; Phenomenex, Torrance, CA), whereas ESI- compounds were analyzed using a Gemini C18 analytical column (3 μm , 100x3 mm; Phenomenex, Torrance, CA). Injection volumes of calibration standards and samples were 500 μL and 1000 μL for ESI+ and ESI-, respectively. All samples, calibration standards, blanks, etc., were prepared in 90:10 water:methanol. Details on the MS parameters and LC conditions can be found in the SI (Appendix C, section C.2).

Target Analysis. Target analytes were identified based on precursor exact mass (mass error < 5 ppm), isotopic pattern (isotopic ratio error < 40%), and retention time ($\Delta RT < 0.05$ min) compared to analytical (native) standards, and quantified using calibration standards in the range of 0.005 $\mu\text{g/L}$ to 25 $\mu\text{g/L}$. Surrogate concentrations in calibration standards (and samples) were either 0.4 $\mu\text{g/L}$ or 0.8 $\mu\text{g/L}$, depending on the ionizability of each compound (see Table C.3). Accuracy of calibration standards was required to be within $\pm 30\%$ and only the linear part of each calibration curve was selected for quantitation ($R \geq 0.99$). The lower LOQ for all analytes was between 0.005 $\mu\text{g/L}$ and 0.01 $\mu\text{g/L}$ for ESI+ compounds and between 0.005 $\mu\text{g/L}$ and 0.10 $\mu\text{g/L}$ for ESI- compounds. Table C.3 contains the LC-QToF-MS parameters for each target analyte; specifically, retention time, exact mass information (quantitation), and MS/MS product ions (qualitative confirmation) in addition to spike recovery data. The following compounds were ultimately excluded from further analysis for several reasons: TCEP (high background levels due to presence of the compound in various flume construction materials), carbaryl (analytical difficulties), metformin (required separate LC/MS methods), and oryzalin (very limited water solubility during dosing).

Suspect Screening. To identify potential TPs of the target analytes, we employed a suspect screening approach published previously (Portmann *et al.*, 2022). LC-QToF-MS data acquired in SWATH[®] mode was screened using a custom extracted ion chromatogram (XIC) list (Table C.6 and C.7) containing molecular formulas and exact masses (precursor and fragments) for TPs identified in a review of extant literature.

4.4 Results and Discussion

4.4.1 Surface Water TOrC Removal (Reach-Scale)

Surface water breakthrough curves (BTCs) for select TOrCs across all four flumes are shown in Figure 4.1 (shown as relative concentrations, normalized by the maximum concentration in the influent, $C_{Su,max}$). For imidacloprid, the reduction in concentration peak in the effluent (Sd) was following the order F3 (69.%) > F4 (17.3%) > F1 (4.1%) > F2 (-3.1%). The majority of TOrCs studied in this experiment exhibited a similar breakthrough behavior and effluent peak reduction as for imidacloprid (see Table C.4). Indeed, the peak reductions for atenolol observed in Flumes 3 and 4 (71.9% and 20.8%, respectively) were very similar to imidacloprid, while effluent peak reductions were slightly greater in F2 and F1 (11.8% and 7.4%, respectively). Atenolol is known to be relatively easily biodegradable (Kern *et al.*, 2010), therefore microbial degradation may have contributed to its removal in F1 (sand control) and F2 (BEST). As is clear in Figure 4.1, removal of the only PFAA examined in this study, PFHxA, was different compared to all other TOrCs and seemed to be predominantly unaffected by the presence of biochar – at least under stormflow conditions: observed concentration peak reductions were only 4.5% in F3 and 0.6% in F4.

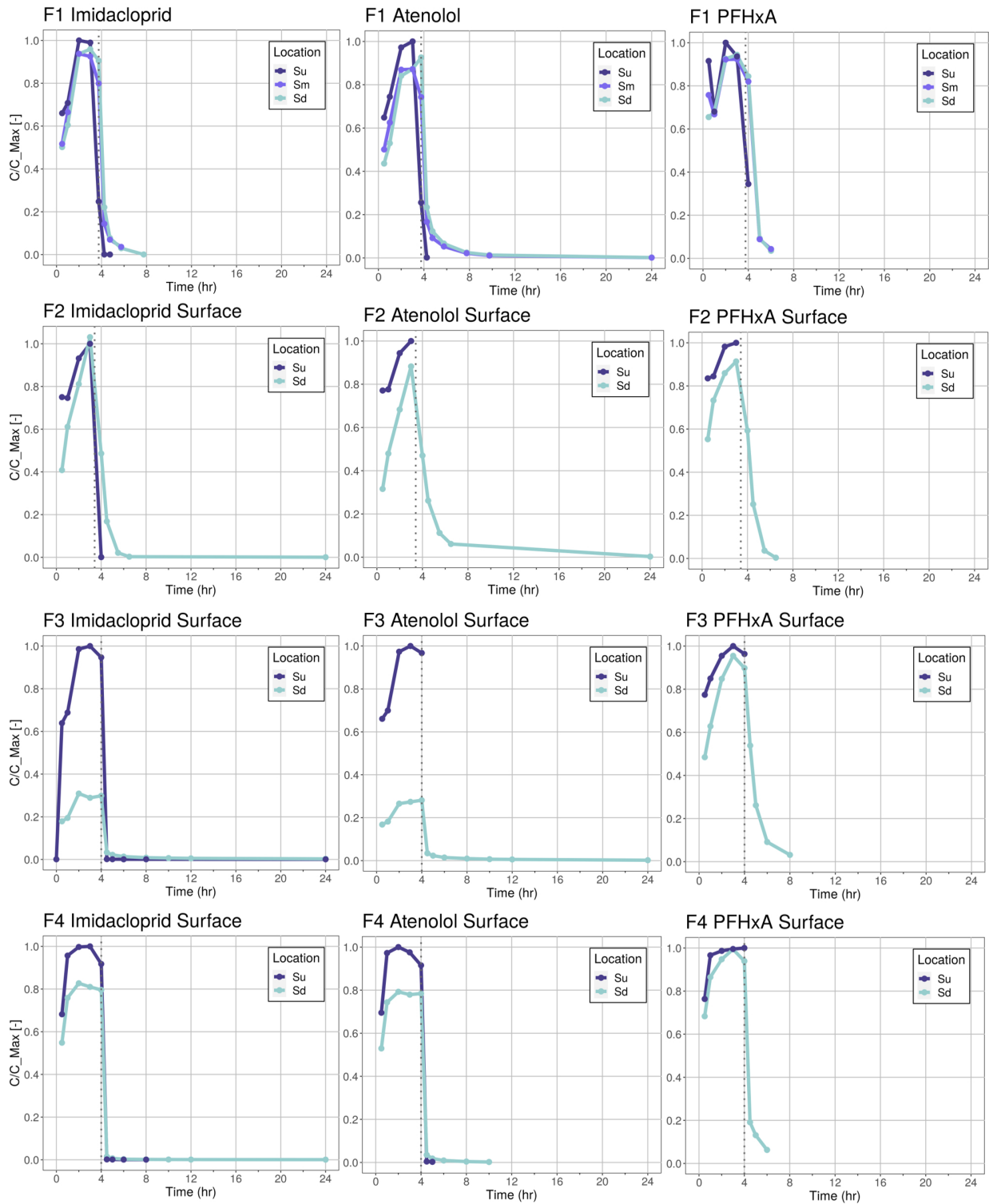


Figure 4.1 Surface water breakthrough curves (BTCs) for select TOxCs during simulated stormflow experiments (single-pass flume operation). Experimental conditions: Control (F1), BEST (F2), BEST + biochar (F3), and BEST + biochar, slow (F4). Dotted vertical lines indicate the time when dosing stopped: 3h 45min (F1), 3h 25min (F2), 4h (F3, F4). Samples with concentrations below the LOQ, which frequently occurred for the Su samples after dosing stopped, were not plotted.

Interestingly, the reductions were slightly greater in the biochar-free flumes (F1: 5.6%; F2: 8.6%), though this is likely within the analytical variability typically observed for PFAAs.

Bundschuh *et al.* (2013) studied the effects of different concentration peak exposure scenarios on freshwater amphipod crustaceans using environmentally relevant concentrations of a representative mix of pesticides (e.g., thiacloprid, a neonicotinoid insecticide). Prolonged exposure to the pesticides at a lower peak concentration considerably decreased the observed freshwater ecotoxicity in contrast to a scenario with a comparably higher peak concentration for a shorter time period (at a constant mass input in both scenarios) (Bundschuh *et al.*, 2013). When the crustaceans were exposed to pesticides at field relevant concentrations over a duration of 120 min, the authors observed a diminished feeding rate, which may have substantial impacts on ecosystem function and local aquatic food-chains. These findings highlight the importance of peak concentration reductions in streams and channels impacted by stormwater runoff in the context of aquatic benchmarks. With the exception of PFHxA, our data indicate that biochar-amended BEST systems are capable of reducing peak concentrations in the surface flow, even over short distances.

Despite the crucial importance of concentration peak reductions for aquatic biota, regulatory water quality standards may not be well represented by concentration reductions and may require a cumulative discharge perspective (i.e., Total Maximum Daily Load, TMDL). Thus, for each TOrC, we conducted a mass balance of the simulated stormflow data comparing the total mass input (nominal mass added to each flume) into a given flume with the observed mass output in the effluent (cumulative concentration–time product for Sd and constant flowrate). The resulting mass differences are summarized in Figure 4.2 as the percent mass either retained in the streambed (positive ΔM) or “produced” by the system (negative ΔM). Data from Flumes 1 and 2, which only contained sand, suggest that cumulative TOrC mass retention in the systems remained <50% in F1 and <60% in F2 for all compounds during the 24-hour observation period. There was a substantial variability in mass removal between the different compounds: average mass retention was 10.1% ($\pm 27.6\%$) and 2.7% ($\pm 28.4\%$) for F1 and F2, respectively, and differences between the two flumes were not significant (Welch’s t-test: $p=0.4222$; $\alpha=0.05$). The herbicide 2,4-D is a striking outlier because the data suggests TOrC mass production of $\geq 80\%$ in both sand streambeds; this number is likely due to a measurement error arising during spiking solution preparation (nominal mass input). Consistent mass retention (positive mass removal) only occurred in the case of the biochar-amended flumes F3 and F4, with the exception of PFHxA in F3 (likely within analytical variability). Across all TOrCs, greatest mass removal percentages were observed for the BEST and biochar flume (F3: $62.1\% \pm 21.0\%$), followed by BEST amended with biochar and fine-grain sand (F4: $38.1\% \pm 19.7\%$).

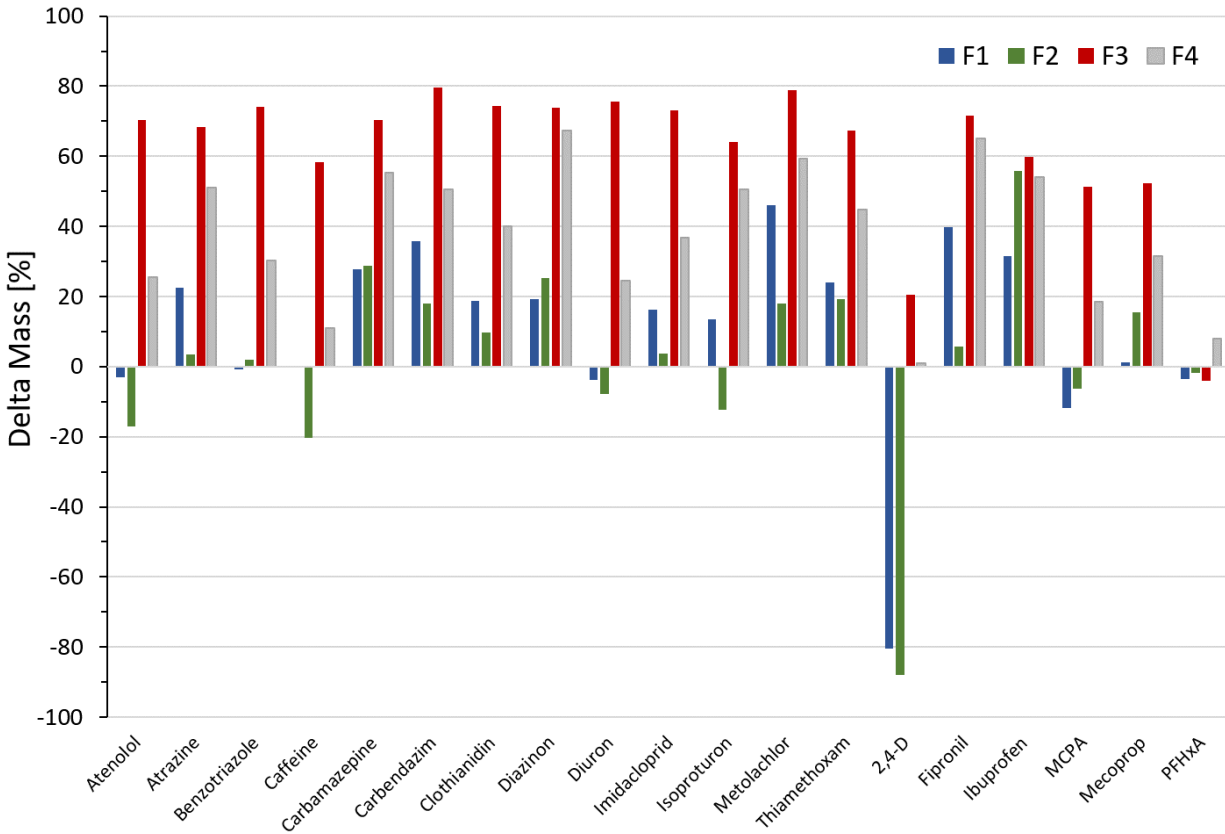


Figure 4.2 Mass balance for each TOxC and flume (F1-F4) for simulated stormflow experiments (single-pass flume operation). Mass differences per flume were calculated as follows: $\Delta M [\%] = (M_{in} - M_{out})/M_{in} * 100$ whereas M_{in} was the nominal mass added to each flume; $M_{out} = \sum(C_{out} * t) * Q$ with $Q = 681.37 \text{ L/h} = \text{constant}$. Experimental conditions: Control (F1), BEST (F2), BEST + biochar (F3), and BEST + biochar, slow (F4).

Our results indicated that over a flume length of 15 meters, the amendment of BEST streambeds with biochar was necessary to provide both reliable TOxC concentration peak reductions and net TOxC mass retention under stormflow conditions. Therefore, under limited space conditions – a common feature of urban stormwater systems – addition of strong geosorbents (e.g., biochar) to BEST streambeds may be essential for effective pollutant removal both in terms of concentration and mass load reductions. Our results are corroborated by a recent modelling study investigating the suitability of SCMs for managing urban pesticide pollution: biochar-amended biofilters led to both a load reduction and cumulatively less toxicity benchmark exceedances, while conventional biofilters only attenuated storm loads (Wolfand *et al.*, 2019). However, the choice of sand and thus the permeability of the streambed seemed to have a substantial impact on reach-scale removal in the flumes: removal of the majority of compounds was

consistently greater in F3 than F4, presumably due to greater hyporheic exchange between the surface and porewater in F3 (more water is routed through the subsurface due to greater streambed permeability).

4.4.2 Subsurface Water TOrC Removal (Module-Scale)

Hydrological Characterization of Select Modules (#3, 7, 11). Hydraulic conductivity of the streambed is one of the most important factors governing the extent and magnitude of hyporheic exchange (Cardenas, 2015; Ward *et al.*, 2011). Saturated hydraulic conductivity (K_{Sat}) and porosity were determined for the different streambed materials under loosely packed (L) and tightly packed (T) conditions using a constant head permeameter (see Table 4.1 on page 64). The streambeds were built without external media compaction and thus initially, conditions have probably resembled the loosely packed case. However, we observed some minor streambed settlement as soon as they became fully water saturated: the material was likely becoming more tightly packed. Resulting K_{Sat} and porosity values in the streambeds were likely somewhere on the continuum of the values provided in Table 4.1. Under tightly packed conditions, K_{Sat} results indicate that the permeabilities of sand (0.73 ± 0.06 cm/s; F2) and the sand-biochar mix (0.67 ± 0.17 cm/s; F3) were comparable. In contrast, average K_{Sat} values of the fine-grain sand with biochar (0.20 ± 0.01 cm/s; F4) were smaller compared to the means of the other two materials (however, the difference was only significant in the case of F2 vs. F4; one-way ANOVA with Dunnett's comparison: $p=0.0160$; $\alpha=0.05$). Thus, it can be expected that subsurface hydraulic residence times in F4 were greater compared to F2 and F3 – based on bromide BTCs, this was generally the case, at least for the three modules studied (#3, #7, and #11; see Figure C.3). Bromide concentration peaks generally occurred within 2-4 hours in F2 and F3, whereas some peaks occurred at >4 hours in the case of F4. With longer subsurface hydraulic residence times (HRTs) in F4, a smaller portion of the overall water flow passes through the subsurface, which may explain why the reach-scale removal for the majority of TOrCs was consistently greater in F3 compared to F4 (see section 4.4.1). In contrast, on the module-scale, greater HRTs are expected to offer more time for contaminants to sorb/react and thus increased removal (see discussion below).

Additionally, the bromide data indicates that there was a greater variance of residence times between the sampling points D, U1, and U2 in F4 compared to flumes F2/F3. None of the three HZ sampling points in a module are necessarily part of a single flowpath, but they could be. Generally, we observed that U2 is physically downstream of U1 and D; thus, it can be concluded that U1 is a shorter HZ flowpath (i.e., shorter residence time) and U2 is a longer HZ flowpath (i.e., longer residence time). However, this was not always the case: for example, in F4 module #7, U1 and U2 were not connected, since U1 showed considerably delayed bromide breakthrough compared to locations D/U2 and was likely part of a different flowpath (Figure C.3).

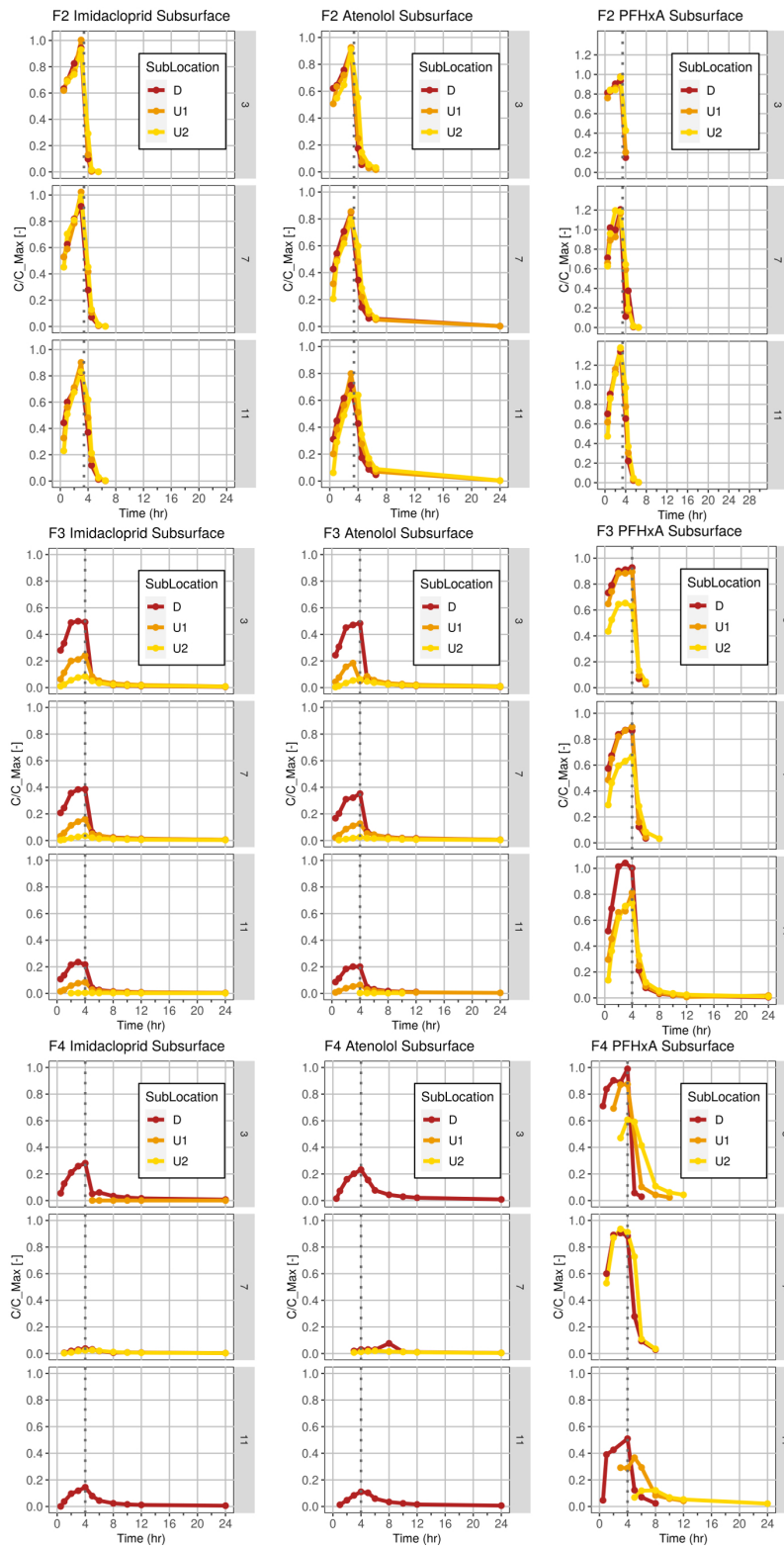


Figure 4.3 Porewater breakthrough curves (BTCs) for select TOxCs and modules (#3, #7, #11) during simulated stormflow experiments (single-pass flume operation). Conditions: BEST (F2), BEST+biochar (F3), and BEST+biochar, slow (F4). Dotted vertical lines indicate dosing end: 3h 25min (F2), 4h (F3, F4).

TOrC Removal in Modules. In streambeds, TOrC removal on the module-scale is likely affected by the existing porewater residence times: flowpaths with longer HZ residence times generally result in greater contaminant removal along HZ flowpaths (Peter *et al.*, 2019). This common hydrologic pattern was observed in Modules #3 and #11 (across F2, F3, and F4) at upwelling sampling locations U1 with shorter HZ residence times vs. U2 characterized by longer HZ residence times (see bromide BTCs; Figure C.3). In F2 (BEST), the greater residence times in U2 compared to U1 only rarely led to greater TOrC removal. This was only observed, for example, in the case of atenolol (Module #11-U2, peak at 64%; Figure 4.3), caffeine (Module #7-U2, peak at 80%; data now shown), or carbendazim (Module #11-U2, peak at 63%; data not shown). For the majority of compounds, including imidacloprid and PFHxA (Figure 4.3), there was no distinct difference in peak height or clear trend in BTC behavior between HZ locations U1 and U2 in F2. The data imply that the difference in hydraulic residence times for U1 vs. U2 was not sufficient for removal of the TOrCs in the HZ of the sand-only BEST. When BEST was amended with biochar (F3), however, we observed a decreasing trend of BTC height in the modules along the length of the flume: for imidacloprid, relative peak concentrations in the downwelling zone (D) decreased from Module #3 to #7 to #11 ($0.50 > 0.39 > 0.23$; Figure 4.3). The same pattern of decreasing BTC height also occurred along the length of a module with $D > U1 > U2$, and was the case for all TOrCs studied here (e.g., atenolol and imidacloprid in Module #3; Figure 4.3), with the exception of PFHxA. PFHxA subsurface BTCs exhibited less alignment compared to F2, but there was no clear trend. For TOrCs that have a high sorption affinity towards the biochar, amendment of sand with biochar led to increased contaminant residence times. Across all flumes, removal in modules was greatest for F4, when the BEST streambeds were amended with fine sand (lower K_{Sat}) and biochar. Breakthrough was consistently observed at the D locations in F4, but the TOrCs were often removed below the LOQ in the upwelling zone (U1, U2); this was observed, for example, for imidacloprid (Module #11) and atenolol (Module #3, #11) (Figure 4.3). Once again, the only exception was PFHxA, but interestingly, F4 data showed both a decreasing trend of BTC height in the modules along the length of the flume and within a module itself ($D > U1 > U2$) – similarly to what we observed for the other TOrCs in F3. It should be noted that Module #7 in F4 was somewhat unique in that both locations D and U2 seemed to break through simultaneously, while typically no TOrCs were detected in U1 (except for carbendazim and diuron). The bromide breakthrough in Module #7 of F4 (see Figure C.3) might explain this observation: probably due to streambed heterogeneities, location U1 showed delayed bromide breakthrough (peak reached at 10 hours compared to 4 hours for the locations D/U1) and thus must have had a prolonged residence time.

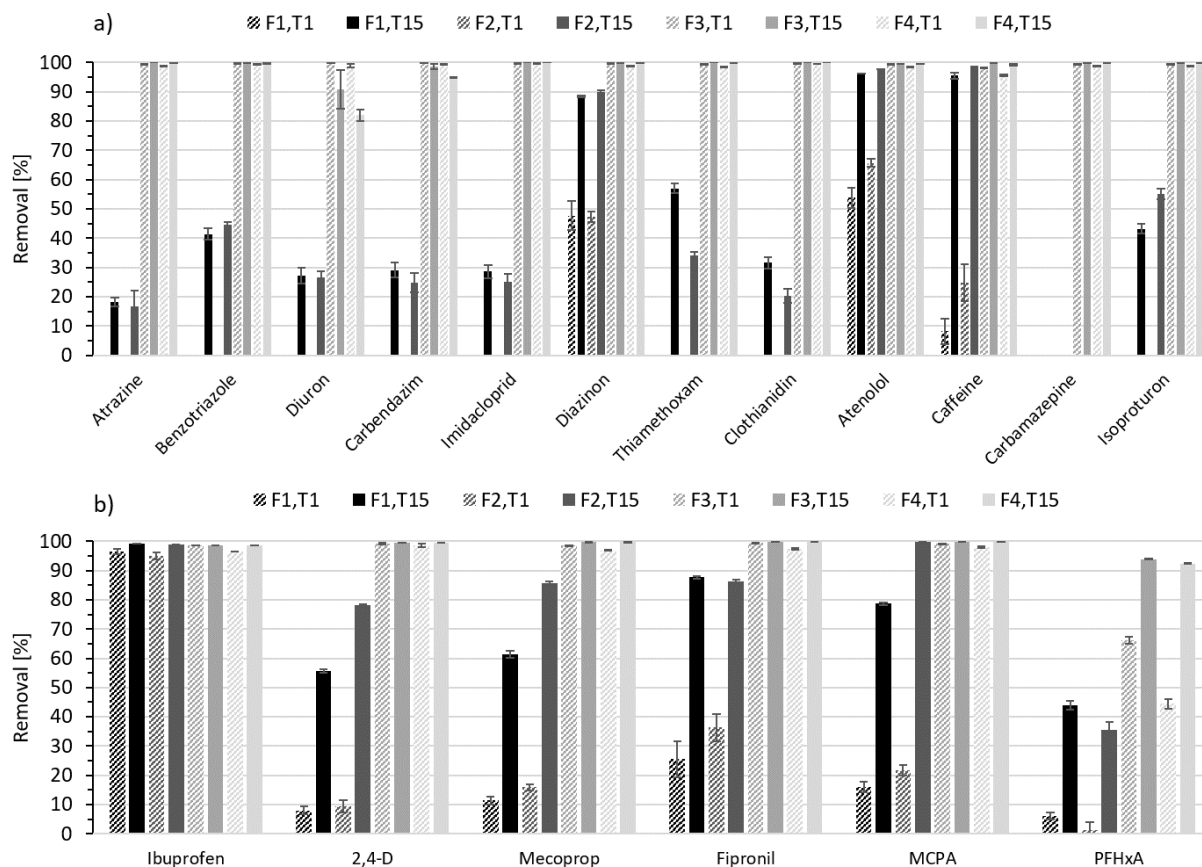


Figure 4.4 Removal of TOxCs during recirculation experiments at 24 hours after dosing onset (T1) and at 15 days (T15); calculated based on concentration reductions between Su and Sd. Net negative removal at T15 for carbamazepine in F1 and F2 is not shown (-28.3% and -43.1%, respectively). Experimental conditions: Control (F1), BEST (F2), BEST + biochar (F3), and BEST + biochar, slow (F4).

4.4.3 Extended Reach-Scale Attenuation

TOxC removal during recirculation experiments (extended contact time between streambeds and contaminants) was greatest in flumes with biochar-amended streambeds (F3, F4; Figure 4.4). It should be noted that removal was calculated based on concentration reductions instead of mass removal. In the biochar-amended flumes (F3, F4), 24 hours were sufficient to provide >95% removal for the majority of compounds (see T1, Figure 4.4), except for PFHxA. Removal of PFHxA was greater in F3 (66.2%) compared to F4 (44.4%) – which is in line with generally greater reach-scale removal observed for F3 (see section 4.4.1). Extended contact time (15 days; T15) increased removal in the sand-only systems, F1 and F2, since net positive removal rates were observed for all TOxCs studied here except for carbamazepine. Carbamazepine exhibited net negative removal, possibly as a result of desorption from previous stormflow experiments or reversion of carbamazepine conjugation products present in the MBR effluent (e.g.,

carbamazepine-N-glucuronide is commonly detected in human urine; Bahlmann *et al.* (2014)); though the definite reasons remain unclear. Nevertheless, at day 15, removal in both F1 and F2 was >78% for only 6 out of 18 TOrCs. Three of these compounds are fairly hydrophobic ($\log K_{OW} > 3.5$; diazinon, fipronil, ibuprofen), whereas the other three are more easily biodegradable (within ‘weeks’ according to BIOWIN3; caffeine, ibuprofen, MCPA) (see Table C.2). Atenolol was the only TOrC that was generally well-removed in F1 and F2 which was neither hydrophobic nor (relatively) more biodegradable, though its biodegradability rating was ‘weeks-months’ according to BIOWIN3. In contrast, the only readily biodegradable compound included in the analysis that did not show good removal in F1 and F2 was benzotriazole, though it was removed to 41% (F1) and 45% (F2) after 15 days. Our results indicate that under conditions of extended streambed contact time, microbial degradation may have played an important role in the removal of the TOrCs in this more relatively biodegradable group (see transformation product analysis in section 4.4.4).

A particularly interesting case was ibuprofen: the pharmaceutical showed excellent removal in all four flumes already at 24 hours after dosing onset ($\geq 95\%$ removal; T1 in Figure 4.4b), even in the flumes without biochar (F1, F2). Rubasinghege *et al.* (2018) found that abiotic ibuprofen removal was associated with adsorption onto clay surface involving silanol groups (SiOH). These findings may explain the fast (abiotic process) and consistent ibuprofen removal in all flume systems, because all streambeds consisted of a high purity silica sand. Silanol groups present on the silica sand surface have likely served as highly specific adsorption sites for ibuprofen.

4.4.4 TOrC Transformation Products

During the recirculation experiments, a total of 30 transformation products (TPs) were detected in the surface (“S”) and subsurface water (“HZ”) – predominantly in sand-only flumes (F1, F2), although positive detections were found in the biochar-systems as well (at lower concentrations and fewer time points; see Table C.6 and C.7). The TP atenolol-acid was detected at by far the greatest concentrations in both flumes F1 and F2 (Figure 4.5a), followed by 1,2-dihydroxy-ibuprofen (1,2-diOH-IBU; Figure 4.5b). Since degradation of both atenolol and ibuprofen occurred at such high rates (<4 hours), their respective influent concentrations measured in F1 and F2 were most likely underestimated: their nominal influent concentrations based on TOrC mass addition and total flume water volume might serve as a better estimate (atenolol: $C_0 = 30.1$ and 34.7 nM for F1 and F2, respectively; ibuprofen: $C_0 = 38.8$ and 44.8 nM for F1 and F2, respectively). Both atenolol-acid and 1,2-diOH-IBU were already present in background water samples (before dosing), presumably stemming from microbial processes during MBR treatment and/or the TPs were produced in the streambeds during preceding simulated stormflow experiments.

Another potential source of atenolol-acid is its presence in municipal wastewater as a human metabolite of the hypertension medication metoprolol (Kern *et al.*, 2010); atenolol-acid is therefore also commonly referred to as metoprolol-acid. Results from activated sludge batch experiments reported a half-life of ~ 4 hours for atenolol under oxic conditions (Kern *et al.*, 2010), while atenolol half-lives of 1.2-1.7 hours were observed during riverbank filtration (Huntscha *et al.*, 2013). Atenolol half-lives between 1.2-4 hours would definitely correspond well with our data, as we observed 76-84% removal of atenolol (based on nominal mass input) in F1 and F2 after 4 hours.

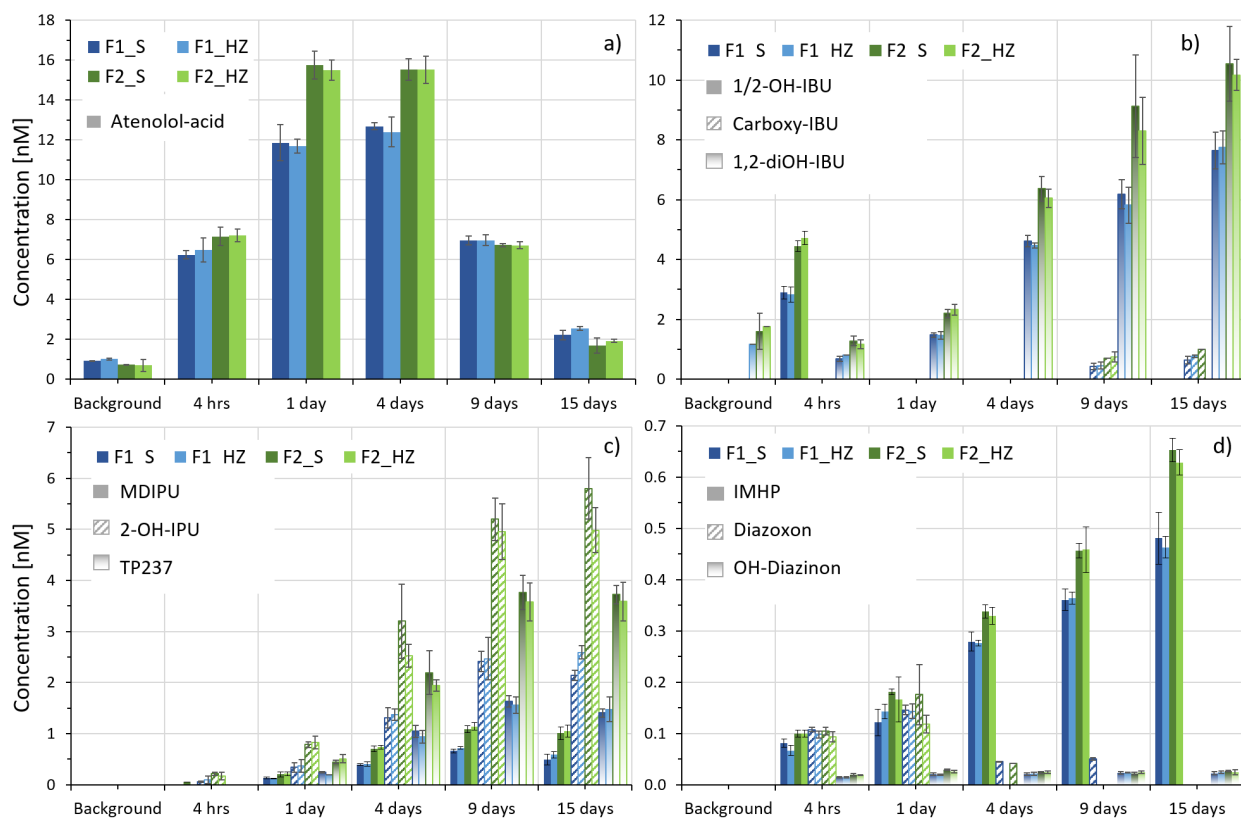


Figure 4.5 Transformation products (TPs) detected in samples from recirculation experiments via suspect screening for the following parent compounds: a) Atenolol (C_0 F1: 4.9 nM; C_0 F2: 8.5 nM); b) Ibuprofen (13.0 nM; 8.2 nM); c) Isoproturon (25.0 nM; 32.5 nM); d) Diazinon (16.7 nM; 16.0 nM). Please note that concentrations for all suspects are semi-quantitative; calibrants were the corresponding parent compounds. Abbreviations: 1/2-hydroxy-ibuprofen (1/2-OH-IBU); carboxy-ibuprofen (carboxy-IBU); 1,2-dihydroxy-ibuprofen (1,2-diOH-IBU); monodesmethyl-isoproturon (MDIPU); 2-hydroxy-isoproturon (2-OH-IPU); 2-isopropyl-6-methyl-4-pyrimidinol (IMHP); hydroxy-diazinon (OH-diazinon).

For ibuprofen, the second highest concentrations were measured for 1/2-hydroxy-ibuprofen (1/2-OH-IBU), followed by carboxy-ibuprofen (carboxy-IBU) (Figure 4.5b). The metabolite 1,2-diOH-IBU has been detected in activated sludge batch studies (Ferrando-Climent *et al.*, 2012) and in ibuprofen degradation experiments involving white-rot fungi (Marco-Urrea *et al.*, 2009). The latter study reported a

fast appearance of 1-OH-IBU and 2-OH-IBU after the first 150 min of the experiment and a subsequent degradation of the initial metabolites into 1,2-diOH-IBU by the fungi. Interestingly, the same pattern was observed in the BEST streambeds: 1/2-OH-IBU was quickly produced within 4 hours and then completely disappeared at all following sampling times, while concentrations of 1,2-diOH-IBU started to increase at Day 1. In contrast to the hydroxylated metabolites, the formation of carboxy-IBU was characterized by a distinct lag time (delayed biodegradation) of ~ 9 days. The absence of a lag phase suggests biodegradation by co-metabolic processes, while the presence of a lag time has been associated with the adaptive expression of TORC-specific enzymes (Amador *et al.*, 2010; Ulrich *et al.*, 2017b). In regard to TPs of ibuprofen, it has been suggested previously that the hydroxylated metabolites and carboxy-IBU occur through separate biodegradation pathways and at different rates (Ferrando-Climent *et al.*, 2012). Based on our observations, microbial transformation may have considerably contributed to the overall removal of ibuprofen observed in the streambeds of F1 and F2 during recirculation – in addition to the presumed abiotic pathway of ibuprofen adsorption onto silica clay surfaces.

Degradation of isoproturon occurred almost exclusively in sand-only flumes (F1, F2) and yielded monodesmethyl-isoproturon (MDIPU), 2-hydroxy-isoproturon (2-OH-IPU), and a novel TP that we denoted “TP237” (2-4-[(dimethyl-carbamoyl)amino]phenylpropanoic acid; Figure 4.5c; Table C.6). It is listed as an intermediate TP in the degradation map for isoproturon in soil in the database Eawag-Soil (www.envipath.org/package; Kiefer *et al.* 2019). Microbial transformation of isoproturon in the environment is relatively well established in the literature and involves distinct transformation pathways, ranging from hydroxylation (2-OH-IPU) and N-demethylation (MDIPU) to hydrolysis of the amide group (4-isopropylaniline; 4-IA) (Penning *et al.*, 2010). We observed 4-IA in F1 and F2 at low concentrations at the beginning of the recirculation experiment (up to 0.065 nM; at 4 hrs - 1 day), but it disappeared quickly. It has been previously reported that it may be difficult to detect the metabolite 4-IA in the environment (Penning *et al.*, 2010) since it was prone to bind to soil organic matter (Scheunert & Reuter, 2000) – which could explain the rapid disappearance observed in our streambed experiments.

Transformation of the insecticide diazinon was predominantly observed in F1 and F2 (Figure 4.5d), while its TPs appeared only at the earliest sampling point (4 hours) in the slow biochar-amended BEST (F4; Table C.6). The main suspect that was identified was 2-isopropyl-6-methyl-4-pyrimidinol (IMHP), whose concentration constantly increased throughout the experiment and peaked at 15 days, whereas other TPs diazoxon and hydroxy-diazinon (OH-diazinon) remained at comparably lower levels. All of these TPs were also detected in a study employing ozonation of diazinon in water, with IMHP being the main product formed via oxidation followed by hydrolysis, while diazoxon was only observed as an intermediate (Lee *et al.*, 2020). OH-diazinon was produced via hydroxylation and remained at trace levels (Lee *et al.*, 2020) –

similar to our study, in which the TP was quickly formed and stayed at a constant and low level throughout the experiment. In addition to abiotic transformation, IMHP is also the major product of diazinon biotransformation, as for example reported for bacterial (Briceño *et al.*, 2016) and fungal communities (Gaber *et al.*, 2020). Most likely, transformation of diazinon occurred through a combination of abiotic (i.e., chemical hydrolysis) and biotic processes (i.e., microbial degradation) in the engineered streambeds.

Surprisingly, we did not observe any TPs of caffeine, most likely due to chromatographic limitations of the LC method employed here. Typically, TPs are more polar (shorter retention times) than their respective parent compounds (Kiefer *et al.*, 2019; Menger *et al.*, 2021). Thus, it is likely that we did not chromatographically retain potential TPs in the case of caffeine, which is already on the highly polar side ($\log K_{OW} = 0.16$).

Li *et al.* (2015) observed exclusive production of certain TPs in the porewater (e.g. carbamazepine-10,11-epoxide), however, this was not the case in this study. Comparable surface and subsurface concentrations were found for all TPs – at least at the temporal resolution of the sampling employed here. As mentioned above, TPs were detected less frequently and at much lower concentration levels in the biochar-amended BEST streambeds (F3, F4) compared to the sand-only flumes (F1, F2). Occurrence of TPs in F3 and F4 typically exhibited the following patterns: they were either formed at the beginning (4 hours, 1 day; Table C.6 and C.7) when more of the parent compound was likely still present in the aqueous phase (not sorbed), or alternatively at later timepoints in the experiment (15 days), most likely due to desorption processes of either the parent compound or the TP itself; for example, DCPMU (15 days; Table C.6). Interestingly, DCPMU can be formed in the environment through a multitude of pathways, including soil photolysis, aerobic soil degradation, and (an)aerobic aqueous metabolism (Mahler *et al.*, 2021).

Overall, the sand-only BEST streambeds (F2) were metabolically active and exhibited substantial biotransformation potential. This could have positive implications during the treatment of non-toxic, nutrient-rich, and well-characterized stormwater influents. Nevertheless, while biotransformation is frequently linked with detoxification mechanisms that yield less toxic TPs compared to the parent compound, this principle cannot be generalized: the toxicity of a metabolite is highly compound-specific and also depends on the type of biota affected (e.g., mammals, fish, insecticides). For example, decreased toxicity of secondary products compared to the parent was observed in the case of abiotic metabolites of ibuprofen towards different bacteria and freshwater algae species (Rubasinghege *et al.*, 2018), while greater toxicity was reported for 1,2-diOH-IBU using standardized Microtox bioassays (Marco-Urrea *et al.*, 2009). Another example is the degradation of the neonicotinoid imidacloprid into desnitro-imidacloprid: this transformation reaction yields a metabolite that causes decreased bee mortality,

whereas its toxicity towards mammals is >300 times greater compared to the parent compound (Tomizawa & Casida, 2003). Given the known (eco)toxicity potential of many TOrCs and some of their metabolites, it is essential to include (bio)transformation products in the evaluation of future stormwater treatment systems. In a study looking at pesticide TPs in small urban streams, Mahler *et al.* (2021) reported occurrence of pesticide TPs during baseflow, which suggests a chronic exposure risk towards aquatic organisms. Based on our findings from the recirculation flume experiments, F1 and F2 could be potential sources of TPs into the environment – possibly rendering the “treated” water more ecotoxic – whereas biochar-amended BEST systems (F3, F4) effectively removed these TPs, though it remains unclear whether TPs were not produced or not released.

4.5 Conclusions

Insights gained from these pilot-scale flume experiments allow the establishment of basic design recommendations for BEST engineered streambeds. The most promising configuration was the biochar-amended BEST system (F3), providing efficient reduction in both concentration peaks and mass loadings – most likely by creating a sufficient extent of hyporheic exchange between surface and porewater. In contrast, peak concentrations and mass retention remained mostly unaffected or were inconsistent in both sand-only flumes (F1, F2), however, they showed promising potential for active biodegradation processes in the streambeds. This may be a desired feature in the case of non-toxic and nutrient-rich stormwater influents, however, for TOrCs-rich stormwater, F1 and F2 could be potential sources of toxic TPs into the environment. An interesting case was F4, the biochar-amended BEST featuring a low K_{Sat} streambed (fine sand): this configuration yielded greater removal per module compared to all other treatments, but failed to provide the same reach-scale peak concentration reductions as observed in F3 – presumably because of limited surface-subsurface water exchange (hyporheic exchange). Limited HZ exchange results in a proportionally smaller total water volume that is routed through the streambed and treated in a given amount of time; therefore, limited reach-scale removal of TOrCs was observed for F4. All in all, these findings highlight the importance of hydraulic conductivity properties of the media of choice (e.g. sand) to optimize HZ exchange, and the addition of strong geosorbents (e.g. biochar) to the sediment for accelerated removal in the design of BEST streambed applications.

CHAPTER 5

CONCLUSIONS

The overall objective of this dissertation was to evaluate the role of biodegradation and biochar in the long-term removal of trace organic contaminants (TOrcs) in novel biochar-amended stormwater control measures (SCMs). Chapter 2 sought to advance the understanding of the impact of a biofilm layer on filter lifetime and shed light on the complex interplay between sorption and biodegradation. The aim of Chapters 3 and 4 was to study the fate of TOrcs in engineered hyporheic zones (i.e., streambed biofilters known as Biohydrochemical Enhancements for Streamwater Treatment; BEST) and evaluate whether biochar amendments were effective in providing enhanced removal of TOrcs. In addition to summarizing the major research findings of each chapter, this chapter provides a discussion of the outcomes and broader significance of the work. Lastly, this dissertation concludes with recommendations for future directions of research.

5.1 Summary of Findings

The following section provides a summary of the most important findings associated with each objective of this dissertation and a discussion of how each of the findings relates to the hypotheses introduced earlier.

5.1.1 Objective 1: The Role of Biofilm in the Removal of Pesticides in Biofilters

The aim of the research presented in Chapter 2 was to assess the long-term fate and relevant removal processes (i.e. sorption, biodegradation) of selected neonicotinoids and the herbicide atrazine in biochar-amended sand columns in the presence of a microbial biofilm. This research was conducted using laboratory-scale columns and its approach was novel as it combined a representative synthetic stormwater matrix with a biofilm layer to create representative biofouling conditions (similar to field situations). In addition, the potential formation of pesticide transformation products (TPs) was carefully assessed using high resolution mass spectrometry (HRMS).

Hypothesis 1: Biodegradation in biofilm-biochar filters is a relevant removal process of TOrcs in the long-term and the presence of a biofilm layer prolongs filter lifetime by >50%. This hypothesis was tested in laboratory-scale exhaustive column tests (three months dosing) to quantify the impact of an active biofilm layer on overall pesticide removal and filter lifetime. Furthermore, column breakthrough curves were used to estimate parameters of a contaminant transport model in porous media to simulate representative biofilter lifetimes in different case study scenarios. Among the most significant findings of this work are the following:

- Despite their higher polarity, neonicotinoid insecticides (i.e., imidacloprid, clothianidin) were efficiently removed by biochar.
- Biological processes accounted for 20-36% of overall TOxC removal in the biotic biochar-amended sand filters. Biological processes were likely a combination of biologically enhanced sorptive removal (i.e., regenerative effect of microbial activity restoring some of the sorption capacity over time) and/or biodegradation of TOxCs in the aqueous and/or sorbed phase.
- At a biochar application rate of 0.5% by weight, the presence of an active biofilm layer prolonged the filter lifetime by 1.8-2.3 times compared to a fouled but inactive filter, where removal was presumably dominated by adsorption.
- All TPs detected in the column effluent remained below 2.5% of their respective parent influent concentrations for the duration of the experiment suggesting that biochar-amended biofilters would not likely constitute a significant source of TPs into the aquatic environment.
- In a representative case study modelling scenario, biochar-amended biofilters could last at least 17 years before exceeding pesticide aquatic life thresholds at biochar application rates as low as 1% by weight (5% by volume).

5.1.2 Objective 2: Attenuation of Metformin in Full-Scale Engineered Streambed Hyporheic Zones

The goal of the study described in Chapter 3 was to investigate the effects of engineered hyporheic zones (HZs) on surface-subsurface water exchange, hyporheic redox conditions, and the attenuation of the highly polar compound metformin. This research was conducted using an outdoor flume facility at the German Environment Agency in Berlin, Germany. The novel aspects of this work include studying pollutant removal in engineered streambed modules (i.e., using subsurface impermeable BEST walls) at a representative field-scale under actual environmental conditions (i.e., temperature, sunlight exposure, aquatic biota, and microorganisms).

Hypothesis 2: a) BEST engineered streambeds will lead to enhanced attenuation of metformin and guanylurea due to increased HZ exchange and streambed redox conditions favorable for their degradation; and b) Biochar addition to BEST engineered streambeds will further accelerate removal along hyporheic flowpaths due to biochar's high sorption capacity. This hypothesis was tested in full-scale BEST modules with and without biochar installed in a recirculating flume under near-natural conditions as well as with limited batch experiments. Two full-scale flume experiments were conducted: in the first experiment, metformin was spiked at 10 ug/L and monitored regularly in the surface and subsurface water (May-August

2018), while in the second experiment, the initial metformin concentration was higher (10 mg/L) and thus ideal to study TP formation (August-November 2018). The major findings of this research include:

- In the biochar batch experiments, the TP guanylyurea exhibited a significantly greater adsorptive removal at equilibrium ($\log K_{d,eq} = 4.87$ L/kg) compared to metformin ($\log K_{d,eq} = 3.96$ L/kg).
- Hydraulic conductivity testing of sediment materials confirmed that the presence of biochar at 30% by volume and at the particle size range applied (0.25-1.00 mm) did not compromise the permeability of the sediment-biochar mixture.
- Metformin removal in the HZ of BEST streambeds was greater with longer flowpaths, suggesting that engineered streambeds with greater HZ residence times will likely lead to enhanced adsorption and biodegradation. As no guanylyurea was detected above the limit of quantitation (LOQ) of the analytical detection method, further degradation may have been occurring (possibly full mineralization).
- Amendment of a BEST streambed with biochar resulted in a pronounced decrease in metformin breakthrough curve amplitude in the downwelling zone of the HZ and complete removal of metformin along the flowpaths (upwelling zone).
- BEST streambeds induced a distinct succession of redox conditions along hyporheic flowpaths that likely created ideal biotransformation conditions for metformin/guanylyurea: whereas the highly oxygenated downwelling zone favored the microbial transformation of metformin to guanylyurea, further degradation of guanylyurea was likely enhanced along the increasingly anoxic HZ flowpaths.
- When metformin was spiked to the flume at a higher dose ($C_0 = 10$ mg/L), four additional transformation products were identified in surface water and porewater samples: 1-methyl-biguanide, 2-4-AMT / 4-2-1-AIMT, 2-4-DAT, and biguanide.

5.1.3 Objective 3: TO_rCs Removal in Pilot-Scale Engineered Streambed Hyporheic Zones

The aim of the research described in Chapter 4 was to evaluate the removal efficiency of different BEST engineered streambed configurations (with subsurface impermeable walls and with/without biochar) for a wide range of TO_rCs with different biogeochemical properties. This research was conducted in a pilot-scale outdoor flume system installed at the Mines Park Water Reclamation Facility at the Colorado School of Mines in Golden, CO. The novel aspects of this work include studying a broad suite of stormwater-relevant TO_rCs in engineered streambed flumes under field conditions (i.e., temperature, sunlight exposure) using a representative recycled water matrix (i.e., municipal wastewater effluent).

Hypothesis 3: The addition of biochar to engineered HZ streambeds will enhance the removal of TOrCs and will result in measurable reach-scale attenuation along 15 meters of BEST streambeds. This hypothesis was tested in different contaminant experiments that allowed determination of the reach-scale attenuation, longer-term performance (extended contact times), and the potential for TOrC biotransformation of different streambed configurations. The following configurations were evaluated: sand-only control streambed (F1), BEST streambeds (F2), BEST streambeds amended with biochar (F3), and BEST streambeds containing fine-grain sand mixed with biochar (F4). The most significant findings of this work include:

- Out of the four tested streambed configurations, the most promising one was the biochar-amended BEST system (F3), providing efficient reduction in both TOrC concentration peaks and mass loadings – most likely by creating a sufficient extent of hyporheic exchange between the surface water and porewater.
- TOrC peak concentrations and mass retention remained mostly unaffected in both sand-only flumes (F1, F2). However, sand-only BEST modules (F2) showed promising potential for active biodegradation processes in the HZ.
- The biochar-amended BEST featuring a low permeability streambed (F4) yielded greater removal per module compared to all other treatments, but failed to provide the same reach-scale peak concentration reductions as observed in F3 – presumably due to limited hyporheic exchange.
- Removal of TOrCs on the module scale was highly dependent on biochar addition: along one-meter length, biochar led to substantial reductions in subsurface breakthrough curve amplitudes, even in the case of highly polar TOrCs. The effect of biochar on subsurface concentrations was greater in streambeds with lower permeability (F4; fine-grain sand) compared to higher permeability (F3; coarser sand).
- The only contaminant whose reach-scale removal under stormflow conditions did not greatly benefit from the addition of biochar and/or longer HZ residence times was the perfluorohexanoate (PFHxA): surface concentration peak reductions stayed below 5% for both F3 and F4, even though some removal occurred on the module-scale (e.g., 38% removal in Module #3 of F4).

5.2 Research Contributions and Significance

The work presented in Chapter 2 has shown that biofilms in biochar-amended biofilters provided sustained TOrC removal through regenerated biochar sorption capacity and a two-fold prolonged filter

lifetime (compared to biofilm inactivated conditions). These findings provide insight into the design of bioinfiltration systems in practice: the addition of biochar in combination with a relatively porous media such as sand may help to establish an active microbial community in the biofilter with an estimated filter lifetime of over 15 years. A self-restoring system would certainly lead to less maintenance efforts and costs over the filter's lifetime. In field applications, the presence of biofilms would most likely not be a design choice but instead an inevitable feature of biofilters due to the presence of dissolved organic carbon (DOC) and microorganisms in stormwater. This observation – that biofilm growth (or biofouling) does not necessarily decrease filtration capacities – is consistent with previous observations in other passive water treatment applications (Chomiak *et al.*, 2015).

Research findings from Chapter 3 highlighted that BEST engineered HZs promoted fast and efficient removal of the highly polar compounds metformin and possibly also the metabolite guanyurea ($\log K_{OW} \leq -2$). BEST streambeds induced a succession of redox conditions (oxic – anoxic – anaerobic) along the hyporheic flowpaths that likely offered favorable biotransformation conditions for metformin and its TPs, which may be beneficial for other TOrCs as well. Furthermore, in pilot-scale BEST flumes (Chapter 4), 30 different TPs of pesticides and pharmaceuticals were observed in sand-only streambeds, which indicates promising potential for active biodegradation processes. These findings suggest that there was a microbially active and likely diverse HZ present in the BEST streambeds, similar to a natural HZ environment. Based on TP analysis, the microbial ecosystem led to a range of different biotic transformation pathways, including e.g., biotic hydrolysis, N-demethylation, and hydroxylation. Thus, BEST streambeds may feature a microbially active HZ, with the added benefit of hydraulic residence time control and the potential for increased streambed reactivity when geomedia is added. The beneficial effect of a biofilm layer on biochar's sustained sorption capacity that was shown for biofilters (Chapter 2) may similarly apply to microbially active streambeds amended with biochar.

In the past, little focus has been placed on the analysis of TOrC metabolites in SCM effluents, likely because there are no regulatory discharge limits for TOrCs or their TPs yet. With recent advancements in analytical measurement capabilities for TOrCs, especially polar compounds (Reemtsma *et al.*, 2016), and the increasing awareness of widespread occurrence of TPs in the aquatic cycle and their potential threat to aquatic and human health (Kiefer *et al.*, 2019; Mahler *et al.*, 2021), greater effort is now being made to include TPs in stormwater management decisions in cities (Wolfand *et al.*, 2019). For example, several TPs of benzotriazole were detected in a monitoring study of a bioretention field-installation, including microbial TPs (e.g., methyl-benzotriazole) and benzotriazole phytotransformation metabolites (Gu *et al.*, 2021). However, available studies are rare and are completely missing in the case of biochar-amended SCMs. In this context, major contributions of this dissertation include the elucidation of dominant microbial

transformation pathways of TOrCs in biofilters and engineered HZ streambeds in the presence/absence of biochar. All work conducted suggests that limited release of TPs in the presence of biochar would occur. Furthermore, some of the TOrCs included in this dissertation are emerging contaminants with a lack of environmental research data (e.g., neonicotinoid insecticides). Experimental data on their fate and transformation pathways in biochar-amended SCMs will help to close some of these research gaps.

Since BEST engineered hyporheic zones are a relatively novel stormwater treatment technology that is not (yet) widely accepted in practice, the collection of contaminant performance data is crucial to facilitate regulatory approval and acceptance of the technology by stormwater managers. Chapter 4 of this dissertation provides critical performance data and basic design recommendations for BEST applications: 14 consecutive 1-m long modules featuring BEST streambeds amended with 7% biochar (by volume) and sand (8-mesh Unimin) resulted in surface peak concentration reductions of >50% for all TOrCs studied (with the exception of PFHxA). Concentration peak reductions in stormwater runoff have important implications for the protection of aquatic life as it decreases acute toxicity impacts (Bundschuh *et al.*, 2013). Decreased freshwater ecotoxicity helps preserve ecosystem function and aquatic food-chains (Bundschuh *et al.*, 2013) of nearby stormwater-impacted surface waters. Moreover, the work in Chapter 4 showed that a streambed configuration consisting of a sand with lower permeability (hydraulic conductivity) resulted in limited hyporheic exchange and thus limited reach-scale removal of TOrCs – even in the presence of biochar. All told, these results highlight the importance of hydraulic conductivity properties of the media of choice (e.g. sand) to optimize HZ exchange and the addition of strong geosorbents (e.g. biochar) to the sediment for accelerated removal in the design of BEST streambed applications.

The work presented in this dissertation indicates that both biochar-amended biofilters and BEST engineered streambeds have great potential to offer broad water quality improvements in urban areas (even under space-limited circumstances). Water quality upgrades culminate in greater protection of stream ecosystems, groundwater resources, and aquatic organisms. Furthermore, biochar additions have been shown to enhance the available water holding capacity of soils (Omondi *et al.*, 2016), thus there is potential to reverse some of the negative impacts that impervious surfaces pose on the urban water cycle by promoting infiltration. The research in this dissertation identified no readily apparent negative impacts of biochar additions to SCMs, which will hopefully benefit the incorporation of these novel technologies in future stormwater management decisions. Both biochar-amended BEST and biofilters offer relatively flexible application depending on space availability and priority contaminants, whereas the decision of horizontal streambeds vs. bioinfiltration might be site-specific. For example, an infiltration system might be less prone to wash-out due to large stormflow volumes and might have a lower land footprint, whereas BEST streambeds could offer ecological benefits and attractive recreation space in cities. In an urban

world that is increasingly decoupled from natural ecosystems (Gómez-Baggethun & Barton, 2013), green infrastructure spaces such as planted biofilters or engineered streambeds could form green islands that provide ecosystem services that go beyond water treatment, including habitat function for aquatic flora and fauna, biodiversity conservation, mitigation of the urban heat island effect, and physical and mental health benefits for humans (Tzoulas *et al.*, 2007).

Lastly, biochar-amended SCMs can be important tools in the combat to mitigate impacts of climate change and water scarcity/degradation on the urban water cycle: local non-potable reuse of stormwater runoff is a valuable measure to alleviate water supply shortages in cities (Luthy *et al.*, 2019) – this could be especially relevant in dry climates, where every drop of water counts. Furthermore, production of biochar through the reuse of local biomass waste materials (e.g., coconut shells, wood waste, algae biomass) is a comparably cost-effective reuse strategy and provides carbon sequestration benefits (Miller-Robbie *et al.*, 2015). While biochar use in the capacity of amendments to SCMs would not necessarily capture large amounts of carbon, it could contribute to a broader use of biochar in environmental applications.

5.3 Recommendations for Future Research

The work presented in this dissertation advanced our understanding of TOrC removal performance and the role of biofilms in biochar-amended SCMs, i.e., biofilters and BEST engineered streambeds. However, open questions remain pertaining to field applications of these novel technologies and emerging contaminants in the urban context. In particular, as real stormwater almost exclusively consists of a mixture of different contaminant classes, e.g. nutrients, TOrCs, and heavy metals, it would be meaningful to study biofilter lifetime (exhaustive breakthrough) in more mixed contaminants studies. Especially in the case of metals and TOrCs, there could be competitive (e.g. related to sorption sites) or potentially synergistic effects (e.g. co-precipitation) in the presence of biochar. Since metals are non-degradable, they might determine when the biochar media needs to be replaced (Ulrich *et al.*, 2015). Moreover, it may be helpful to understand how the presence of a biofilm layer affects metals retention in biofilters.

Additional TOrC sampling of the HZ of biochar-amended BEST engineered streambeds are also needed to collect high-resolution data (both spatially and temporally) that could be used for the calibration of a surface-subsurface coupled contaminant transport model (i.e., in COMSOL Multiphysics). A contaminant transport model could help elucidate the contribution of different processes (i.e., sorption and biodegradation) in TOrC removal. Additionally, it would be valuable to investigate if TOrC sorption kinetics related to biochar are diffusion controlled, similar to what has been reported for TOrCs in vertical biofilters (Ulrich *et al.*, 2015). Depending on the design and streambed conditions (i.e., surface flow rate, hydraulic conductivity of the sediment), porous media flow in horizontal biofilters might be sufficiently slow

so that diffusion effects on TOrC sorption kinetics could be ignored – which would vastly simplify modelling efforts including parameter estimation and model calibration.

There is also a need for empirical studies of both these novel SCMs in the field, most importantly under dynamic conditions. The research presented in this dissertation focused on constant flow rates and constant water quality of the influent. However, variable flow rates (i.e., baseflow vs. stormflow) and extended dry periods could substantially change the media properties, microbial community composition, and likely the sorption properties or reactivity of the biochar. Moreover, in geographic locations with four seasons, freeze-thaw cycles might greatly impact the overall performance and TOrC removal in field-scale SCMs. Most importantly, long-term performance data that goes beyond singular storm-event water quality monitoring may be needed by some stormwater managers to justify the installation of biochar-amended systems (compared to a conventional biofilter or no installation at all). Specifically for BEST, strategies for easy geomedia installation and replacement need to be tested in the field. For a novel technology to be attractive to stormwater managers, the benefits of enhanced performance need to outweigh potentially added cost related to media, installation, and maintenance.

Finally, in relation to TOrCs released to urban environments, there are two main areas of research needs. First, metabolites of TOrCs need to be included regularly in future research efforts. For example, there is a need for studies on removal and adsorption mechanisms of TPs by biochars (or comparable geomedia), similar to the work of Webb *et al.* (2020) conducted for TPs of neonicotinoid insecticides. This type of knowledge will aid in estimating the leaching risk of TPs from biochar-amended SCMs for other TOrCs without necessarily performing laborious field studies. Second, the research presented in this dissertation highlights the shortcomings in the removal of poly- and perfluoroalkyl substances (PFASs, as exemplified by PFHxA) in biochar-amended stormwater treatment systems, which has important environmental implications beyond water quality and warrants future research. Development/design of biochars or alternative (carbonaceous) adsorbents with greater sorption capacities for PFASs under fast flow conditions are urgently needed.

REFERENCES

- Abromaitis, V, Racys, V, van der Marel, P, & Meulepas, R J W. 2016. Biodegradation of persistent organics can overcome adsorption–desorption hysteresis in biological activated carbon systems. *Chemosphere*, **149**, 183–189.
- Ahmad, Mahtab, Rajapaksha, Anushka Upamali, Lim, Jung Eun, Zhang, Ming, Bolan, Nanthi, Mohan, Dinesh, Vithanage, Meththika, Lee, Sang Soo, & Ok, Yong Sik. 2014. Biochar as a sorbent for contaminant management in soil and water: A review. *Chemosphere*, **99**(Mar.), 19–33.
- Aktaş, Özgür, & Çeçen, Ferhan. 2007. Bioregeneration of activated carbon: A review. *International Biodeterioration & Biodegradation*, **59**(4), 257–272.
- Amador, Cristina I., Canosa, Inés, Govantes, Fernando, & Santero, Eduardo. 2010. Lack of CbrB in *Pseudomonas putida* affects not only amino acids metabolism but also different stress responses and biofilm development. *Environmental Microbiology*, **12**(6), 1748–1761. Publisher: John Wiley & Sons, Ltd.
- Anderson, Brian S., Phillips, Bryn M., Voorhees, Jennifer P., Siegler, Katie, & Tjeerdema, Ronald. 2016. Bioswales reduce contaminants associated with toxicity in urban storm water. *Environmental Toxicology and Chemistry*, **35**(12), 3124–3134. Publisher: John Wiley & Sons, Ltd.
- Aronson, Dallas, Boethling, Robert, Howard, Philip, & Stiteler, William. 2006. Estimating biodegradation half-lives for use in chemical screening. *Chemosphere*, **63**(11), 1953–1960.
- Ashoori, Negin, Teixido, Marc, Spahr, Stephanie, LeFevre, Gregory H, Sedlak, David L, & Luthy, Richard G. 2019. Evaluation of pilot-scale biochar-amended woodchip bioreactors to remove nitrate, metals, and trace organic contaminants from urban stormwater runoff. *Water Research*, **154**, 1–11.
- Bach, Peter M., McCarthy, David T., & Deletic, Ana. 2010. Redefining the stormwater first flush phenomenon. *Water Research*, **44**(8), 2487–2498.
- Bahlmann, Arnold, Brack, Werner, Schneider, Rudolf J., & Krauss, Martin. 2014. Carbamazepine and its metabolites in wastewater: Analytical pitfalls and occurrence in Germany and Portugal. *Water Research*, **57**(June), 104–114.
- Berset, J D, Mermer, S, Robel, A E, Walton, V M, Chien, M L, & Field, J A. 2017. Direct residue analysis of systemic insecticides and some of their relevant metabolites in wines by liquid chromatography – mass spectrometry. *Journal of Chromatography A*, **1506**, 45–54.
- Bertrand-Krajewski, Jean-Luc, Chebbo, Ghassan, & Saget, Agnes. 1998. Distribution of pollutant mass vs volume in stormwater discharges and the first flush phenomenon. *Water Research*, **32**(8), 2341–2356.
- Blair, Benjamin D, Crago, Jordan P, Hedman, Curtis J, Treguer, Ronan J F, Magruder, Christopher, Royer, L Scott, & Klaper, Rebecca D. 2013. Evaluation of a model for the removal of pharmaceuticals, personal care products, and hormones from wastewater. *Science of The Total Environment*, **444**, 515–521.

- B Boehm, Alexandria B, Bell, Colin D, Fitzgerald, Nicole J M, Gallo, Elizabeth, Higgins, Christopher P, Hogue, Terri S, Luthy, Richard G, Portmann, Andrea C, Ulrich, Bridget A, & Wolfand, Jordyn M. 2020. Biochar-augmented biofilters to improve pollutant removal from stormwater—can they improve receiving water quality? *Environmental Science: Water Research & Technology*, **6**(6), 1520–1537. Publisher: Royal Society of Chemistry.
- Bonmatin, J.-M., Giorio, C, Girolami, V, Goulson, D, Kreutzweiser, D P, Krupke, C, Liess, M, Long, E, Marzaro, M, Mitchell, E A D, Noome, D A, Simon-Delso, N, & Tapparo, A. 2015. Environmental fate and exposure; neonicotinoids and fipronil. *Environmental Science and Pollution Research*, **22**(1), 35–67.
- Boulton, Andrew J, Findlay, Stuart, Marmonier, Pierre, Stanley, Emily H, & Valett, H Maurice. 1998. THE FUNCTIONAL SIGNIFICANCE OF THE HYPORHEIC ZONE IN STREAMS AND RIVERS. *Annual Review of Ecology and Systematics*, **29**(1), 59–81. Publisher: Annual Reviews.
- Bradley, Paul M, Journey, Celeste A, Button, Daniel T, Carlisle, Daren M, Clark, Jimmy M, Mahler, Barbara J, Nakagaki, Naomi, Qi, Sharon L, Waite, Ian R, & VanMetre, Peter C. 2016. Metformin and Other Pharmaceuticals Widespread in Wadeable Streams of the Southeastern United States. *Environmental Science & Technology Letters*, **3**(6), 243–249. Publisher: American Chemical Society.
- Bradley, Paul M, Journey, Celeste A, Romanok, Kristin M, Barber, Larry B, Buxton, Herbert T, Foreman, William T, Furlong, Edward T, Glassmeyer, Susan T, Hladik, Michelle L, Iwanowicz, Luke R, Jones, Daniel K, Kolpin, Dana W, Kuivila, Kathryn M, Loftin, Keith A, Mills, Marc A, Meyer, Michael T, Orlando, James L, Reilly, Timothy J, Smalling, Kelly L, & Villeneuve, Daniel L. 2017. Expanded Target-Chemical Analysis Reveals Extensive Mixed-Organic-Contaminant Exposure in U.S. Streams. *Environmental Science & Technology*, **51**(9), 4792–4802. Publisher: American Chemical Society.
- Briceño, G., Schalchli, H., Rubilar, O., Tortella, G.R., Mutis, A., Benimeli, C.S., Palma, G., & Diez, M.C. 2016. Increased diazinon hydrolysis to 2-isopropyl-6-methyl-4-pyrimidinol in liquid medium by a specific *Streptomyces* mixed culture. *Chemosphere*, **156**(Aug.), 195–203.
- Brunner, Andrea Mizzi, Vughs, Dennis, Siegers, Wolter, Bertelkamp, Cheryl, Hofman-Caris, Roberta, Kolkman, Annemieke, & ter Laak, Thomas. 2019. Monitoring transformation product formation in the drinking water treatments rapid sand filtration and ozonation. *Chemosphere*, **214**(Jan.), 801–811.
- Bundschuh, Mirco, Zubrod, Jochen P., Klemm, Patricia, Elsaesser, David, Stang, Christoph, & Schulz, Ralf. 2013. Effects of peak exposure scenarios on *Gammarus fossarum* using field relevant pesticide mixtures. *Ecotoxicology and Environmental Safety*, **95**(Sept.), 137–143.
- Burant, Aniela, Selbig, William, Furlong, Edward T., & Higgins, Christopher P. 2018. Trace organic contaminants in urban runoff: Associations with urban land-use. *Environmental Pollution*, **242**(Nov.), 2068–2077.
- Burke, Victoria, Greskowiak, Janek, Asmuß, Tina, Bremermann, Rebecca, Taute, Thomas, & Massmann, Gudrun. 2014. Temperature dependent redox zonation and attenuation of wastewater-derived organic micropollutants in the hyporheic zone. *Science of The Total Environment*, **482**, 53–61.
- Caldwell, Daniel J, D’Aco, Vincent, Davidson, Todd, Kappler, Kelly, Murray-Smith, Richard J, Owen, Stewart F, Robinson, Paul F, Simon-Hettich, Brigitte, Straub, Jürg Oliver, & Tell, Joan. 2019. Environmental risk assessment of metformin and its transformation product guanylurea: II. Occurrence in surface waters of Europe and the United States and derivation of predicted no-effect concentrations. *Chemosphere*, **216**, 855–865.
- Cardenas, M Bayani. 2015. Hyporheic zone hydrologic science: A historical account of its emergence and a prospectus. *Water Resources Research*, **51**(5), 3601–3616.

- Chen, Shanshan, Rotaru, Amelia-Elena, Shrestha, Pravin Malla, Malvankar, Nikhil S, Liu, Fanghua, Fan, Wei, Nevin, Kelly P, & Lovley, Derek R. 2014. Promoting Interspecies Electron Transfer with Biochar. *Scientific Reports*, **4**(May), 5019. Publisher: Nature Publishing Group.
- Chomiak, A., Traber, J., Morgenroth, E., & Derlon, N. 2015. Biofilm increases permeate quality by organic carbon degradation in low pressure ultrafiltration. *Water Research*, **85**(Nov.), 512–520.
- Clark, Shirley E, & Pitt, Robert. 2012. Targeting treatment technologies to address specific stormwater pollutants and numeric discharge limits. *Water Research*, **46**(20), 6715–6730.
- Crago, Jordan, Bui, Cindy, Grewal, Sanji, & Schlenk, Daniel. 2016. Age-dependent effects in fathead minnows from the anti-diabetic drug metformin. *General and Comparative Endocrinology*, **232**, 185–190.
- Cui, Hao, & Schröder, Peter. 2016. Uptake, translocation and possible biodegradation of the antidiabetic agent metformin by hydroponically grown *Typha latifolia*. *Journal of Hazardous Materials*, **308**(Supplement C), 355–361.
- Dalahmeh, Sahar, Ahrens, Lutz, Gros, Meritxell, Wiberg, Karin, & Pell, Mikael. 2018. Potential of biochar filters for onsite sewage treatment: Adsorption and biological degradation of pharmaceuticals in laboratory filters with active, inactive and no biofilm. *Science of The Total Environment*, **612**(Jan.), 192–201.
- Dalahmeh, Sahar S, Alziq, Nancy, & Ahrens, Lutz. 2019. Potential of biochar filters for onsite wastewater treatment: Effects of active and inactive biofilms on adsorption of per- and polyfluoroalkyl substances in laboratory column experiments. *Environmental Pollution*, **247**, 155–164.
- De Bhowmick, Goldy, Briones, Rowena M., Thiele-Bruhn, Sören, Sen, Ramkrishna, & Sarmah, Ajit K. 2022. Adsorptive removal of metformin on specially designed algae-lignocellulosic biochar mix and techno-economic feasibility assessment. *Environmental Pollution*, **292**(Jan.), 118256.
- Desiante, Werner L., Minas, Nora S., & Fenner, Kathrin. 2021. Micropollutant biotransformation and bioaccumulation in natural stream biofilms. *Water Research*, **193**(Apr.), 116846.
- Dick, Ryan A., Kanne, David B., & Casida, John E. 2006. Substrate Specificity of Rabbit Aldehyde Oxidase for Nitroguanidine and Nitromethylene Neonicotinoid Insecticides. *Chemical Research in Toxicology*, **19**(1), 38–43. Publisher: American Chemical Society.
- Douglass, James F., Radosevich, Mark, & Tuovinen, Olli H. 2014. Mineralization of atrazine in the river water intake and sediments of a constructed flow-through wetland. *The Olentangy River Wetland Research Park: Two Decades of Research on Ecosystem Services*, **72**(Nov.), 35–39.
- Fang, Hua, Cai, Lin, Yang, Ying, Ju, Feng, Li, Xiangdong, Yu, Yunlong, & Zhang, Tong. 2014. Metagenomic analysis reveals potential biodegradation pathways of persistent pesticides in freshwater and marine sediments. *Science of The Total Environment*, **470-471**(Feb.), 983–992.
- Ferrando-Climent, Laura, Collado, Neus, Buttiglieri, Gianluigi, Gros, Meritxell, Rodriguez-Roda, Ignasi, Rodriguez-Mozaz, Sara, & Barceló, Damià. 2012. Comprehensive study of ibuprofen and its metabolites in activated sludge batch experiments and aquatic environment. *Science of The Total Environment*, **438**(Nov.), 404–413.
- Fischer, Helmut, Kloep, Frank, Wilzcek, Sabine, & Pusch, Martin T. 2005. A River's Liver – Microbial Processes within the Hyporheic Zone of a Large Lowland River. *Biogeochemistry*, **76**(2), 349–371.

- Flanagan, Kelsey, Branchu, Philippe, Boudahmane, Lila, Caupos, Emilie, Demare, Dominique, Deshayes, Steven, Dubois, Philippe, Meffray, Laurent, Partibane, Chandirane, Saad, Mohamed, & Gromaire, Marie-Christine. 2018. Field performance of two biofiltration systems treating micropollutants from road runoff. *Water Research*, **145**, 562–578.
- Flanagan, Kelsey, Blecken, Godecke-Tobias, Österlund, Heléne, Nordqvist, Kerstin, & Viklander, Maria. 2021. Contamination of Urban Stormwater Pond Sediments: A Study of 259 Legacy and Contemporary Organic Substances. *Environmental Science & Technology*, **55**(5), 3009–3020. Publisher: American Chemical Society.
- Frankel, Mathew L, Bhuiyan, Tazul I, Veksha, Andrei, Demeter, Marc A, Layzell, David B, Helleur, Robert J, Hill, Josephine M, & Turner, Raymond J. 2016. Removal and biodegradation of naphthenic acids by biochar and attached environmental biofilms in the presence of co-contaminating metals. *Bioresource Technology*, **216**, 352–361.
- Gaber, Seleem E, Hussain, Mohammed T, & Jahin, Hossam S. 2020. Bioremediation of diazinon pesticide from aqueous solution by fungal-strains isolated from wastewater. *World J Chem*, **15**(1), 15–23.
- Gasperi, J, Sebastian, C, Ruban, V, Delamain, M, Percot, S, Wiest, L, Mirande, C, Caupos, E, Demare, D, Kessoo, M Diallo Kessoo, Saad, M, Schwartz, J J, Dubois, P, Fratta, C, Wolff, H, Moilleron, R, Chebbo, G, Cren, C, Millet, M, Barraud, S, & Gromaire, M C. 2014. Micropollutants in urban stormwater: occurrence, concentrations, and atmospheric contributions for a wide range of contaminants in three French catchments. *Environmental Science and Pollution Research*, **21**(8), 5267–5281.
- Giroud, Barbara, Vauchez, Antoine, Vulliet, Emmanuelle, Wiest, Laure, & Buleté, Audrey. 2013. Trace level determination of pyrethroid and neonicotinoid insecticides in beebread using acetonitrile-based extraction followed by analysis with ultra-high-performance liquid chromatography–tandem mass spectrometry. *Journal of Chromatography A*, **1316**(Nov.), 53–61.
- Grebel, Janel E, Mohanty, Sanjay K, Torkelson, Andrew A, Boehm, Alexandria B, Higgins, Christopher P, Maxwell, Reed M, Nelson, Kara L, & Sedlak, David L. 2013. Engineered Infiltration Systems for Urban Stormwater Reclamation. *Environmental Engineering Science*, **30**(8), 437–454. Publisher: Mary Ann Liebert, Inc., publishers.
- Grebel, Janel E, Charbonnet, Joseph A, & Sedlak, David L. 2016. Oxidation of organic contaminants by manganese oxide geomedia for passive urban stormwater treatment systems. *Water Research*, **88**(Jan.), 481–491.
- Greskowiak, Janek, Hamann, Enrico, Burke, Victoria, & Massmann, Gudrun. 2017. The uncertainty of biodegradation rate constants of emerging organic compounds in soil and groundwater – A compilation of literature values for 82 substances. *Water Research*, **126**, 122–133.
- Gu, Xinyao, Rodgers, Timothy F. M., Spraakman, Sylvie, Van Seters, Tim, Flick, Robert, Diamond, Miriam L., Drake, Jennifer, & Passeport, Elodie. 2021. Trace Organic Contaminant Transfer and Transformation in Bioretention Cells: A Field Tracer Test with Benzotriazole. *Environmental Science & Technology*, **55**(18), 12281–12290. Publisher: American Chemical Society.
- Guillon, Amélie, Videloup, Christyne, Leroux, Clara, Bertin, Héloïse, Philibert, Marc, Baudin, Isabelle, Bruchet, Auguste, & Esperanza, Mar. 2018. Occurrence and fate of 27 triazines and metabolites within French drinking water treatment plants. *Water Supply*, **19**(2), 463–471.
- Gómez-Baggethun, Erik, & Barton, David N. 2013. Classifying and valuing ecosystem services for urban planning. *Ecological Economics*, **86**(Feb.), 235–245.

- Hale, Lauren, Luth, Madeline, & Crowley, David. 2015. Biochar characteristics relate to its utility as an alternative soil inoculum carrier to peat and vermiculite. *Soil Biology and Biochemistry*, **81**, 228–235.
- Hao, Chunyan, Noestheden, Matthew R, Zhao, Xiaoming, & Morse, David. 2016. Liquid chromatography–tandem mass spectrometry analysis of neonicotinoid pesticides and 6-chloronicotinic acid in environmental water with direct aqueous injection. *Analytica Chimica Acta*, **925**, 43–50.
- Harvey, Judson W, Böhlke, J K, Voytek, Mary A, Scott, Durrelle, & Tobias, Craig R. 2013. Hyporheic zone denitrification: Controls on effective reaction depth and contribution to whole-stream mass balance. *Water Resources Research*, **49**(10), 6298–6316.
- Hernández, Belén, Pflüger, Fernando, Kruglik, Sergei G., Cohen, Régis, & Ghomi, Mahmoud. 2015. Protonation–deprotonation and structural dynamics of antidiabetic drug metformin. *Journal of Pharmaceutical and Biomedical Analysis*, **114**(Oct.), 42–48.
- Herzog, S P, Higgins, C P, & McCray, J E. 2016. Engineered Streambeds for Induced Hyporheic Flow: Enhanced Removal of Nutrients, Pathogens, and Metals from Urban Streams. *Journal of Environmental Engineering*, **142**(1). Publisher: American Society of Civil Engineers.
- Herzog, Skuyler P., Higgins, Christopher P., Singha, Kamini, & McCray, John E. 2018. Performance of Engineered Streambeds for Inducing Hyporheic Transient Storage and Attenuation of Resazurin. *Environmental Science and Technology*, **52**(18), 10627–10636.
- Herzog, Skuyler P, Eisenstein, William A, Halpin, Brittnee N, Portmann, Andrea C, Fitzgerald, Nicole J M, Ward, Adam S, Higgins, Christopher P, & McCray, John E. 2019. Co-Design of Engineered Hyporheic Zones to Improve In-Stream Stormwater Treatment and Facilitate Regulatory Approval. *Water*, **11**(12), 2543. ISBN: 2073-4441.
- Hormazabal, V, & Ostensvik, O. 2011. Determination of metformin in cultivated plant species and soil by liquid chromatography-mass spectrometry. **33**(17-20), 1630–1639.
- Huntscha, Sebastian, Rodriguez Velosa, Diana M, Schroth, Martin H, & Hollender, Juliane. 2013. Degradation of Polar Organic Micropollutants during Riverbank Filtration: Complementary Results from Spatiotemporal Sampling and Push–Pull Tests. *Environmental Science & Technology*, **47**(20), 11512–11521. Publisher: American Chemical Society.
- Huntscha, Sebastian, Hofstetter, Thomas B, Schymanski, Emma L, Spahr, Stephanie, & Hollender, Juliane. 2014. Biotransformation of Benzotriazoles: Insights from Transformation Product Identification and Compound-Specific Isotope Analysis. *Environmental Science & Technology*, **48**(8), 4435–4443. Publisher: American Chemical Society.
- Hussain, Sarfraz, Hartley, Carol J, Shettigar, Madhura, & Pandey, Gunjan. 2016. Bacterial biodegradation of neonicotinoid pesticides in soil and water systems. *FEMS microbiology letters*, **363**(23). Publisher: Oxford University Press.
- Jaeger, Anna, Posselt, Malte, Betterle, Andrea, Schaper, Jonas, Mechelke, Jonas, Coll, Claudia, & Lewandowski, Joerg. 2019. Spatial and Temporal Variability in Attenuation of Polar Organic Micropollutants in an Urban Lowland Stream. *Environmental Science & Technology*, **53**(5), 2383–2395. Publisher: American Chemical Society.
- Jones, D L, Edwards-Jones, G, & Murphy, D V. 2011. Biochar mediated alterations in herbicide breakdown and leaching in soil. *Soil Biology and Biochemistry*, **43**(4), 804–813.

- Kah, Melanie, Sigmund, Gabriel, Xiao, Feng, & Hofmann, Thilo. 2017. Sorption of ionizable and ionic organic compounds to biochar, activated carbon and other carbonaceous materials. *Water Research*, **124**, 673–692.
- Kappler, Andreas, Wuestner, Marina Lisa, Ruecker, Alexander, Harter, Johannes, Halama, Maximilian, & Behrens, Sebastian. 2014. Biochar as an Electron Shuttle between Bacteria and Fe(III) Minerals. *Environmental Science & Technology Letters*, **1**(8), 339–344. Publisher: American Chemical Society.
- Kern, Susanne, Baumgartner, Rebekka, Helbling, Damian E, Hollender, Juliane, Singer, Heinz, Loos, Martin J, Schwarzenbach, Rene P, & Fenner, Kathrin. 2010. A tiered procedure for assessing the formation of biotransformation products of pharmaceuticals and biocides during activated sludge treatment. *Journal of Environmental Monitoring*, **12**(11), 2100–2111. Publisher: The Royal Society of Chemistry.
- Kiefer, Karin, Müller, Adrian, Singer, Heinz, & Hollender, Juliane. 2019. New relevant pesticide transformation products in groundwater detected using target and suspect screening for agricultural and urban micropollutants with LC-HRMS. *Water Research*, **165**, 114972.
- Kim, Bo Mi, Park, Joon-Seong, Choi, Jeong-Heui, Abd El-Aty, A M, Na, Tae Woong, & Shim, Jae-Han. 2012. Residual determination of clothianidin and its metabolites in three minor crops via tandem mass spectrometry. *Food Chemistry*, **131**(4), 1546–1551.
- Klarich, Kathryn L, Pflug, Nicholas C, DeWald, Eden M, Hladik, Michelle L, Kolpin, Dana W, Cwiertny, David M, & LeFevre, Gregory H. 2017. Occurrence of Neonicotinoid Insecticides in Finished Drinking Water and Fate during Drinking Water Treatment. *Environmental Science & Technology Letters*, **4**(5), 168–173. Publisher: American Chemical Society.
- Klimenko, N, Smolin, S, Grechanyk, S, Kofanov, V, Nevynna, L, & Samoylenko, L. 2003. Bioregeneration of activated carbons by bacterial degraders after adsorption of surfactants from aqueous solutions. *Colloids and Surfaces A: Physicochemical and Engineering Aspects*, **230**(1), 141–158.
- Klüpfel, Laura, Keiluweit, Marco, Kleber, Markus, & Sander, Michael. 2014. Redox Properties of Plant Biomass-Derived Black Carbon (Biochar). *Environmental Science & Technology*, **48**(10), 5601–5611. Publisher: American Chemical Society.
- Koba, Olga, Golovko, Oksana, Kodešová, Radka, Klement, Aleš, & Grabic, Roman. 2016. Transformation of atenolol, metoprolol, and carbamazepine in soils: The identification, quantification, and stability of the transformation products and further implications for the environment. *Environmental Pollution*, **218**(Nov.), 574–585.
- Kolekar, Parag D., Phugare, Swapnil S., & Jadhav, Jyoti P. 2014. Biodegradation of atrazine by *Rhodococcus* sp. BCH2 to N-isopropylammelide with subsequent assessment of toxicity of biodegraded metabolites. *Environmental Science and Pollution Research*, **21**(3), 2334–2345.
- Kosma, Christina I, Lambropoulou, Dimitra A, & Albanis, Triantafyllos A. 2015. Comprehensive study of the antidiabetic drug metformin and its transformation product guanylyurea in Greek wastewaters. *Water Research*, **70**(Supplement C), 436–448.
- Kwon, Seokjoon, & Pignatello, Joseph J. 2005. Effect of Natural Organic Substances on the Surface and Adsorptive Properties of Environmental Black Carbon (Char): Pseudo Pore Blockage by Model Lipid Components and Its Implications for N₂-Probed Surface Properties of Natural Sorbents. *Environmental Science & Technology*, **39**(20), 7932–7939. Publisher: American Chemical Society.

- Launay, Marie A, Dittmer, Ulrich, & Steinmetz, Heidrun. 2016. Organic micropollutants discharged by combined sewer overflows – Characterisation of pollutant sources and stormwater-related processes. *Water Research*, **104**, 82–92.
- Lawrence, Justin E, Skold, Magnus E, Hussain, Fatima A, Silverman, David R, Resh, Vincent H, Sedlak, David L, Luthy, Richard G, & McCray, John E. 2013. Hyporheic Zone in Urban Streams: A Review and Opportunities for Enhancing Water Quality and Improving Aquatic Habitat by Active Management. *Environmental Engineering Science*, **30**(8), 480–501. Publisher: Mary Ann Liebert, Inc., publishers.
- Lee, Haejin, Lau, Sim-Lin, Kayhanian, Masoud, & Stenstrom, Michael K. 2004. Seasonal first flush phenomenon of urban stormwater discharges. *Water Research*, **38**(19), 4153–4163.
- Lee, Yunhee, Kim, Yun-Ji, Khan, Muhammad Saiful Islam, & Na, Yun-Cheol. 2020. Identification and determination of by-products originating from ozonation of chlorpyrifos and diazinon in water by liquid chromatography–mass spectrometry. *Journal of Separation Science*, **43**(21), 4047–4057. Publisher: John Wiley & Sons, Ltd.
- LeFevre, Gregory H, Novak, Paige J, & Hozalski, Raymond M. 2012. Fate of Naphthalene in Laboratory-Scale Bioretention Cells: Implications for Sustainable Stormwater Management. *Environmental Science & Technology*, **46**(2), 995–1002. Publisher: American Chemical Society.
- LeFevre, Gregory H, Paus, Kim H, Natarajan, Poornima, Gulliver, John S, Novak, Paige J, & Hozalski, Raymond M. 2015. Review of dissolved pollutants in urban storm water and their removal and fate in bioretention cells. *Journal of Environmental Engineering*, **141**(1), 04014050. Publisher: American Society of Civil Engineers.
- Lewandowski, Jörg, Putschew, Anke, Schwesig, David, Neumann, Christiane, & Radke, Michael. 2011. Fate of organic micropollutants in the hyporheic zone of a eutrophic lowland stream: Results of a preliminary field study. *Science of The Total Environment*, **409**(10), 1824–1835.
- Li, Xiaojing, Li, Yue, Zhang, Xiaolin, Zhao, Xiaodong, Chen, Xiaodong, & Li, Yongtao. 2020. The metolachlor degradation kinetics and bacterial community evolution in the soil bioelectrochemical remediation. *Chemosphere*, **248**(June), 125915.
- Li, Zhe, Sobek, Anna, & Radke, Michael. 2015. Flume Experiments To Investigate the Environmental Fate of Pharmaceuticals and Their Transformation Products in Streams. *Environmental Science & Technology*, **49**(10), 6009–6017. Publisher: American Chemical Society.
- Lin, Kunde, Haver, Darren, Oki, Lorence, & Gan, Jay. 2008. Transformation and Sorption of Fipronil in Urban Stream Sediments. *Journal of Agricultural and Food Chemistry*, **56**(18), 8594–8600. Publisher: American Chemical Society.
- Liu, Charlie J, Werner, David, & Bellona, Christopher. 2019. Removal of per- and polyfluoroalkyl substances (PFASs) from contaminated groundwater using granular activated carbon: a pilot-scale study with breakthrough modeling. *Environmental Science: Water Research & Technology*, **5**(11), 1844–1853. Publisher: The Royal Society of Chemistry.
- Liu, Jie, Ding, Yanli, Ma, Lili, Gao, Guanghai, & Wang, Yingying. 2017a. Combination of biochar and immobilized bacteria in cypermethrin-contaminated soil remediation. *International Biodeterioration & Biodegradation*, **120**, 15–20.

- Liu, Junguo, Yang, Hong, Gosling, Simon N, Kummu, Matti, Flörke, Martina, Pfister, Stephan, Hanasaki, Naota, Wada, Yoshihide, Zhang, Xinxin, Zheng, Chunmiao, Alcamo, Joseph, & Oki, Taikan. 2017b. Water scarcity assessments in the past, present, and future. *Earth's Future*, **5**(6), 545–559. Publisher: John Wiley & Sons, Ltd.
- Loos, Robert, Locoro, Giovanni, Comero, Sara, Contini, Serafino, Schwesig, David, Werres, Friedrich, Balsaa, Peter, Gans, Oliver, Weiss, Stefan, Blaha, Ludek, Bolchi, Monica, & Gawlik, Bernd Manfred. 2010. Pan-European survey on the occurrence of selected polar organic persistent pollutants in ground water. *Water Research*, **44**(14), 4115–4126.
- Luo, Y, Durenkamp, M, De Nobili, M, Lin, Q, Devonshire, B J, & Brookes, P C. 2013. Microbial biomass growth, following incorporation of biochars produced at 350 °C or 700 °C, in a silty-clay loam soil of high and low pH. *Soil Biology and Biochemistry*, **57**, 513–523.
- Luthy, Richard G, Sharvelle, Sybil, & Dillon, Peter. 2019. Urban Stormwater to Enhance Water Supply. *Environmental Science & Technology*, **53**(10), 5534–5542. Publisher: American Chemical Society.
- López-Muñoz, M.J., Revilla, A., & Aguado, J. 2013. Heterogeneous photocatalytic degradation of isoproturon in aqueous solution: Experimental design and intermediate products analysis. *SELECTED CONTRIBUTIONS OF THE 7th EUROPEAN MEETING ON SOLAR CHEMISTRY AND PHOTOCATALYSIS: ENVIRONMENTAL APPLICATIONS (SPEA 7)*, **209**(June), 99–107.
- Ma, Li Ya, Zhang, Shu Hao, Zhang, Jing Jing, Zhang, Ai Ping, Li, Na, Wang, Xin Qiang, Yu, Qian Qian, & Yang, Hong. 2018. Jasmonic Acids Facilitate the Degradation and Detoxification of Herbicide Isoproturon Residues in Wheat Crops (*Triticum aestivum*). *Chemical Research in Toxicology*, **31**(8), 752–761. Publisher: American Chemical Society.
- Mahler, Barbara J., Nowell, Lisa H., Sandstrom, Mark W., Bradley, Paul M., Romanok, Kristin M., Konrad, Christopher P., & Van Metre, Peter C. 2021. Inclusion of Pesticide Transformation Products Is Key to Estimating Pesticide Exposures and Effects in Small U.S. Streams. *Environmental Science & Technology*, **55**(8), 4740–4752. Publisher: American Chemical Society.
- Malev, Olga, Klobučar, Roberta Sauerborn, Fabbretti, Elsa, & Trebše, Polonca. 2012. Comparative toxicity of imidacloprid and its transformation product 6-chloronicotinic acid to non-target aquatic organisms: Microalgae *Desmodesmus subspicatus* and amphipod *Gammarus fossarum*. *Pesticide Biochemistry and Physiology*, **104**(3), 178–186.
- Maragou, Niki C., Thomaidis, Nikolaos S., & Koupparis, Michael A. 2011. Optimization and Comparison of ESI and APCI LC-MS/MS Methods: A Case Study of Irgarol 1051, Diuron, and their Degradation Products in Environmental Samples. *Journal of the American Society for Mass Spectrometry*, **22**(10). Publisher: American Society for Mass Spectrometry. Published by the American Chemical Society. All rights reserved.
- Marco-Urrea, Ernest, Pérez-Trujillo, Miriam, Vicent, Teresa, & Caminal, Gloria. 2009. Ability of white-rot fungi to remove selected pharmaceuticals and identification of degradation products of ibuprofen by *Trametes versicolor*. *Chemosphere*, **74**(6), 765–772.
- Markiewicz, Marta, Jungnickel, Christian, Stolte, Stefan, Białk-Bielińska, Anna, Kumirska, Jolanta, & Mroziak, Wojciech. 2017. Primary degradation of antidiabetic drugs. *Journal of Hazardous Materials*, **324**(Feb.), 428–435.

- Masoner, Jason R., Kolpin, Dana W., Cozzarelli, Isabelle M., Barber, Larry B., Burden, David S., Foreman, William T., Forshay, Kenneth J., Furlong, Edward T., Groves, Justin F., Hladik, Michelle L., Hopton, Matthew E., Jaeschke, Jeanne B., Keefe, Steffanie H., Krabbenhoft, David P., Lowrance, Richard, Romanok, Kristin M., Rus, David L., Selbig, William R., Williams, Brianna H., & Bradley, Paul M. 2019. Urban Stormwater: An Overlooked Pathway of Extensive Mixed Contaminants to Surface and Groundwaters in the United States. *Environmental Science & Technology*, **53**(17), 10070–10081. Publisher: American Chemical Society.
- McKnight, Ursula S, Rasmussen, Jes J, Kronvang, Brian, Binning, Philip J, & Bjerg, Poul L. 2015. Sources, occurrence and predicted aquatic impact of legacy and contemporary pesticides in streams. *Environmental Pollution*, **200**, 64–76.
- Menger, Frank, Boström, Gustaf, Jonsson, Ove, Ahrens, Lutz, Wiberg, Karin, Kreuger, Jenny, & Gago-Ferrero, Pablo. 2021. Identification of Pesticide Transformation Products in Surface Water Using Suspect Screening Combined with National Monitoring Data. *Environmental Science & Technology*, **55**(15), 10343–10353. Publisher: American Chemical Society.
- Meyer, Armin H, Penning, Holger, & Elsner, Martin. 2009. C and N Isotope Fractionation Suggests Similar Mechanisms of Microbial Atrazine Transformation Despite Involvement of Different Enzymes (AtzA and TrzN). *Environmental Science & Technology*, **43**(21), 8079–8085. Publisher: American Chemical Society.
- Miles, Thomas R, Rasmussen, Erin M, & Gray, Myles. 2016. Aqueous Contaminant Removal and Stormwater Treatment Using Biochar. *Pages 341–376 of: Agricultural and Environmental Applications of Biochar: Advances and Barriers*. Madison, WI: Soil Science Society of America, Inc. Series Title: SSSA Special Publication SV - 63.
- Miller, Janet L, Schmidt, Travis S, Van Metre, Peter C, Mahler, Barbara J, Sandstrom, Mark W, Nowell, Lisa H, Carlisle, Daren M, & Moran, Patrick W. 2020. Common insecticide disrupts aquatic communities: A mesocosm-to-field ecological risk assessment of fipronil and its degradates in US streams. *Science advances*, **6**(43), eabc1299. Publisher: American Association for the Advancement of Science.
- Miller-Robbie, Leslie, Ulrich, Bridget A, Ramey, Dotti F, Spencer, Kathryn S, Herzog, Skuyler P, Cath, Tzahi Y, Stokes, Jennifer R, & Higgins, Christopher P. 2015. Life cycle energy and greenhouse gas assessment of the co-production of biosolids and biochar for land application. *Journal of Cleaner Production*, **91**, 118–127.
- Mnif, Wissem, Hassine, Aziza Ibn Hadj, Bouaziz, Aicha, Bartegi, Aghleb, Thomas, Olivier, & Roig, Benoit. 2011. Effect of endocrine disruptor pesticides: a review. *International journal of environmental research and public health*, **8**(6), 2265–2303. Publisher: Molecular Diversity Preservation International.
- Mohanty, Sanjay K, Valenca, Renan, Berger, Alexander W, Yu, Iris K M, Xiong, Xinni, Saunders, Trenton M, & Tsang, Daniel C W. 2018. Plenty of room for carbon on the ground: Potential applications of biochar for stormwater treatment. *Science of The Total Environment*, **625**, 1644–1658.
- Mori, Toshio, Wang, Jianqiao, Tanaka, Yusuke, Nagai, Kaoru, Kawagishi, Hirokazu, & Hirai, Hirofumi. 2017. Bioremediation of the neonicotinoid insecticide clothianidin by the white-rot fungus *Phanerochaete sordida*. *Journal of Hazardous Materials*, **321**(Jan.), 586–590.
- Mudhoo, Ackmez, & Garg, VK. 2011. Sorption, transport and transformation of atrazine in soils, minerals and composts: a review. *Pedosphere*, **21**(1), 11–25. Publisher: Elsevier.
- Muerdter, Claire P, & LeFevre, Gregory H. 2019. Synergistic Lemna Duckweed and Microbial Transformation of Imidacloprid and Thiacloprid Neonicotinoids. *Environmental Science & Technology Letters*, **6**(12), 761–767. Publisher: American Chemical Society.

- Mulligan, Rebecca A, Tomco, Patrick L, Howard, Megan W, Schempp, Tabitha T, Stewart, Davis J, Stacey, Phillip M, Ball, David B, & Tjeerdema, Ronald S. 2016. Aerobic versus Anaerobic Microbial Degradation of Clothianidin under Simulated California Rice Field Conditions. *Journal of Agricultural and Food Chemistry*, **64**(38), 7059–7067. Publisher: American Chemical Society.
- Nauen, Ralf, Reckmann, Udo, Armbrorst, Stefan, Stupp, Hans-Peter, & Elbert, Alfred. 1999. Whitefly-active metabolites of imidacloprid: biological efficacy and translocation in cotton plants. *Pesticide Science*, **55**(3), 265–271. Publisher: John Wiley & Sons, Ltd.
- Niemuth, Nicholas J, & Klaper, Rebecca D. 2015. Emerging wastewater contaminant metformin causes intersex and reduced fecundity in fish. *Chemosphere*, **135**, 38–45.
- Niemuth, Nicholas J, & Klaper, Rebecca D. 2018. Low-dose metformin exposure causes changes in expression of endocrine disruption-associated genes. *Aquatic Toxicology*, **195**, 33–40.
- Nikolaivits, Efstratios, Agrafiotis, Andreas, Termentzi, Aikaterini, Machera, Kyriaki, Le Goff, Géraldine, Álvarez, Pedro, Chavanich, Suchana, Benayahu, Yehuda, Ouazzani, Jamal, & Fokialakis, Nikolas. 2019. Unraveling the detoxification mechanism of 2, 4-dichlorophenol by marine-derived mesophotic symbiotic fungi isolated from marine invertebrates. *Marine drugs*, **17**(10), 564. Publisher: Multidisciplinary Digital Publishing Institute.
- OECD. 2000 (Jan.). *Guideline 106 for the testing of chemicals- Adsorption - Desorption Using a Batch Equilibrium Method*. Tech. rept. OECD. Publication Title: OECD Organisation for Economic Co-Operation and Development Issue: January ISBN: 9789264069602.
- Ogata, Yuka, Toyama, Tadashi, Yu, Ning, Wang, Xuan, Sei, Kazunari, & Ike, Michihiko. 2013. Occurrence of 4-tert-butylphenol (4-t-BP) biodegradation in an aquatic sample caused by the presence of *Spirodela polyrrhiza* and isolation of a 4-t-BP-utilizing bacterium. *Biodegradation*, **24**(2), 191–202. Place: Dordrecht Publisher: Springer Nature B.V.
- Ogbonnaya, Uchenna, & Semple, Kirk T. 2013. Impact of biochar on organic contaminants in soil: a tool for mitigating risk? *Agronomy*, **3**(2), 349–375. Publisher: Multidisciplinary Digital Publishing Institute.
- Oh, Kye-Heon, & Tuovinen, Olli H. 1994. Biodegradation of the phenoxy herbicides MCPP and 2, 4-D in fixed-film column reactors. *International biodeterioration & biodegradation*, **33**(1), 93–99. Publisher: Elsevier.
- Oh, Seok-Young, Son, Jong-Gil, & Chiu, Pei C. 2013. Biochar-mediated reductive transformation of nitro herbicides and explosives. *Environmental Toxicology and Chemistry*, **32**(3), 501–508. Publisher: John Wiley & Sons, Inc.
- Omondi, Morris Oduor, Xia, Xin, Nahayo, Alphonse, Liu, Xiaoyu, Korai, Punhoon Khan, & Pan, Genxing. 2016. Quantification of biochar effects on soil hydrological properties using meta-analysis of literature data. *Geoderma*, **274**, 28–34.
- Pandey, Gunjan, Dorrian, Susan J, Russell, Robyn J, & Oakeshott, John G. 2009. Biotransformation of the neonicotinoid insecticides imidacloprid and thiamethoxam by *Pseudomonas* sp. 1G. *Biochemical and Biophysical Research Communications*, **380**(3), 710–714.
- Penning, Holger, Sørensen, Sebastian R., Meyer, Armin H., Aamand, Jens, & Elsner, Martin. 2010. C, N, and H Isotope Fractionation of the Herbicide Isoproturon Reflects Different Microbial Transformation Pathways. *Environmental Science & Technology*, **44**(7), 2372–2378. Publisher: American Chemical Society.

- Peter, Katherine T., Tian, Zhenyu, Wu, Christopher, Lin, Peter, White, Sarah, Du, Bowen, McIntyre, Jenifer K., Scholz, Nathaniel L., & Kolodziej, Edward P. 2018. Using High-Resolution Mass Spectrometry to Identify Organic Contaminants Linked to Urban Stormwater Mortality Syndrome in Coho Salmon. *Environmental Science & Technology*, **52**(18), 10317–10327. Publisher: American Chemical Society.
- Peter, Katherine T, Herzog, Skuyler, Tian, Zhenyu, Wu, Christopher, McCray, John E, Lynch, Katherine, & Kolodziej, Edward P. 2019. Evaluating emerging organic contaminant removal in an engineered hyporheic zone using high resolution mass spectrometry. *Water Research*, **150**, 140–152.
- Peter, Katherine T, Hou, Fan, Tian, Zhenyu, Wu, Christopher, Goehring, Matt, Liu, Fengmao, & Kolodziej, Edward P. 2020. More Than a First Flush: Urban Creek Storm Hydrographs Demonstrate Broad Contaminant Pollutographs. *Environmental Science & Technology*, **54**(10), 6152–6165. Publisher: American Chemical Society.
- Piai, Laura, Blokland, Marco, van der Wal, Albert, & Langenhoff, Alette. 2020. Biodegradation and adsorption of micropollutants by biological activated carbon from a drinking water production plant. *Journal of Hazardous Materials*, **388**, 122028.
- Pignatello, Joseph J, Kwon, Seokjoon, & Lu, Yufeung. 2006. Effect of Natural Organic Substances on the Surface and Adsorptive Properties of Environmental Black Carbon (Char): Attenuation of Surface Activity by Humic and Fulvic Acids. *Environmental Science & Technology*, **40**(24), 7757–7763. Publisher: American Chemical Society.
- Pitt, Robert, Clark, Shirley, & Field, Richard. 1999. Groundwater contamination potential from stormwater infiltration practices. *Urban Water*, **1**(3), 217–236.
- Portmann, Andrea C., LeFevre, Gregory H., Hankawa, Rennosuke, Werner, David, & Higgins, Christopher P. 2022. The regenerative role of biofilm in the removal of pesticides from stormwater in biochar-amended biofilters. *Environmental Science: Water Research & Technology*, **8**(5), 1092–1110. Publisher: The Royal Society of Chemistry.
- Posselt, Malte. 2020. *Transformation of Micropollutants in the Hyporheic Zone*. Doctoral thesis, comprehensive summary, Department of Environmental Science, Stockholm University, Stockholm. ISBN: 978-91-7911-038-3 (ISBN).
- Posselt, Malte, Jaeger, Anna, Schaper, Jonas L, Radke, Michael, & Benskin, Jonathan P. 2018. Determination of polar organic micropollutants in surface and pore water by high-resolution sampling-direct injection-ultra high performance liquid chromatography-tandem mass spectrometry. *Environmental Science: Processes & Impacts*. Publisher: Royal Society of Chemistry.
- Posselt, Malte, Mechelke, Jonas, Rutere, Cyrus, Coll, Claudia, Jaeger, Anna, Raza, Muhammad, Meinikmann, Karin, Krause, Stefan, Sobek, Anna, Lewandowski, Jörg, Horn, Marcus A, Hollender, Juliane, & Benskin, Jonathan P. 2020. Bacterial Diversity Controls Transformation of Wastewater-Derived Organic Contaminants in River-Simulating Flumes. *Environmental Science & Technology*, Apr. Publisher: American Chemical Society.
- Puhakka, Jaakko A, Melin, Esa S, Järvinen, Kimmo T, Koro, Päivi M, Rintala, Jukka A, Hartikainen, Päivi, Shieh, Wen K, & Ferguson, John F. 1995. Fluidized-bed biofilms for chlorophenol mineralization. *Water Science and Technology*, **31**(1), 227–235. Publisher: IWA Publishing Place: London.
- Quilliam, Richard S, Glanville, Helen C, Wade, Stephen C, & Jones, Davey L. 2013. Life in the ‘charosphere’ – Does biochar in agricultural soil provide a significant habitat for microorganisms? *Soil Biology and Biochemistry*, **65**, 287–293.

- Raina-Fulton, R., & Behdarvandan, A. 2016. Liquid Chromatography-mass spectrometry for the determination of neonicotinoid insecticides and their metabolites in biological, environmental and food commodity matrices. *Trends Chromatogr*, **10**, 51–79.
- Ray, Jessica R, Shabtai, Itamar A, Teixidó, Marc, Mishael, Yael G, & Sedlak, David L. 2019. Polymer-clay composite geomedia for sorptive removal of trace organic compounds and metals in urban stormwater. *Water Research*, **157**, 454–462.
- Reemtsma, Thorsten, Alder, Lutz, & Banasiak, Ursula. 2013. Emerging pesticide metabolites in groundwater and surface water as determined by the application of a multimethod for 150 pesticide metabolites. *Water Research*, **47**(15), 5535–5545.
- Reemtsma, Thorsten, Berger, Urs, Arp, Hans Peter H., Gallard, Hervé, Knepper, Thomas P., Neumann, Michael, Quintana, José Benito, & Voogt, Pim de. 2016. Mind the Gap: Persistent and Mobile Organic Compounds—Water Contaminants That Slip Through. *Environmental Science & Technology*, **50**(19), 10308–10315. Publisher: American Chemical Society.
- Rippy, Megan A, Deletic, Ana, Black, Jeff, Aryal, Rupak, Lampard, Jane-Louise, Tang, Janet Yat-Man, McCarthy, David, Kolotelo, Peter, Sidhu, Jatinder, & Gernjak, Wolfgang. 2017. Pesticide occurrence and spatio-temporal variability in urban run-off across Australia. *Water Research*, **115**(May), 245–255.
- Rubasinghege, Gayan, Gurung, Rubi, Rijal, Hom, Maldonado-Torres, Sabino, Chan, Andrew, Acharya, Shishir, Rogelj, Snezna, & Piyasena, Menake. 2018. Abiotic degradation and environmental toxicity of ibuprofen: Roles of mineral particles and solar radiation. *Water Research*, **131**(Mar.), 22–32.
- Sagarkar, Sneha, Mukherjee, Shinjini, Nousiainen, Aura, Björklöf, Katarina, Purohit, Hemant J., Jørgensen, Kirsten S., & Kapley, Atya. 2013. Monitoring bioremediation of atrazine in soil microcosms using molecular tools. *Environmental Pollution*, **172**(Jan.), 108–115.
- Saquin, Jovita M, Yu, Yu-Han, & Chiu, Pei C. 2016. Wood-Derived Black Carbon (Biochar) as a Microbial Electron Donor and Acceptor. *Environmental Science & Technology Letters*, **3**(2), 62–66. Publisher: American Chemical Society.
- Sbardella, Luca, Comas, Joaquim, Fenu, Alessio, Rodriguez-Roda, Ignasi, & Weemaes, Marjoleine. 2018. Advanced biological activated carbon filter for removing pharmaceutically active compounds from treated wastewater. *Science of The Total Environment*, **636**, 519–529.
- Schaefer, Charles E., M., Drennan Dina, N., Tran Danielle, Raymmah, Garcia, Emerson, Christie, P., Higgins Christopher, & A., Field Jennifer. 2019. Measurement of Aqueous Diffusivities for Perfluoroalkyl Acids. *Journal of Environmental Engineering*, **145**(11), 6019006. Publisher: American Society of Civil Engineers.
- Schaper, Jonas L, Seher, Wiebke, Nützmänn, Gunnar, Putschew, Anke, Jekel, Martin, & Lewandowski, Jörg. 2018. The fate of polar trace organic compounds in the hyporheic zone. *Water Research*, **140**, 158–166.
- Schaper, Jonas L, Posselt, Malte, Bouchez, Camille, Jaeger, Anna, Nuetzmänn, Gunnar, Putschew, Anke, Singer, Gabriel, & Lewandowski, Joerg. 2019. Fate of Trace Organic Compounds in the Hyporheic Zone: Influence of Retardation, the Benthic Biolayer, and Organic Carbon. *Environmental Science & Technology*, **53**(8), 4224–4234. Publisher: American Chemical Society.
- Scheunert, I, & Reuter, S. 2000. Formation and release of residues of the ¹⁴C-labelled herbicide isoproturon and its metabolites bound in model polymers and in soil. *Environmental Pollution*, **108**(1), 61–68.

- Scheurer, Marco, Michel, Amandine, Brauch, Heinz-Jürgen, Ruck, Wolfgang, & Sacher, Frank. 2012. Occurrence and fate of the antidiabetic drug metformin and its metabolite guanylurea in the environment and during drinking water treatment. *Water Research*, **46**(15), 4790–4802.
- Schulz-Jander, Daniel A., Leimkuehler, William M., & Casida, John E. 2002. Neonicotinoid Insecticides: Reduction and Cleavage of Imidacloprid Nitroimine Substituent by Liver Microsomal and Cytosolic Enzymes. *Chemical Research in Toxicology*, **15**(9), 1158–1165. Publisher: American Chemical Society.
- Schymanski, Emma L, Jeon, Junho, Gulde, Rebekka, Fenner, Kathrin, Ruff, Matthias, Singer, Heinz P, & Hollender, Juliane. 2014. Identifying Small Molecules via High Resolution Mass Spectrometry: Communicating Confidence. *Environmental Science & Technology*, **48**(4), 2097–2098. Publisher: American Chemical Society.
- Seller, Carolin, Honti, Mark, Singer, Heinz, & Fenner, Kathrin. 2020. Biotransformation of Chemicals in Water–Sediment Suspensions: Influencing Factors and Implications for Persistence Assessment. *Environmental Science & Technology Letters*, **7**(11), 854–860. Publisher: American Chemical Society.
- Sharma, Smriti, Singh, Balwinder, & Gupta, V. K. 2014. Assessment of imidacloprid degradation by soil-isolated *Bacillus alkalinitrilicus*. *Environmental Monitoring and Assessment*, **186**(11), 7183–7193.
- Sharma, Teena, Rajor, Anita, & Toor, Amrit Pal. 2015. Potential of *Enterobacter* sp. Strain ATA1 on imidacloprid degradation in soil microcosm: Effects of various parameters. *Environmental Progress & Sustainable Energy*, **34**(5), 1291–1297. Publisher: John Wiley & Sons, Ltd.
- Shearer, Lisa, Pap, Sabolc, & Gibb, Stuart W. 2022. Removal of pharmaceuticals from wastewater: A review of adsorptive approaches, modelling and mechanisms for metformin and macrolides. *Journal of Environmental Chemical Engineering*, **10**(4), 108106.
- Shieh, Wen K, & Keenan, John D. 1986. Fluidized bed biofilm reactor for wastewater treatment BT - Bioproducts. Berlin, Heidelberg: Springer Berlin Heidelberg.
- Singh, Anil Kumar, & Cameotra, Swaranjit Singh. 2014. Influence of microbial and synthetic surfactant on the biodegradation of atrazine. *Environmental Science and Pollution Research*, **21**(3), 2088–2097.
- Singh, Simranjeet, Kumar, Vijay, Chauhan, Arun, Datta, Shivika, Wani, Abdul Basit, Singh, Nasib, & Singh, Joginder. 2018. Toxicity, degradation and analysis of the herbicide atrazine. *Environmental Chemistry Letters*, **16**(1), 211–237.
- Spahr, Stephanie, Teixidó, Marc, Sedlak, David L, & Luthy, Richard G. 2020. Hydrophilic trace organic contaminants in urban stormwater: occurrence, toxicological relevance, and the need to enhance green stormwater infrastructure. *Environmental Science: Water Research & Technology*, **6**(1), 15–44. Publisher: The Royal Society of Chemistry.
- Stone, Wesley W, Gilliom, Robert J, & Ryberg, Karen R. 2014. Pesticides in U.S. Streams and Rivers: Occurrence and Trends during 1992–2011. *Environmental Science & Technology*, **48**(19), 11025–11030. Publisher: American Chemical Society.
- Straub, Jürg Oliver, Caldwell, Daniel J, Davidson, Todd, D’Aco, Vincent, Kappler, Kelly, Robinson, Paul F, Simon-Hettich, Brigitte, & Tell, Joan. 2019. Environmental risk assessment of metformin and its transformation product guanylurea. I. Environmental fate. *Chemosphere*, **216**, 844–854.
- Suchail, Séverine, Guez, David, & Belzunces, Luc P. 2001. Discrepancy between acute and chronic toxicity induced by imidacloprid and its metabolites in *Apis mellifera*. *Environmental Toxicology and Chemistry*, **20**(11), 2482–2486. Publisher: John Wiley & Sons, Ltd.

- Sutton, Rebecca, Xie, Yina, Moran, Kelly D, & Teerlink, Jennifer. 2019. Occurrence and Sources of Pesticides to Urban Wastewater and the Environment. *Pages 5–63 of: Pesticides in Surface Water: Monitoring, Modeling, Risk Assessment, and Management*, vol. 1308. American Chemical Society. Series Title: ACS Symposium Series.
- Sánchez-Hernández, Laura, Hernández-Domínguez, Deamelys, Martín, María T, Nozal, María J, Higes, Mariano, & Bernal Yagüe, José L. 2016. Residues of neonicotinoids and their metabolites in honey and pollen from sunflower and maize seed dressing crops. *Journal of Chromatography A*, **1428**, 220–227.
- Tang, Xiaoyan, Yang, Yang, Tao, Ran, Chen, Peijun, Dai, Yunv, Jin, Congcong, & Feng, Xu. 2016. Fate of mixed pesticides in an integrated recirculating constructed wetland (IRCW). *Science of The Total Environment*, **571**, 935–942.
- Thompson, Darrin A., Lehmler, Hans-Joachim, Kolpin, Dana W., Hladik, Michelle L., Vargo, John D., Schilling, Keith E., LeFevre, Gregory H., Peeples, Tonya L., Poch, Matthew C., LaDuca, Lauren E., Cwiertny, David M., & Field, R. William. 2020. A critical review on the potential impacts of neonicotinoid insecticide use: current knowledge of environmental fate, toxicity, and implications for human health. *Environmental Science: Processes & Impacts*, **22**(6), 1315–1346. Publisher: The Royal Society of Chemistry.
- Tian, Zhenyu, Zhao, Haoqi, Peter, Katherine T., Gonzalez, Melissa, Wetzel, Jill, Wu, Christopher, Hu, Ximin, Prat, Jasmine, Mudrock, Emma, Hettlinger, Rachel, Cortina, Allan E., Biswas, Rajshree Ghosh, Kock, Flávio Vinicius Crizóstomo, Soong, Ronald, Jenne, Amy, Du, Bowen, Hou, Fan, He, Huan, Lundeen, Rachel, Gilbreath, Alicia, Sutton, Rebecca, Scholz, Nathaniel L., Davis, Jay W., Dodd, Michael C., Simpson, Andre, McIntyre, Jenifer K., & Kolodziej, Edward P. 2021. A ubiquitous tire rubber-derived chemical induces acute mortality in coho salmon. *Science*, **371**(6525), 185–189. Publisher: American Association for the Advancement of Science.
- Tisler, Selina, & Zwiener, Christian. 2018. Formation and occurrence of transformation products of metformin in wastewater and surface water. *Science of The Total Environment*, **628–629**, 1121–1129.
- Tisler, Selina, & Zwiener, Christian. 2019. Aerobic and anaerobic formation and biodegradation of guanlyl urea and other transformation products of metformin. *Water Research*, **149**, 130–135.
- Tomizawa, Motohiro, & Casida, John E. 2003. SELECTIVE TOXICITY OF NEONICOTINOIDS ATTRIBUTABLE TO SPECIFICITY OF INSECT AND MAMMALIAN NICOTINIC RECEPTORS. *Annual Review of Entomology*, **48**(1), 339–364. Publisher: Annual Reviews.
- Tomizawa, Motohiro, Zhang, Nanjing, Durkin, Kathleen A., Olmstead, Marilyn M., & Casida, John E. 2003. The Neonicotinoid Electronegative Pharmacophore Plays the Crucial Role in the High Affinity and Selectivity for the Drosophila Nicotinic Receptor: An Anomaly for the Nicotinoid Cation- π Interaction Model. *Biochemistry*, **42**(25), 7819–7827. Publisher: American Chemical Society.
- Tong, Yiran, McNamara, Patrick J, & Mayer, Brooke K. 2019. Adsorption of organic micropollutants onto biochar: a review of relevant kinetics, mechanisms and equilibrium. *Environmental Science: Water Research & Technology*, **5**(5), 821–838. Publisher: The Royal Society of Chemistry.
- Trautwein, Christoph, & Kümmerer, Klaus. 2011. Incomplete aerobic degradation of the antidiabetic drug Metformin and identification of the bacterial dead-end transformation product Guanylurea. *Chemosphere*, **85**(5), 765–773.
- Tzoulas, Konstantinos, Korpela, Kalevi, Venn, Stephen, Yli-Pelkonen, Vesa, Kaźmierczak, Aleksandra, Niemela, Jari, & James, Philip. 2007. Promoting ecosystem and human health in urban areas using Green Infrastructure: A literature review. *Landscape and Urban Planning*, **81**(3), 167–178.

- Ulrich, Bridget A, Im, Eugenia A, Werner, David, & Higgins, Christopher P. 2015. Biochar and Activated Carbon for Enhanced Trace Organic Contaminant Retention in Stormwater Infiltration Systems. *Environmental Science & Technology*, **49**(10), 6222–6230. Publisher: American Chemical Society.
- Ulrich, Bridget A., Loehnert, Megan, & Higgins, Christopher P. 2017a. Improved contaminant removal in vegetated stormwater biofilters amended with biochar. *Environmental Science: Water Research & Technology*, **3**(4), 726–734. Publisher: The Royal Society of Chemistry.
- Ulrich, Bridget A, Loehnert, Megan, & Higgins, Christopher P. 2017b. Improved contaminant removal in vegetated stormwater biofilters amended with biochar. *Environmental Science: Water Research & Technology*. Publisher: The Royal Society of Chemistry.
- Ussery, Erin, Bridges, Kristin N., Pandelides, Zacharias, Kirkwood, Andrea E., Guchardi, John, & Holdway, Douglas. 2019. Developmental and Full-Life Cycle Exposures to Guanylurea and Guanylurea–Metformin Mixtures Results in Adverse Effects on Japanese Medaka (*Oryzias latipes*). *Environmental Toxicology and Chemistry*, **38**(5), 1023–1028. Publisher: John Wiley & Sons, Ltd.
- Van der Velde-Koerts, T., Van Hoeven-Arentzen, P. H., & Mahieu, C. M. 2011. *Clothianidin (238). Pesticide Residues in Food 2010: Evaluations Part I-Residues; FAO Plant Production and Protection Paper 206*. Tech. rept. World Health Organization & Food and Agriculture Organization of the United States, Rome.
- Vaux, W G. 1968. Intragravel flow and interchange of water in a streambed. *United States Fish And Wildlife Service Fishery Bulletin*, **66**(3), 479.
- Venkataramanan, Vidya, Packman, Aaron I, Peters, Daniel R, Lopez, Denise, McCuskey, David J, McDonald, Robert I, Miller, William M, & Young, Sera L. 2019. A systematic review of the human health and social well-being outcomes of green infrastructure for stormwater and flood management. *Journal of Environmental Management*, **246**, 868–880.
- Vignet, Caroline, Cappello, Tiziana, Fu, Qiuguo, Lajoie, Kévin, De Marco, Giuseppe, Clérandeau, Christelle, Mottaz, Hélène, Maisano, Maria, Hollender, Juliane, Schirmer, Kristin, & Cachot, Jérôme. 2019. Imidacloprid induces adverse effects on fish early life stages that are more severe in Japanese medaka (*Oryzias latipes*) than in zebrafish (*Danio rerio*). *Chemosphere*, **225**, 470–478.
- Wackett, L, Sadowsky, M, Martinez, B, & Shapir, N. 2002. Biodegradation of atrazine and related s-triazine compounds: from enzymes to field studies. *Applied Microbiology and Biotechnology*, **58**(1), 39–45.
- Walsh, Christopher J, Roy, Allison H, Feminella, Jack W, Cottingham, Peter D, Groffman, Peter M, & Morgan, Raymond P. 2005. The urban stream syndrome: current knowledge and the search for a cure. *Journal of the North American Benthological Society*, **24**(3), 706–723. Publisher: The University of Chicago Press.
- Ward, Adam S, Gooseff, Michael N, & Johnson, Peggy A. 2011. How can subsurface modifications to hydraulic conductivity be designed as stream restoration structures? Analysis of Vaux’s conceptual models to enhance hyporheic exchange. *Water Resources Research*, **47**(8), n/a–n/a.
- Webb, Danielle T, Nagorzanski, Matthew R, Powers, Megan M, Cwiertny, David M, Hladik, Michelle L, & LeFevre, Gregory H. 2020. Differences in Neonicotinoid and Metabolite Sorption to Activated Carbon Are Driven by Alterations to the Insecticidal Pharmacophore. *Environmental Science & Technology*, **54**(22), 14694–14705. Publisher: American Chemical Society.

- Webb, Danielle T., Nagorzanski, Matthew R., Cwiertny, David M., & LeFevre, Gregory H. 2022. Combining Experimental Sorption Parameters with QSAR to Predict Neonicotinoid and Transformation Product Sorption to Carbon Nanotubes and Granular Activated Carbon. *ACS ES&T Water*, **2**(1), 247–258. Publisher: American Chemical Society.
- Werner, David, Ghosh, Upal, & Luthy, Richard G. 2006. Modeling Polychlorinated Biphenyl Mass Transfer after Amendment of Contaminated Sediment with Activated Carbon. *Environmental Science & Technology*, **40**(13), 4211–4218. Publisher: American Chemical Society.
- Werner, David, Karapanagioti, Hrisi K, & Sabatini, David A. 2012. Assessing the effect of grain-scale sorption rate limitations on the fate of hydrophobic organic groundwater pollutants. *Journal of Contaminant Hydrology*, **129**, 70–79.
- Wolfand, Jordyn M, Seller, Carolin, Bell, Colin D, Cho, Yeo-Myoung, Oetjen, Karl, Hogue, Terri S, & Luthy, Richard G. 2019. Occurrence of Urban-Use Pesticides and Management with Enhanced Stormwater Control Measures at the Watershed Scale. *Environmental Science & Technology*, **53**(7), 3634–3644. Publisher: American Chemical Society.
- Xiao, Feng, & Pignatello, Joseph J. 2015a. Interactions of triazine herbicides with biochar: Steric and electronic effects. *Water Research*, **80**(Sept.), 179–188.
- Xiao, Feng, & Pignatello, Joseph J. 2015b. $\pi+\pi$ Interactions between (Hetero)aromatic Amine Cations and the Graphitic Surfaces of Pyrogenic Carbonaceous Materials. *Environmental Science & Technology*, **49**(2), 906–914. Publisher: American Chemical Society.
- Xie, Wen, Han, Chao, Qian, Yan, Ding, Huiying, Chen, Xiaomei, & Xi, Junyang. 2011. Determination of neonicotinoid pesticides residues in agricultural samples by solid-phase extraction combined with liquid chromatography–tandem mass spectrometry. *Journal of Chromatography A*, **1218**(28), 4426–4433.
- Yan, Yulin, Ma, Mengsi, Liu, Xiang, Ma, Weifang, Li, Miao, & Yan, Lijuan. 2017. Effect of biochar on anaerobic degradation of pentabromodiphenyl ether (BDE-99) by archaea during natural groundwater recharge with treated municipal wastewater. *International Biodeterioration & Biodegradation*, **124**, 119–127.
- Young, Alexander, Kochenkov, Valentin, McIntyre, Jenifer K., Stark, John D., & Coffin, Allison B. 2018. Urban stormwater runoff negatively impacts lateral line development in larval zebrafish and salmon embryos. *Scientific Reports*, **8**(1), 2830.
- Yu, Linpeng, Yuan, Yong, Tang, Jia, Wang, Yueqiang, & Zhou, Shungui. 2015. Biochar as an electron shuttle for reductive dechlorination of pentachlorophenol by *Geobacter sulfurreducens*. *Scientific Reports*, **5**(1), 16221.
- Yu, Xiang-Yang, Ying, Guang-Guo, & Kookana, Rai S. 2006. Sorption and Desorption Behaviors of Diuron in Soils Amended with Charcoal. *Journal of Agricultural and Food Chemistry*, **54**(22), 8545–8550. Publisher: American Chemical Society.
- Yu, Xin, Qi, Zhihua, Zhang, Xiaojian, Yu, Ping, Liu, Bo, Zhang, Limin, & Fu, Liang. 2007. Nitrogen loss and oxygen paradox in full-scale biofiltration for drinking water treatment. *Water Research*, **41**(7), 1455–1464.
- Zhang, Chao, Schilirò, Tiziana, Gea, Marta, Bianchi, Silvia, Spinello, Angelo, Magistrato, Alessandra, Gilardi, Gianfranco, & Di Nardo, Giovanna. 2020. Molecular basis for endocrine disruption by pesticides targeting aromatase and estrogen receptor. *International Journal of Environmental Research and Public Health*, **17**(16), 5664. Publisher: Multidisciplinary Digital Publishing Institute.

- Zhang, Kefeng, Randelovic, Anja, Page, Declan, McCarthy, David T, & Deletic, Ana. 2014. The validation of stormwater biofilters for micropollutant removal using in situ challenge tests. *Ecological Engineering*, **67**, 1–10.
- Zhang, Meng, Shen, Xiaofang, Zhang, Haiyun, Werner, David, Wang, Bin, Yang, Yu, Tao, Shu, & Wang, Xilong. 2019. Humic Acid Can Enhance the Mineralization of Phenanthrene Sorbed on Biochars. *Environmental Science & Technology*, **53**(22), 13201–13208. Publisher: American Chemical Society.
- Zhang, Peng, Sun, Hongwen, Yu, Li, & Sun, Tiejing. 2013. Adsorption and catalytic hydrolysis of carbaryl and atrazine on pig manure-derived biochars: Impact of structural properties of biochars. *Journal of Hazardous Materials*, **244**, 217–224.
- Zhang, Peng, Ren, Chao, Sun, Hongwen, & Min, Lujuan. 2018a. Sorption, desorption and degradation of neonicotinoids in four agricultural soils and their effects on soil microorganisms. *Science of The Total Environment*, **615**(Feb.), 59–69.
- Zhang, Peng, Sun, Hongwen, Ren, Chao, Min, Lujuan, & Zhang, Huiming. 2018b. Sorption mechanisms of neonicotinoids on biochars and the impact of deashing treatments on biochar structure and neonicotinoids sorption. *Environmental Pollution*, **234**(Mar.), 812–820.
- Zhou, Guang-can, Wang, Ying, Zhai, Shan, Ge, Feng, Liu, Zhong-hua, Dai, Yi-jun, Yuan, Sheng, & Hou, Jun-yi. 2013. Biodegradation of the neonicotinoid insecticide thiamethoxam by the nitrogen-fixing and plant-growth-promoting rhizobacterium *Ensifer adhaerens* strain TMX-23. *Applied Microbiology and Biotechnology*, **97**(9), 4065–4074.

APPENDIX A
SUPPORTING INFORMATION FOR CHAPTER 2

A.1 TOrC Analysis

Aqueous TOrC concentrations were quantified by liquid chromatography quadrupole time-of-flight mass spectrometry (LC-QToF-MS). Source and purity of TOrC analytical standards (natives and surrogates) are shown in Table A.1, while Table A.2 contains the LC-QToF-MS parameters for each target analyte: precursor accurate mass, MS/MS fragment masses, retention time, LOQ, and spike recovery data.

Table A.1 Native and surrogate standard sources for investigated trace organic chemicals (TOrCs).

Compound Name	Abbreviation	Chemical Formula	CAS #	Analytical Standard Source	Spiking Standard Source
Atrazine	ATZ	C ₈ H ₁₄ ClN ₅	1912-24-9	Fluka, Pestanal®	TCI America, >97%
Desethyl-Atrazine	DEA	C ₆ H ₁₀ ClN ₅	6190-65-4	Sigma-Aldrich, Pestanal®	-
De(s)isopropyl-Atrazine	DIA	C ₅ H ₈ ClN ₅	1007-28-9	Sigma-Aldrich, Pestanal®	-
2-Hydroxy-Atrazine	OH-ATZ	C ₈ H ₁₅ N ₅ O	2163-68-0	Sigma-Aldrich, Pestanal®	-
Imidacloprid	IMI	C ₉ H ₁₀ ClN ₅ O ₂	138261-41-3	SPEX CertiPrep, Certified Reference Material	Sigma-Aldrich, Pestanal®
Desnitro-Imidacloprid	Desnitro-IMI	C ₉ H ₁₁ ClN ₄	127202-53-3	Sigma-Aldrich, Pestanal®	-
Imidacloprid-Urea	IMI-Urea	C ₉ H ₁₀ ClN ₃ O	120868-66-8	LGC Standards	-
Imidacloprid-Olefin	IMI-Olefin	C ₉ H ₈ ClN ₅ O ₂	115086-54-9	Toronto Research Chemicals	-
6-Chloronicotinic acid	6-CNA	C ₆ H ₄ ClNO ₂	5326-23-8	Toronto Research Chemicals	-
Clothianidin	CLO	C ₆ H ₈ ClN ₅ O ₂ S	210880-92-5	SPEX CertiPrep, Certified Reference Material	Sigma-Aldrich, Pestanal®
Atrazine-d ₅	ATZ-d ₅	C ₈ H ₉ 2H ₅ ClN ₅	163165-75-1	C/D/N Isotopes, 99% D	-
Imidacloprid-d ₄	IMI-d ₄	C ₉ 2H ₄ H ₆ ClN ₅ O ₂	1015855-75-0	C/D/N Isotopes, 99% D	-
Clothianidin-d ₃	CLO-d ₃	C ₆ 2H ₃ H ₅ ClN ₅ O ₂ S	1262776-24-8	C/D/N Isotopes, 98% D	-

Table A.2 LC-QToF-MS parameters for target analytes including parent compounds, transformation products, and surrogates. Analysis was performed in ESI+ ionization mode.

Compound name	LOQ [ug/L]	Spike recovery ^a [%]	Precursor Mass (Q1) [Da], [M+H] ⁺	Fragment Mass (Q3) [Da]	RT [min]	Fragments [Da], Literature	References
Atrazine	0.005	80	216.10105	174.05390	6.07	174.2, 103.9	Ulrich <i>et al.</i> 2017b
Imidacloprid	0.005	75	256.05958	175.0977	5.51	209.0585, 175.0982	Pandey <i>et al.</i> 2009; Xie <i>et al.</i> 2011
Clothianidin	0.005 – 0.025	76	250.01600	169.05390	5.25	169.0, 131.9	Xie <i>et al.</i> 2011
Desethyl-Atrazine	0.005	95	188.06975	146.0228, 104.0010	5.19	146.2, 104.1	Ulrich <i>et al.</i> 2017b
Desisopropyl-Atrazine	0.005	96	174.05410	146.0228, 132.0322	4.67	146.2, 132.3	
Hydroxy-Atrazine	0.005	111	198.13494	156.0878, 86.0348	4.74	156.1, 85.9	
Desnitro-/guanidine-Imidacloprid	0.005	91	211.07450	126.0105, 90.0335	4.55	126, 90	Raina-Fulton & Behdarvandan 2016
Imidacloprid-Urea	0.005	83	212.05852	128.0256, 99.0551	5.15	128, 99	
Imidacloprid-Olefin	0.005	97	254.04393	236.0340, 171.0667	5.11	236, 171	
6-Chloro-nicotinic acid ^b	0.05	-	158.00033	122.02320, 78.0338	4.99	122.0, 78.0	Berset <i>et al.</i> 2017; Hao <i>et al.</i> 2016
Atrazine-d5	-	-	221.13243	-	6.07	179.2	Ulrich <i>et al.</i> 2017b
Imidacloprid-d4	-	-	260.08469	-	5.51	213.1, 179.2	Xie <i>et al.</i> 2011
Clothianidin-d3	-	-	253.03483	-	5.25	172, 132	Raina-Fulton & Behdarvandan 2016

^a Surrogate corrected spike recovery in synthetic stormwater.

^b Data not available due to late addition of TP to analyte list.

LC Conditions

HPLC eluents, analysis blanks and double blanks, and sample dilutions (column effluents) were prepared using Optima® LC/MS-grade water and methanol and HPLC-grade acetonitrile (Fisher Scientific). The aqueous mobile phase (A) was 1 mM ammonium formate (Sigma-Aldrich) and 0.1% formic acid (Fluka) in Optima® LC/MS-grade water and the organic mobile phase (B) was 100% HPLC-grade acetonitrile. A flowrate of 0.6 mL/min was employed and the temperature of the column oven was held at 40°C. The HPLC gradient started out at 5% B, increased to 95% B within 5 min, stayed constant at this level for 5.5 min, until it quickly receded to 5% B for another 7.5 min to establish equilibrium conditions. Select samples and calibration standards for analysis of 6-CNA were acidified with formic acid (0.225% final concentration in sample vial) to avoid peak splitting issues during liquid chromatography.

MS Parameters

Precursor ion data (TOF MS) was collected for m/z 50-1000 Da for 2271 cycles with a total scan time of 0.476 s and an accumulation time of 0.1 s, with ion spray voltage set at 5500 V and temperature set to 500 °C. The ion source gas 1 and 2, curtain gas, and collision (CAD) gas were set to 50 psi, 40 psi, 25 psi, and 10 psi, respectively. The collision energy (CE) was set to 5 V and the declustering potential (DP) to 50 V, each with no spread. Product ion (TOF MS/MS) scanning was conducted for m/z 50-1000 Da. The accumulation time for each SWATH window was 0.05 s and the CE was set to 30 V with 20 V spread, whereas the DP was kept at 50 V without spread. The instrument was mass calibrated every five injections using SCIEX ESI Positive Calibration Solution.

A.2 Microbial Transformation Pathways

Using the EAWAG Biocatalysis/Biodegradation Database and Pathway Prediction System (EAWAG-BBD/PPS; <http://eawag-bbd.ethz.ch/index.html>) and microbial transformation data available in literature biotransformation studies, we compiled an extracted ion chromatogram (XIC) list of known and suspected transformation products of atrazine, imidacloprid, and clothianidin (Table A.3). The most widely identified transformation products were then used to develop an overview of common microbial transformation pathways for each of the three parent compounds, as shown in Figure A.1 for atrazine, Figure A.2 for imidacloprid and Figure A.3 for clothianidin. The here presented pathways may be non-exhaustive and were compiled to the best of our knowledge.

Table A.3 Extracted ion chromatogram (XIC) list of microbial transformation products of atrazine, imidacloprid, and clothianidin.

Organic Contaminant	Formula	Exact Mass	Source / Reference
ATRAZINE	C ₈ H ₁₄ ClN ₅	215.093781	
Hydroxyatrazine	C ₈ H ₁₅ N ₅ O	197.12766	EAWAG Pathway Predictor; Mudhoo & Garg, 2011; Singh et al. 2018; Fang et al. 2014; Kolekar et al. 2014; Sagarkar et al. 2013
Desethylatrazine	C ₆ H ₁₀ ClN ₅	187.062473	EAWAG Pathway Predictor; Mudhoo & Garg, 2011; Singh et al. 2018; Fang et al. 2014; Kolekar et al. 2014; Singh & Cameotra, 2014; Sagarkar et al. 2013
Deisopropylatrazine	C ₅ H ₈ ClN ₅	173.046823	EAWAG Pathway Predictor; Mudhoo & Garg, 2011; Singh et al. 2018; Fang et al. 2014; Kolekar et al. 2014; Singh & Cameotra, 2014; Sagarkar et al. 2013
Acetone	C ₃ H ₆ O	58.041865	EAWAG Pathway Predictor
N-Isopropylammelide	C ₆ H ₁₀ N ₄ O ₂	170.080376	EAWAG Pathway Predictor; Singh et al. 2018; Fang et al. 2014; Kolekar et al. 2014; Sagarkar et al. 2013
2,4-Dihydroxy-6-(N'-ethyl)amino-1,3,5-triazine/ N-Ethylammelide	C ₅ H ₈ N ₄ O ₂	156.064726	EAWAG Pathway Predictor; Singh et al. 2018; Fang et al. 2014; Sagarkar et al. 2013
Isopropylamine	C ₃ H ₉ N	59.073499	EAWAG Pathway Predictor
	C ₆ H ₁₁ N ₅ O	169.09636	EAWAG Pathway Predictor
Deisopropylhydroxyatrazine	C ₅ H ₉ N ₅ O	155.08071	EAWAG Pathway Predictor; Singh et al. 2018; Fang et al. 2014; Kolekar et al. 2014; Sagarkar et al. 2013
	C ₆ H ₉ ClN ₄ O	188.046489	EAWAG Pathway Predictor
Deisopropyldeethylatrazine / Didealkylatrazine	C ₃ H ₄ ClN ₅	145.015523	EAWAG Pathway Predictor; Mudhoo & Garg, 2011; Singh et al. 2018; Fang et al. 2014; Kolekar et al. 2014; Singh & Cameotra, 2014; Sagarkar et al. 2013
	C ₅ H ₇ ClN ₄ O	174.030839	EAWAG Pathway Predictor
Cyanuric acid	C ₃ H ₃ N ₃ O ₃	129.017442	EAWAG Pathway Predictor; Singh et al. 2018; Fang et al. 2014; Sagarkar et al. 2013
2,4-Dihydroxy-6-amino- 1,3,5-triazine / Ammelide	C ₃ H ₄ N ₄ O ₂	128.033426	EAWAG Pathway Predictor; Singh et al. 2018; Fang et al. 2014; Singh & Cameotra, 2014; Sagarkar et al. 2013

Table A.3 Continued.

Organic Contaminant	Formula	Exact Mass	Source / Reference
2-Hydroxy-4,6-diamino-1,3,5-triazine	C3H5N5O	127.04941	EAWAG Pathway Predictor
	C3H2ClN3O2	146.983555	EAWAG Pathway Predictor
2-Chloro-4-hydroxy-6-amino-1,3,5-triazine	C3H3ClN4O	145.999539	EAWAG Pathway Predictor; Singh et al. 2018; Fang et al. 2014; Sagarkar et al. 2013
Biuret	C2H5N3O2	103.038177	Fang et al. 2014; Sagarkar et al. 2013
Allophanate	C2H4N2O3	104.022193	Sagarkar et al. 2013
IMIDACLOPRID	C9H10ClN5O2	255.052303	EAWAG Pathway Predictor; Hussain et al. 2016; Pandey et al. 2009; Sharma et al. 2015
Imidacloprid-Urea	C9H10ClN3O	211.05124	EAWAG Pathway Predictor
Imidazolidinone	C3H6N2O	86.048013	EAWAG Pathway Predictor
	C6H4ClNO	140.998142	EAWAG Pathway Predictor
	C9H11ClN3O2	228.05398	EAWAG Pathway Predictor
	C3H7N2O2	103.050753	EAWAG Pathway Predictor; Hussain et al. 2016; Sharma et al. 2014; Sharma et al. 2015
Base form of 6-Chloronicotinic Acid	C6H3ClNO2	155.985232	EAWAG Pathway Predictor
	C6H7ClN2	142.029776	EAWAG Pathway Predictor
	C3H4NO3	102.019119	EAWAG Pathway Predictor
	C8H12ClN3	185.071975	EAWAG Pathway Predictor; Hussain et al. 2016; Pandey et al. 2009; Sharma et al. 2015
5-Hydroxyimidacloprid	C9H10ClN5O3	271.047218	Hussain et al. 2016; Sharma et al. 2014
Imidacloprid-Olefin	C9H8ClN5O2	253.036653	Hussain et al. 2016
Nitrosoguanidine metabolite / Nitrosimine imidacloprid	C9H10ClN5O	239.057388	Hussain et al. 2016; Pandey et al. 2009; Sharma et al. 2014
Aminoguanidine metabolite	C9H12ClN5	225.078123	Hussain et al. 2016; Pandey et al. 2009
Desnitro/guanidine metabolite / Imidacloprid NTG	C9H11ClN4	210.067224	Hussain et al. 2016; Pandey et al. 2009; Sharma et al. 2014; Sharma et al. 2015
6-Hydroxynicotinic acid	C6H5NO3	139.026944	Hussain et al. 2016
6-Oxo-1,4,5,6-tetrahydronicotinic acid	C6H7NO3	141.042594	Hussain et al. 2016

Table A.3 Continued.

Organic Contaminant	Formula	Exact Mass	Source / Reference
2-Formyl glutarate	C6H6O5	158.021525	Hussain et al. 2016
1-[(6-Chloropyridin-3-yl)methyl]imidazolidine-2,4-dione	C9H8ClN3O2	225.030505	Sharma et al. 2015
???	C9H10N4	174.090546	Sharma et al. 2015
2-Chloro-5-methylpyridine	C6H6ClN	127.018877	Sharma et al. 2015
CLOTHIANIDIN	C6H8ClN5O2S	249.008725	
1-[(2-Chloro-1,3-thiazol-5-yl)methyl]-3-nitrourea; CTNU	C5H5ClN4O3S	235.977091	EAWAG Pathway Predictor
	C4H5ClN2S	147.986198	EAWAG Pathway Predictor
	C5H4ClN2O2S	190.968203	EAWAG Pathway Predictor
	C5H5ClN4O4S	251.972006	EAWAG Pathway Predictor
	C4H2ClNOS	146.954564	EAWAG Pathway Predictor
	C4H5ClN2OS	163.981113	EAWAG Pathway Predictor
	C5H4ClN2O3S	206.963117	EAWAG Pathway Predictor
	C5H5ClN4O5S	267.966921	EAWAG Pathway Predictor
	C4H2ClNO2S	162.949479	EAWAG Pathway Predictor
	C4HClNO2S	161.941654	EAWAG Pathway Predictor
	C4H5ClN2O2S	179.976028	EAWAG Pathway Predictor
N-(2-chlorothiazol-5-yl-methyl)-N'-methylurea; thiazolylmethylurea; TZMU; clothianidin-urea	C6H8ClN3OS	205.007662	Van der Velde-Koerts et al. 2011; Mori et al. 2017; Zhang et al. 2018
N-(2-chlorothiazol-5-yl-methyl)-N'-nitroguanidine; thiazolylnitroguanidine; TZNG	C5H6ClN5O2S	234.993075	Van der Velde-Koerts et al. 2011
N-methyl-N'-nitroguanidine; 1-methyl-2-nitroguanidine; MNG	C2H6N4O2	118.049076	Van der Velde-Koerts et al. 2011
Nitroguanidine; NTG	CH4N4O2	104.033426	Van der Velde-Koerts et al. 2011
3-Methyl-1-[(1,3-thiazol-5-yl)methyl]urea	C6H9N3OS	171.046634	Zhang et al. 2018

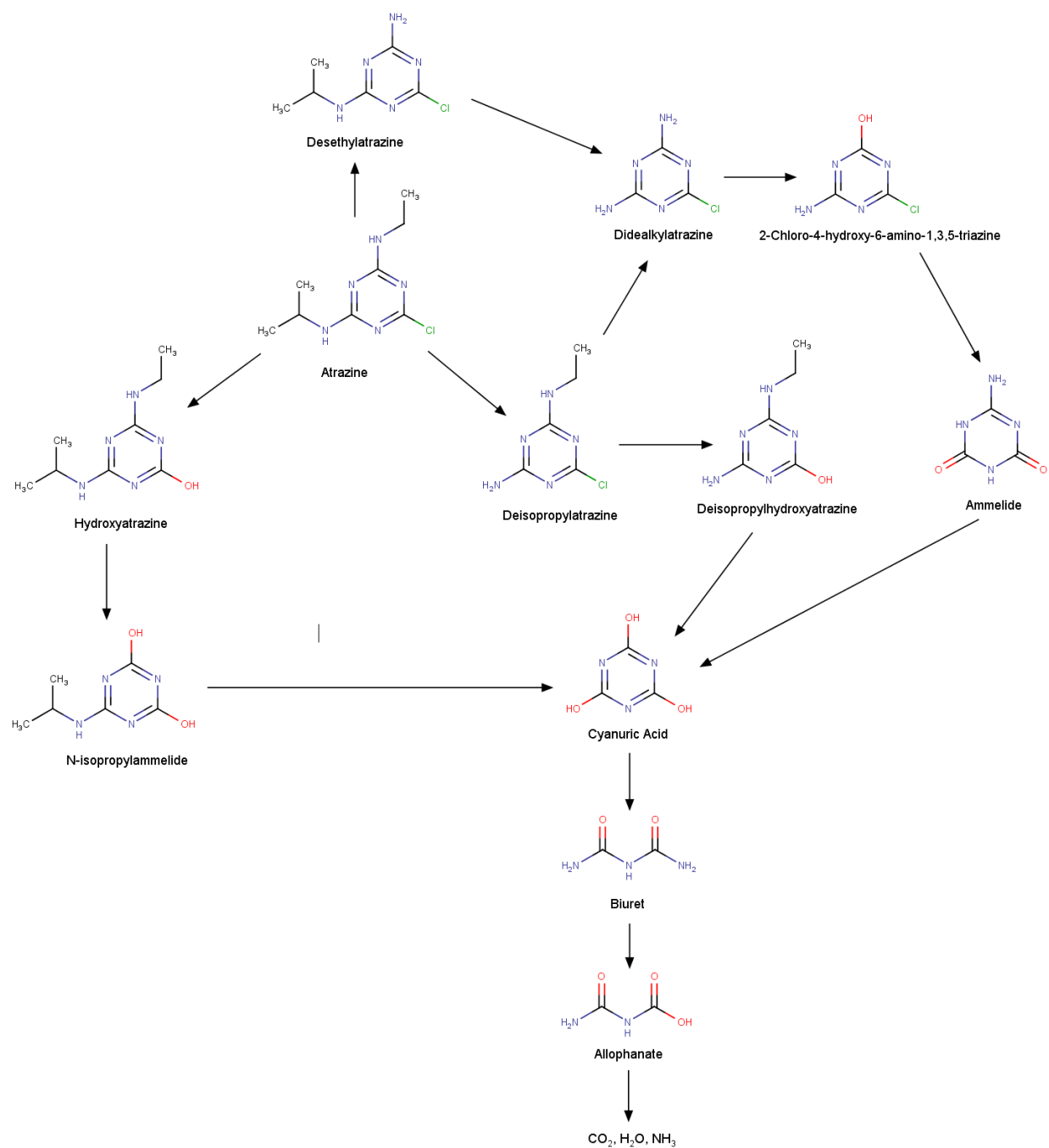


Figure A.1 Literature-established major microbial transformation pathways for atrazine. Sources: Fang *et al.* (2014); Kolekar *et al.* (2014); Mudhoo & Garg (2011); Sagarkar *et al.* (2013); Singh & Cameotra (2014); Singh *et al.* (2018).

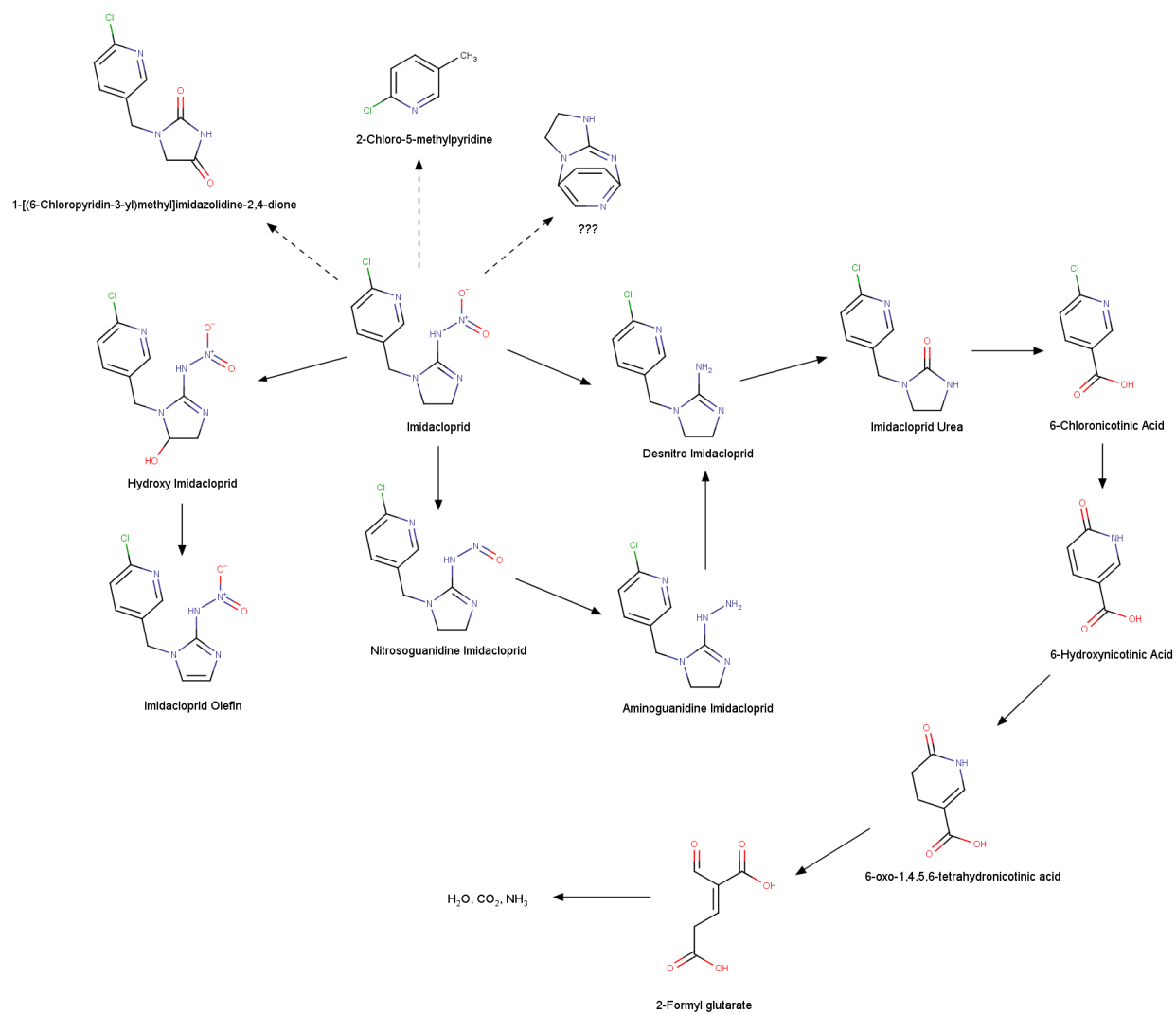


Figure A.2 Literature-established major microbial transformation pathways for imidacloprid. Sources: Hussain *et al.* (2016); Pandey *et al.* (2009); Sharma *et al.* (2014, 2015).

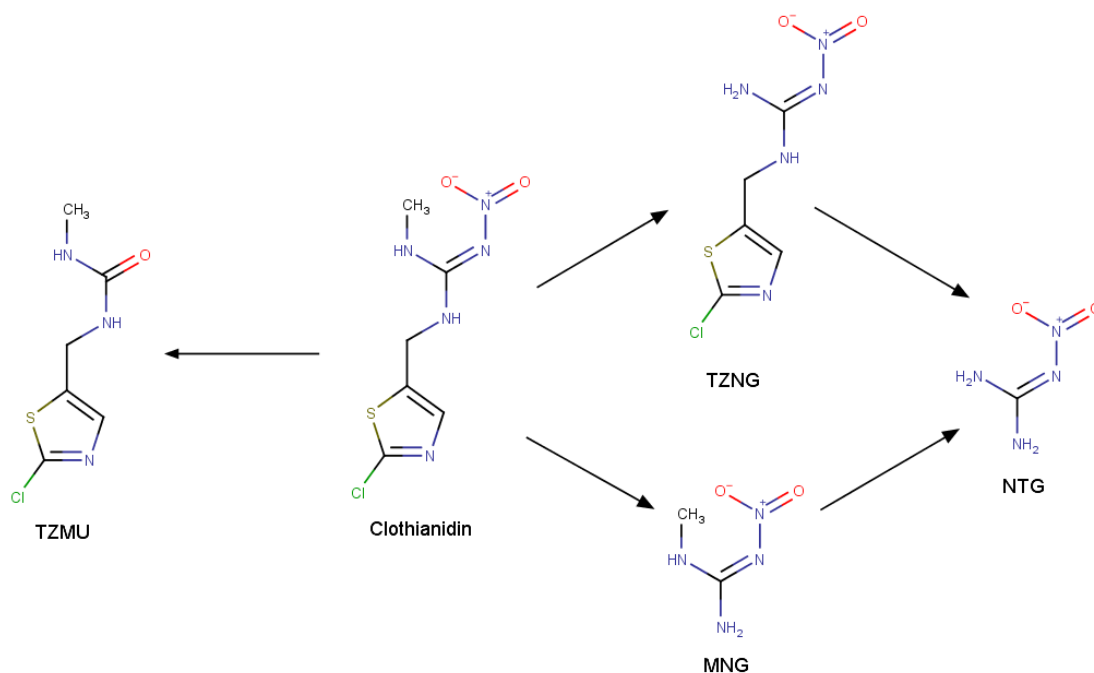


Figure A.3 Literature-established major microbial transformation pathways for clothianidin. Sources: Mori *et al.* (2017); Van der Velde-Koerts *et al.* (2011); Zhang *et al.* (2018a).

A.3 Materials

Biochar Characterization

To characterize the physical properties of the biochar used, the Brunauer-Emmett-Teller specific surface area (BET SSA) and the total pore volume (PV) were measured using a Micromeritics Gemini V surface area and pore size analyzer (Norcross, GA). Total pore volume and pore size distributions for macropores (>50 nm) and mesopores (2-50 nm) were calculated from Barrett, Joyner, and Halenda (BJH) desorption isotherms. Estimation of micropore (<2 nm) volumes was based on t-Plot micropore volume measurements using the same instrument. Prior to measurement, sample masses were added to the analysis tubes (<0.1 g for pure biochar samples, >0.5 g for mixed sand-biochar samples) and degassed overnight at 100 °C at <50 mTorr. BET SSA measurements were acquired using 11 points, whereas BJH adsorption and desorption isotherms were measured using 40 points each. Detection limits for BET analysis were $\sim 1 \text{ m}^2/\text{g}$. t-Plot micropore volume measurements of aged sand-biochar samples were below the limit of detection due to the low mass percentages of biochar (0.5 wt%) in these samples.

DOC Extract Solutions (“DOC Teas”)

The DOC extract solutions (DOC teas) were prepared as follows: Five gallons of nearby creek water (Clear Creek, Golden, CO) were collected and grass and leaves from residential curbs and stormwater ditches and woody plant-based EcoGrow compost (A1 Organics; Eaton, CO) were added as DOC sources. The solution was incubated for three weeks at room temperature (18-20°C) and shaken occasionally. The leachate was then centrifuged in small batches at 500 rpm and the supernatant was subsequently filtered employing a three-step membrane filtration process starting with 2.7 µm (Whatman, GF/D Glass Microfiber Filters), followed by 0.7 µm (Whatman, GF/F Glass Microfiber Filters), and finally a 0.45 µm filter (Supor-450, PALL). The filtered DOC solution was distributed into separate 1L and 2L PYREX glass bottles, which were autoclaved for sterilization at 121°C for 1.5 hours, and then refrigerated at 4°C.

During the total four months of column operation and influent preparation, we started with one bottle and as soon it was used up (typically within 2 weeks), we moved on to the next one. To avoid microbial contamination, necessary DOC solution volumes were poured into separate beakers for use (extra volumes were discarded), and no pipet tips or similar were ever introduced into the glass storage bottles. The DOC concentration of each newly opened bottle was determined via TOC-L Laboratory Total Organic Carbon Analyzer to determine the correct volume to use for the influent preparation. Furthermore, DOC concentrations in the prepared influent were measured twice a week during the first seven weeks, and then weekly after that. Visual inspection of the solution in the clear glass bottles in addition to changes in smell (due to bacterial growth) were performed during each influent preparation.

A.4 Batch Sorption Experiments

Sorption Isotherms

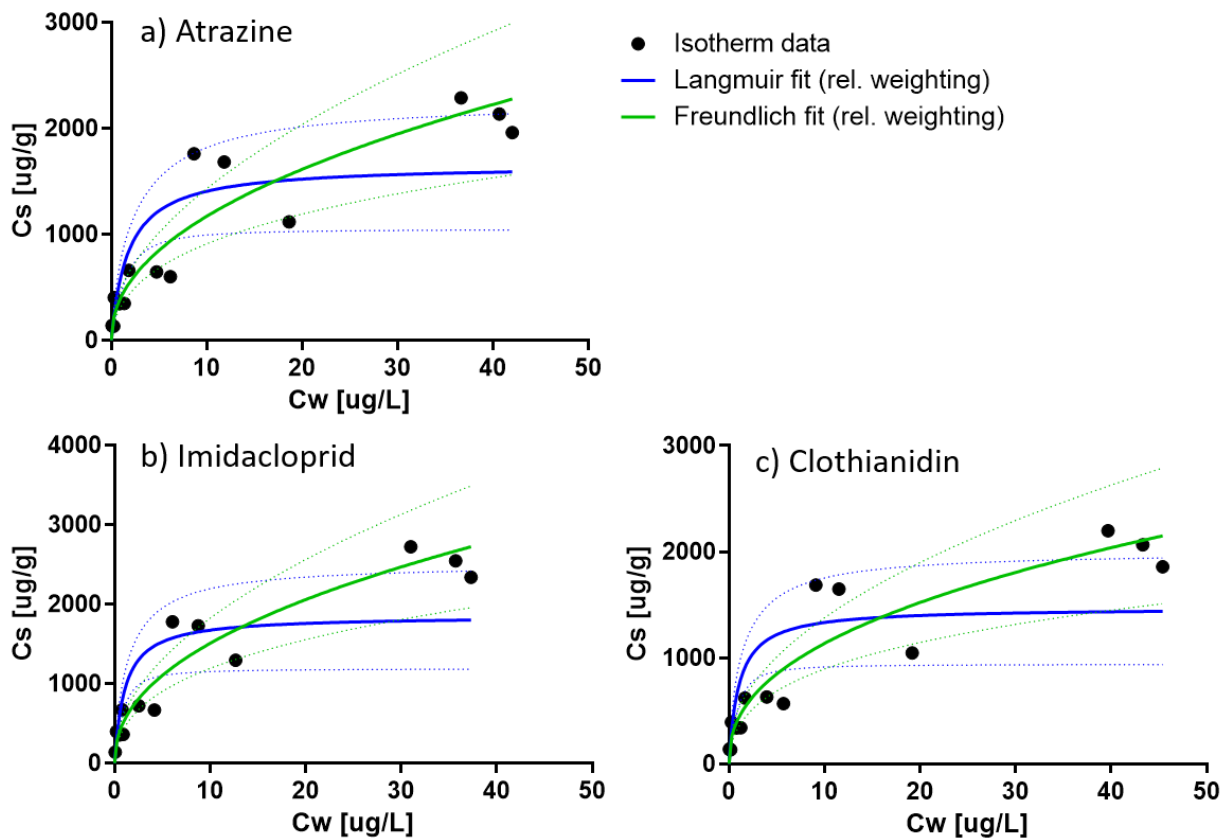


Figure A.4 Solid lines represent best fits of the Freundlich and Langmuir equations to batch sorption isotherm data using non-linear regression and relative weighting ($1/Y^2$). Dotted lines represent the 95% confidence intervals of the fitted curves. The systematic error in the observed datapoints across all three pesticides was likely caused by uncertainties in dry biochar mass (due to its extremely light weight and hydrostatic behavior).

Table A.4 Best-fit values for Freundlich and Langmuir parameters obtained in GraphPad Prism (version 9.1.1). AICc designates the Akaike's Information Criterion corrected for low sample size. Please note that the K_F values are not significantly different from each other ($p=0.1261$), the same is true for the parameter n ($p=0.7542$; One-way ANOVA, $\alpha = 0.05$). Abbreviations: Confidence interval (CI), Root Mean Square Error (RMSE).

	Atrazine	Imidacloprid	Clothianidin
<i>Freundlich</i>			
K_F [(ug/g)/((ug/L) ⁿ)]	402.2	535.0	429.6
K_F 95% CI [(ug/g)/((ug/L) ⁿ)]	356.8 to 610.3	483.5 to 723.9	384.0 to 617.4
n [-]	0.4638	0.4495	0.4221
n 95% CI [-]	0.3546 to 0.5484	0.3612 to 0.5197	0.3312 to 0.4970
Weighted Sum of Squares (1/Y ²)	1.502	1.151	1.365
RMSE	0.3276	0.2867	0.3122
AICc	-26.33	-30.33	-27.78
AIC probability that the model is correct [%]	94.76	99.18	98.96
<i>Langmuir</i>			
Q_{max} [ug/g]	1658	1850	1472
Q_{max} 95% CI [ug/g]	1340 to 2722	1518 to 3097	1216 to 2532
K_L [L/ug]	0.5590	0.9412	0.9614
K_L 95% CI [L/ug]	0.3398 to 1.078	0.5664 to 1.676	0.5645 to 1.841
Weighted Sum of Squares (1/Y ²)	2.210	2.180	2.506
RMSE	0.3973	0.3946	0.4231
AICc	-20.54	-20.75	-18.66
AIC probability that the model is correct [%]	5.241	0.825	1.036

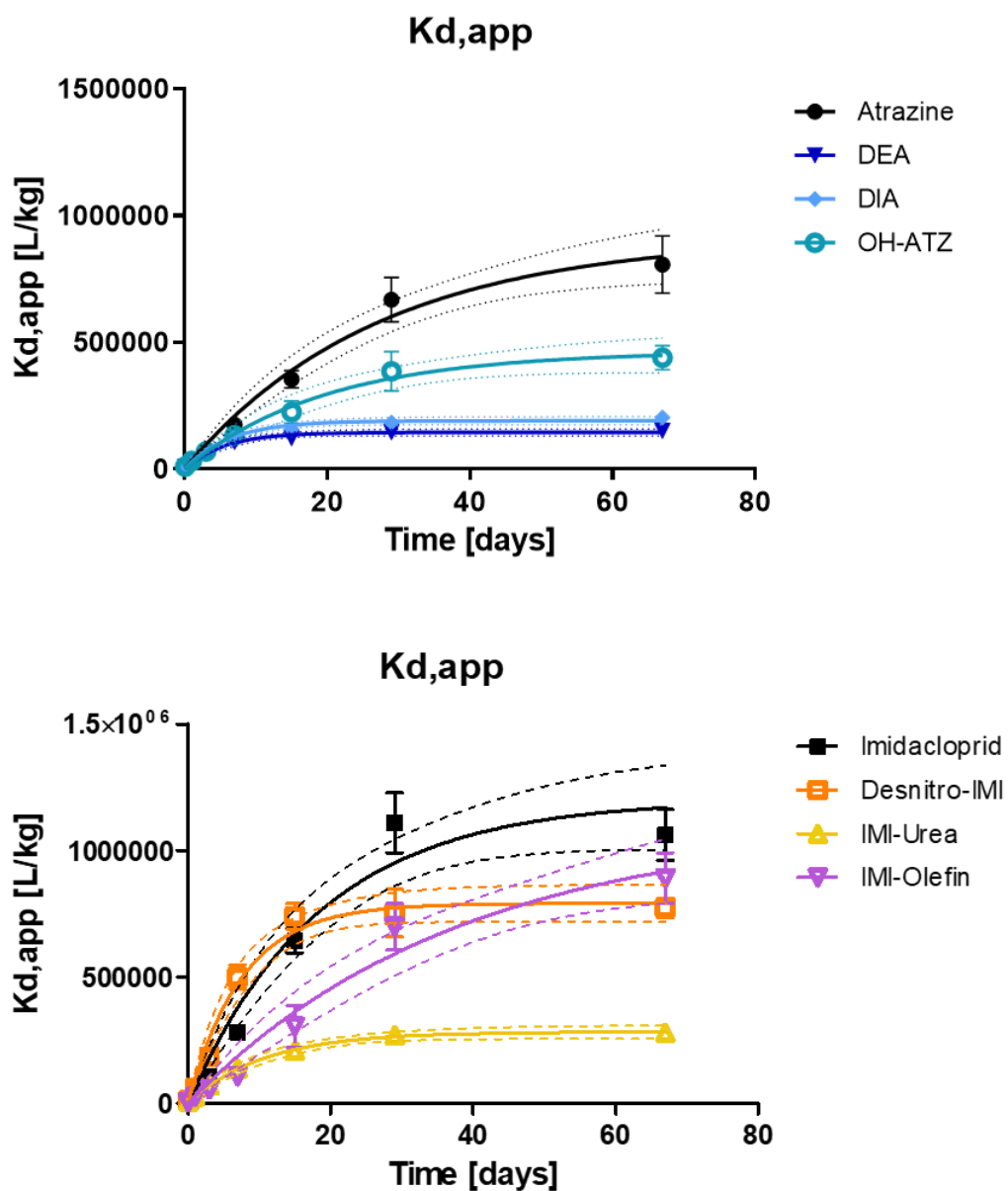


Figure A.5 Kinetic batch sorption data plotted as apparent distribution coefficient, $K_d = C_S/C_W$ (C_S = biochar-sorbed concentration, C_W = aqueous concentration). The solid lines represent pseudo-first order fits and the dashed lines represent the 95% confidence intervals; the fit was simply done for better visualization.

Table A.5 Equilibrium K_d (\pm standard deviation) calculated from kinetic batch sorption data at timepoint $t=67$ days ($K_{d,eq} = C_{S,eq}/C_{W,eq}$). It was concluded that sorption equilibrium had been established for all compounds since linear regression analysis between $t=29$ days and 67 days revealed that slopes did not significantly deviate from zero ($p \geq 0.7498$). Tukey's multiple comparisons test (following ANOVA) was computed in GraphPad Prism (version 9.1.1). "ns" denotes "not significant". Abbreviations: Confidence interval (CI), Difference (Diff.); others: see Table A.1.

Compound Name	$K_{d,eq}$ [L/g]
Atrazine	807.24 \pm 159.4
DEA	151.01 \pm 16.63
DIA	203.44 \pm 14.19
OH-ATZ	439.23 \pm 82.72
Imidacloprid	1061.55 \pm 141.15
Desnitro-IMI	772.54 \pm 63.43
IMI-Urea	279.52 \pm 45.72
IMI-Olefin	890.55 \pm 172.37
Clothianidin	1112.03 \pm 250.86

Tukey's multiple comparisons test	Mean Diff.	95% CI of Diff.	Below threshold?	Summary	Adjusted P Value
Atrazine vs. Imidacloprid	-254.3	-663.2 to 154.5	No	ns	0.4334
Atrazine vs. Clothianidin	-304.8	-713.6 to 104.1	No	ns	0.2345
Atrazine vs. DEA	656.2	283.0 to 1029	Yes	***	0.0004
Atrazine vs. DIA	603.8	230.6 to 977.0	Yes	***	0.0009
Atrazine vs. OH-ATZ	368.0	-5.221 to 741.2	No	ns	0.0547
Imidacloprid vs. Clothianidin	-50.48	-459.3 to 358.4	No	ns	>0.9999
Imidacloprid vs. Desnitro-IMI	289.0	-84.22 to 662.2	No	ns	0.1998
Imidacloprid vs. IMI-Urea	782.0	408.8 to 1155	Yes	****	<0.0001
Imidacloprid vs. IMI-Olefin	171.0	-202.2 to 544.2	No	ns	0.7682
DEA vs. DIA	-52.43	-386.3 to 281.4	No	ns	0.9996
DEA vs. OH-ATZ	-288.2	-622.0 to 45.61	No	ns	0.1185
DIA vs. OH-ATZ	-235.8	-569.6 to 98.04	No	ns	0.2888
Desnitro-IMI vs. IMI-Urea	493.0	159.2 to 826.8	Yes	**	0.0021
Desnitro-IMI vs. IMI-Olefin	-118.0	-451.8 to 215.8	No	ns	0.9259
IMI-Urea vs. IMI-Olefin	-611.0	-944.9 to -277.2	Yes	***	0.0002

A.5 Column Experiments

Salt Tracer Data

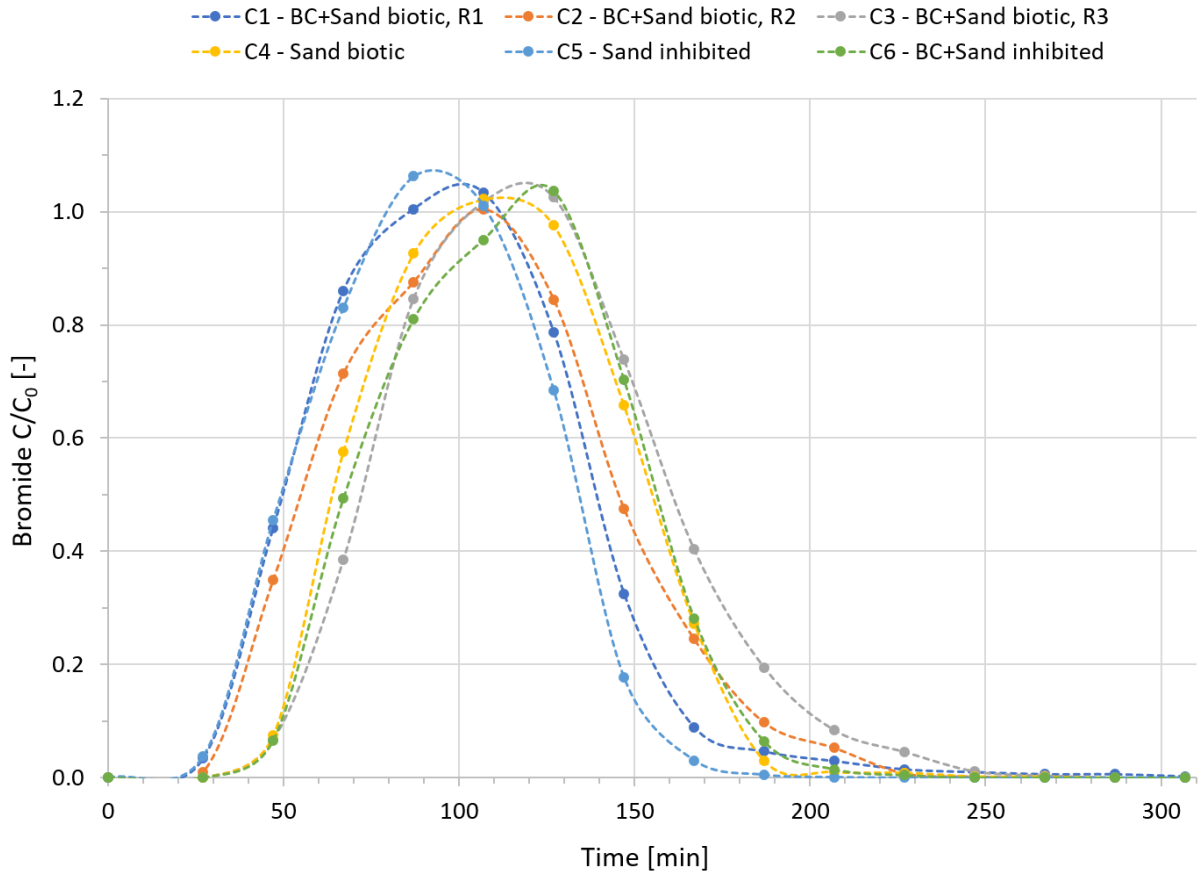


Figure A.6 Salt tracer breakthrough curves in column effluents using a potassium bromide (KBr) tracer. Data is adjusted for hold-up time outside of porous media; ideal plug-flow conditions were assumed in tubing and in glass beads/glass wool mixture at the inlet and outlet of columns.

Growth Procedure of Microbial Enrichment Solutions (Multi-Cycle Inoculation)

Local sediment-creek water slurries served as the inoculum to the enrichment solutions. Duplicates of 1 L creek water each containing 100 mL of creek sediment, leaves, and silt were collected and let sit at room temperature overnight. Slurries were put on a shaker table for 24 h for pre-equilibration and were then centrifuged at 800 RCF for 5 min to remove large particles and leaves. All supernatant was combined and transferred to a glass bottle for storage. Microbial cultures for the enrichment solutions were grown over two stages of three successive inoculation-incubation cycles as follows: Initial cultures were prepared by combining 100 mL of autoclaved DOC extract solution (~ 250 mg/L) with 10 mL of sediment-creek water inoculum in 500 mL Erlenmeyer flasks and aerobically incubated at 30°C on a shaker table in the dark. Growth of cultures was monitored visually (see Figure A.7) and by measurement of the optical density (O.D.) every 2-3 days. After one week (7 d), cultures of the second cycle were prepared by combining 10 mL of the initial cultures with 100 mL of autoclaved DOC growth media and inoculated for another week (9 d). For the third cycle, the entire 110 mL of media was transferred to a 2000 mL Erlenmeyer flask containing 500 mL of autoclaved DOC extract solution and incubated again. The second incubation stage was carried out following the same method as described in the first stage, except for the following modifications: The DOC concentration of the growth media was higher (~ 650 mg/L), incubation cycles only lasted four days, and O.D. measurements were taken daily. O.D. values increased considerably 1-2 days after the culture was transferred to a new DOC growth media and dropped afterwards due to pronounced aggregation (see Figure A.8). This observation reemphasizes the need to consider that O.D. measurements are only suitable for assessing growth of microbial cultures in the aqueous phase, as aggregates quickly sink to the bottom of the measurement cuvette and are hence not detected by the optical measurement.



Figure A.7 Seeding cultures used for column inoculation and microcosms during the last stage (4 days) of the second inoculation cycle. Optical density (O.D.) at 600 nm of the culture was measured in a subsample each day and was as follows (chronological order): a) 0.183, b) 0.585, c) 0.643, d) 0.474. The seeding culture depicted in d) was used for column and microcosms inoculation the following day.

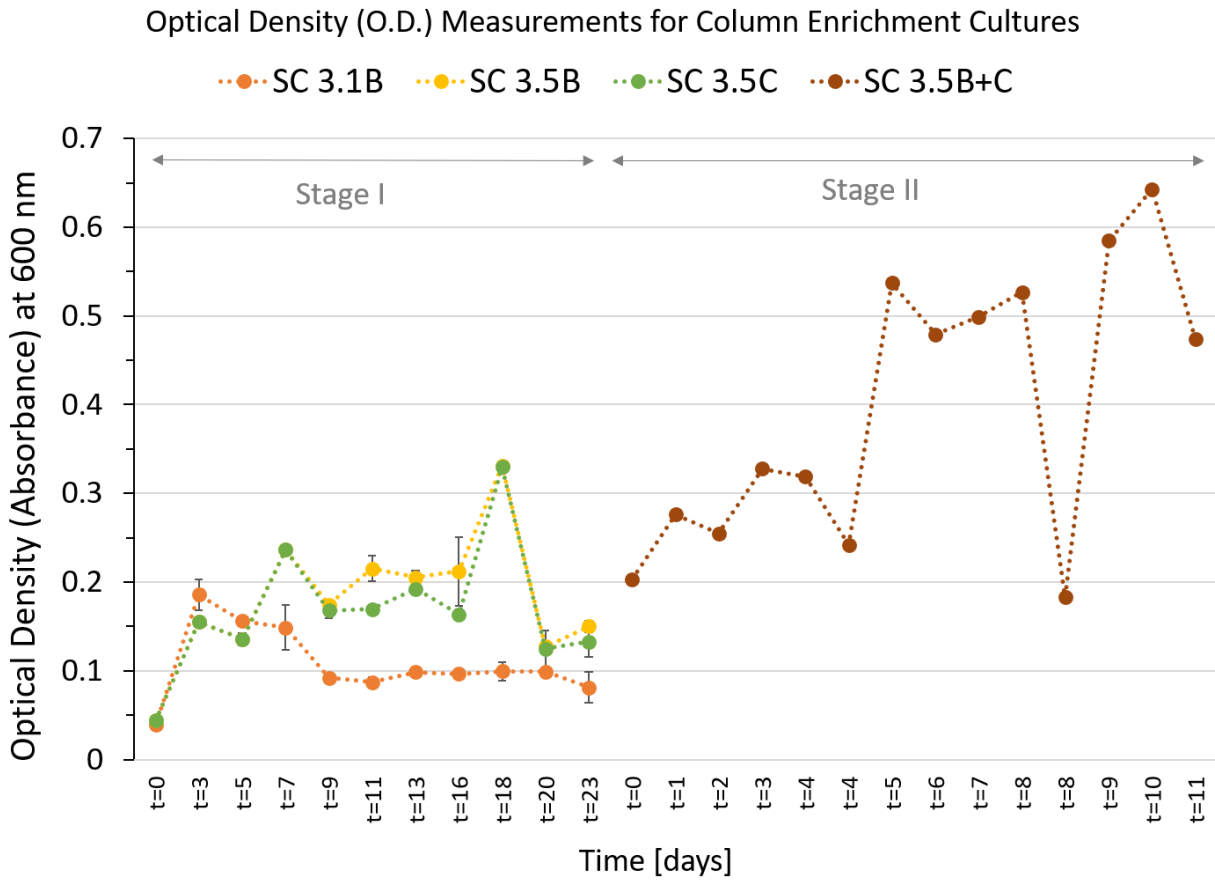


Figure A.8 Optical density (O.D.) measurements of column enrichment cultures or seeding cultures (SC). In the beginning, several replicate batches were incubated and only the ones with most observed growth (highest O.D. values) were kept for continued multi-cycle inoculation. Cultures 3.5B and 3.5C were combined for stage II incubation, which resulted in the final culture 3.5B+C, which was used for column and microcosm biofilm seeding. Error bars during stage I represent standard deviation occurring from repeated measurement of the same sample (analytical variability).

A.6 Transformation Products & Suspect Screening

Suspect Compounds in Microcosms

Three suspect TPs were identified in microcosm (and column) samples: 5-hydroxy-imidacloprid (5-OH-IMI; Figure A.9), nitrosoguanidine-imidacloprid (NG-IMI; Figure A.10), and clothianidin-urea (CLO-urea; Figure A.11). LC-HRMS parameters of suspect TPs are summarized in Table A.6.

The *absolute* average precursor mass error (in ppm) in Table A.6 was calculated based on the suspect peaks identified in 20 microcosm samples total: for both biotic replicates (M1, M2), we analyzed five time points each (T8, T13, T15, T17, T19), while each sample was analyzed twice (R1, R2).

Table A.6 MRM transitions of suspect analytes (all in ESI+ mode): The exact precursor mass was used for compound identification and at least one of the exact fragment masses was used for compound verification. The level of suspect confidence refers to the scale proposed by E. Schymanski, Schymanski *et al.* (2014).

Compound name	5-Hydroxy- Imidacloprid (5-OH-IMI)	Nitrosoguanidine- Imidacloprid (NG-IMI)/ Nitrosoimine- Imidacloprid	Clothianidin- Urea (CLO-urea, TZMU)
Formula	C9H10ClN5O3	C9H10ClN5O	C6H8ClN3OS
Precursor Mass (Q1) [Da] [M+H]⁺	272.05449	240.06466	206.01494
Av. Mass error [ppm]	1.41	1.42	0.80
Fragment Mass 1 (Q3) [Da]	225.0569	209.0591	131.9671
Fragment Mass 2 (Q3) [Da]	191.0949	175.0981	119.9675
RT [min]	5.13	5.09	4.67
Fragments [Da], Literature	225, 191 ^a	209, 175, 84 ^b	131.97, 120.01 ^c
Confidence level (Schymanski scale)	Level 4	Level 3	Level 3

^a Giroud *et al.* (2013)

^b Dick *et al.* (2006); Schulz-Jander *et al.* (2002)

^c Kim *et al.* (2012); Sánchez-Hernández *et al.* (2016)

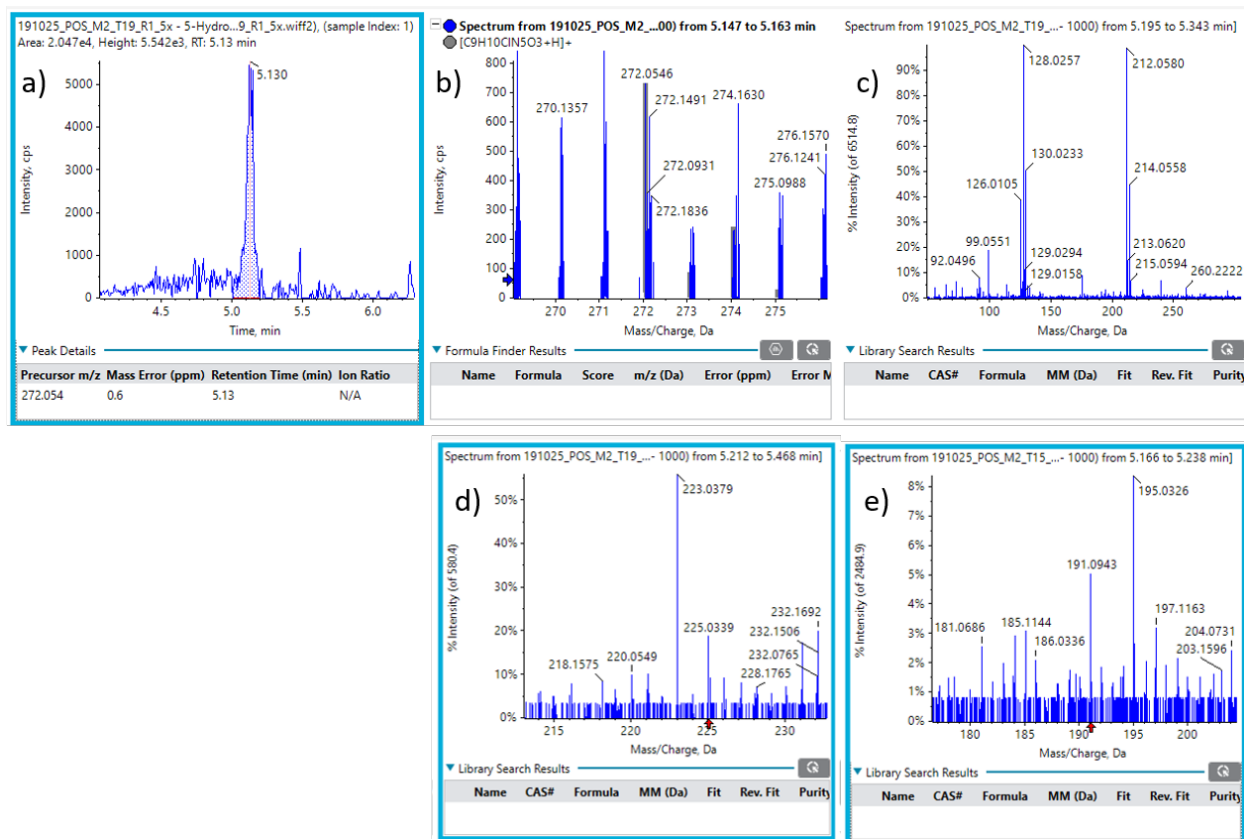


Figure A.9 Representative MS and MS² scans for 5-Hydroxyimidacloprid. a) Precursor ion extracted chromatogram, b) Isotope spectrum of precursor ion, c) MS² scan, d) Zoomed in MS² scan at 225.05 Da (fragment), e) Zoomed in MS² scan at 191.09 Da (fragment).

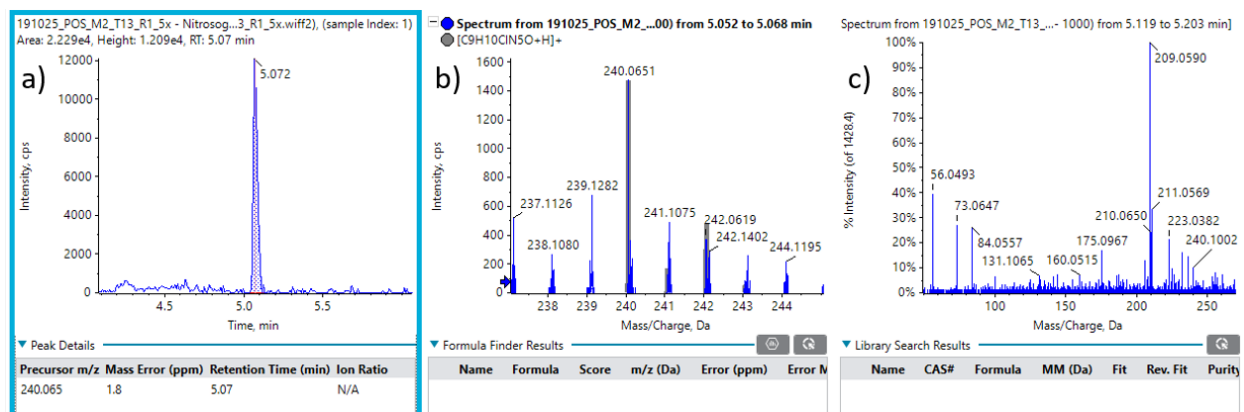


Figure A.10 Representative MS and MS² scans for Nitrosoguanidine-Imidacloprid. a) Precursor ion extracted chromatogram, b) Isotope spectrum of precursor ion, c) MS² scan including fragments at 209.05 Da and 175.09 Da.

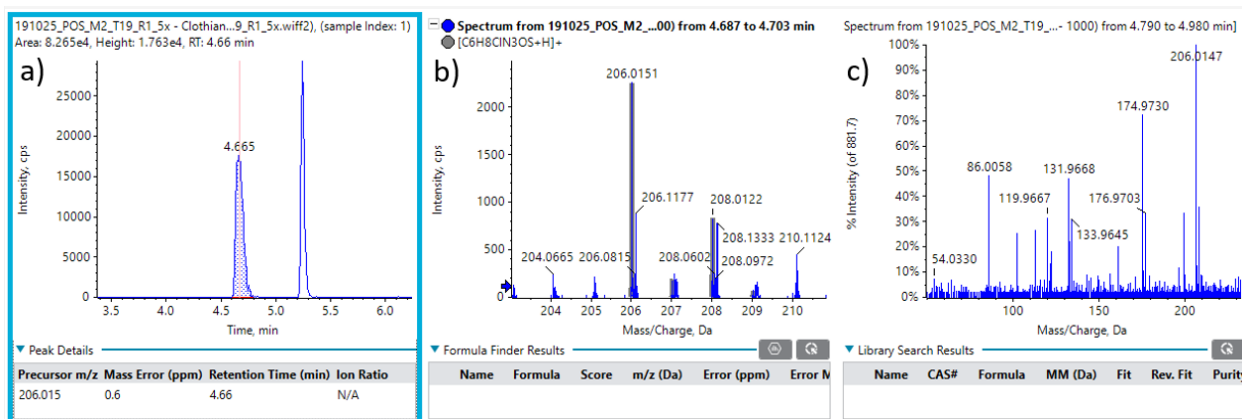


Figure A.11 Representative MS and MS² scans for Clothianidin-Urea. a) Precursor ion extracted chromatogram, b) Isotope spectrum of precursor ion, c) MS² scan including fragments at 131.96 Da and 119.96 Da.

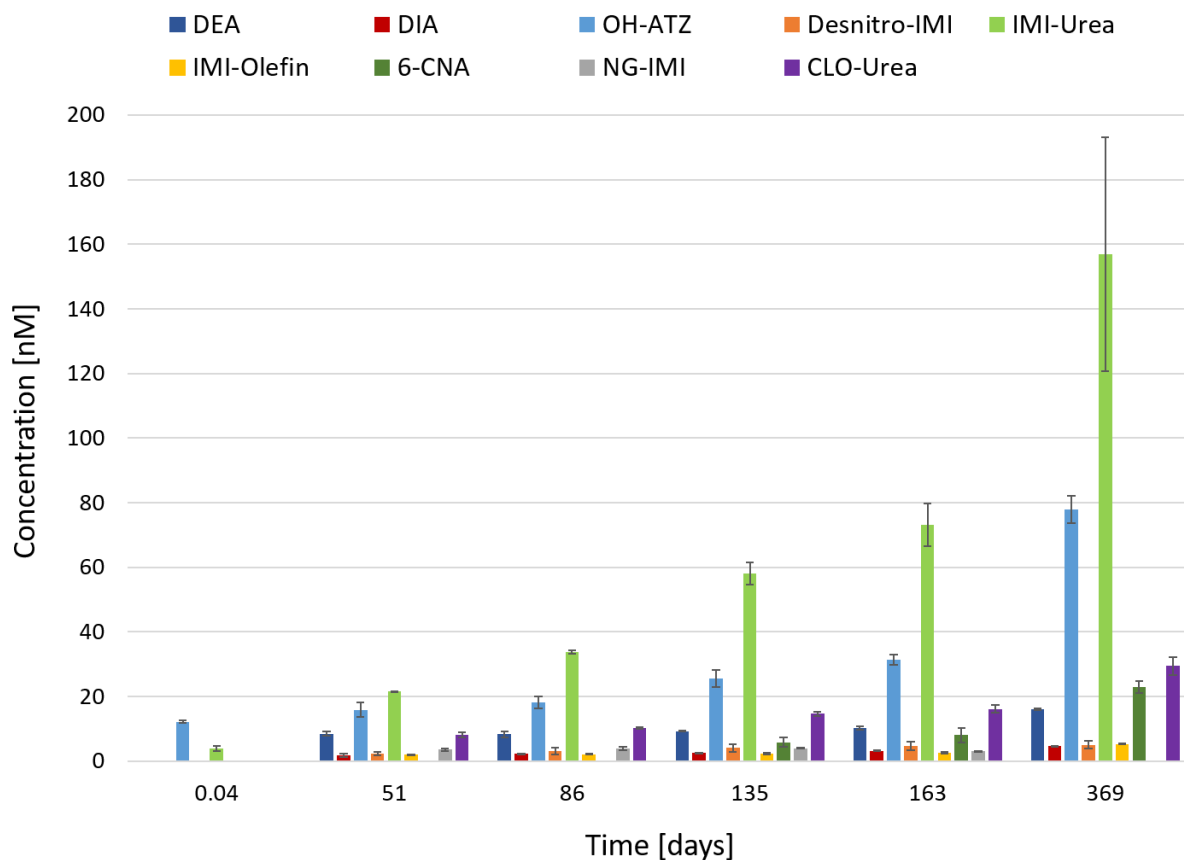


Figure A.12 Target and suspect transformation products in microcosms over time. Error bars represent the standard deviation between experimental replicates (n=2). Abbreviations: desethylatrazine (DEA), desisopropylatrazine (DIA), and 2-hydroxy-atrazine (OH-ATZ), desnitro-imidacloprid (desnitro-IMI), imidacloprid-urea (IMI-urea), imidacloprid-olefin (IMI-olefin), 6-chloronicotinic acid (6-CNA), nitrosoguanidine-imidacloprid (NG-IMI), and clothianidin-urea (CLO-urea). Note that concentrations for NG-IMI and CLO-urea are semi-quantitative.

Additional Transformation Products & Suspect Compounds in Columns

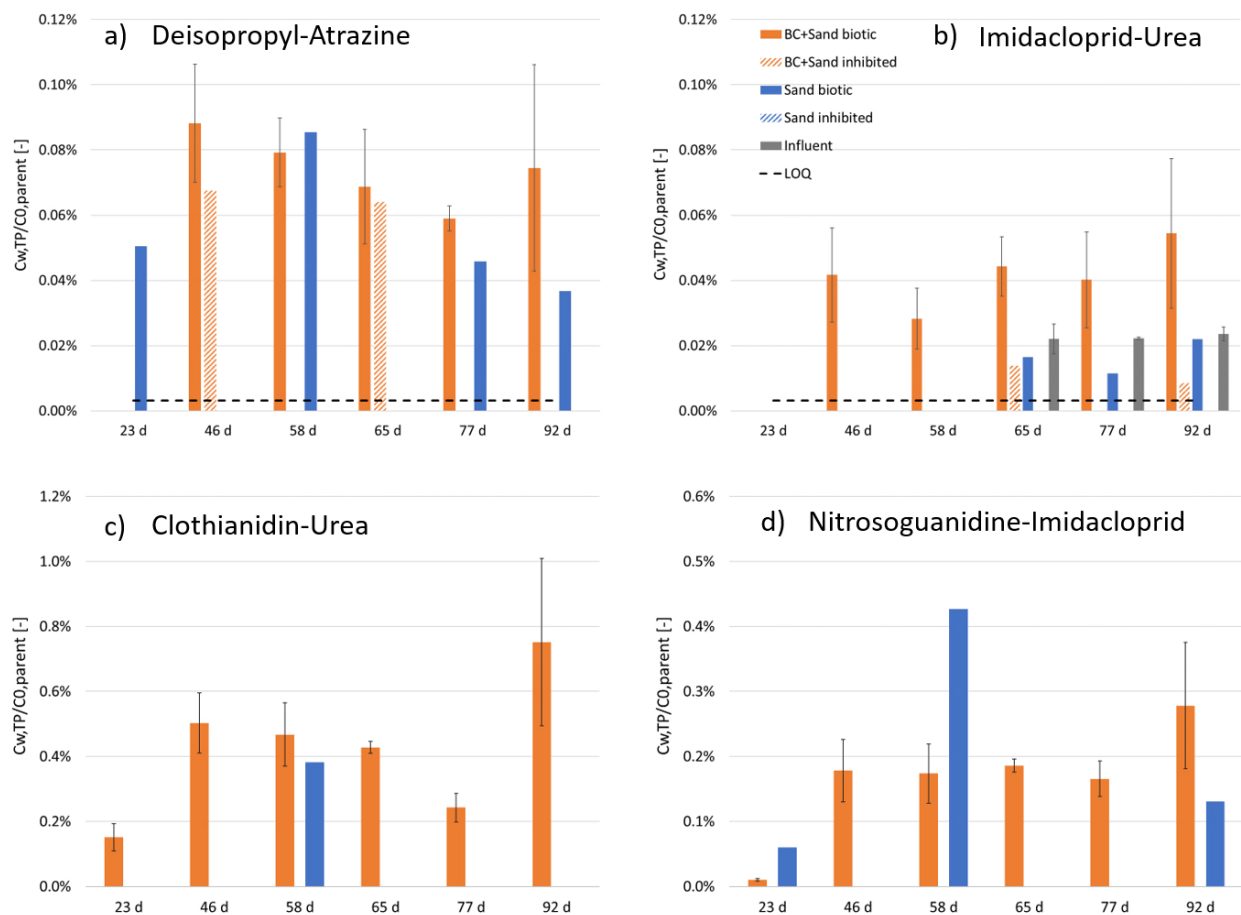


Figure A.13 Additional target and suspect transformation products (TPs) of atrazine, imidacloprid, and clothianidin in column effluents (and influent) identified by LC-QToF-MS analysis: a) deisopropyl-atrazine, b) imidacloprid-urea, c) clothianidin-urea (suspect; semi-quantitative), d) nitrosoguanidine-imidacloprid (suspect; semi-quantitative). Y-axis shows TP concentrations normalized by the average parent influent concentration ($C_{W,TP}/C_{W,0,Parent}$). Dotted black lines represent the limit of quantitation (LOQ) for each TP (not available for suspects).

Semi-Quantitation

Approach:

1. Choose calibrant matches for all suspect compounds. Ideally, the calibrant has similar or the same ionizable groups as the suspect. We chose imidacloprid as the calibrant for 5-OH-IMI and NG-IMI, and clothianidin was the calibrant for CLO-urea.
2. Determine a response factor (RF) for each calibrant (= slope of calibration curve). When using internal standards (IS), this is actually a relative response factor to the IS.
3. Calculate the suspect concentration:

$$C_{suspect} = (Area_{suspect} * C_{IS}) / (Area_{IS} * RF) * (MW_{suspect} / MW_{calibrant})$$

where $C_{IS} = 1$ (relative concentration of IS in samples vs. standards) and MW refers to the molecular weight of compounds. Further, it is essential that both calibrant and suspect compounds were acquired with the same extracted ion chromatogram (XIC) window; in our study 0.02 Da was used consistently.

Target and Suspect Transformation Products in Columns and Microcosms

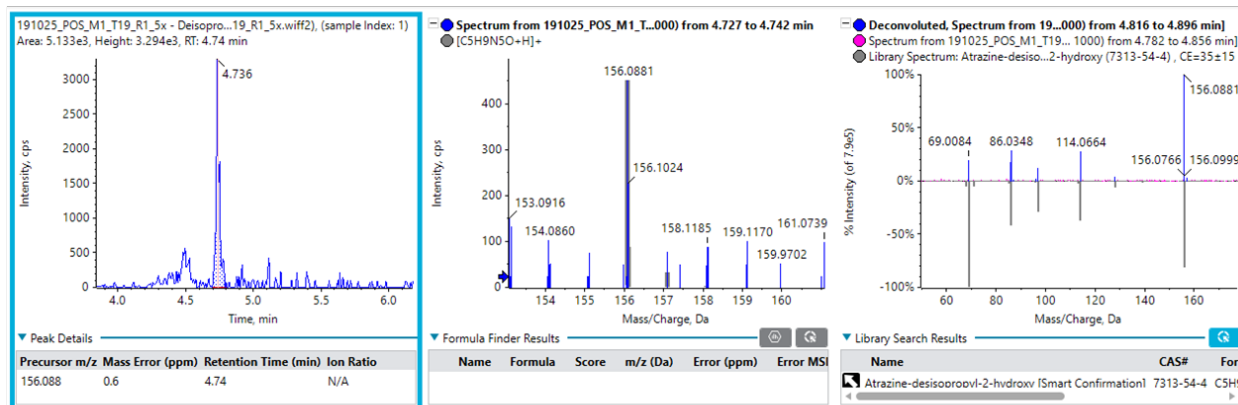
A summary of all target and suspect transformation products (TPs) detected in biotic columns (BC+Sand) and in microcosms is presented in Table A.7; given is the observed concentration range over the entire experiment duration.

Table A.7 Range of (average) TP concentrations observed in the biotic BC+Sand columns and in the microcosms. Please note that concentrations for NG-IMI and CLO-urea are semi-quantitative.

Transformation product	Columns (BC+Sand biotic) [$\mu\text{g/L}$]	Microcosms [$\mu\text{g/L}$]
Desethyl-atrazine (DEA)	n.d. - 0.147	n.d. - 3.015
Deisopropyl-atrazine (DIA)	n.d. - 0.138	n.d. - 0.817
2-Hydroxy-atrazine (OH-ATZ)	0.037 - 3.192	2.41 - 15.343
Desnitro-imidacloprid (Desnitro-IMI)	n.d. - 0.448	n.d. - 1.075
Imidacloprid-urea (IMI-urea)	n.d. - 0.084	0.833 - 33.206
Imidacloprid-olefin (IMI-olefin)	n.d. - 0.298	n.d. - 1.348
6-chloronicotinic acid (6-CNA)	n.d. - 0.091	n.d. - 3.616
Nitrosoguanidine-imidacloprid (NG-IMI)	0.018 - 0.487	n.d. - 0.946
Clothianidin-urea (CLO-urea)	0.236 - 1.171	n.d. - 6.053

In-Source Fragmentation

a) Sample (RT=4.73 min):



b) Analytical standard (RT=4.73 min):

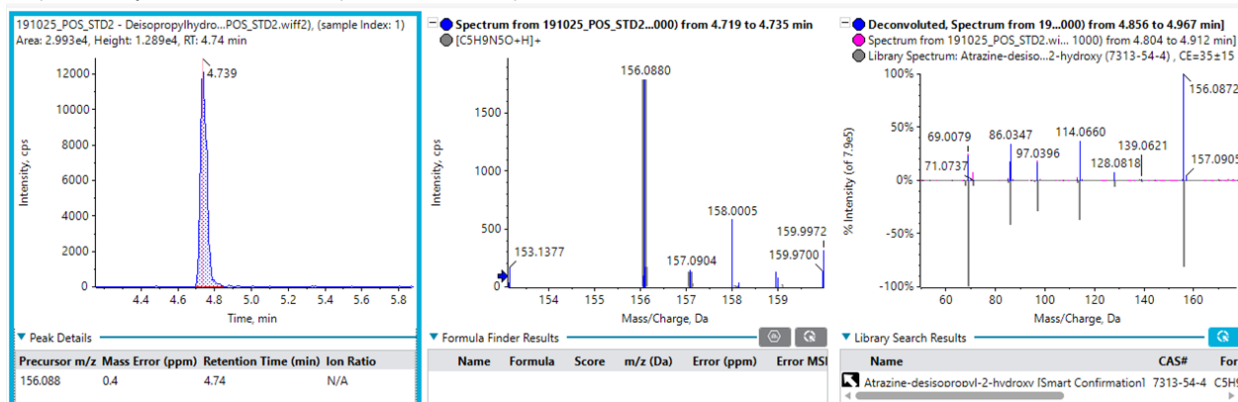
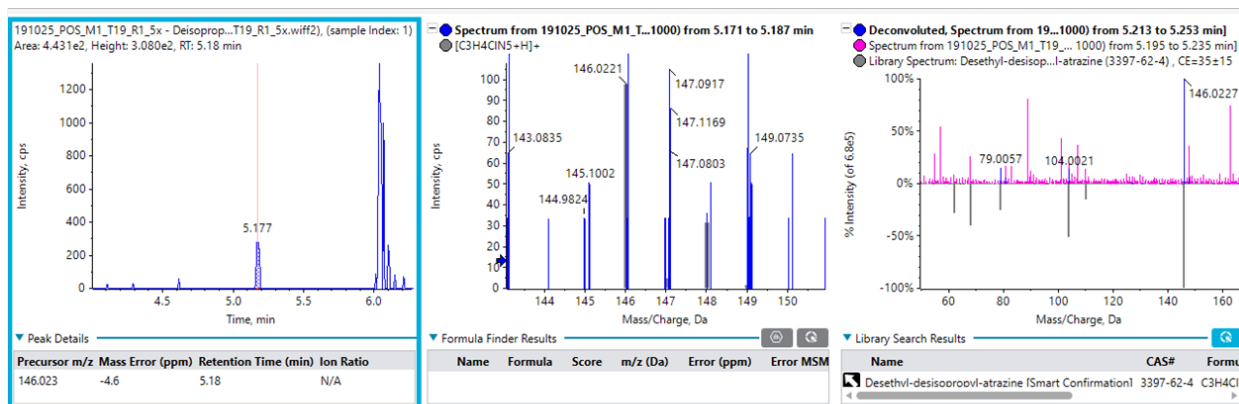


Figure A.14 The suspect deisopropylhydroxy-atrazine as a product of in-source fragmentation of 2-hydroxy-atrazine (OH-ATZ) at identical retention times of 4.73 min, found both in microcosm samples (a) and analytical standards (b). Both precursor peaks were confirmed by library hits (score >99).

a) Sample (RT=5.17 min):



b) Analytical standard (RT=5.17 min and 4.67 min):

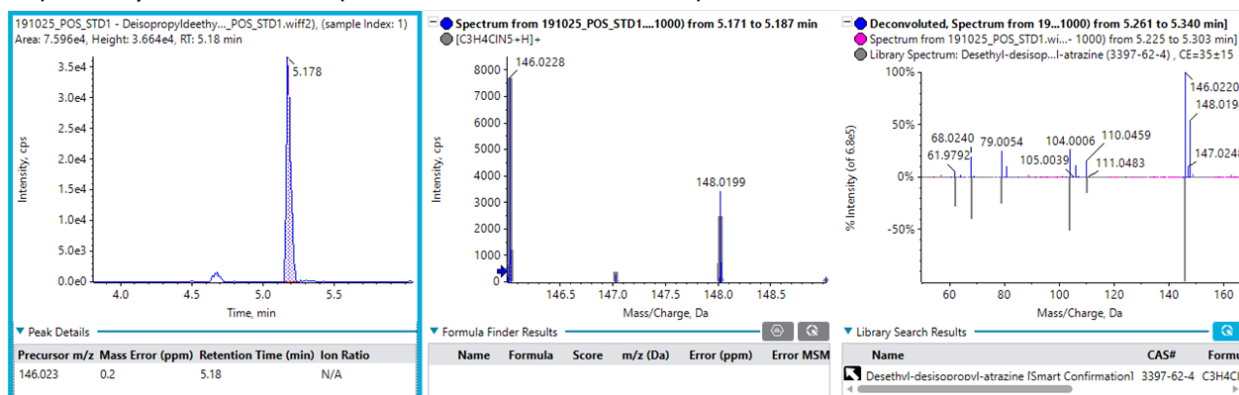


Figure A.15 The suspect desethyldeisopropyl-atrazine (or didealkyl-atrazine) as a product of in-source fragmentation of desethyl-atrazine (DEA) at identical retention times of 5.17 min, found both in microcosm samples (a) and analytical standards (b). Both precursor peaks were confirmed by library hits (score >93). The peak to the left in panel b) is the product of in-source fragmentation of deisopropyl-atrazine (DIA) in the analytical standard, but was not found in the sample.

A.7 Transport Modelling

Column Pollutant Transport Model

The column model considers pollutant transport by advection and dispersion of mobile water in addition to the sorption and biodegradation processes. Two types of column medium particles are considered, non-porous S particles (i.e. sand) and porous BC particles (i.e. biochar or activated carbon). The instantaneous equilibrium model assumes local sorption equilibrium between mobile water and these particles, whereas the kinetic sorption model considers first-order rate uptake of pollutants by the S particles, and pollutant diffusion in the water-filled pore network of the BC particles retarded by sorption to the BC solid matrix. Biodegradation of pollutants is assumed to occur in the water in between the S and BC particles and is described by first-order rate biodegradation kinetics. Parameters are expressed in SI units of moles, seconds, kilograms, and meters (see Table A.8). The pollutant concentration in the mobile water in between the S and BC particles, C_W , the pollutant concentration in the S particles, C_S , and the pollutant concentration in the BC intraparticle porewater $C_{BC,ippw}$, are all dependent on the distance from the column inlet x , and time t . $C_{BC,ippw}$ additionally varies as a function of the distance r from the particle centre. Values of transport model input parameters are summarized in Table A.9 and governing mathematical equations are presented in the following section.

Column medium composition:

The volume fraction of the column filled with S particles, θ_S , can be calculated as

$$\theta_S = \frac{M_S}{d_S L \pi R^2} \quad (\text{A.1})$$

where M_S is the dry mass of S particles in the column, d_S is the S particle density, L is the column length and R the column radius.

The volume fraction of the column filled with BC particles, θ_{BC} , can be calculated as

$$\theta_{BC} = \frac{M_{BC}}{(1 - \theta_{BC,ippw}) * d_{BC} L \pi R^2} \quad (\text{A.2})$$

where M_{BC} is the dry mass of BC particles in the column, $\theta_{BC,ippw}$ is the water-filled intraparticle porosity, and d_{BC} is the density of the solid matrix of the BC particles.

The volume fraction of the column space in between the S and BC particles, which is assumed to be filled with mobile water, θ_W , can be calculated as

$$\theta_W = 1 - \theta_S - \theta_{BC} \quad (\text{A.3})$$

Table A.8 Independent and dependent column model variables and input parameters and their dimensions.

Variable / Input Parameter	Description
t (s)	Time
x (m)	Distance from the column inlet
r (m)	Radial distance from the BC particle centre
L (m)	Length of the column
R (m)	Radius of the column
θ_S (-)	Volume fraction of the column filled with S particles
θ_{BC} (-)	Volume fraction of the column filled with BC particles
θ_W (-)	Volume fraction of the column filled with mobile water (water in between the S and BC particles)
C_W (moles m ⁻³)	Pollutant concentration in the mobile water in the column (water in between the BC and S particles)
C_{in} (moles m ⁻³)	Pollutant concentration in the column influent
C_S (moles kg ⁻¹)	Pollutant concentration associated with the S particles
$C_{BC,solid}$ (moles kg ⁻¹)	Pollutant concentration in the BC solid matrix
$C_{BC,ippw}$ (moles m ⁻³)	Pollutant concentration in the BC intraparticle porewater
$C_{min,Fr}$ (moles m ⁻³)	Pollutant concentration in the BC intraparticle porewater below which an alternative isotherm model is substituted to avoid division by zero.
K_S (m ³ kg ⁻¹)	S particle-water partitioning coefficient for the pollutant
k_S (s ⁻¹)	First-order kinetic sorption rate for pollutants sorbed by the S particles
$K_{Fr,BC}$ (moles kg ⁻¹ (m ³ moles ⁻¹) ^{1/n_{Fr,BC}})	Freundlich isotherm coefficient for the pollutant
$n = 1/n_{Fr,BC}$ (-)	Freundlich isotherm exponent for the pollutant
k_{deg} (s ⁻¹)	First-order biodegradation rate for the pollutant in the mobile water (in between the S and BC particles)
v_x (m s ⁻¹)	Velocity of the mobile water flowing in between the S and BC particles in the x direction
D_{disp} (m ² s ⁻¹)	Dispersion coefficient for pollutants in the mobile water flowing in between the S and BC particles in the x direction
M_S (kg)	Dry mass of S particles in the column
d_S (kg m ⁻³)	Solid density of the S particles
M_{BC} (kg)	Dry BC mass in the column
R_{BC} (m)	BC particle radius
$\theta_{BC,ippw}$ (-)	Water-filled BC intraparticle porosity
d_{BC} (kg m ⁻³)	Solid density of the BC skeleton/solid matrix
τ_{BC} (-)	BC pore network tortuosity factor
D_{aq} (m ² s ⁻¹)	The molecular diffusion coefficient of the pollutant in water

Intraparticle diffusion of the pollutant in the pore network of BC particles:

Freundlich isotherm model:

The Freundlich isotherm model describes the sorption equilibrium distribution of pollutants between water and the BC solid matrix

$$C_{BC,solid} = K_{Fr,BC} * (C_{BC,ippw})^{1/n_{Fr,BC}} \quad (A.4)$$

where $C_{BC,solid}$ is the pollutant concentration in the solid matrix of the BC particles, $C_{BC,ippw}$ is the pollutant concentration in the intraparticle porewater of the BC particles, $K_{Fr,BC}$ is the Freundlich isotherm coefficient for the pollutant sorption by the BC solid matrix, and $1/n_{Fr,BC}$ is the Freundlich exponent. To avoid issues with the derivative when $C_{BC,ippw}$ is zero, the Freundlich isotherm is substituted with an alternative isotherm below a threshold intraparticle concentration value $C_{min,Fr}$

$$C_{BC,solid} = a * C_{BC,ippw} + b * (C_{BC,ippw})^2 \quad (A.5)$$

Parameters a and b are chosen so that the substituted isotherm has the same value and slope as the Freundlich isotherm at $C_{BC,ippw} = C_{min,Fr}$.

Effective diffusion coefficient:

The effective diffusion coefficient of the pollutant in the BC particle pore network is defined as

$$D_{eff,BC} = \frac{\theta_{BC,ippw} * D_{aq}}{\tau_{BC}} \quad (A.6)$$

where τ_{BC} is the BC particle pore network tortuosity factor, $\theta_{BC,ippw}$ the intraparticle porosity of the BC particles, which is assumed to be filled with immobile water, and D_{aq} is the molecular diffusion coefficient of the pollutant in water.

The following partial differential equation governs the pollutant concentration in BC intraparticle pore water, $C_{BC,ippw}$, for the Freundlich isotherm model

$$\begin{aligned} \frac{d}{dt} \left(\theta_{BC,ippw} * C_{BC,ippw} + (1 - \theta_{BC,ippw}) * d_{BC} * K_{Fr,BC} * (C_{BC,ippw})^{1/n_{Fr,BC}} \right) \\ = \frac{D_{eff,BC}}{r^2} * \frac{\partial}{\partial r} r^2 * \frac{\partial}{\partial r} C_{BC,ippw} \end{aligned} \quad (A.7)$$

Differentiation of the left-hand side results in

$$\begin{aligned} \left(\theta_{BC,ippw} + (1 - \theta_{BC,ippw}) * d_{BC} * K_{Fr,BC} * (C_{BC,ippw})^{(1/n_{Fr,BC}-1)} * 1/n_{Fr,BC} \right) * \frac{d}{dt} C_{BC,ippw} \\ = \frac{D_{eff,BC}}{r^2} * \frac{\partial}{\partial r} r^2 * \frac{\partial}{\partial r} C_{BC,ippw} \end{aligned} \quad (A.8)$$

Pollutant mass transfer from BC particles to the mobile water in the column (in between the S and BC particles):

The BC particles to mobile water pollutant mass transfer rate, $r_{ippwd,out}$, is described by

$$\begin{aligned} r_{ippwd,out} &= -\frac{\theta_{BC}}{\frac{4}{3}\pi R_{BC}^3} * 4\pi R_{BC}^2 * D_{eff,BC} * \frac{\partial}{\partial r} C_{BC,ippw} \Big|_{r=R_{BC}} \\ &= -3 * \frac{\theta_{BC}}{R_{BC}} * D_{eff,BC} * \frac{\partial}{\partial r} C_{BC,ippw} \Big|_{r=R_{BC}} \end{aligned} \quad (A.9)$$

where R_{BC} is the BC particle radius.

Pollutant mass transfer from the mobile water in the column (in between the S and BC particles) to the S particles:

The following differential equation governs the pollutant concentration in S particles

$$\theta_S d_S * \frac{d}{dt} C_S = r_S = -\theta_W k_S \left(\frac{C_S}{K_S} - C_W \right) \quad (A.10)$$

where k_S is the first-order kinetic sorption rate, and K_S the linear S particle to water partitioning coefficient for the pollutant.

Pollutant removal by biodegradation from the mobile water in the column (in between the S and BC particles):

The first-order pollutant mass removal rate from mobile water by biodegradation, r_{deg} , is described by

$$r_{deg} = \theta_W k_{deg} C_W \quad (A.11)$$

where k_{deg} is a first-order biodegradation rate for the pollutant in mobile water.

Pollutant fate in mobile water in the column (in between the S and BC particles) for the kinetic sorption model:

The following partial differential equation governs the pollutant concentration in the mobile water phase for the kinetic sorption model:

$$\theta_W * \frac{d}{dt} C_W = \theta_W D_{disp} * \frac{\partial^2}{\partial x^2} C_W - \theta_W v_x * \frac{\partial}{\partial x} C_W + r_{ippwd,out} - r_S - r_{deg} \quad (A.12)$$

where D_{disp} is the dispersion coefficient for pollutants in the mobile water, and v_x is the velocity of this water when flowing within the column in between the S and BC particles in the x direction.

Pollutant fate in mobile water in the column (in between the S and BC particles) for the sorption equilibrium model:

The following partial differential equation governs the pollutant concentration in the mobile water phase for the instantaneous sorption equilibrium model:

$$\left(\theta_W + \theta_S d_S K_S + \theta_{BC} * \theta_{BC,ippw} + \theta_{BC} * (1 - \theta_{BC,ippw}) * d_{BC} K_{Fr,BC} * (C_W)^{(1/n_{Fr,BC}-1)} * 1/n_{Fr,BC} \right) * \frac{d}{dt} C_W = \theta_W D_{disp} * \frac{\partial^2}{\partial x^2} C_W - \theta_W v_x * \frac{\partial}{\partial x} C_W - r_{deg} \quad (\text{A.13})$$

Boundary conditions:

Column boundary conditions:

It was assumed that flux into the column is by advection only with influent concentration, C_{in} ,

$$\left(-D_{disp} * \frac{\partial}{\partial x} C_W + v_x * C_W \right) \Big|_{x=0} = v_x * C_{in} \quad (\text{A.14})$$

and flux out of the column is also by advection only,

$$\left(-D_{disp} * \frac{\partial}{\partial x} C_W + v_x * C_W \right) \Big|_{x=L} = v_x * C_W \quad (\text{A.15})$$

For the intraparticle diffusion model, a zero-concentration gradient boundary condition is enforced at $r=0$ in the centre of the BC particles due to the assumed spherical symmetry of the particles

$$\frac{\partial}{\partial r} C_{BC,ippw} \Big|_{r=0} = 0 \quad (\text{A.16})$$

and the pollutant concentration in BC intraparticle pore water at the mobile water-BC interface is set equal to the pollutant concentration in the mobile water phase, C_W , at the corresponding location within the column (i.e. it is assumed that there is no external aqueous film mass transfer resistance)

$$C_{BC,ippw} \Big|_{r=R_{BC}} = C_W \quad (\text{A.17})$$

Input Parameters Column Model

Sorption to sand media:

The sand partitioning coefficient (K_S) and the first-order kinetic sorption rate (k_S) for pollutants sorbed by the sand particles were estimated via best-fit to the inhibited Sand column data:

$K_S [m^3 kg^{-1}] = 0.0028, 0.0011, \text{ and } 0.0023$ for atrazine, imidacloprid, and clothianidin.

$k_S [s^{-1}] = 0.0025, 0.0253, \text{ and } 0.0052$ for atrazine, imidacloprid, and clothianidin.

Table A.9 General input parameters for column pollutant transport model for parameter estimation (fitting).

Parameter	Value	Common Units	Value (SI)	Model units (SI)	Comments
For all three pesticides					
Flow rate, Q	0.2114	[mL/min]	3.523E-09	[m ³ /s]	
Column length, L	5.6	[cm]	0.056	[m]	
Inner column radius, R	1.25	[cm]	0.0125	[m]	
Total dry mass of biochar in the column, M_{BC}	0.23665	[g]	0.00023665	[kg]	0.5wt% BC
Total dry mass of S particles in the column, M_S	47.33	[g]	0.04733	[kg]	Average value as measured during column packing
Skeletal density of biochar, d_{BC}	1.7	[g/cm ³]	1700	[kg/m ³]	Ulrich <i>et al.</i> 2015
Sand solid density, d_S	2.54	[g/cm ³]	2540	[kg/m ³]	Ulrich <i>et al.</i> 2015
Biochar particle size	53-250	[μ m]	(53-250)*10 ⁻⁶	[m]	Sieve sizes
Radius of biochar particle, R_{BC}	57.6	[μ m]	0.0000576	[m]	Geometric mean of particle size range
Sand particles size, R_S	210-297	[μ m]	(210-297)*10 ⁻⁶	[m]	Per manufacturer
Radius of sand particle	126.75	[μ m]	0.000127	[m]	Average value
Atrazine					
Molecular weight, MW	215.68	[g/mol]	215.68*10 ⁻³	[kg/mol]	
Influent concentration, C_{In}	194.53	[μ g/L]	0.000902	[moles/m ³]	Average value over 92 days
Imidacloprid					
Molecular weight, MW	255.66	[g/mol]	255.66*10 ⁻³	[kg/mol]	
Influent concentration, C_{In}	187.10	[μ g/L]	0.000732	[moles/m ³]	Average value over 92 days
Clothianidin					
Molecular weight, MW	249.68	[g/mol]	249.68*10 ⁻³	[kg/mol]	
Influent concentration, C_{In}	189.15	[μ g/L]		[moles/m ³]	Average value over 92 days

Column Breakthrough Curve Predictions based on Batch Data

See Table A.10 for the batch-derived input parameters (K_F , n , τ).

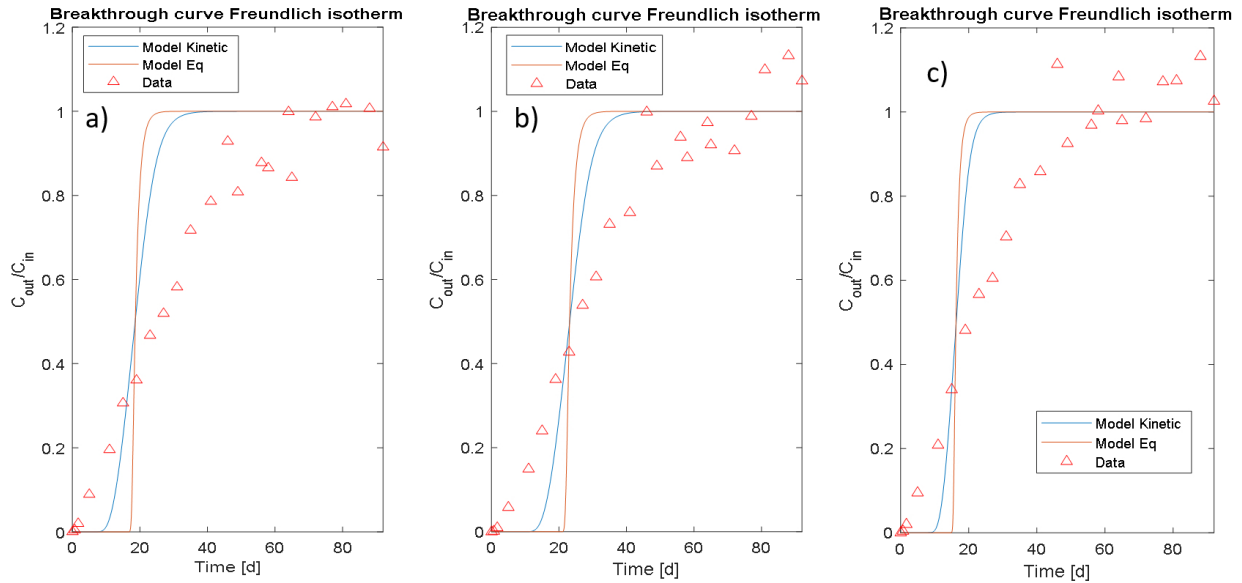


Figure A.16 Prediction of inhibited BC+Sand column breakthrough curves using the batch-derived Freundlich sorption isotherm (K_F , n) and kinetic (tortuosity) parameters in the MATLAB transport model. a) Atrazine, b) imidacloprid, c) clothianidin.

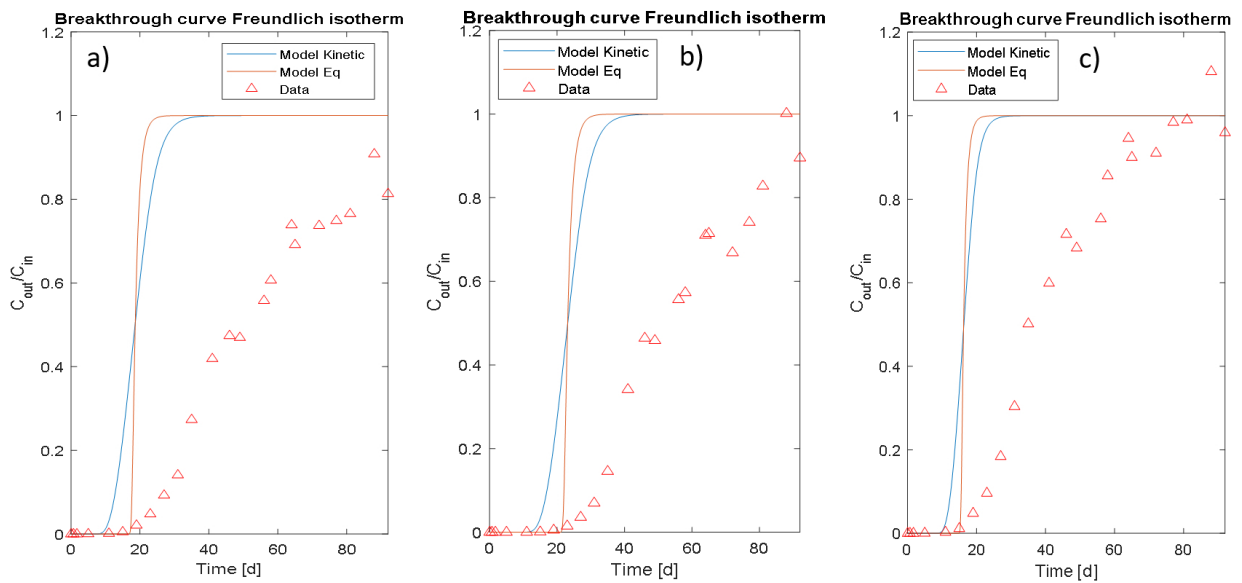


Figure A.17 Prediction of biotic BC+Sand column breakthrough curves using the batch-derived Freundlich sorption isotherm (K_F , n) and kinetic (tortuosity) parameters in the MATLAB transport model. a) Atrazine, b) imidacloprid, c) clothianidin.

Parameter Estimation based on Column Data (Best-Fit)

See Table A.10 for the best-fit parameters (K_F , n , τ) of the inhibited and biotic column data.

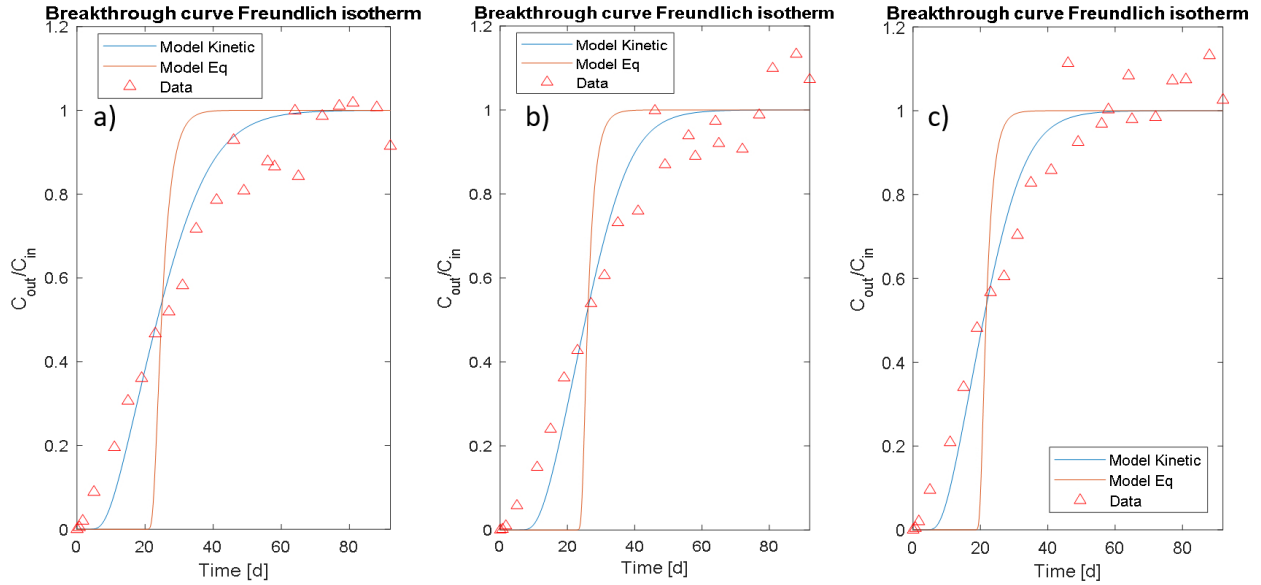


Figure A.18 Best-fit simulations of inhibited BC+Sand column breakthrough curves using the transport model in MATLAB and assuming Freundlich non-linear sorption behavior. a) Atrazine, b) imidacloprid, c) clothianidin.

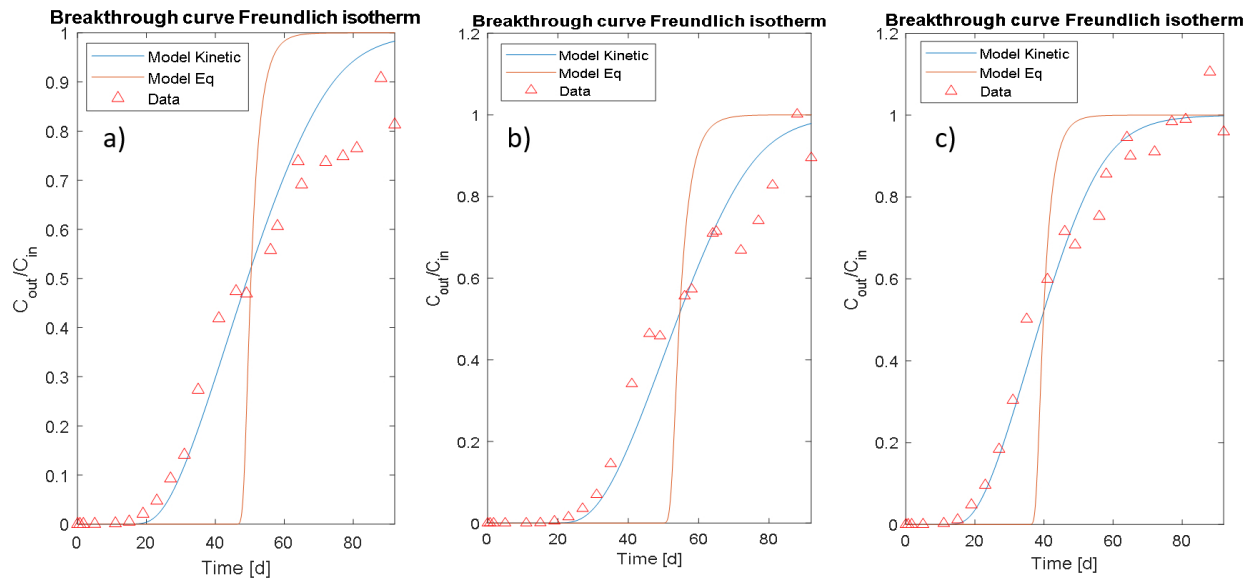


Figure A.19 Best-fit simulations of biotic BC+Sand column breakthrough curves using the transport model in MATLAB and assuming Freundlich non-linear sorption behavior. a) Atrazine, b) imidacloprid, c) clothianidin.

Table A.10 Freundlich sorption parameters, kinetic fitting parameter (tortuosity), goodness of fit, and linearized distribution coefficients for batch (abiotic) and column systems (inhibited and biotic) (Figures A.16-A.19). Linearization of isotherms is presented for comparison only.

	<i>Common units</i>		<i>Transport model units (SI)</i>		<i>Kinetics</i>	<i>Goodness of fit</i>	<i>Linearization of isotherms</i>	
Pesticide	K_F [(ug/g)/ ((ug/L) ⁿ)]	n [-]	$K_{Fr,BC}$ [(moles/kg)* (m ³ /moles) ^(1/n _{Fr,BC})]	$n_{Fr,BC}$ [-] (n = 1/n _{Fr,BC})	Tortuosity, τ [-]	Sum of squared residuals, SSR [moles/kg]	K_d [L/kg] at $C_W=$ 50 μ g/L	K_d [L/kg] at $C_W=$ 10 μ g/L
Batch-derived input parameters (from sorption isotherms and kinetic fit)								
ATZ	402.2	0.464	0.5552	2.156	15.4893	-	49000	117000
IMI	535.0	0.450	0.5642	2.225	11.2236	-	62000	151000
CLO	429.6	0.422	0.3265	2.369	10.1021	-	45000	114000
Best-fit simulations of column data: inhibited BC+Sand								
ATZ	263.3	0.6013	1.9679	1.663	28.2160	1.2168e-07	55000	105000
IMI	439.6	0.5102	0.9873	1.960	21.2937	8.3175e-08	65000	142000
CLO	287.2	0.5562	1.1558	1.798	23.5926	8.2505e-08	51000	103000
Best-fit simulations of column data: biotic BC+Sand								
ATZ	1519	0.4022	0.9847	2.4861	25.1389	1.3027e-07	147000	384000
IMI	1499	0.4170	1.0545	2.3983	17.8317	7.0867e-08	153000	392000
CLO	892.0	0.4565	1.0401	2.1904	19.8953	3.4946e-08	106000	255000

Estimation of Biodegradation Rate

To estimate the biodegradation rate (k_{deg}) for the biotic BC+Sand data set, we used the sorption (K_F , n) and kinetic parameters (τ) derived from the best-fit to the inhibited BC+Sand column data and let the transport model fit k_{deg} by minimizing the sum of squared residuals (SSR). As can be taken from Figure A.20, the way the transport model handles biodegradation (as a simple first-order rate only affecting the pesticide concentration in the aqueous phase) was not suitable to adequately describe our biotic BC+Sand column data set. The expansion of the existing transport model with mechanisms to account for biotransformation in all its possible forms was not feasible within the current study. For this reason, as described in the manuscript, we decided to *assume* that for our modelling purposes, the observed mass removal difference between biotic and inhibited BC+Sand columns was due to biologically enhanced sorption only (in order to be conservative and not overestimate the contribution of biodegradation in the subsequent scenario modelling).

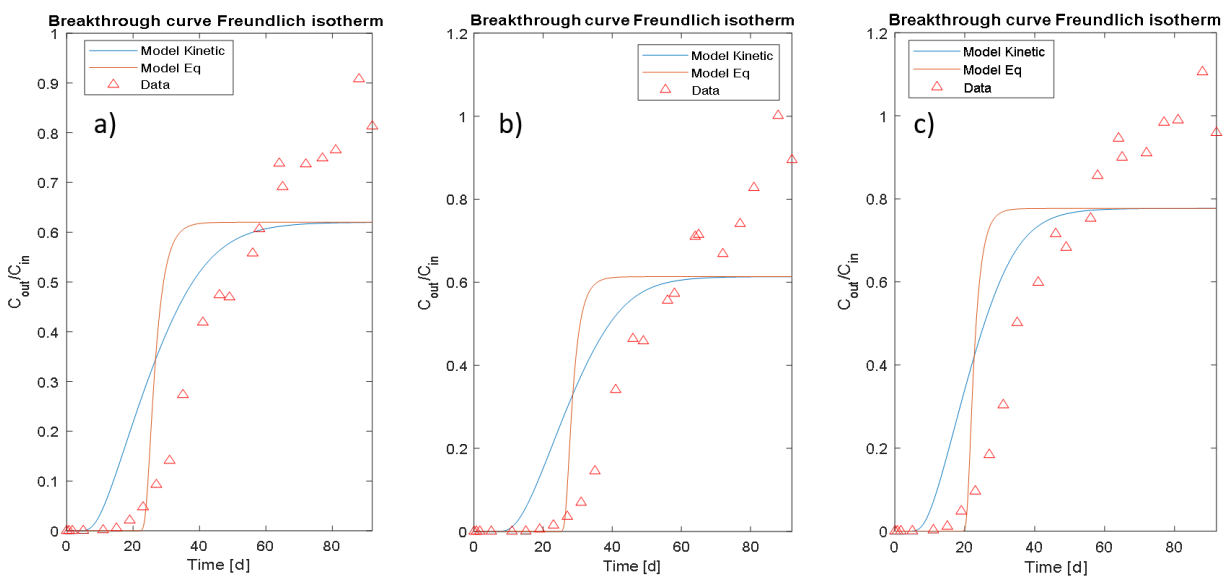


Figure A.20 Estimation of first-order biodegradation rate (k_{deg}) for biotic BC+Sand column breakthrough curves using the transport model in MATLAB and assuming Freundlich non-linear sorption behavior. Input values for the sorption and kinetic parameters were taken from the best-fit shown in Figure A.18 (best-fit to inhibited BC+Sand data). a) Atrazine, b) imidacloprid, c) clothianidin.

Biofilter Lifetime Simulations (Scenarios)

The best-fit sorption parameters were used to predict TOC breakthrough and biofilter lifetime in several case study simulations (scenarios). The simulated continuous filter lifetimes were then adjusted based on a representative field-scale biofilter (infiltration basin) for a residential area in Denver, CO, receiving a representative amount of rainfall. Input numbers and calculations are presented in Table A.11.

Table A.11 Calculations to adjust simulated continuous filter lifetimes based on a representative field-scale biofilter (infiltration basin) for a residential area of 3 acres and 16 inches per year of average annual rainfall in Denver, CO.

Variable	Formula	Parameter	Value	Comments
Column Experiment				
Diameter		D [cm]	2.5	Measured
Length		L [cm]	5.6	Measured
Area (cross section)	$A = (D/2)^2 * \pi$	A [cm ²]	4.91	
Total porous media volume	$V = A * h$	V [cm ³]	27.49	
Pore volume (BC+Sand)	$PV = V * n$	PV [cm ³]	9.62	~10 mL
Flow rate		Q [ml/min]	0.2114	Measured
		Q [L/year]	111.1	Total volume treated assuming continuous flow
Infiltration rate	$q = Q/A$	q [cm/min]	0.04	Darcy velocity
		q [cm/h]	2.58	Ulrich <i>et al.</i> 2017b: "Linear velocity", 2.6 cm/h
Porosity (BC+Sand)		n [-]	0.35	Ulrich <i>et al.</i> 2017b
Linear pore velocity	$v = q/n$	v [cm/min]	0.12	For BC+Sand media
Modelling Case Study				
Catchment size (residential)		A _{catch} [acres]	3	Ulrich <i>et al.</i> 2015
Area of infiltration basin (biofilter)		A _{IB} [ft ²]	1112	Ulrich <i>et al.</i> 2015, per recommendation of Denver Urban Drainage and Flood Control District
		A _{IB} [m ²]	103.3	
Denver annual precip.		P _{annual} [in]	16	Ulrich <i>et al.</i> 2015
		P _{annual} [cm]	40.64	
Total precipitation volume		V _{precip,annual} [acre-ft]	4	Ulrich <i>et al.</i> 2015
Treatment volume (assume: 50%)		V _{treat,annual} [acre-ft]	2	Ulrich <i>et al.</i> 2015
		V _{treat,annual} [L]	2.47E+06	
Biofilter Lifetime Adjustment				
Area ratio (biofilter/columns)	A_{IB}/A	Area ratio [-]	210456	
Treatment volume columns	$V_{treat,annual} / \text{Area ratio}$	V _{treat,annual,col} [L]	11.72	
Biofilter lifetime adjustment factor	$Q / V_{treat,annual,col}$	Factor [-]	9.5	To account for the filter not running continuously.

APPENDIX B
SUPPORTING INFORMATION FOR CHAPTER 3

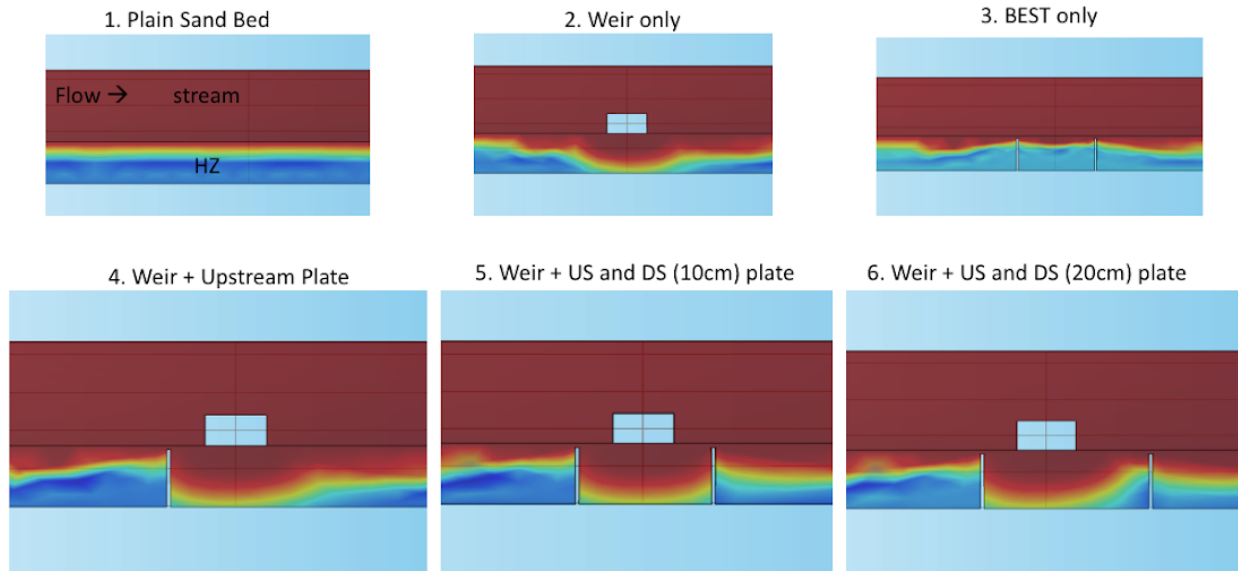
B.1 Flume System & Experimental Set-up

Outdoor Flumes System (Berlin, Germany)



Figure B.1 Full-scale outdoors flume system at the German Environment Agency (Umweltbundesamt; UBA) in Berlin, Germany. Photo was taken in 2018.

Preliminary Study of Experimental Set-up (COMSOL)



These results are all from $t=60$ minutes for a conservative tracer. Red indicates $C/C_0 = 1$, dark blue indicates $C/C_0 = 0$.

Figure B.2 Preliminary evaluation of experimental set-up and impact of different BEST streambed structures (submerged dam, subsurface steel plates) on HZ flow and residence times of flowpaths in a 1-D flow model in COMSOL Multiphysics®. Finally, the configuration of condition 6 was chosen for the full-scale flume study (with and without biochar).

Flume: Surface Water Quality Data

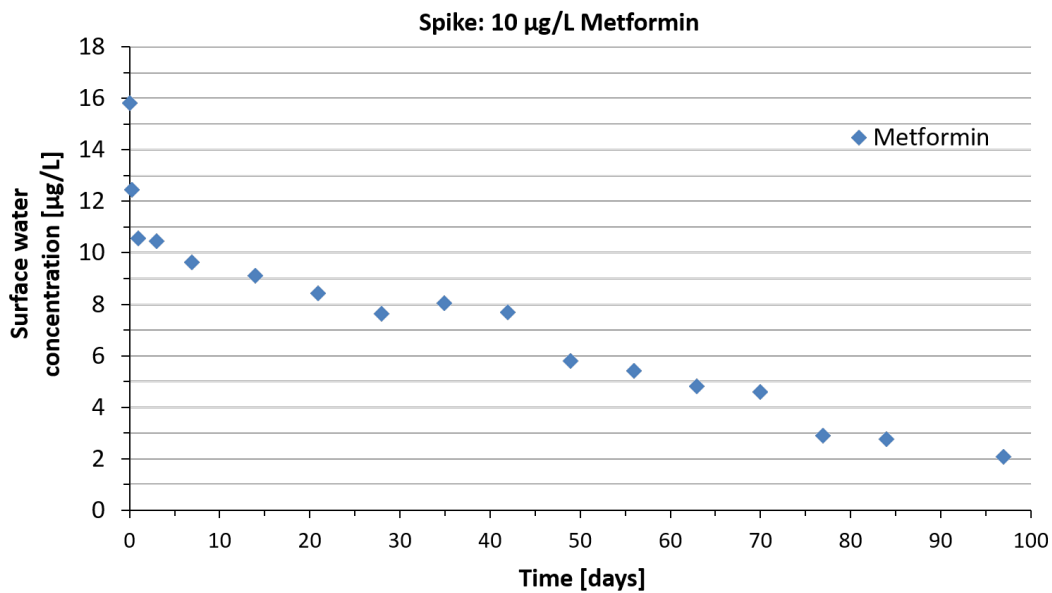


Figure B.3 Flume surface water concentrations of metformin over time during Experiment A (10 µg/L spike). Data is volume-corrected (using lithium-bromide tracer data).

Table B.1 Representative surface water quality data for the treatment flume. Nitrite, phosphate, and ammonia were 0 mg/L at all measured timepoints; nitrate was consistently <0.5 mg/L.

Sample Date	F⁻ [mg/L]	Cl⁻ [mg/L]	Br⁻ [mg/L]	SO₄²⁻ [mg/L]	Li⁺ [mg/L]	Na⁺ [mg/L]	K⁺ [mg/L]	Mg²⁺ [mg/L]	Ca²⁺ [mg/L]
17.04.2018	0.113	37.058	<0.3	93.2575	<0.2	25.7635	1.8965	7.115	79.7605
07.05.2018 ^a	<0.1	27.455	<0.3	64.2935	<0.2	28.785	4.502	6.3375	55.2025
08.05.2018	<0.1	41.6745	5.4915	91.273	0.4875	30.348	4.783	6.877	55.185
08.05.2018	<0.1	41.7075	5.723	91.1125	0.5115	30.4075	4.619	6.836	54.195
09.05.2018	<0.1	42.1915	5.8325	91.7445	0.5175	30.6445	4.596	6.967	55.2345
11.05.2018	0.113	40.736	5.405	85.854	0.4785	29.9	4.4025	4.6235	52.2645
15.05.2018	0.108	41.8905	5.4125	84.905	0.4665	30.849	4.268	6.751	52.513
22.05.2018	<0.1	41.662	5.128	79.2455	0.4285	30.7195	3.8435	6.465	49.4145
29.05.2018	0.1005	43.283	5.236	76.845	0.413	32.08	3.778	6.3425	52.473
05.06.2018	0.1035	43.498	5.0205	79.2455	0.4055	32.7355	4.161	6.3745	54.3795
12.06.2018	<0.1	34.4715	3.861	49.268	0.3825	33.725	3.4205	5.9805	46.3775
26.06.2018	0.11	48.479	4.675	79.593	0.36	38.6995	3.173	7.007	51.352
03.07.2018	0.111	49.2895	4.6725	78.055	0.3595	39.304	3.1175	6.9335	50.211
10.07.2018	0.13	49.923	4.8975	75.906	0.353	39.594	3.1095	6.7925	48.151
17.07.2018	<0.1	46.4505	4.2145	68.221	0.329	38.2445	2.8915	6.2955	43.052
24.07.2018	<0.1	52.0175	4.42	78.0205	0.34	43.0695	3.0605	6.984	46.6305
31.07.2018	<0.1	52.944	4.4495	72.803	0.339	43.509	3.07	6.878	44.0405
07.08.2018	<0.1	3.2875	<0.6	<20.0	<0.2	<10.0	<0.75	<2.0	<20.0

^a Spiking of metformin and tracer LiBr occurred on the 7th of May, 2018.

B.2 TOrC Analysis

Table B.2 List of target analytes analyzed by LC-QToF-MS including information on the source of analytical standards and surrogates.

Compound Name	Abbreviation	Chemical Formula	CAS #	Standard Source
Metformin	-	C ₄ H ₁₁ N ₅	1115-70-4	Metformin HCl, Sigma-Aldrich, 1 mg/ml in MeOH
Metformin-d ₆	-	C ₄ 2H ₆ H ₅ N ₅	1185166-01-1	1,1-Dimethyl-d ₆ -biguanide HCl, C/D/N Isotopes, 99 atom % D
Guanylylurea	GUA	C ₂ H ₆ N ₄ O	926-72-7	Carbamoyl-guanidine amidino urea salt, Toronto Research Chemicals
Guanylylurea- ¹⁵ N ₄	GUA-15N ₄	C ₂ H ₆ ¹⁵ N ₄ O	926-72-7	Guanylylurea-15N ₄ HCl, Toronto Research Chemicals
1-Methylbiguanide	MBG	C ₃ H ₉ N ₅	1674-62-0	1-Methylbiguanide HCl, Toronto Research Chemicals

LC Conditions

HPLC eluents, analysis blanks, double blanks, and sample dilutions (sorption isotherms) were prepared using Optima® LC/MS-grade water and methanol and HPLC-grade acetonitrile (Fisher Scientific). The aqueous mobile phase (A) was 5 mM ammonium formate (Sigma-Aldrich) and 0.1% formic acid (Fluka) in Optima® LC/MS-grade water and the organic mobile phase (B) consisted of 0.1% formic acid in HPLC-grade acetonitrile. The eluent flowrate was set to 1.0 mL/min and the temperature of the column oven was held at 40°C. The HPLC gradient started out at 0% B and was increased to 80% B within 4 min, returned to 0% B at 4.1 min, stayed constant at this level to establish equilibrium conditions until stopped at 8 min. The sample injection volume was 15 µL. Calibration standards were prepared over a calibration range of 0.25 – 250 µg/L in 90:10 water:acetonitrile. Surrogate concentrations in calibration standards, analysis blanks, and samples were 10 µg/L (metformin/MBG) and 50 µg/L (GUA).

Table B.3 LC-QToF-MS parameters for target analytes including native compounds and surrogates, plus suspect compounds (transformation products (TPs) of metformin). All analytes were analyzed in positive electrospray ionization (ESI+) mode. Abbreviations: 2-amino-4-methylamino-1,3,5-triazine (2,4-AMT), 4-amino-2-imino-1-methyl-1,2-dihydro-1,3,5-triazine (4,2,1-AIMT), and 2,4-diamino-1,3,5-triazine (2,4-DAT).

Native Compound Name	Chemical Formula	Precursor Mass (Q1) [Da], [M+H] ⁺	RT [min]	LOQ [$\mu\text{g/L}$]	Spike Recovery [%] ^a	Surrogate Name	Precursor Mass (Q1) [Da], [M+H] ⁺
Target analysis:							
Metformin	C4H11N5	130.10872	2.23	0.25	105	Metformin-d6	136.14638
Guanylurea	C2H6N4O	103.06144	1.86	1.00	138	Guanylurea-15N4	107.04958
1-Methylbiguanide	C3H9N5	116.09307	1.76	0.25	109	Metformin-d6	136.14638
Suspect screening (XIC list):							
Biuret	C2H5N3O2	104.04545	2.07	-	-		
2-4-AMT ^b	C4H7N5	126.07742	2.89	-	-		
4-2-1-AIMT ^b	C4H7N5	126.07742	2.89				
2-4-DAT	C3H5N5	112.06177	2.09	-	-		
Biguanide	C2H7N5	102.07742	1.66	-	-		
Dimethylguanidine	C3H9N3	88.08692	2.23	-	-		
Urea	CH4N2O	61.03964	n.d.	-	-		
Guanidine	CH5N3	60.05562	n.d.	-	-		
Allophanate	C2H3N2O3-	104.02164	n.d.	-	-		

^a Surrogate corrected average spike recovery in synthetic stormwater over a concentration range of 3-100 and 9-300 $\mu\text{g/L}$ for metformin / MBG and GUA, respectively.

^b These two suspects could not be distinguished with the LC-HRMS data collected; results will be summarized as one product "2-4-AMT/4-2-1-AIMT".

MS Parameters

Precursor ion data (TOF MS) was collected in ESI+ mode for m/z 50-500 Da for 1139 cycles with a total scan time of 0.421 s and an accumulation time of 0.1 s, with ion spray voltage set at 2500 V and temperature set to 500 °C. The ion source gas 1 and 2 were both set to 60 psi, the curtain gas and collision (CAD) gas were set to 50 psi and 10 psi, respectively. The collision energy (CE) was set to 5 V and the declustering potential (DP) to 50 V, each with no spread. Product ion (TOF MS/MS) scanning was conducted for m/z 50-1000 Da. The accumulation time for each SWATH window was 0.05 s and the CE was set to 30 V with 20 V spread, whereas the DP was kept at 50 V without spread. The instrument was mass calibrated every five injections using SCIEX ESI Positive Calibration Solution.

Metformin Transformation Products (Suspect Screening)

We built the extracted ion chromatogram (XIC) list for suspect analysis based on literature data. However, there are only a few studies reporting the detection of metformin transformation products (TPs) other than guanylurea: 2,4-diamino-1,3,5-triazine (2,4-DAT), 1-methylbiguanide (MBG), 2-amino-4-methylamino-1,3,5-triazine (2,4-AMT) and 4-amino-2-imino-1-methyl-1,2-dihydro-1,3,5-triazine (4,2,1-AIMT) were formed by electrochemical degradation of metformin in water samples (Tisler & Zwiener, 2018). Increasing concentrations of 2,4-AMT and 2,4-DAT were reported for wastewater treatment plant effluents, while MBG and 2,4-DAT were detected in wastewater impacted surface water (Tisler & Zwiener, 2018). Markiewicz *et al.* (2017) identified biguanide to be a potential intermediate in the formation of guanylurea. The compound biuret was detected for the first time in porewater samples of recirculating flumes as a TP of guanylurea (Posselt *et al.*, 2020). Lastly, Posselt (2020) suggested the formation of dimethylguanidine via removal of two urea molecules as another potential degradation pathway for metformin.

B.3 Batch Sorption Experiments

Kinetic Sorption Experiments

Kinetic data (aqueous concentration, C_W , over time) for metformin and guanylurea is shown in Figure B.4. Aqueous concentrations in control conditions (no biochar) were significantly different from treatment conditions: $p = 0.0341$ for metformin and $p = 0.0145$ for guanylurea (paired t-test; $\alpha = 0.05$).

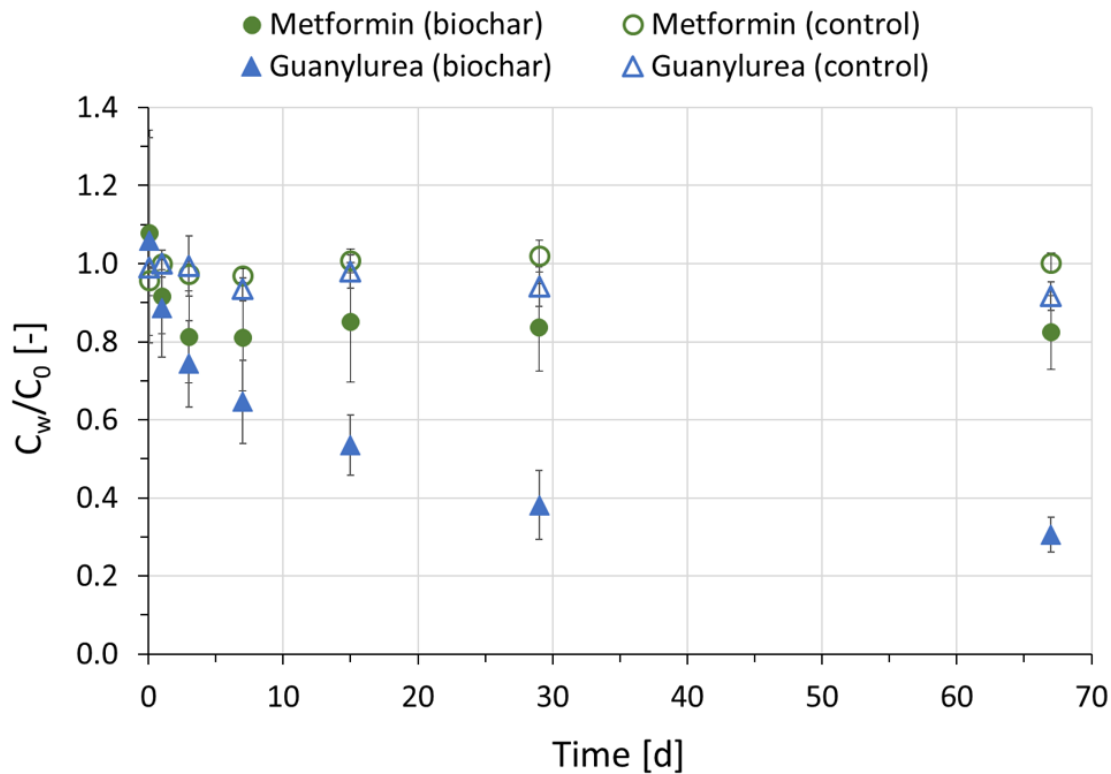


Figure B.4 Kinetic sorption of metformin and guanylurea to MCG biochar; shown as relative aqueous concentrations over time (67 days total). Initial TO_{RC} concentration was 10 $\mu\text{g/L}$ each. Control batches were set up without biochar (water only).

To compare sorption kinetics between compounds, a pseudo-first order (PFO) adsorption model (assumption: desorption is negligible) was fitted to the apparent distribution coefficient ($K_{d,app} = C_S/C_W$) data over time; best-fit parameters are summarized in Table B.4:

$$K_{d,app} = K_{d,eq} * (1 - e^{-k_{ad}*t})$$

where $K_{d,app}$ is the apparent distribution coefficient [L/kg] at any time t [days], $K_{d,eq}$ is the distribution coefficient at sorption equilibrium [L/kg], and k_{ad} is the adsorption rate constant [1/d].

Table B.4 Kinetic data: Pseudo-first order fit of the apparent distribution coefficient ($K_{d,app} = C_S/C_W$) over time using GraphPad Prism (version 9.1.1).

Best-fit Parameters	Metformin	Guanylurea
$K_{d,eq}$ [L/kg]	8626	81254
$K_{d,eq}$ 95% CI [L/kg]	5699 to 11932	63350 to 125999
k_{ad} [1/d]	0.6618	0.03536
k_{ad} 95% CI [1/d]	0.1547 to ? ^a	0.01514 to 0.06290
RMSE	4439	9663
AICc	275.7	300.6
Shapiro Wilk normality test (Residuals)	Yes (p = 0.2658)	Yes (p = 0.7569)

^a Calculation of confidence interval (CI) for k_{ad} in the case of metformin was incomplete, thus best-fit value should be interpreted with caution.

Sorption Isotherms

Table B.5 Best-fit values for Freundlich and Langmuir parameters obtained from equilibrium biochar sorption data using non-linear regression with relative weighting ($1/Y^2$) in GraphPad Prism (version 9.1.1). AICc designates the Akaike's Information Criterion corrected for low sample size.

	Metformin	Guanylurea	1-Methylbiguanide
Freundlich			
K_F [(ug/g)/((ug/L) ⁿ)]	13.74	230.0	18.46
K_F 95% CI [(ug/g)/((ug/L) ⁿ)]	11.22 to 17.22	201.3 to 270.5	13.62 to 54.15
n [-]	0.6667	0.4459	0.4637
n 95% CI [-]	0.6031 to 0.7577	0.4030 to 0.4907	0.2146 to 0.6294
Weighted Sum of Squares ($1/Y^2$)	0.4580	0.1298	2.055
RMSE	0.1809	0.1086	0.3831
AICc	-44.15	-45.32	-21.64
AIC probability that model is correct [%]	97.03	99.99	1.95
Langmuir			
Q_{max} [ug/g]	289.4	1934	135.1
Q_{max} 95% CI [ug/g]	236.1 to 512.8	1613 to 2739	108.9 to 228.3
K_L [L/ug]	0.0363	0.0797	0.0940
K_L 95% CI [L/ug]	0.0186 to 0.0514	0.0504 to 0.1235	0.0498 to 0.1732
Weighted Sum of Squares ($1/Y^2$)	0.7290	0.5873	1.219
RMSE	0.2282	0.2311	0.2950
AICc	-37.18	-27.21	-29.47
AIC probability that model is correct [%]	2.97	0.01	98.05

In-Field Bottles Experiments

Removal of metformin was studied under more controlled conditions in glass bottles to assess the relative importance of sorption and biodegradation in sediment compared to sediment + biochar and to identify other abiotic processes (e.g. hydrolysis, photolysis) potentially affecting metformin removal in the flumes. Results are summarized in Figure B.5.

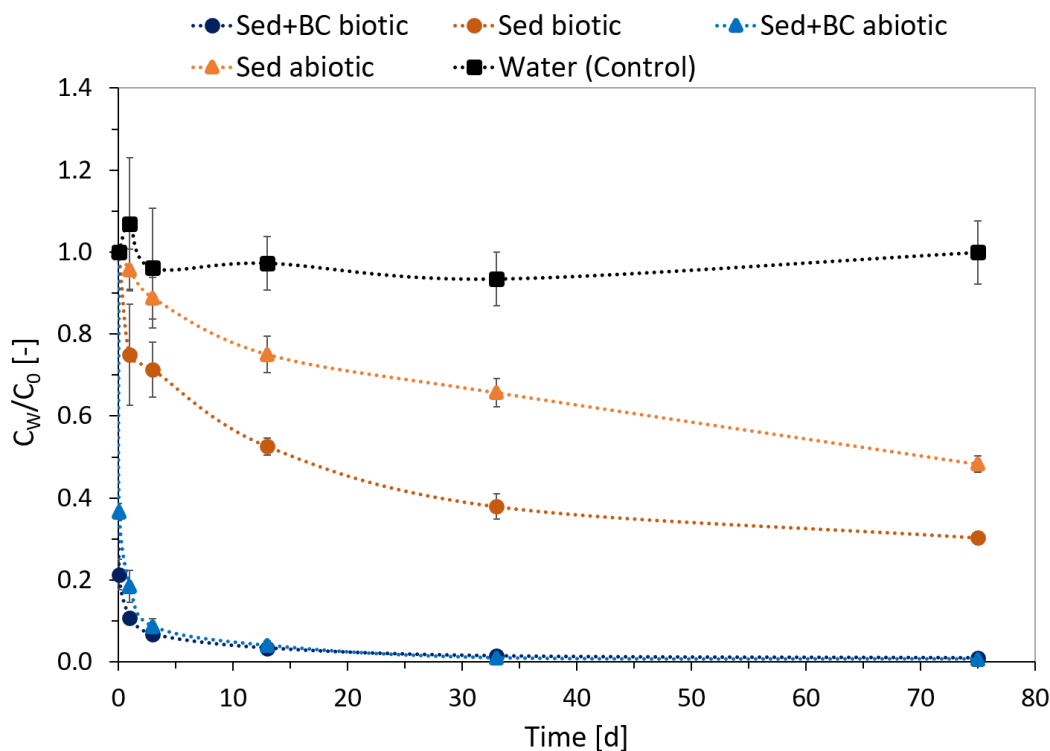


Figure B.5 Removal of metformin during bottle incubation experiment (75 days). Error bars represent standard deviation from triplicate experiments. All experiments were carried out outside to mimic temperature and sunlight exposure conditions of flumes. Biotic experiments were aerated continuously.

Figure B.5 indicates that sorption of metformin to the flume sediment was relatively slow, but overall still a relevant removal process (on average 52% removal after 75 d). The biotic sediment led to a quick removal of 25% after only one day, whereas an overall removal of 70% was observed at the end of the experiment. By comparing the removal in sediment under biotic conditions with abiotic conditions (assuming sorption only), it can be concluded that overall, biodegradation may have accounted for up to 18% of metformin removal. However, given the initially faster observed kinetics of metformin dissipation under biotic compared to abiotic conditions, it is hypothesized that biodegradation may have contributed to >>18% removal in the current experiment. Furthermore, it is possible that biodegradation may have still occurred in the abiotic treatment due to incomplete inactivation of microbial activity following sterilization (autoclaving). Loss of metformin due to abiotic processes other than sorption appeared to be

irrelevant under the conditions employed in this experiment: linear regression of the control data (water only) over time indicated that the slope was not significantly different from zero ($p = 0.737$; $\alpha=0.05$).

As for the biochar treatments, after only one day of exposure, the presence of MCG biochar led to 89% and 82% removal of metformin under biotic and abiotic conditions, respectively - owing to the high mass of biochar present in the bottles (33 vol% of the sediment/biochar mixture). After 75 days, nearly all metformin was removed from the water in both biochar conditions (on average 99%). In the presence of biochar, sterilization had no significant effect on the disappearance of metformin from the water (Wilcoxon matched-pairs signed rank test: $p=0.1563$; $\alpha=0.05$). The greater mass of biochar to mass of metformin ratio in the bottle experiments may explain the faster kinetics compared to the batch sorption experiments (see Figure 3.5a).

Overall, we conclude that the disappearance of metformin in the bottles followed the order we would expect: Sed+BC biotic = Sed+BC abiotic > Sed biotic > Sed abiotic > Control. Furthermore, there were no other relevant loss processes besides sorption and biodegradation affecting metformin disappearance; a finding that can be translated to the flumes. Under the studied conditions in the bottles (no continuous source of metformin), the effect of biodegradation on removal in the presence of biochar was negligible. However, the conditions in the flumes were different insofar as there was a continuous source of metformin through HZ exchange from the surface water. This might lead to the saturation of biochar sorption sites over time and thus a portion of metformin may remain bioaccessible for microbial transformation even in the presence of biochar.

B.4 Redox Conditions in Streambeds

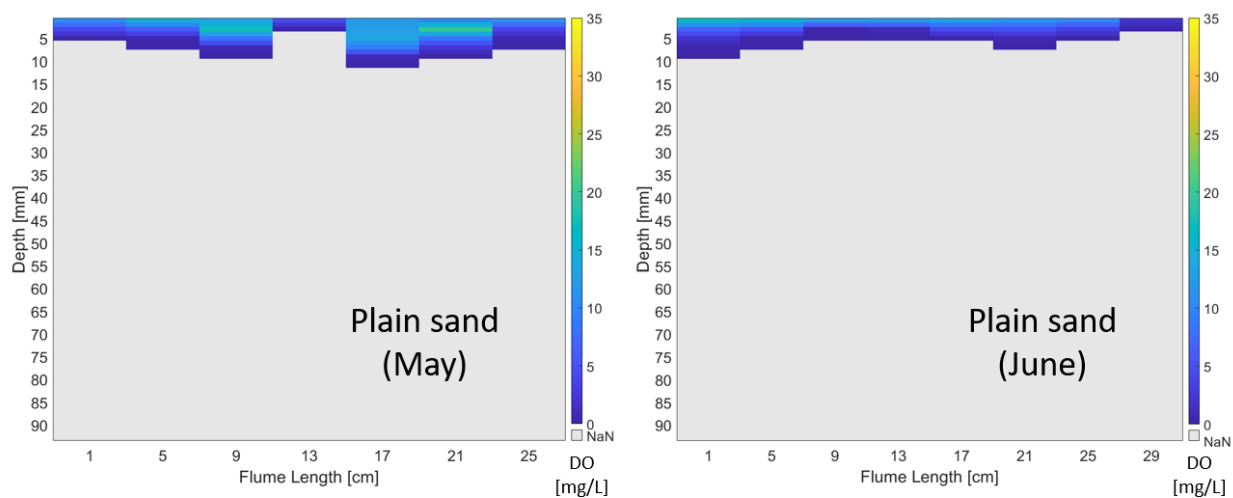


Figure B.6 Subsurface dissolved oxygen (DO) profiles of plain sand (un-altered) streambed sections. Measurements were taken in May and June 2018.

B.5 Particle Tracing (Transport Model)

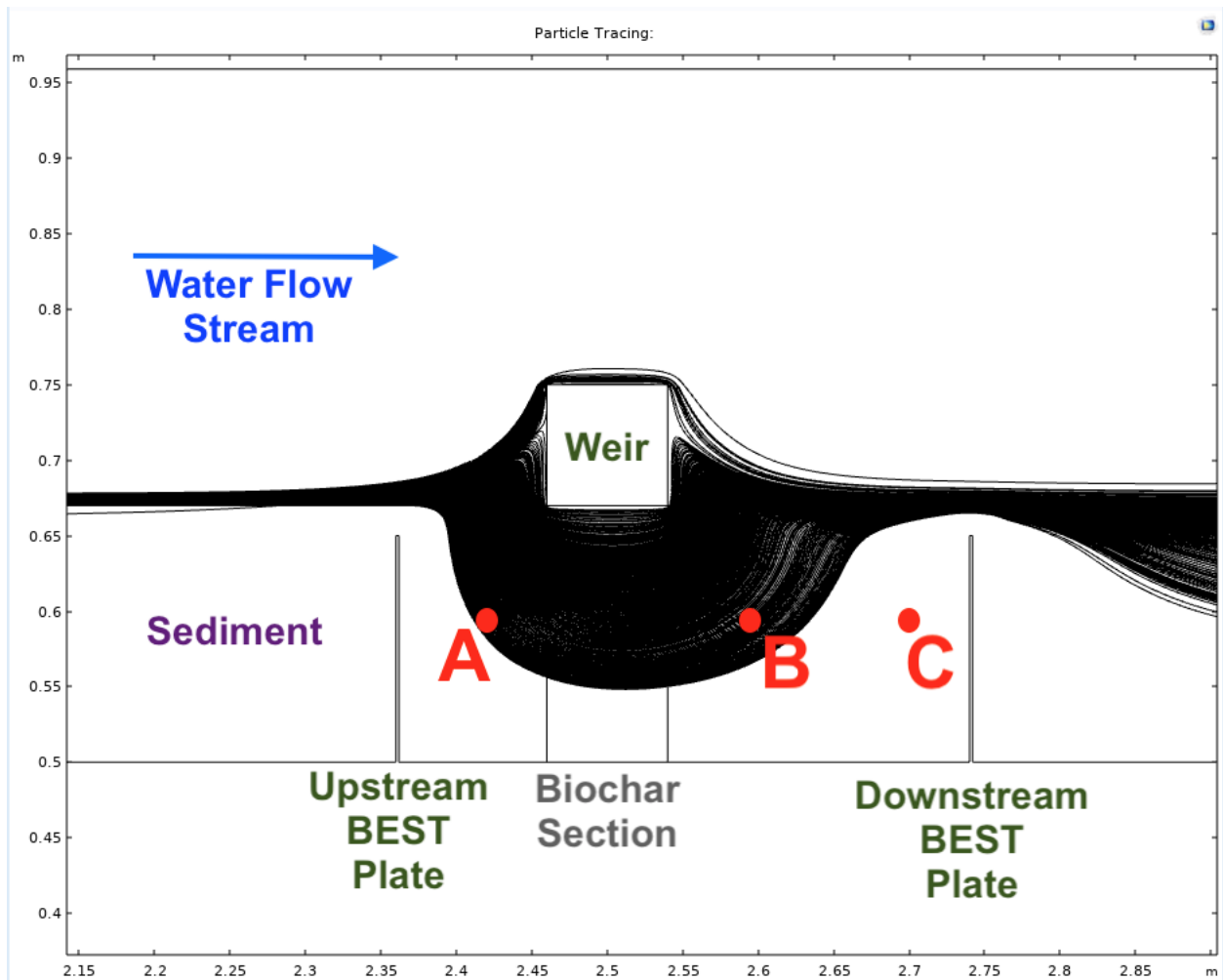


Figure B.7 Particle tracing in a 1-D flow model using COMSOL Multiphysics®. The coupled surface-subsurface model was built based on geometry measurements, material properties and flow information (not calibrated).

B.6 Experiment B (10 mg/L Metformin), Suspect Screening

Concentrations of Metformin/Guanylurea

Concentrations of metformin and guanylurea in the HZ measured during Experiment B at 10 days after spiking (~ 10 mg/L metformin) are shown in Figure B.8. No guanylurea was detected in any of the sampling locations in the biochar-amended BEST streambed sections (2A-C), presumably due to strong retention of metformin to the biochar surface and thus limited bioaccessibility.

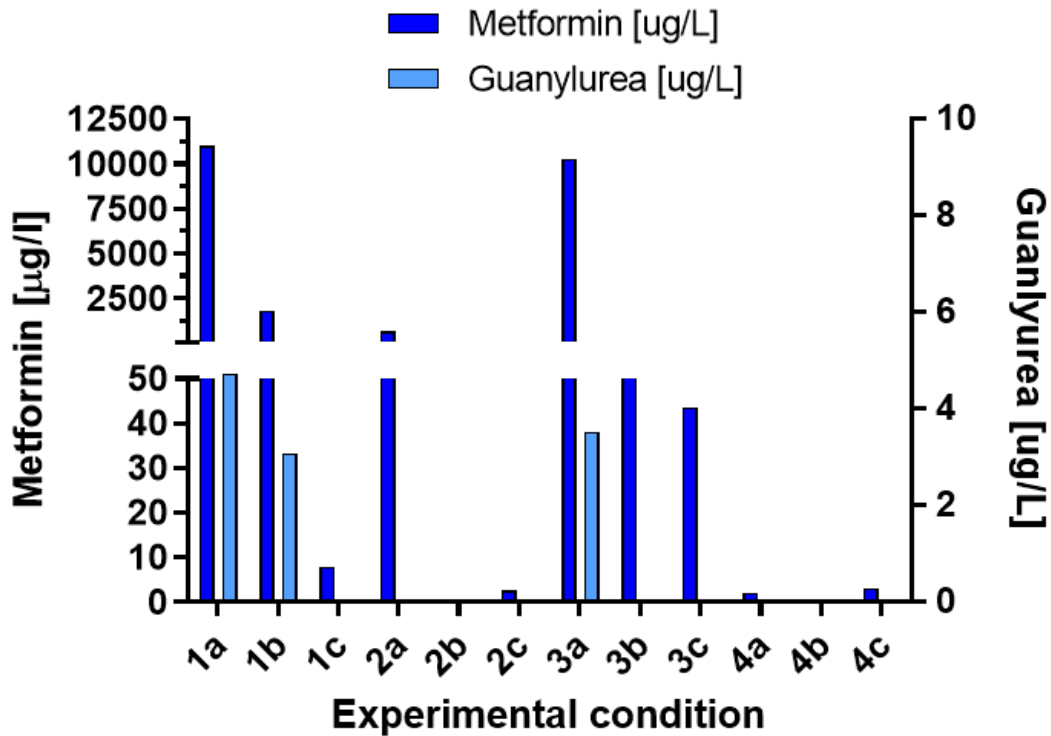


Figure B.8 Metformin and guanylurea concentrations in the subsurface of different conditions during Experiment B (~ 10 mg/L spike) measured at $t = 10$ days after spiking. Conditions: 1) BEST, 2) BEST + biochar, 3) Surface sand dunes, 4) Plain sediment (un-altered).

APPENDIX C

SUPPORTING INFORMATION FOR CHAPTER 4

C.1 Pilot-Scale Flume System & Experimental Set-up

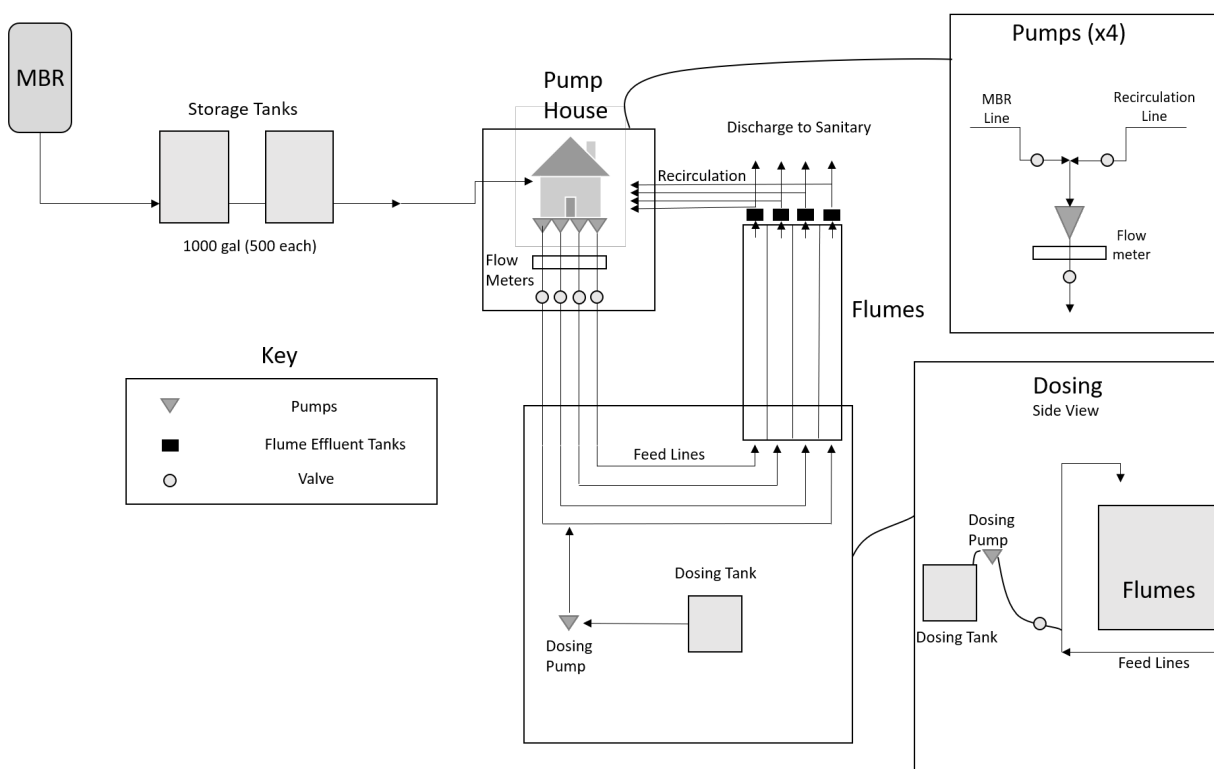


Figure C.1 Process diagram of the pilot-scale outdoor stream flumes at the Mines Park Water Reclamation Facility at the Colorado School of Mines in Golden, CO. Four individual flumes with different configurations can be operated in parallel in recirculation mode or one at a time in single-pass mode.

Porewater Sampling Locations (BEST Module)

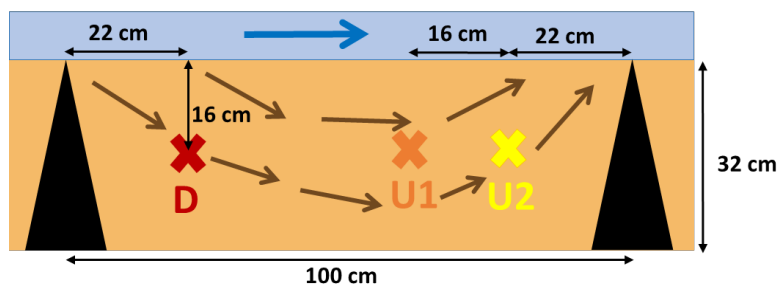


Figure C.2 Location of porewater sampling points in BEST modules. The “X” denotes the location of the tip of the sampling rod, from where pore water was drawn. Black triangles represent BEST walls.

Influent Water Quality Data

Table C.1 Representative water quality data for the Membrane Batch Reactor (MBR) system treating wastewater from nearby university student housing. The effluent of the MBR served as the source water for all flume experiments conducted in this study (August-October 2020).

Abbreviations: sCOD = soluble chemical oxygen demand; pCOD = particulate chemical oxygen demand; T-N = total nitrogen; T-P = total phosphorus.

Analyte	Influent^a 5/26/20	Effluent^a 5/26/20	Influent^a 7/02/20	Effluent^a 7/02/20	Influent^a 7/10/20	Effluent^a 7/10/20
sCOD [mg/L]	78.6	19.80	104.3	21.0	109.7	17.7
pCOD [mg/L]	156.3	-	177.0	-	195.7	-
T-N [mg/L]	6.5	7.77	7.5	6.5	7.0	4.9
T-P [mg/L]	6.4	9.40	7.8	5.6	6.6	5.3
NO ₃ ⁻ [mg N/L]	-	8.35	-	5.4	-	6.3
NO ₂ ⁻ [mg N/L]	-	-	-	-	-	-
NH ₄ ⁺ [mg N/L]	18.7	<1	23.9	<1	20.8	<1
pH [-]	7.15	5.19	7.22	7.06	7.06	6.30
Conductivity [μS/cm]	641	630	684	535	645	546
Alkalinity [mg/L CaCO ₃]	207	1	133	12	88	9

Analyte	Effluent^b 7/26/20	Effluent^b 8/07/20	Effluent^b 8/21/20
DOC [mg/L]	6.08	5.95	4.48
T-N [mg/L]	13.87	17.78	8.93
F ⁻ [mg/L]	0.50	0.48	0.47
Cl ⁻ [mg/L]	94.94	82.32	67.52
NO ₂ ⁻ [mg/L]	n.a.	n.a.	n.a.
Br ⁻ [mg/L]	n.a.	n.a.	0.03
NO ₃ ⁻ [mg/L]	74.81	81.20	41.42
PO ₄ ³⁻ [mg/L]	9.68	12.66	13.17
SO ₄ ²⁻ [mg/L]	61.41	67.30	71.58

^a Average values from grab samples (n=3).

^b Average values from composite samples (n=2).

C.2 TOrC Analysis

Table C.2 List of spiked target compounds analyzed by LC-QToF-MS including information on hydrophobicity ($\log K_{OW}$) and biodegradability (BIOWIN3). $\log K_{OW}$ = octanol-water partition coefficient; source: KOWWIN v1.68 estimates (EPI SuiteTM).

Compound Class	Compound Name	CAS #	Spiked Source & Purity	Native & Pu- rity	$\log K_{OW}$ [-]	BIOWIN3 (Ultimate degradation survey model; EPI Suite TM)
Herbicides	Atrazine	1912-24-9	TCI	America, >97%	2.82	2.0002 (months)
	Diuron	330-54-1	Sigma-Aldrich,	$\geq 98\%$	2.67	2.2709 (weeks-months)
	Metolachlor	51218-45-2	Sigma-Aldrich,	PESTANAL®	3.24	2.1862 (months)
	Isoproturon	34123-59-6	Sigma-Aldrich,	PESTANAL®	2.84	2.6684 (weeks-months)
	2,4-D	94-75-7	TCI	America, >97%	2.62	2.6040 (weeks-months)
	Mecoprop	93-65-2	Sigma-Aldrich,	PESTANAL®	2.94	2.7499 (weeks-months)
	Oryzalin	19044-88-3	Sigma-Aldrich,	PESTANAL®	2.73	1.8398 (months)
	MCPA	94-74-6	Sigma-Aldrich,	PESTANAL®	2.52	2.7809 (weeks)
Fungicides	Carbendazim	10605-21-7	Sigma-Aldrich,	97%	1.55	2.7300 (weeks-months)
Insecticides	Carbaryl	63-25-2	Sigma-Aldrich,	PESTANAL®	2.35	2.7078 (weeks-months)
	Diazinon	333-41-5	Sigma-Aldrich,	PESTANAL®	3.86	2.5306 (weeks-months)
	Fipronil	120068-37-3	TCI	America, >97%	6.64	0.5767 (recalcitrant)
Neonicotinoid insecticides (systemic)	Imidacloprid	138261-41-3	Sigma-Aldrich,	PESTANAL®	0.56	2.2134 (months)
	Thiamethoxam	153719-23-4	Sigma-Aldrich,	PESTANAL®	0.80	2.3393 (weeks-months)
	Clothianidin	210880-92-5	Sigma-Aldrich,	PESTANAL®	0.64	2.4408 (weeks-months)
Corrosion inhibitors	1H-Benzotriazole	95-14-7	Sigma-Aldrich,	ReagentPlus 99%	1.17	2.9359 (weeks)
Flame retardants	TCEP	115-96-8	Sigma-Aldrich,	97%	1.63	2.2025 (months)

Table C.2 Continued.

Compound Class	Compound Name	CAS #	Spiked Native Source & Purity	logK _{OW} [-]	BIOWIN3 (Ultimate degradation survey model; EPI Suite TM)
Pharmaceuticals & Personal Care Products (PPCPs)	Caffeine	58-08-2	Sigma-Aldrich, ReagentPlus	0.16	2.7700 (weeks)
	Atenolol	29122-68-7	Sigma-Aldrich, ≥98%	-0.03	2.6078 (weeks-months)
	Carbamazepine	298-46-4	TCI America, >97%	2.25	2.6770 (weeks-months)
	Metformin	1115-70-4	Sigma-Aldrich, certified reference material	-2.64	2.9137 (weeks)
	Ibuprofen	15687-27-1	Sigma-Aldrich, ≥98%	3.79	2.9582 (weeks)
Perfluoroalkyl Acids (PFAAs)	PFHxA	307-24-4	Liquid	3.48	1.5083 (recalcitrant)

LC Conditions

HPLC eluents, analysis blanks, double blanks, and sample dilutions (surface and subsurface samples) were prepared using Optima® LC/MS-grade water and methanol and HPLC-grade acetonitrile (Fisher Scientific). In the ESI+ method (Kinetex Biphenyl column), the aqueous mobile phase (A) was 1 mM ammonium formate (Sigma-Aldrich) and 0.1% formic acid (Fluka) in Optima® LC/MS-grade water and the organic mobile phase (B) was 100% HPLC-grade acetonitrile. The flowrate was set to 0.6 mL/min and the temperature of the column oven was held at 40°C. The HPLC gradient started out at 5% B, increased to 95% B within 5 min, stayed constant at this level for 5.5 min, until it quickly receded to 5% B for another 7.5 min to re-establish equilibrium conditions in the column.

Analysis of ESI- compounds was performed on a Gemini C18 column using the following eluents: the aqueous mobile phase (A) was 4 mM ammonium acetate in Optima® LC/MS-grade water and the organic mobile phase (B) consisted of 4 mM ammonium acetate in Optima® LC/MS-grade methanol. The flowrate was set to 0.5 mL/min and the temperature of the column oven was held steady at 40°C. LC Gradient elution started out at 10% B, increased to 90% B within 10 min, stayed constant at this level for another 10 min, until it quickly receded to 10% B for 5 min to allow for equilibrium conditions to establish.

Table C.3 LC-QToF-MS parameters for target analytes including native compounds and surrogates. § Variabilities in limit of quantitation (LOQ) were due to instrument variability (ESI-) or lab blank contamination (ESI+). * Spike Recovery was assessed by adding 10 µL of Standard solution (in MeOH) to 500 mL deionized water. Unfiltered samples were compared with PVDF (0.2 µm, 13 mm) filtered samples to determine the average recovery (n = 2) during sample processing.

Native Compound Name	ESI mode (+/-)	Chemical formula	For-	Precursor Mass (Q1) [Da], [M+H] ⁺	RT [min]	LOQ [µg/L] §	Spike Recovery [%] *	Surrogate Name	Precursor Mass (Q1) [Da], [M+H] ⁺
Atrazine	+	C ₈ H ₁₄ ClN ₅		216.1010496	5.80	0.005	103	Atrazine-d ₅	221.1324333
Benzotriazole	+	C ₆ H ₅ N ₃		120.0556236	4.55	0.01–0.025	93	Benzotriazole-d ₄	124.0807306
Diuron	+	C ₉ H ₁₀ Cl ₂ N ₂ O		233.0242948	5.90	0.005	94	Diuron-d ₆	239.0619552
Carbendazim	+	C ₉ H ₉ N ₃ O ₂		192.076753	4.25	0.005	99	Carbendazim-d ₄	196.10186
Imidacloprid	+	C ₉ H ₁₀ ClN ₅ O ₂		256.0595787	5.23	0.005	97	Imidacloprid-d ₄	260.0846857
Diazinon	+	C ₁₂ H ₂₁ N ₂ O ₃ PS		305.1083272	6.74	0.005	89	Diazinon-(dyethyl-d ₁₀)	315.1710946
Thiamethoxam	+	C ₈ H ₁₀ ClN ₅ O ₃ S		292.0265645	4.89	0.005	95	Thiamethoxam-d ₃	295.0453947
Clothianidin	+	C ₆ H ₈ ClN ₅ O ₂ S		250.0159998	4.98	0.005	95	Clothianidin-d ₃	253.0348301
Metolachlor	+	C ₁₅ H ₂₂ ClNO ₂		284.1411831	6.54	0.005–0.01	104	Metolachlor-d ₆	290.1788436
Atenolol	+	C ₁₄ H ₂₂ N ₂ O ₃		267.170319	3.78	0.01–0.025	94	Atenolol-d ₇	274.2142563
Caffeine	+	C ₈ H ₁₀ N ₄ O ₂		195.087652	4.53	0.01–0.025	97	Caffeine-(trimethyl-d ₉)	204.1441427
Carbamazepine	+	C ₁₅ H ₁₂ N ₂ O		237.1022395	5.69	0.005	105	Carbamazepine-d ₁₀	247.1650069
Isoproturon	+	C ₁₂ H ₁₈ N ₂ O		207.1491897	5.88	0.005	102	Isoproturon-d ₃	210.1680199
Ibuprofen	-	C ₁₃ H ₁₈ O ₂		205.1234034	12.50	0.01–0.025	93	Ibuprofen-d ₃	208.1422336
2,4-D	-	C ₈ H ₆ Cl ₂ O ₃		218.962123	10.73	0.01–0.025	100	2,4-D-d ₃	221.9809532

Table C.3 Continued.

Native Compound Name	ESI mode (+/-)	Chemical formula	For- Precursor Mass (Q1) [Da], [M+H] ⁺	RT [min]	LOQ [$\mu\text{g/L}$] §	Spike Recovery [%] *	Surrogate Name	Precursor Mass (Q1) [Da], [M+H] ⁺
Mecoprop	-	C ₁₀ H ₁₁ ClO ₃	213.0323954	11.38	0.005–0.025	100	Mecoprop-d ₃	216.0512257
Fipronil	-	C ₁₂ H ₄ Cl ₂ F ₆ N ₄ O ₅	434.9314298	12.99	0.005	99	Fipronil des F ₃	380.9596954
Oryzalin	-	C ₁₂ H ₁₈ N ₄ O ₆ S	345.087429	12.84	0.005	101	Fipronil des F ₃	380.9596954
MCPA	-	C ₉ H ₉ ClO ₃	199.0167454	10.71	0.01 – 0.10	107	MCPA-d ₃	202.0355756
PFHxA	-	C ₆ H ₁₁ O ₂	312.9728126	11.74	0.25	<i>n.a.</i>	M2PFHxA	314.9795223

MS Parameters

The MS settings of the ESI+ method are described elsewhere (Portmann *et al.*, 2022). ESI- method: Precursor ion data (TOF MS) was collected for m/z 50-1000 Da for 2397 cycles with a total scan time of 0.626 s and an accumulation time of 0.25 s, with the ion spray voltage set at -4500 V and temperature set to 500 °C. The ion source gas 1 and 2, curtain gas, and CAD gas were set to 50 psi, 40 psi, 25 psi, and 10 psi, respectively. The CE was set to -5 V and the DP was set to -50 V, each with no spread. Product ion (TOF MS/MS) scanning was conducted for m/z 50-1000 Da. The accumulation time for each SWATH window was 0.05 s and the CE was set to -30 V with 20 V spread, while the DP was kept at -50 V without spread. The instrument was mass calibrated every five injections using SCIEX ESI Neg. Calibration Solution.

C.3 Flume Contaminant Experiments

Bromide BTCs (Simulated Stormflow Experiments)

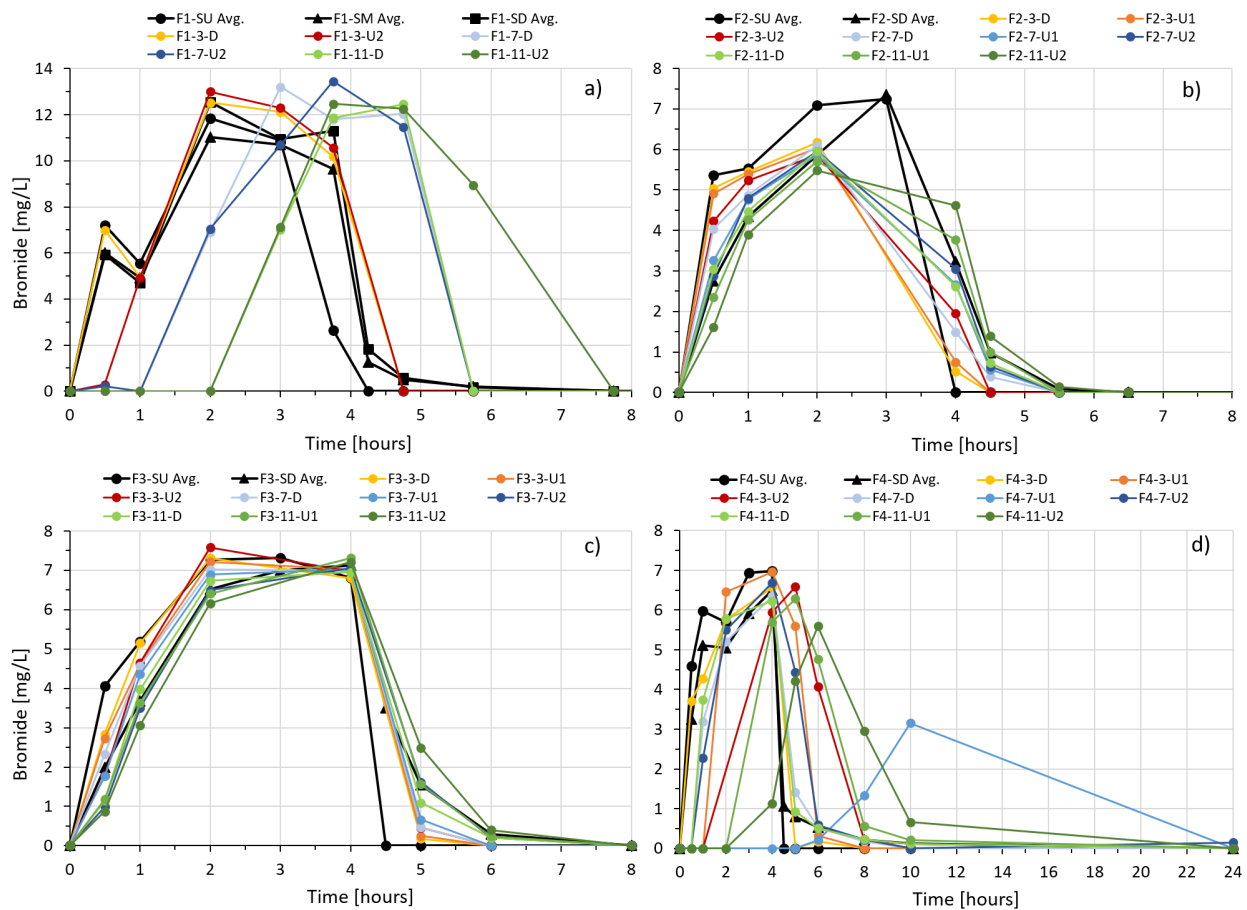


Figure C.3 Subsurface bromide breakthrough curves (BTCs) during simulated stormflow experiments: a) Control (F1), b) BEST (F2), c) BEST + biochar (F3), and d) BEST + biochar, slow (F4). Please note the difference in scaling of the y-axis for F1 and the x-axis for F4.

Concentration Peak Reductions (Simulated Stormflow Experiments)

An overview of concentration peak reductions in the surface (Sd) and subsurface (Module #3, D-U2) determined from TOrC breakthrough curves observed in simulated stormflow experiments is provided in Table C.4.

Table C.4 TOrC concentration peak reductions observed during single-pass experiments (4h-rainfall simulation). Surface attenuation was determined as peak reduction in Sd (effluent) compared to influent concentrations (Su); subsurface attenuation was determined exemplarily in Module #3 (across all flumes), as measured removal between HZ sampling locations D and U2.

Single-Pass Experiments	Sd [%]	Module 3 (D-U2) [%]						
	F1		F2		F3		F4	
Atrazine	-4.9	9.2	-6.8	-14.5	64.3	40.2	19.4	48.5
Benzotriazole	0.0	-0.3	-4.0	1.0	72.6	39.8	20.8	16.6
Diuron	4.4	-14.1	-10.0	-8.7	76.1	34.5	18.4	4.7
Carbendazim	-35.6	3.8	-2.4	2.0	71.2	43.2	11.0	8.7
Imidacloprid	4.1	-1.3	-3.1	1.2	69.1	41.5	17.3	28.0
Diazinon	1.0	1.0	10.6	7.8	70.0	40.9	18.7	23.5
Thiamethoxam	3.2	0.8	-2.1	-5.6	63.3	36.0	19.0	52.4
Clothianidin	0.0	2.4	-6.7	-7.9	70.7	42.0	20.4	28.1
Metolachlor	0.7	-7.4	3.5	9.3	66.1	38.1	9.3	47.3
Atenolol	7.4	24.8	11.8	0.8	71.9	42.1	20.8	23.0
Caffeine	15.7	38.2	14.1	-2.4	67.8	43.1	15.8	33.8
Carbamazepine	2.8	-8.6	5.3	-32.5	66.0	42.1	18.1	34.3
Isoproturon	3.3	-5.8	-7.4	-18.9	65.2	43.2	18.9	40.3
Ibuprofen	12.2	n.a.	29.1	3.8	58.8	24.8	23.2	50.4
2,4-D	-4.6	n.a.	0.6	-1.5	59.6	33.6	18.9	58.7
Mecoprop	7.0	n.a.	3.7	-2.4	54.7	24.0	19.0	64.8
Fipronil	-62.5	n.a.	-3.6	22.6	59.4	50.9	-5.9	51.6
MCPA	5.4	n.a.	5.6	-2.1	58.6	30.2	17.4	62.1
PFHxA	5.6	n.a.	8.6	-3.4	4.5	27.4	0.6	38.2
Min [%]	-62.5	-14.1	-10.0	-32.5	4.5	24.0	-5.9	4.7
Max [%]	15.7	38.2	29.1	22.6	76.1	50.9	23.2	64.8
Average [%]	-1.8	3.3	2.5	-2.7	62.6	37.8	15.8	37.6
Stdev. [%]	17.9	14.1	9.5	11.5	15.2	7.1	7.3	17.6

Mass Balance (Simulated Stormflow Experiments)

A summary of the mass balance conducted for each flume and compound using the single-pass simulated stormflow surface water data are presented in Table C.5 (page 163). The mass difference was calculated using the method of moments for the downstream concentration (Sd) and the nominal TOrC mass added to each flume (M_{in}).

C.4 Transformation Products (Suspect Screening)

TOrCs transformation products (TPs) observed via LC-HRMS suspect screening in samples of recirculation experiments (15 days observation period) are summarized in Table C.6 (ESI+ mode/method; pages 164-166) and Table C.7 (ESI- mode/method; page 167). The tables provide information on precursor and fragments exact masses, retention time, suspect confidence level according to the Schymanski scale (Schymanski *et al.*, 2014), literature references, and temporal occurrence in experimental flumes F1-F4 during the recirculation experiment (extended contact time).

Table C.5 TOrc mass balance conducted for each TOrc and flume for simulated stormflow data (single-pass), using the method of moments for the downstream concentration (Sd) and the nominal TOrc mass added to each flume (M_{in}). $M_{in} = 36$ mg of each TOrc in F1/F3/F4, and 30 mg in F2.

Compound Name	Mass Su [mg]	Mass Sd [mg]	$\Delta M/M_{in}$ [%]	$\Delta M/M_{in}$ [%]	$\Delta M/M_{in}$ [%]	$\Delta M/M_{in}$ [%]						
	F1	F2	F3	F4	F1	F2	F3	F4				
Atenolol	31.9	37.1	24.0	35.1	31.4	10.6	32.9	26.8	-3.0	-17.1	70.4	25.5
Atrazine	22.5	27.9	25.2	29.0	26.9	11.4	20.8	17.6	22.6	3.4	68.3	51.0
Benzotriazole	28.8	36.3	21.1	29.4	31.5	9.3	30.9	25.1	-0.8	2.0	74.0	30.2
Caffeine	30.0	36.1	29.4	36.1	34.9	15.0	38.6	32.0	-0.4	-20.4	58.2	11.1
Carbamazepine	22.1	26.0	19.0	21.3	27.7	10.7	18.9	16.1	27.8	28.9	70.3	55.3
Carbendazim	13.7	23.1	19.5	24.6	23.9	7.3	20.1	17.8	35.7	18.0	79.6	50.6
Clothianidin	24.3	29.3	20.1	27.1	28.6	9.2	26.9	21.6	18.7	9.7	74.3	39.9
Diazinon	24.1	29.1	18.6	22.4	28.5	9.4	14.8	11.8	19.2	25.3	73.8	67.2
Diuron	30.5	37.4	28.2	32.3	34.3	8.8	33.2	27.1	-3.8	-7.7	75.7	24.6
Imidacloprid	26.1	30.2	26.3	28.9	30.0	9.7	27.4	22.8	16.2	3.7	73.1	36.7
Isoproturon	26.3	31.2	29.1	33.7	33.6	13.0	21.1	17.8	13.4	-12.3	64.0	50.7
Metolachlor	16.3	19.4	21.8	24.6	19.2	7.6	17.3	14.6	46.0	18.0	78.8	59.3
Thiamethoxam	23.6	27.4	17.9	24.2	24.7	11.8	23.9	19.9	23.9	19.3	67.2	44.7
2,4-D	51.4	65.0	44.0	56.4	55.0	28.6	42.8	35.7	-80.5	-87.9	20.6	0.9
Fipronil	11.7	21.6	18.5	28.3	20.2	10.2	10.9	12.5	39.9	5.7	71.6	65.1
Ibuprofen	21.3	24.7	15.0	13.3	28.0	14.4	20.8	16.6	31.4	55.7	59.9	54.0
MCPA	32.7	40.3	25.4	31.9	34.8	17.5	33.1	29.3	-11.9	-6.3	51.3	18.5
Mecoprop	28.6	35.6	20.1	25.3	27.6	17.1	29.3	24.7	1.2	15.6	52.4	31.4
PFHxA	30.4	37.3	22.8	30.5	33.1	37.5	30.5	33.2	-3.6	-1.8	-4.0	7.9
Average									10.1	2.7	62.1	38.1
Stdev									27.6	28.4	21.0	19.7

Table C.6 Suspect transformation products (TPs) detected in surface and subsurface samples of recirculation experiments via LC-HRMS Positive Ionization Mode (ESI+). Experimental conditions: Control (F1), BEST (F2), BEST + biochar (F3), and BEST + biochar, slow (F4).

Transformation Product (TP)	Parent	TP Chemical Formula	Precursor Mass (Q1) [Da], [M+H] ⁺	MS2 Fragments (Q3) [Da]	References MS2 Data	RT [min]	Confidence Level	F1	F2	F3	F4
Desethyl-Atrazine	Atrazine (5.80 min)	C6H10ClN5	188.0697	146.0228, 104.0010	Chem. Ref. Standard	4.91	Level 1	4hrs-15d	4hrs-15d	-	-
2-Hydroxy-Atrazine		C8H15N5O	198.1349	156.0878, 86.0348	Chem. Ref. Standard	4.43	Level 1	4hrs-15d	4hrs-15d	-	-
1-Methyl-1H-Benzotriazole	Benzo-triazole (4.54 min)	C7H7N3	134.0713	106.0636, 91.0409	Gu <i>et al.</i> 2021; Huntscha <i>et al.</i> 2014	5.07	Level 2b	4d-15d	1d-15d	-	-
4/5-Methoxy-1H-Benzotriazole		C7H7N3O	150.0662	135.0446	Gu <i>et al.</i> 2021	4.83	Level 2b	4hrs-15d	4hrs-15d	-	-
DCPMU	Diuron (5.89 min)	C8H8Cl2N2O	219.0086	162, 127.0183	Maragou <i>et al.</i> 2011	5.70	Level 2b	4hrs-15d	4hrs-15d	4hrs-1d, 15d	1d, 15d
Desnitro-Imidacloprid	Imida-cloprid (5.22 min)	C9H11ClN4	211.0745	126.0105, 90.0335	Chem. Ref. Standard	4.25	Level 1	9d-15d	9d-15d	-	-
Imidacloprid-Urea		C9H10ClN3O	212.0585	128.0256, 99.0551	Chem. Ref. Standard	4.84	Level 1	15d	15d	-	-
5-Hydroxy-Imidacloprid		C9H10ClN5O3	272.0545	225.0569, 191.0949	Giroud <i>et al.</i> 2013	4.87	Level 3	1d-15d	1d-15d	-	-
IMHP	Diazinon (6.73 min)	C8H12N2O	153.1022	84.0443, 70.0650	Lee <i>et al.</i> 2020	3.80	Level 2b	4hrs-15d	4hrs-15d	-	4hrs
Diazoxon		C12H21N2O4P	289.1312	153.1021		5.80	Level 2b	4hrs-9d	4hrs-4d	-	4hrs
Hydroxy-Diazinon (OH-diazinon)		C12H21N2O4PS	321.1032	303.0929, 167.0640		6.38	Level 2b	4hrs-15d	4hrs-15d	-	4hrs

Table C.6 Continued.

Trans-formation Product (TP)	Parent	TP Chemical Formula	Precursor Mass (Q1) [Da], [M+H] ⁺	MS2 Fragments (Q3) [Da]	References MS2 Data	RT [min]	Confidence Level	F1	F2	F3	F4
Thiamethoxam-Urea (THX-urea)	Thiamethoxam (4.88 min)	C ₈ H ₁₀ ClN ₃ O ₂ S	248.0255	174.9728, 131.9672	Zhou <i>et al.</i> 2013	5.08	Level 2b	4hrs-15d	4hrs-15d	4hrs	4hrs-1d
Clothianidin-Urea (CLO-urea)	Clothianidin (4.97 min)	C ₆ H ₈ ClN ₃ O ₂ S	206.0149	131.9671, 119.9675	Kim <i>et al.</i> 2012	4.40	Level 3	9d-15d	4d-15d	-	-
Dechloro-Metolachlor	Metolachlor (6.54 min)	C ₁₅ H ₂₃ N ₂ O ₂	250.1802	176.1431, 218.1531	Brunner <i>et al.</i> 2019	6.20	Level 2b	9d-15d	4d-15d	-	-
CGA 50267		C ₁₂ H ₁₇ N ₂ O ₂	208.1332	135.0252, 120.0734	Reemtsma <i>et al.</i> 2013	4.48	Level 3	4hrs-15d	4hrs-15d	-	-
Atenolol-Acid/ Metoprolol-Acid	Atenolol (3.84 min)	C ₁₄ H ₂₁ N ₂ O ₄	268.1543	145.0650, 191.0704	Koba <i>et al.</i> 2016	4.29	Level 2b	4hrs-15d	4hrs-15d	4hrs-1d	4hrs-1d
Carbamazepine-10,11-epoxide	Carbamazepine (5.68 min)	C ₁₅ H ₁₂ N ₂ O ₂	253.0972	236.0706, 210.0915, 180.0810	Koba <i>et al.</i> 2016	5.36	Level 2b	4d-15d	4hrs-15d	-	-
Monodesmethyl-Isoproturon (MDIPU)	Isoproturon (5.87 min)	C ₁₁ H ₁₆ N ₂ O	193.1335	151.0863, 94.0649	Reemtsma <i>et al.</i> 2013	5.68	Level 2b	1d-15d	4hrs-15d	-	-
2-OH-Isoproturon (2-OH-IPU)		C ₁₂ H ₁₈ N ₂ O ₂	223.1441	59.0492, 72.0444, 165.1024	López-Muñoz <i>et al.</i> 2013; Ma <i>et al.</i> 2018	4.79	Level 2b	4hrs-15d	4hrs-15d	-	4hrs
4-isopropylaniline (4-IA)		C ₉ H ₁₃ N	136.1121	91.0537	This study	3.84	Level 3	4hrs	4hrs-1d	-	-

Table C.6 Continued.

Trans-formation Product (TP)	Parent	TP Chemical Formula	Precursor Mass (Q1) [Da], [M+H]⁺	MS2 Fragments (Q3) [Da]	References MS2 Data	RT [min]	Confidence Level	F1	F2	F3	F4
2-{4-[(dimethyl-carbamoyl) amino]phenyl} propanoic acid (TP237)		C ₁₂ H ₁₆ N ₂ O ₃	237.1234	72.0446, 120.0810	This study	4.93	Level 3	1d- 15d	1d- 15d	-	-

Table C.7 Suspect transformation products (TPs) detected in surface and subsurface samples of recirculation experiments via LC-HRMS Negative Ionization Mode (ESI-). Note: Metolachlor oxanilic acid and metolachlor ethane sulfonic acid had to be analyzed in ESI- mode despite the parent (metolachlor) being an ESI+ compound, see Li *et al.* (2020). For Fipronil sulfone, impurities may be present in calibration standards, possibly due to in-vial oxidation. References: Miller *et al.* (2020) refers to the following online dataset: <https://www.sciencebase.gov/catalog/item/5e6cdf5e4b01d509265a1fc>.

TP Name	Parent	TP Chemical Formula	Precursor Mass (Q1) [Da], [M+H] ⁻	MS2 Fragments (Q3) [Da]	References MS2 Data	RT [min]	Confidence Level	F1	F2	F3	F4
1/2-Hydroxy-Ibuprofen (1/2-OH-IBU)	Ibuprofen (12.55 min)	C13H18O3	221.1183	177.1286; 159.0394 (1-OH-IBU)	Ferrando-Climent <i>et al.</i> 2012	9.45	Level 2b	4hrs	4hrs	4hrs	4hrs
Carboxy-Ibuprofen		C13H16O4	235.0976	191.1075		10.48	Level 3	9d-15d	9d-15d	-	-
1,2-Dihydroxy-Ibuprofen (1,2-diOH-IBU)		C13H18O4	237.1132	135.0998, 193.1232		11.44	Level 3	4hrs-15d	4hrs-15d	-	-
2,4-Dichlorophenol (2,4-DCP)	2,4-D (10.76 min)	C6H4Cl2O	160.9566	124.9798	Nikolaiivits <i>et al.</i> 2019	10.31	Level 3	1d-15d	1d-15d	-	-
Fipronil sulfone	Fipronil (13.01 min)	C12H4Cl2F6N4O2S	450.9263	414.9504, 281.9931	Miller <i>et al.</i> 2020	13.26	Level 3	4hrs-15d	4hrs-15d	-	-
Fipronil desulfinyl		C12H4Cl2F6N4	386.9644	281.9926, 350.9875		12.89	Level 2b	4hrs-15d	4hrs-15d	4hrs	4hrs
Fipronil amide		C12H6Cl2F6N4O2S	452.9420	303.9571, 347.9703		11.81	Level 2b	4hrs-15d	4hrs-15d	4hrs	4hrs
Metolachlor oxanilic acid (OXA)	Metolachlor (ESI+)	C15H21NO4	278.1398	206.1543	Li <i>et al.</i> 2020	11.38	Level 3	4d-15d	4d-15d	-	-
Metolachlor ethane sulfonic acid (ESA)		C15H23NO5S	328.1224	79.9560, 120.9606		11.25	Level 2b	4d-15d	4d-15d	-	-

APPENDIX D
COPYRIGHT PERMISSIONS

Publisher and co-author copyright permissions for the already published manuscript (Portmann *et al.*, 2022) reproduced in Chapter 2 of this dissertation are compiled in a separate file and uploaded to ProQuest as a Supplemental File.